

2012

# DEVELOPMENT OF MINERAL PARTICLE SURFACES FOR THE ADSORPTION OF PITCH FROM WOOD PROCESSING AND RECYCLING OF PAPER

Gantenbein , Daniel

<http://hdl.handle.net/10026.1/1175>

---

<http://dx.doi.org/10.24382/1431>

University of Plymouth

---

*All content in PEARL is protected by copyright law. Author manuscripts are made available in accordance with publisher policies. Please cite only the published version using the details provided on the item record or document. In the absence of an open licence (e.g. Creative Commons), permissions for further reuse of content should be sought from the publisher or author.*

## Copyright statement

This copy of the thesis has been supplied on condition that anyone who consults it is understood to recognise that its copyright rests with its author and that no quotation from the thesis and no information derived from it may be published without the author's prior consent.

Signed.....

Daniel Gantenbein

**DEVELOPMENT OF MINERAL PARTICLE SURFACES  
FOR THE ADSORPTION OF PITCH FROM WOOD  
PROCESSING AND RECYCLING OF PAPER**

by

**DANIEL GANTENBEIN**

A thesis submitted to the University of Plymouth in partial fulfilment for the degree of

**DOCTOR OF PHILOSOPHY**

Environmental and Fluid Modelling Group

Centre for Research in Earth Sciences

School of Geography, Earth and Environmental Sciences

University of Plymouth

In collaboration with

Omya Development AG

**May 2012**

## **Supervisory team**

**Professor G. Peter Matthews**

Environmental and Fluid Modelling Group

School of Geography, Earth and Environmental Sciences

University of Plymouth

Plymouth

Devon

PL4 8AA

UK

Tel: 01752 584798

[P.Matthews@plymouth.ac.uk](mailto:P.Matthews@plymouth.ac.uk)

**Professor Patrick A. C. Gane**

Head of Research and Development

Omya Development AG

Baslerstrasse 42

CH-4665 Oftringen

Switzerland

Tel: +41 62 789 2422

[Patrick.Gane@omya.com](mailto:Patrick.Gane@omya.com)

**Dr Joachim Schoelkopf**

Head of RD-MSD

Omya Development AG

Baslerstrasse 42

CH-4665 Oftringen

Switzerland

Tel: +41 62 789 2229

[Joachim.Schoelkopf@omya.com](mailto:Joachim.Schoelkopf@omya.com)

# Abstract

**By Daniel Gantenbein**

**Development of mineral particle surfaces for the adsorption of pitch from wood processing and recycling of paper.**

During the production of paper in paper mills, detrimental wood resin is released into the water circuit of the mill during the pulping process of the wood into fibres. This wood resin, termed pitch, can detrimentally deposit on the paper and on the paper machine equipment. The deposits mark the paper or can lead to a tear of the paper web involving a loss of output and a reduction in paper quality. Furthermore, the wood resinous compounds in paper mill effluents need to be reduced in order to minimise their toxic effects on water organisms.

Talc has been the benchmark for many years as a mineral additive in pitch control. Since the papermaking process has changed over the years, the concept of mineral addition needs to be redefined and adopted towards the new circumstances. By understanding the fundamentals behind the adsorption of wood resin compounds from aqueous systems on to talc new mineral additives can be developed.

A model for the determination of the aspect ratio of platy and rod-like particles has been developed, based on commonly available characterisations such as particle size, specific surface area and shape.

It was found that the adsorption capacity of a mineral is directly proportional to its specific surface area, but only within its mineral family. Including the effect of surface hydrophilicity and hydrophobicity allowed fine tuning of the adsorption capacity of newly developed calcium carbonate grades. Furthermore, size exclusion effects, in porous, high surface area modified calcium carbonate, were seen to hinder complete coverage of the surface area by wood resin.

With increasing pH, the adsorption efficiency of talc for colloidal wood resin was found to decrease. Under these alkaline conditions, which are common in modern paper making processes, talc preferentially adsorbed dissolved species. The use of the newly developed surface treated and modified calcium carbonates allowed more efficient adsorption of the colloidal fraction and, therefore, represent an efficient alternative to talc in pitch control.

An increase in temperature led to an increased adsorption capacity of talc. This observation indicates the type of interaction that controls the adsorption of hydrophobic pitch particles onto talc, i.e. the entropically favoured release of water from the hydrophobic talc surface as well as the hydrophobic methylene backbone of the hemicellulose.

# Table of contents

Copyright statement .....	I
Title page.....	II
Supervisory team.....	III
Abstract .....	V
Table of contents .....	VI
Table of figures .....	XIII
Table of tables .....	XXIII
Table of equations .....	XXVII
Acknowledgements .....	XXX
Author's declaration.....	XXXI
Conferences, Seminars and Workshops.....	XXXII
Publications and Book chapters .....	XXXIII
Patents .....	XXXV
Nomenclature .....	XXXVII
1 Introduction .....	1
1.1 Aim and thesis description .....	1
1.2 Hypotheses .....	1
1.3 Structure of the thesis.....	2
1.4 The collaborative basis of this research project .....	3
2 Theory and literature review .....	4
2.1 Paper and Papermaking.....	4
2.1.1 History.....	5

2.1.2	The papermaking process.....	6
2.1.2.1	Wood.....	6
2.1.2.2	Fibre and stock preparation.....	7
2.1.2.3	Sheet formation.....	8
2.1.2.4	Press and dryer section .....	8
2.1.2.5	Surface treatment .....	9
2.1.2.6	Paper recycling .....	10
2.2	Wood components.....	13
2.2.1	Origin and composition of Wood resin.....	13
2.2.2	Lignin .....	17
2.2.3	Polysaccharides .....	17
2.2.4	Wood resin in aqueous environment.....	18
2.2.5	Environmental aspects of wood resinous compounds .....	21
2.2.6	Analysis and quantification of dissolved and colloidal substances, and of pitch control measures.....	23
2.2.6.1	Analysis of dissolved and colloidal substances .....	23
2.2.6.2	Deposition tests.....	25
2.3	Pitch Control .....	28
2.3.1	Retention .....	28
2.3.2	Dispersion .....	29
2.3.3	Deresination .....	30
2.4	Minerals in paper making.....	30
2.4.1	Talc and related minerals .....	32
2.4.1.1	History of talc in paper .....	32
2.4.1.2	Mineralogy of phyllosilicates .....	32
2.4.1.2.1	Occurrence of talc and chlorite .....	35
2.4.1.2.1.1	(A) Magnesium carbonate derivative ore bodies .....	36
2.4.1.2.1.2	(B) Serpentine derivative ore bodies.....	37
2.4.1.2.1.3	(C) Silica aluminous rock derivative ore bodies.....	38
2.4.1.2.1.4	(D)Magnesium sedimentary deposit derivative ore bodies....	39



2.4.1.3	Surface properties of talc, chlorite and pyrophyllite.....	39
2.4.2	Calcium carbonate.....	42
2.4.3	Particle size and aspect ratio .....	47
2.4.3.1	Importance and definitions of aspect ratio.....	47
2.4.3.2	Methods to evaluate the aspect ratio.....	50
2.5	Minerals in Pitch control.....	54
2.5.1	Talc.....	54
2.5.2	Bentonite .....	61
2.5.3	Kaolin.....	61
2.5.4	Calcium carbonate.....	62
2.5.5	Other minerals.....	63
2.6	Adsorption.....	63
2.6.1	Langmuir isotherm.....	66
2.6.2	Freundlich isotherm .....	67
2.6.3	Other useful isotherms .....	67
2.6.4	Brunauer, Emmett, Teller isotherm.....	68
2.6.5	Colloidal Deposition .....	71
3	Techniques .....	73
3.1	Preparation of the mineral particles .....	73
3.1.1	Talc, chlorite and pyrophyllite.....	73
3.1.2	Hydrophobised calcium carbonate.....	74
3.1.3	Modified calcium carbonate.....	75
3.2	Particle characterisation .....	75
3.2.1	Particle size .....	75
3.2.1.1	Sedimentation .....	76
3.2.1.2	Laser light scattering.....	77
3.2.1.3	Dynamic light scattering – photon correlation spectroscopy.....	79
3.2.2	Specific surface area .....	81
3.2.3	Scanning electron microscopy (SEM) and image analysis.....	82

3.2.4	Mineral analysis .....	84
3.2.4.1	X-ray fluorescence .....	84
3.2.4.2	Loss on ignition LOI.....	84
3.2.4.3	X-ray diffraction .....	85
3.2.5	Pore size .....	86
3.2.6	Zeta potential and electrophoretic mobility .....	87
3.2.7	Polyelectrolyte titration and streaming current detector .....	91
3.2.8	Wetting properties of minerals.....	94
3.3	Preparation of the dissolved and colloidal substances and the adsorption experiments .....	95
3.4	Quantification of dissolved and colloidal substances .....	97
3.4.1	Turbidity.....	98
3.4.2	Chemical oxygen demand (COD).....	99
3.4.3	Gravimetric analysis.....	99
3.4.4	Analysis of extractives .....	100
3.4.5	Analysis of carbohydrates and lignin.....	103
3.4.6	Analysis of inorganic ions.....	104
3.4.7	Thermo gravimetric analysis.....	107
3.4.8	Equilibrium .....	109
3.4.9	Statistical considerations.....	110
3.4.9.1	Linear and non-linear regression .....	111
4	Determining the size distribution-defined aspect ratio of platy and rod-like particles .....	114
4.1	Introduction .....	114
4.1.1	Hohenberger model (2001) .....	115
4.2	Platy particles .....	121
4.2.1	Material and Methods .....	121
4.2.1.1	Minerals .....	121
4.2.1.2	Methods .....	122

4.2.2	Results and Discussion.....	124
4.3	Rod-like particles .....	132
4.3.1	Material and Methods .....	132
4.3.1.1	Minerals .....	132
4.3.1.2	Methods .....	133
4.3.1.2.1	Image analysis.....	134
4.3.2	Results and Discussion.....	135
4.4	Conclusions.....	141
5	Efficiency of colloidal pitch adsorption onto phyllosilicates: comparing talc, chlorite and pyrophyllite .....	145
5.1	Introduction.....	145
5.2	Materials and Methods.....	146
5.2.1	Materials.....	146
5.2.2	Methods.....	149
5.3	Results and Discussion.....	150
5.3.1	Effect of mineral on pH – correction for turbidity.....	150
5.3.2	Modelling the adsorption .....	153
5.3.3	Application to data .....	154
5.4	Conclusions.....	165
6	Influence of pH and temperature on the adsorption of dissolved and colloidal substances from thermo mechanical pulp filtrates onto talc .....	167
6.1	Influence of pH .....	167
6.1.1	Introduction.....	167
6.1.2	Materials and Methods.....	169
6.1.2.1	Materials .....	169
6.1.2.2	Methods .....	170
6.1.3	Results and Discussion.....	172
6.2	Influence of temperature .....	189
6.2.1	Introduction.....	189

6.2.2	Materials and Methods.....	190
6.2.2.1	Materials .....	190
6.2.2.2	Methods .....	191
6.2.3	Results and Discussion.....	192
6.3	Conclusions .....	202
7	The development of hydrophobised ground calcium carbonate and the use of porous high surface area calcium carbonate for the adsorption of dissolved and colloidal substances from thermo mechanical pulp filtrates .....	204
7.1	Development of hydrophobised Calcium carbonate particles .....	205
7.1.1	Introduction .....	205
7.1.2	Materials and Methods.....	205
7.1.2.1	Materials .....	205
7.1.2.1.1	Stearic acid treatment and semi-quantitative wetting test.....	206
7.1.2.2	Methods .....	207
7.1.3	Results.....	209
7.1.3.1	Screening – 0, 30 and 60 % surface treatment.....	211
7.1.3.2	Optimisation – defining the degree of surface coverage with stearic acid	215
7.1.3.3	Application – quantify the benefit of surface treatment and chemical analysis	217
7.1.4	Discussion .....	223
7.2	The use of porous high surface area calcium carbonate .....	228
7.2.1	Introduction .....	228
7.2.1.1	Surface properties .....	229
7.2.2	Materials and Methods.....	229
7.2.2.1	Materials .....	229
7.2.2.2	Methods .....	230
7.2.3	Results.....	231
7.2.3.1	Effective adsorption isotherm.....	232
7.2.3.2	Chemical analysis – selective adsorption properties .....	235

7.2.4	Discussion .....	240
7.3	Influence of electrolytes on pitch stability .....	245
7.3.1	Introduction .....	245
7.3.2	Materials and Methods .....	246
7.3.2.1	Materials .....	246
7.3.2.2	Methods .....	246
7.3.3	Results and Discussion.....	247
7.4	Conclusions .....	250
8	Overview .....	254
8.1	Findings.....	254
8.2	Conclusions .....	256
8.2.1	Industrial applications and limitations .....	260
8.3	Related work .....	262
8.4	Future work .....	263
9	Literature .....	265

## Table of figures

Figure 2-1: Schematic of the papermaking process. ....	6
Figure 2-2: Dissection of the cyclic carbon skeleton of primaric acid into isoprene units linked tail to head (Back, Allen 2000). ....	14
Figure 2-3: Common resin acids in softwood canal resin (Back, Allen 2000). ....	15
Figure 2-4: Characteristic parenchyma wood resin constituents (Back, Allen 2000). ....	16
Figure 2-5: Chemical structure of some common sterols in wood resin: (1) sitosterol, (2) campesterol, (3) sitostanol, (4) campestanol and (5) citrostadienol, (6) cycloartenol, (7) 24-methylene cycloartanol, and (8) butyrospermol (Back, Allen 2000). ....	17
Figure 2-6: Possible structure of <i>O</i> -acetylgalactoglucomannan. ....	18
Figure 2-7: Tentative illustration of pitch globules and their equilibrium with the surrounding bulk solution. ....	20
Figure 2-8: Flowsheet of the apparatus used for the Hydro-Pulsed Colloidal Deposition (HPCD) test (McGregor, Philippaerts 1998). ....	27
Figure 2-9: Simplified geological cross section through a magnesium carbonate ore. ( <a href="http://www.luzenac.com/geology.htm">http://www.luzenac.com/geology.htm</a> ). ....	37
Figure 2-10: Schematic illustration of the different talc ore origins. Serpentine derivative ore bodies are upgraded by flotation to reach a high talc content and high whiteness. ( <a href="http://www.mondominerals.com/geology.asp">http://www.mondominerals.com/geology.asp</a> ). ....	37
Figure 2-11: Simplified geological cross section through a serpentine derivative ore. ( <a href="http://www.luzenac.com/geology.htm">http://www.luzenac.com/geology.htm</a> ). ....	38
Figure 2-12; Simplified geological cross section through a siliceous derivative ore ( <a href="http://www.luzenac.com/geology.htm">http://www.luzenac.com/geology.htm</a> ). ....	39
Figure 2-13: Ratio between hydrophilic and hydrophobic surface area for different talc / chlorite mixtures with approximately $10 \text{ m}^2 \text{ g}^{-1}$ specific surface area (Charnay et al. 2001). ....	42

Figure 2-14: Crystal structure of calcite. The schematic shows both (left) the true unit cell the calcite rhombohedron, which contains $2[\text{CaCO}_3]$ and (right) an alternative cell based on the cleavage rhombohedron. ....	43
Figure 2-15: SEM image of a ground natural calcium carbonate (marble) [Omya]......	45
Figure 2-16: a) SEM image of a scalenohedral precipitated calcium carbonate (S-PCC) and b) a aragonitic precipitated calcium carbonate A-PCC [Omya]......	46
Figure 2-17: SEM image of a modified calcium carbonate with a rosy structure [Omya]. .....	47
Figure 2-18: Definition of the disc-like approximation for a high aspect ratio platelet.	48
Figure 2-19: Definition of the aspect ratio of a rod. ....	49
Figure 2-20: Definitions of particles and particle shape (Allen 1990)......	49
Figure 2-21: Model of talc as an adsorbent for tacky particles (left) and adsorbed onto tacky aggregates (right) (Hubbe et al. 2006)......	55
Figure 2-22: General scheme of adsorption on a two-dimensional surface (grey) with various adsorption sites (green and orange cylinders) and the adsorbate that adsorbs onto available surface sites (orange cones)......	64
Figure 2-23: Adsorption reaction scheme. ....	65
Figure 2-24: BET plot for a modified calcium carbonate [Omya]......	69
Figure 2-25: Overview of the different adsorption isotherms. a) Freundlich isotherms with $K_F=1$ and $n=0.5$ (blue), $n=1.0$ (black), and $n=1.5$ (red). b) Langmuir isotherm with $K_L=1$ and $\Gamma_{\max}=1$ . c) Langmuir-Freundlich (black) with $K_{LF}=1$ , $\Gamma_{\max}=1$ and $n=0.5$ ; Redlich-Peterson isotherm (red) with $K_{RP}=1$ , $\Gamma_{\max}=1$ and $n=0.5$ ; and Tóth isotherm (blue) with $K_T=1$ , $\Gamma_{\max}=1$ and $n=2.0$ . d) BET isotherm with $K_{BET}=1$ , $\Gamma_{\max} =1$ and $c_{\text{sat}}=2.1$ . The equilibrium concentration in solution, $c_{\text{eq}}$ , and on the surface, $\Gamma_{\text{eq}}$ , are both dimensionless. ....	71
Figure 3-1: Schematic drawing of the grinding and exfoliation/delamination of a platelet shaped material.....	74

Figure 3-2: Geometry and laser light scattering detection as used for particle sizing (Schoelkopf et al. 2008a). .....	78
Figure 3-3: Dynamic light scattering geometry and principle of autocorrelation (Schoelkopf et al. 2008a). .....	80
Figure 3-4: Schematic representation of zeta potential (Hiemenz, Rajagopalan 1997)..	89
Figure 3-5: Schematic representation of the total potential energy ( $U_e$ ) against the distance of separation for a pair of electrostatically stabilised particles according to the DLCO theory (Napper 1983). .....	91
Figure 3-6: Surface tension of aqueous ethanol mixtures (Lide 2002). .....	95
Figure 3-7: Ion chromatograph 882 Compact IC plus with autosampler (left), dialysis unit (middle) and the two 882 Compact IC plus units for anions (second from right) and cations (right). .....	105
Figure 3-8: Calibration curves for a) chloride ions and b) calcium ions. Only the steepness is significant according to the $t$ -test resulting in a $p$ -value of 0.00 in both cases. The intercept is not significantly different from 0 having a $p$ -value of 0.13 in the chloride calibration curve and 0.47 in the calcium calibration curve. ....	106
Figure 3-9: Example of a TGA (black)/SDTA (violet) curves for a talc/pitch composite. ....	109
Figure 3-10: Adsorption kinetic of colloidal pitch onto HSA-talc. The starting turbidity was 425 NTU. Talc dosage was 10 (grey diamonds) and 20 (dark squares) $\text{gdm}^{-3}$ .....	110
Figure 4-1: SEM pictures of the four investigated minerals Finntalc P05 (a + b), Westmin PCS (c + d), Comminuted high surface area talc (e + f) and Laponite <sup>®</sup> RD (g + h). .....	123
Figure 4-2: Particle size distribution by photon correlation spectroscopy (PCS), static laser light scattering (SLLS) and sedimentation for the three talc grades (number based). .....	125
Figure 4-3: Particle size distribution measured by photon correlation spectroscopy for the Laponite <sup>®</sup> RD. ....	131



Figure 4-4: Platelet thickness of Laponite <sup>®</sup> RD calculated with Equation 4-21 and with the $d_{N50} = 13$ nm and $d_{N84} = 17$ nm. ....	132
Figure 4-5: SEM pictures of aragonite (a + b) and palygorskite (c + d). The palygorskite needles aggregate in dry state. ....	133
Figure 4-6: a) SEM micrograph with very high contrast of aragonite used for image analysis. Image width corresponds to 22.9 $\mu$ m. b) Binary image of the SEM micrograph for aragonite used for image analysis. Image width corresponds to 22.9 $\mu$ m. c) SEM micrograph of palygorskite used for image analysis. Image width corresponds to 5.7 $\mu$ m. d) Binary image of palygorskite used for image analysis. Image width corresponds to 5.7 $\mu$ m. ....	135
Figure 4-7: Nitrogen adsorption and desorption isotherm on palygorskite. ....	136
Figure 4-8: Particle size distribution measured by photon correlation spectroscopy (PCS), static laser light scattering (SLLS) (Fraunhofer and Mie optics) and sedimentation of aragonite. The corresponding lines are based on a cumulative log normal distribution calculated by the $d_{N50}$ , $d_{N84}$ or $d_{N16}$ giving an $R^2 > 0.99$ . ....	137
Figure 4-9: Cumulative aspect ratio distribution based on the image analysis. The line corresponds to a fitted log normal distribution with $\rho_{N50}$ of 2.14 and $\rho_{N84}$ of 3.33. ....	138
Figure 4-10: Particle size distribution measured by photon correlation spectroscopy for the rod-like palygorskite particles, Attagel 50. The fitted log normal distribution is based on $d_{N50}$ and $d_{N16}$ . ....	140
Figure 5-1: Light microscope picture of the TMP filtrate used showing colloidal pitch droplets and the elimination of disturbing fibrils. ....	147
Figure 5-2: Turbidity as a function of the pH in the range of pH 5.5 to 10.8. The pH reached after treatment with each of the high surface area minerals is also shown on the plot. The TMP filtrate has an incoming pH of 6.8 and a turbidity of 577 NTU, which here corresponds to a relative turbidity of 100 %. ....	153
Figure 5-3: Influence of talc and chlorite on the turbidity of a TMP filtrate normalised with the untreated reference TMP filtrate. 100 % corresponds to 577 NTU in the upper liquid phase at pH 7.0. Values have been corrected to those expected at pH 7.4. ....	156

Figure 5-4: Influence of talc and chlorite on Chemical Oxygen Demand (COD) of a TMP filtrate normalised with the untreated reference TMP filtrate. 100 % corresponds to 4 914 mg O <sub>2</sub> per dm <sup>3</sup> of the upper liquid phase. ....	156
Figure 5-5: Influence of talc and chlorite on gravimetric analysis of the remaining material in a TMP filtrate treated with mineral, normalised to the untreated reference TMP filtrate and with the dissolved fraction of minerals subtracted. 100 % corresponds to 3.52 gdm <sup>-3</sup> residue in the upper liquid phase. ....	157
Figure 5-6: TGA analysis from 200 °C to 1 000 °C on the talc-, chlorite- and pyrophyllite-containing residues in the lower centrifuged phase, showing the cumulative weight loss.....	160
Figure 5-7: Normalised Gravimetry and COD against normalised turbidity for talc and chlorite. Each point is the average of three measurements and the error bars represent the standard deviation of the three measurements. ....	162
Figure 5-8: Analysis of the upper liquid phase after the treatment with pyrophyllite. The analyses of the talc treatment are given as references for each method, having the corresponding unfilled symbols. ....	163
Figure 5-9: Particle size distributions (PSD) for the investigated pyrophyllite samples P-LSSA, P-MSSA and P-HSSA compared with the FT-HSSA talc. The particle size is given as an Equivalent Spherical Diameter ( <i>esd</i> ). The data were measured on a Micromeritics Sedigraph <sup>®</sup> 5100. P-HSSA is seen to have significantly more ultrafines than the finest talc, which are suspected to become dispersion stabilised during adsorption of pitch.....	165
Figure 6-1: Turbidity of the TMP filtrate as a function of pH. The pH was adjusted by either hydrochloric acid or sodium hydroxide (0.1 M). The data set labelled with “Ref samples” was recorded 3 hours after the addition of acid or base. ....	173
Figure 6-2: Electrophoretic mobility of the pitch particles as a function of pH. Measurements were performed 3 hours after the addition of the acid (hydrochloric) or base (sodium hydroxide), respectively.....	173
Figure 6-3: Particle size distribution of the pH adjusted TMP filtrates as well as of the talc. The distribution curve is number based. ....	174

Figure 6-4: pH of the trials, commencing at a range of pH from 4.2 to 9.1, as a function of talc dosage..... 175

Figure 6-5: Development of the electrophoretic mobility of the particles in the TMP filtrates as a result of increasing talc addition and of pH. The grey shaded line represents the electrophoretic mobility of the original TMP filtrate as already shown in Figure 6-2. Talc dosage increases from there in the direction of the arrows..... 176

Figure 6-6: Adsorption isotherms of the trials for turbidity analysis..... 177

Figure 6-7:  $\Gamma_{\max}^{\tau}$  (a) and  $K_L^{\tau}$  (b) of the isotherm obtained through turbidity analysis against pH. The error bars represent the 95 % confidence intervals..... 179

Figure 6-8: Equilibrium COD  $c_{\text{eq}}^{\text{COD}}$  of all trials against equilibrium turbidity  $c_{\text{eq}}^{\tau}$  after adsorption in the supernatant. The arrow shows the direction of increasing talc dosage. The slope of the linear regression line above 50 NTU is  $2.07 \text{ mgdm}^{-3}\text{NTU}^{-1}$ , and its intercept at zero turbidity is  $3\ 030 \text{ mgdm}^{-3}$ .  $R^2=0.91$  and  $p$  for both parameters  $< 0.01$ .  
..... 179

Figure 6-9: Adsorption isotherm of the trials for the COD analysis. The grey area between  $3030 \text{ mg dm}^{-3}$   $4\ 100 \text{ mgdm}^{-3}$  represents the region in which colloids are present in the liquid phase. The scatter of the results in this region is due to the uncertainty of the COD analysis, quantified by the vertical error bars. The error bars were calculated based on the error propagation of Equation 6-1 with the standard deviation of  $c_0$  of  $80 \text{ mg dm}^{-3}$  (Table 6-2). The thick line represents a two-stage smoothing curve explained in the text..... 180

Figure 6-10: Equilibrium gravimetry  $c_{\text{eq}}^{\text{grav}}$  versus equilibrium COD  $c_{\text{eq}}^{\text{COD}}$ : enabling the COD to represent mass of organic remaining after adsorption. Both fitted parameters are significant ( $p < 0.01$ ). ..... 182

Figure 6-11: Adsorption isotherm at pH 5 for the dissolved and colloidal fractions (black), adsorption isotherm for the colloidal fraction only (blue) and adsorption isotherm for the dissolved fraction only (red). The direction of the arrows indicates the increasing talc dosage, which reduces the equilibrium concentration. The phases are described in the Discussion section..... 184

Figure 6-12: Adsorption isotherm at pH 7 for the dissolved and colloidal fractions (black), adsorption isotherm for the colloidal fraction only (blue) and adsorption

isotherm for the dissolved fraction only (red). The dotted line indicates the loading of colloidal and dissolved material on talc below the equilibrium concentration of $1.21 \text{ gdm}^{-3}$ . .....	184
Figure 6-13: Adsorption isotherm at pH 9 for the dissolved and colloidal fractions (black), adsorption isotherm for the colloidal fraction only (blue) and adsorption isotherm for the dissolved fraction only (red). .....	185
Figure 6-14: Schematic drawing of the adsorption process. Starting point refers to the untreated TMP filtrate. Talc dosage is increased from left to right whereas the equilibrium concentration decreases from left to right. ....	185
Figure 6-15: Adsorption equilibriums for the adsorption of colloidal and dissolved species. ....	187
Figure 6-16: Electrophoretic mobility of the colloidal fraction of the TMP filtrate as a function of pH. ....	191
Figure 6-17: Equilibrium turbidity of the TMP filtrate after the removal of the mineral versus equilibrium gravimetry after the removal of the mineral. The presented linear regression is based on all data points with $x > 45$ NTU. Both fitted parameters are significant ( $p < 0.01$ ). .....	194
Figure 6-18: Equilibrium COD $c_{\text{eq}}^{\text{COD}}$ of the TMP filtrate after the removal of the mineral versus equilibrium gravimetry $c_{\text{eq}}^{\text{grav}}$ after the removal of the mineral. Both fitted parameters are significant ( $p < 0.01$ ). .....	194
Figure 6-19: Mass-based adsorption isotherm for the colloidal fraction of the TMP filtrate based on turbidity data. ....	197
Figure 6-20: Sorption data for the total organic material in the TMP filtrate at various temperatures. The equilibrium concentration in the aqueous phase was determined by COD and transferred into equivalent mass by Equation 6-5. The loading was obtained by TGA $\Gamma_{\text{eq}}^{\text{TGA}}$ and refers to mg volatile ( $200 \text{ }^\circ\text{C} - 1000 \text{ }^\circ\text{C}$ ) material per gram mineral. The fit is based on a linear regression between 900 and $1662 \text{ mgdm}^{-3}$ and a Langmuir for concentrations $> 1662 \text{ mgdm}^{-3}$ . .....	199

Figure 6-21: Overlay of the total organic adsorption isotherm and the colloidal isotherm with the calculated isotherm for the dissolved fraction at 60 °C. In addition, the measured data points are also shown as $\Gamma_{eq}^{TGA}$ and $c_{eq}^{COD}$ .....	201
Figure 7-1: Mean electrophoretic mobility ( $u$ ) of the particles in the TMP filtrates 1-4 against pH. The pH was adjusted with 0.1 M sodium hydroxide and 0.1 M hydrochloric acid. ....	210
Figure 7-2: Normalised turbidity after the mineral treatment of the TMP filtrate. 100 % corresponds to 349 NTU. ....	212
Figure 7-3: Normalised COD after the mineral treatment of the TMP filtrate. 100 % corresponds to 3 644 mg O <sub>2</sub> dm <sup>-3</sup> .....	214
Figure 7-4: Thermo gravimetric analysis of the mineral after the adsorption. The weight fraction lost was recorded between 200 and 1 000 °C and is corrected with the weight loss of the corresponding mineral powder). ....	214
Figure 7-5: Normalised COD, gravimetry and turbidity of the TMP filtrate after the adsorption experiment with the mineral powders against the surface coverage of the mineral powders with stearic acid. The results are normalised with the values obtained for the untreated TMP filtrate. ....	216
Figure 7-6: Thermo gravimetric analysis of the mineral phase after the adsorption experiments against the surface coverage of the mineral powders with stearic acid. The weight loss of the starting mineral powders (prior the addition to the TMP filtrate) is subtracted (net loss).....	216
Figure 7-7: Apparent hydrophobicity of the tested mineral powders with their range of stearic acid coverage $X_{SA}$ including also the HSA-talc sample. The larger the area on the right side of each line the greater the hydrophobicity. The grey area reflects the situation for talc. ....	217
Figure 7-8: Adsorption isotherm based on turbidity data for the untreated gcc-1, the treated (15 % surface coverage) gcc and the HSA-talc.....	219
Figure 7-9: Adsorption isotherm based on turbidity data for the untreated gcc-1, the treated (15 % surface coverage) gcc and the HSA-talc. The loading $\Gamma_{eq}^{\tau}$ is normalised with the specific surface area of the minerals. ....	219

Figure 7-10: Petroleum ether extractives content of the TMP filtrate 4 prior and post adsorption. The extractives are split into the groups; fatty acids, resin acids, lignans, sterols, sterylesters, triglycerides and an unknown fraction. ....	221
Figure 7-11: Relative composition of the extractives groups in the TMP filtrate prior and post adsorption. ....	222
Figure 7-12: Carbohydrate, acid soluble and acid insoluble content in the TMP filtrates prior and post adsorption.....	222
Figure 7-13: Equilibrium COD against equilibrium turbidity. ....	224
Figure 7-14: Proposed mechanism for the adsorption of dissolved and colloidal substances onto cross-section views of talc platelet (upper route) and gcc rhomboid (lower route).....	226
Figure 7-15: Extractives content against turbidity. ....	228
Figure 7-16: Mean electrophoretic mobility of the particles in the TMP filtrates 1 and 2 against pH. The pH was adjusted with 0.1 M sodium hydroxide and 0.1 M hydrochloric acid. ....	231
Figure 7-17: Extractives content against turbidity. ....	233
Figure 7-18: Adsorption isotherms for the colloidal fraction of the TMP filtrate measured by turbidity.....	234
Figure 7-19: Electrochemical charge of the TMP filtrate after mineral separation as a function of added mineral. ....	235
Figure 7-20: Extractives concentration of the original TMP filtrate 2 and after the treatment with HSA-talc at 0.4 and 4 gdm <sup>-3</sup> , gcc at 8 and 40 gdm <sup>-3</sup> , and mcc at 0.4 and 8 gdm <sup>-3</sup> . ....	237
Figure 7-21: Concentration of the carbohydrates, acid soluble (lignin) and acid insoluble content of the TMP filtrate 2 before and after the various mineral treatments.....	238
Figure 7-22: Carbohydrate monomer composition of the original TMP filtrate 2 and after the various mineral treatments. ....	240

Figure 7-23: Overlay of the particle size distribution for the colloidal fraction of the TMP filtrate and the pore size structure of the mcc. ....	241
Figure 7-24: Turbidity against chemical oxygen demand (COD) of the recorded isotherm. The linear regression was performed using all data points > 50 NTU. All fitted parameters are significant with $p < 0.01$ .....	242
Figure 7-25: Electrophoretic mobility of the particles in the TMP filtrate as a function of $\text{Ca}^{2+}$ and $\text{Na}^+$ addition. An ionic strength $I$ of 0.01 M corresponds to Calcium ion concentration of ~ 3.3 mM.....	247
Figure 7-26: Immediate turbidity change during electrolyte addition. Turbidity is dilution corrected. ....	249
Figure 7-27: Stability of the TMP filtrate with increasing electrolyte concentration quantified by the turbidity prior and after addition of the electrolyte addition.....	249

## Table of tables

Table 2-1: Overview of the three phyllosilicates: talc, chlorite and pyrophyllite.....	35
Table 2-2: Values of the interfacial surface free energy components of talc and pyrophyllite (Giese et al. 1991).....	40
Table 2-3: Definitions of particles and particle shapes (Allen 1990). ....	50
Table 2-4: Formulae to calculate the disc diameter, $d_d$ , and rod length, $l$ , based on the <i>esd</i> ( $d_s$ , $d_a$ , $d_v$ and $d_T$ ) response from the corresponding particle sizing method.....	51
Table 3-1: GC-FID method settings for the analysis of wood extractive groups. ....	102
Table 3-2: Reproducibility of the TMP effluent extraction and quantification by GC-FID. $n$ refers to the amount of data points used for the calculation of the mean and the standard deviation .....	102
Table 3-3: Reproducibility of the method to determine the monosaccharide composition of the same bleached softwood pulp sample determined in five different laboratories. ....	104
Table 3-4: Method parameter for anion and cation analysis on the ion chromatograph. ....	105
Table 3-5: Limit of detection according to the user manual of Metrohm and Sigma Aldrich order number of the various ions. ....	107
Table 4-1: Specific surface area determined by nitrogen adsorption and density of the investigated minerals.....	124
Table 4-2: $d_{N50}$ and $d_{N84}$ based on a fitted logarithmic cumulative distribution performed with TableCurve 2D.....	126
Table 4-3: Calculated aspect ratio for the three talc particles. The aspect ratios were calculated by Equation 4-19. In addition the aspect ratios were calculated based on the model of Pabst and Berthold (2007) (Equation 2-8) and on the model of Jennings and Parslow (1988) for oblate spheroids (Equation 2-5) and discs (Equation 2-6). All calculations were based on the mode value from the corresponding $d_{N50}$ and $d_{N84}$ values in Table 4-2. ....	127



Table 4-4: Particle disc diameter $d_d$ and disc thickness $t_d$ in nm. ....	128
Table 4-5: Aspect ratio of the three different talc particles based on the various models. The values were obtained by inserting the mode value of the volume or mass based distribution data.....	130
Table 4-6: Aspect ratio calculated with the original Hohenberger model (Equation 4-1) based on number and volume or mass based distribution data. ....	130
Table 4-7: Measured $d_{N50}$ and $d_{N84}$ or $d_{N16}$ for aragonite particles. ....	137
Table 4-8: Calculated aspect ratios, determined by the different particle size and specific surface area measurements, compared with calculated values based on the model of Jennings and Parslow (1988) and those measured by image analysis. ....	138
Table 4-9: Rod dimensions for the rod-like particles: rod length $l$ and rod width $w$ for the aragonite. ....	140
Table 5-1: Loss on ignition and XRF analyses for raw talc, chlorite and pyrophyllite samples (before grinding). Error range for the LOI values is based on the standard deviation of three measurements. XRF values were measured only once. ....	147
Table 5-2: Physical properties of the mineral samples, characterised according to origin and specific surface area. ....	148
Table 5-3: pH values of the upper liquid phase after the treatment with the respective mineral, each as a function of increasing specific surface area. ....	151
Table 5-4: Constants $A$ and $B$ and regression coefficient for the gravimetric analysis of the talc and chlorite treated TMP samples. Only constant $A$ for talc is significant ( $p < 0.01$ ). The other fitted parameters are not significant ( $p > 0.05$ ). ....	158
Table 5-5: Comparison of the electrolyte balance of the supernatant in the reference sample, the talc treated samples and the chlorite treated samples. ....	159
Table 5-6: Electrolytic balance of the pyrophyllite treated samples (supernatant).....	163
Table 6-1: Properties of the investigated talc grade. Electrophoretic mobilities were measured in 0.01 M NaCl solution. The $d_{50}$ measured by Sedigraph is weight based whereas the value from the Malvern Zetasizer NS measurement is number based.....	170

Table 6-2: Trial labelling and corresponding pH adjusted with either hydrochloric acid or sodium hydroxide. For trial point pH 7 no additional acid or base was added. Measured turbidity, COD and gravimetric residue of the pH adjusted TMP filtrates. .	171
Table 6-3: Summary of the fitting values derived from the turbidity data. The two constants lie all within the confidence interval of 95 %, except for $K_L^\tau$ at pH 4 and 9 (Given by the t-test with the value of $P >  t $ ). .....	178
Table 6-4: Summary of the fitting parameters for the colloidal fraction of the TMP filtrate described by a Langmuir isotherm (Equation 2-17). The shown range represents the 95 % confidence interval of the constants and $P >  t $ is the probability that the value lies within the confidence interval. ....	196
Table 6-5: Summary of the fitting parameter of the total organic sorption data. The fit is characterised by a linear region in the form of $y = mx + b$ and the Langmuir region in the form of Equation 2-17. The standard error of the steepness, $m$ , is in all cases $\sim 0.01$ . The fitted parameters for the linear regression are significant ( $p < 0.05$ ) except $m$ and $b$ at 20 °C which are not significant ( $p > 0.05$ ). .....	198
Table 7-1: Specific surface area, particle size ( $d_{50}$ ) and electrophoretic mobility in a 0.01 M NaCl solution of the investigated minerals. <sup>a)</sup> not analysed due to settling problems. <sup>b)</sup> not analysed.....	206
Table 7-2: Properties of the TMP samples 1 to 4. The presented range is based on the standard deviation of three independent experiments. n.a. → not analysed.....	210
Table 7-3: Number based particle size (photon correlation spectroscopy) of the colloidal fraction in the TMP filtrate prior to and post treatment with the minerals. ....	213
Table 7-4: Adsorption isotherm parameters based on a non-linear least squares (NLLS) fit to the Langmuir equation (Equation 2-17) performed by TableCurve® 2D.....	218
Table 7-5: Extractives (petroleum ether) group content, carbohydrate content, acid soluble (lignin) content and acid insoluble content of the TMP filtrate. ....	220
Table 7-6: Ratio between dissolved and colloidal material adsorbed from the TMP filtrate. ....	225
Table 7-7: Specific surface area, particle size ( $d_{50}$ ) and electrophoretic mobility $u$ in a 0.01 M NaCl solution of the investigated minerals. ....	230

Table 7-8: Properties of the TMP samples 1 and 2. The presented range for TMP filtrate 1 is based on the standard deviation of six independent experiments. For TMP filtrate 2 only the COD was measured six times. <sup>1)</sup> Titrated with N-methylglycol-chitosan. ....	232
Table 7-9: Detailed overview of the fitted Langmuir parameters. The fit was done with TableCurve® 2D using a non-linear least squares (NLLS) fit. ....	234
Table 7-10: Extractives (petroleum ether) group content, carbohydrate content, acid soluble (lignin) content and acid insoluble content of the TMP filtrate 2. ....	236
Table 7-11: Ratios of removed carbohydrates plus lignin relative to the removed extractives. ....	239

## Table of equations

Equation 2-1 .....	40
Equation 2-2 .....	45
Equation 2-3 .....	49
Equation 2-4 .....	49
Equation 2-5 .....	52
Equation 2-6 .....	52
Equation 2-7 .....	52
Equation 2-8 .....	52
Equation 2-9 .....	53
Equation 2-10 .....	53
Equation 2-11 .....	65
Equation 2-12 .....	65
Equation 2-13 .....	65
Equation 2-14 .....	65
Equation 2-15 .....	65
Equation 2-16 .....	65
Equation 2-17 .....	66
Equation 2-18 .....	67
Equation 2-19 .....	67
Equation 2-20 .....	68
Equation 2-21 .....	68
Equation 2-22 .....	68

Equation 2-23 .....	69
Equation 2-24 .....	69
Equation 2-25 .....	69
Equation 2-26 .....	70
Equation 2-27 .....	70
Equation 3-1 .....	76
Equation 3-2 .....	77
Equation 3-3 .....	80
Equation 3-4 .....	81
Equation 3-5 .....	85
Equation 3-6 .....	86
Equation 3-7 .....	88
Equation 3-8 .....	90
Equation 3-9 .....	99
Equation 4-1 .....	115
Equation 4-2 .....	116
Equation 4-3 .....	117
Equation 4-4 .....	117
Equation 4-5 .....	117
Equation 4-6 .....	117
Equation 4-7 .....	117
Equation 4-8 .....	118
Equation 4-9 .....	118
Equation 4-10 .....	118

Equation 4-11 .....	118
Equation 4-12 .....	118
Equation 4-13 .....	119
Equation 4-14 .....	119
Equation 4-15 .....	119
Equation 4-16 .....	119
Equation 4-17 .....	120
Equation 4-18 .....	120
Equation 4-19 .....	120
Equation 4-20 .....	121
Equation 4-21 .....	131
Equation 5-1 .....	152
Equation 5-2 .....	152
Equation 5-3 .....	154
Equation 5-4 .....	154
Equation 6-1 .....	177
Equation 6-2 .....	182
Equation 6-3 .....	183
Equation 6-4 .....	196
Equation 6-5 .....	196
Equation 6-6 .....	196
Equation 7-1 .....	247
Equation 7-2 .....	248

## Acknowledgements

I wish to thank my internal supervisor and director of study, Prof. Dr. Peter G. Matthews for his support, guidance and encouragement. Further, I would like to thank my external supervisor Dr. Joachim Schölkopf for the fundamental discussions, his encouragement, his inputs and his friendship. Very special thanks to Prof. Dr. Patrick Gane, my external supervisor, for his belief in me and the effort spent to guide me. His patience, support, inputs and friendship were key to my progress.

Many thanks are given OMYA DEVELOPMENT AG for providing the financial support, the opportunity and facilities for me to work on this thesis. Also to all the people in OMYA's research laboratories especially Jörg Nikas, Silvan Fischer, Pascale Poffet, Daniel Oswald and Daniel Frey for all the help in analytical support. I am grateful to Dr. Philipp Hunziker for his valuable inputs concerning the mineralogy of phyllosilicates. Many thanks to Dr. Daniel Gerard for his support and valuable discussions. A special thanks to Dr. Cathy Ridgway for her help, support and encouragement. Also many thanks to my research group members, Roman Lack and Christian Fritz, for their practical help and support. Thanks also to Dr. Christopher Gribble for making my visits to Plymouth that much more pleasant.

To my girlfriend Annina: for always believing in me and for your encouragement, thank you.

To my parents, I thank you for all your love and continued encouragement during the "ups" and support even through the "downs" of my life.

Meinen Eltern danke ich für all ihre Liebe, stete Ermutigung und Unterstützung während den guten und vorallem auch während den schlechten Zeiten in meinem Leben.

## **Author's declaration**

At no time during the registration for the degree of Doctor of Philosophy has the author been registered for any other University award.

This study was financed with the aid of Omya Development AG.

Seminars and conferences were regularly attended throughout the period of study at which research findings were presented.

Word Count: 61'084 words

Signed.....

Date.....

Daniel Gantenbein



## **Conferences, Seminars and Workshops**

PTS-Sticky Seminarreihe: Bekämpfung und Vermeidung von Stickys für einen wirtschaftlichen Altpapiereinsatz, Dresden (Germany); 24<sup>th</sup> – 25<sup>th</sup> April 2007

PTS – CTP Deinking Symposium, Leipzig (Germany); 15<sup>th</sup> – 17<sup>th</sup> April 2008

PTS-Workshop: Membrantechnik in der Papierindustrie, Munich (Germany): 27<sup>th</sup> – 28<sup>th</sup> May 2008

Omya-Workshop: Team leader, Bettlach (Switzerland); 16<sup>th</sup> – 17<sup>th</sup> September 2010

Omya Academy: Intellectual Property Training, Oftringen (Switzerland); 21<sup>st</sup> September 2011

11<sup>th</sup> Advanced Coating Fundamentals Symposium, Munich (Germany); 11<sup>th</sup> – 13<sup>th</sup> October 2011 – Determining a size distribution-defined representative particle aspect ratio for platy and rod-like minerals. Poster Presentation.

YKI Member Days 2012, Stockholm (Sweden); 18<sup>th</sup> – 19<sup>th</sup> April 2012

Omya Academy: Leadership Training, Olten (Switzerland); 23<sup>rd</sup> – 25<sup>th</sup> April 2012

8<sup>th</sup> International Paper and Coating Chemistry Symposium, Stockholm (Sweden); 10<sup>th</sup> – 14<sup>th</sup> June 2012 – The development of controlled hydrophobisation of calcium carbonate particles for the effective adsorption of dissolved and colloidal substances. Oral Presentation.

## **Publications and Book chapters**

- Gantenbein, D., Schoelkopf, J., Hunziker, P., Matthews, G.P., and Gane, P.A.C.: Efficiency of colloidal pitch adsorption onto phyllosilicates: comparing talc, chlorite and pyrophyllite, *Nordic Pulp and Paper Research Journal*, 24 (2009) 448-458. doi:10.3183/npprj-2009-24-04-p448-458
- Gantenbein, D., Schoelkopf, J., Gane, P.A.C., and Matthews, G.P.: Influence of pH on the adsorption of dissolved and colloidal substances in a thermo-mechanical pulp filtrate onto talc, *Nordic Pulp and Paper Research Journal*, 25 (2010) 288-299. doi:10.3183/npprj-2010-25-03-p288-299
- Gantenbein, D., Schoelkopf, J., Matthews, G.P., and Gane, P.A.C.: Influence of the temperature on the adsorption of dissolved and colloidal substances from a thermo mechanical pulp filtrate onto talc, *Nordic Pulp and Paper Research Journal*, 26 (2011) 329-335. doi:10.3183/npprj-2011-26-03-p329-335
- Gantenbein, D., Schoelkopf, J., Matthews, G.P., and Gane, P.A.C.: The development of hydrophobised ground calcium carbonate particles for the effective adsorption of dissolved and colloidal substances (DCS) from thermo mechanical pulp (TMP) filtrates, *Nordic Pulp and Paper Research Journal*, 27 (2012) 93-103. doi:10.3183/npprj-2012-27-01-p093-103
- Gantenbein, D., Schoelkopf, J., Matthews, G.P., and Gane, P.A.C.: The use of porous high surface area calcium carbonate for the adsorption of dissolved and colloidal substances from thermo mechanical pulp filtrates, *Nordic Pulp and Paper Research Journal*, 27 (2012) 631-638. doi:10.3183/npprj-2012-27-03-p631-638
- Gantenbein, D., Schoelkopf, J., Matthews, G.P., and Gane, P.A.C.: Determining the size distribution-defined aspect ratio of platy particles, *Applied Clay Science*, 53 (2011) 544-552. doi:10.1016/j.clay.2011.04.020

- Gantenbein, D., Schoelkopf, J., Matthews, G.P., and Gane, P.A.C.: Determining the size distribution-defined aspect ratio of rod-like particles, *Applied Clay Science*, 53 (2011) 538-543. doi:10.1016/j.clay.2011.01.034
- Gantenbein, D., Schoelkopf, J., Matthews, G.P., and Gane, P.A.C.: Adsorption and detackification of a polyacrylic model colloid on talc and modified calcium carbonate, in preparation.
- Schoelkopf, J., Gantenbein, D., Dukhin, A.S., Goetz, J.P., and Gane, P.A.C.: Novel Particle Size Characterization of Coating Pigments: Comparing Acoustic Spectroscopy with Laser Light Scattering and Sedimentation Techniques, *Advanced Coating Fundamentals Symposium, Montréal Canada, Tappi*, (2008) 427-441.
- Benecke, F., Gantenbein, D., Schoelkopf, J., Gane, P.A.C., and Gliese, T.: Organic contaminants in recycled paper: a model study of the adsorbent properties of talc for idealised component suspensions, *Nordic Pulp and Paper Research Journal*, 24 (2009) 219-224.
- Gribble, C.M., Matthews, G.P., Gantenbein, D., Turner, A., Schoelkopf, J., and Gane, P.A.C.: Adsorption of surfactant-rich stickies onto mineral surfaces, *Journal of Colloids and Interface Science*, 352 (2010) 483-490.
- Gribble, C.M., Matthews, G.P., Gantenbein, D., Turner, A., Schoelkopf, J., and Gane, P.A.C.: Equilibrium coefficients for the adsorption of colloidal stickies onto mineral suspension particulates to improve paper recycling, *Nordic Pulp and Paper Research Journal*, 26 (2011) 421-427.
- Pigment Coating and Surface Sizing of Paper (2009), *Pigments – Talc (Chapter 5.3)*, Book 11, 2<sup>nd</sup> Edition, pp. 110-124, Editor: J. Paltakari, Paperi ja Puu, Helsinki (Finland) ISBN 978-952-5216-27-1

## Patents

Buri, M., Karth, B., Gantenbein, D., Gane, P.A.C. (2007): Method for processing crude bentonite, EP2144850.

Schoelkopf, J., Gantenbein, D., Gane, P.A.C. (2008): Method for controlling the shape of talc particles, EP2146793.

Gane, P.A.C., Gantenbein, D., Schoelkopf, J. (2008): Treatment of talc in a solvent, WO2008148666.

Gane, P.A.C., Schoelkopf, J., Gantenbein, D., Gerard, D.E. (2008) Surface treated calcium carbonate and its use in waste water treatment, EP2180944.

Gantenbein, D., Schoelkopf, J., Gane, P.A.C. (2008): Process for the control of pitch, WO2008113839.

Gantenbein, D., Schoelkopf, J., Gane, P.A.C. (2008): Process for the purification of water, EP2180945.

Gane, P.A.C., Schoelkopf, J., Gantenbein, D., Gerard, D.E. (2008): Process for the removal of endocrine disrupting compounds, EP2180943.

Gane, P.A.C., Gantenbein, D., Schoelkopf, J. (2008): Surface-reacted calcium carbonate in combination with hydrophobic adsorbents for water treatment, WO2008151991.

Gane, P.A.C., Schoelkopf, J., Gantenbein, D., Schenker, M., Pohl, M., Kuebler, B. (2010): Process for the production of nano-fibrillar cellulose suspensions, WO2010112519.

Gane, P.A.C., Schoelkopf, J., Gantenbein, D., Schenker, M. (2010): Process for the production of nano-fibrillar cellulose gels, WO2010115785.

Buri, M., Rentsch, S., Gane, P.A.C., Gantenbein, D., Schoelkopf, J. (2011): Process for the preparation of surface-treated calcium carbonate material and use of same in the control of organic material in an aqueous medium, WO2012010466.

Gantenbein, D., Schoelkopf, J., Gane, P.A.C. (2011): Hydrophobised calcium carbonate particles, EPA11173471.1.

Gane, P.A.C., Gantenbein, D., Schoelkopf, J. (2011): Self-binding pigment hybrid, EPA11179604.1.

Gantenbein, D., Schoelkopf, J., Gane, P.A.C. (2011): Process for preparing self-binding pigment particle suspensions, EPA11179604.1.

## Nomenclature

$a$	linear slope of the BET plot
$A, B$	Fitting constants
$A_{SA}$	Surface area covered by one stearic acid molecule
$b$	intercept on the linear BET plot
$c'$	numerical particle concentration
$c_0$	starting concentration
$c_{eq}$	equilibrium concentration
$c_{sat}$	maximum solubility of adsorbate in a solvent
$c_{sol}$	concentration of the adsorbate in solution
$d$	diameter
$d_d$	disc diameter
$D$	pore diameter
$d_{50}$	particle size at which 50 % by weight of the sample is finer
$d_{84}$	particle size at which 84 % by weight of the sample is finer
$d_a$	equivalent spherical diameter based on projected area
$d_N$	mode value
$d_S$	equivalent spherical diameter based on sedimentation
$d_T$	equivalent spherical diameter based on translatory diffusion
$D_T$	translational diffusion coefficient
$d_V$	equivalent spherical diameter based on volume
$E_1$	adsorption energy for the first gas layer

$E_L$	adsorption energy for the second and higher gas layers
$esd$	equivalent spherical diameter
$f(\text{pH})$	function of pH
$ g $	gravitational acceleration constant
$h$	settling distance
$I$	ionic strength
$I(t)$	varying light scattering intensity
$k_{\text{ads}}$	adsorption rate
$k_B$	Boltzmann constant
$K_{\text{BET}}$	BET constant
$K_{\text{Coll}}$	equilibrium constant for the adsorption of colloidal material
$k_{\text{des}}$	desorption rate
$K_{\text{Diss}}$	equilibrium constant for the adsorption of dissolved material
$K_{\text{eq}}$	equilibrium constant
$K_F$	Freundlich constant
$K_L$	Langmuir constant
$K_{\text{LF}}$	Langmuir-Freundlich constant
$K_{\text{RP}}$	Redlich-Peterson constant
$K_T$	Tóth constant
$l$	Rod length
$\text{LC}_{50}$	(lethal) concentration at which 50 % of the organism population die
$m$	steepness of linear regression
$m_M$	mass of added mineral
$m_{\text{SA}}$	mass of stearic acid

$M_{wSA}$	molecular weight of stearic acid
$n$	refractive index
$N_A$	Avogadro constant
NTU	Nephelometric Turbidity Units
$P$	equilibrium pressure
$P_0$	saturation pressure
$q$	elementary charge
$r$	particle radius
$R$	universal gas constant
$R^2$	regression coefficient
$R_p$	particle radius
$s$	surface area of one particle
$t$	time
$t_d$	disc thickness
$T$	temperature
$u$	electrophoretic mobility
$U_e$	potential energy
UV	ultra violet light
$v$	settling speed of a particle
$v_p$	volume of gas adsorbed
Vis	visible light
$V_m$	Molar volume of adsorbate gas
$v_m$	volume of gas adsorbed in a monolayer
$V_p$	volume of a scattering particle



$w$	rod width
$X_{SA}$	surface coverage fraction by stearic acid
$z$	valency
$\Gamma$	fractional covered surface sites / loading
$\gamma$	surface tension or surface free energy
$\Gamma_{eq}^{colloidal}(c_{eq})$	loading of colloidal material as a function of equilibrium concentration
$\Gamma_{eq}^{dissolved}(c_{eq})$	loading of dissolved material as a function of equilibrium concentration
$\Gamma_{eq}^{total}(c_{eq})$	loading of Total material as a function of equilibrium concentration
$\gamma^{AB}$	acid-base component of surface free energy
$\gamma^{LW}$	Lifshitz- van der Waals component of surface free energy
$\Gamma_{max}$	maximum loading of adsorbate on adsorbent
$\Gamma_{mono}$	adsorbed amount of adsorbate in a monolayer
$\delta$	density
$\delta_l$	liquid density
$\delta_p$	particle density
$\epsilon_0$	permittivity of free space
$\epsilon_{BET}$	specific surface area determined by BET isotherm
$\epsilon$	specific surface area of a single particle
$\epsilon_{gas}$	cross sectional area of adsorbate gas
$\epsilon_r$	dielectric constant
$\zeta$	zeta potential
$\eta$	dynamic viscosity
$\theta$	scattering angle / contact angle
$\kappa$	inverse Debye length

$A$	decay or e-folding parameter
$\lambda$	wavelength
$\mu$	geometric mean
$\rho$	aspect ratio
$\sigma$	standard deviation
$\tau$	turbidity
$v_{\text{ads}}$	adsorption reaction speed
$v_{\text{des}}$	desorption reaction speed

# **1 Introduction**

## **1.1 Aim and thesis description**

The aim of this project is to improve the environmental aspects involved in paper recycling and wood processing components within the papermaking process. The main focus will be the study of the adsorption properties of organic contaminants on the surface of a variety of mineral particles depending principally on hydrophobic and charged species selection. This will include a mechanistic study of the size and surface chemistry relationships between the organic contaminant (pitch) and the mineral particle, with special reference to their morphology. To achieve this, systematic studies of the influence of the mineralogy, the effect of the surface area, the effect of the particle shape parameters and the influence of several crucial process conditions on the adsorption behaviour will be made. Following an initial survey of the current literature, new techniques will be designed to measure the adsorption efficiency and removal of contaminants from real water circuits of industrial relevance. The aims of the project are to deliver a working model for the mechanism of contaminant removal by mineral, a practical test for the efficiency of removal, and optimised design of speciality mineral pigments for the purpose of improving recyclability of paper and paper coating pigments. The results have been published in a series of publications in the academic literature, focused on environmental aspects of water circuit and treatment within the forest and paper industry.

## **1.2 Hypotheses**

**H1** The traditional (Hohenberger) equation relating the aspect ratio of a particle to its diameter and surface area contains false assumptions and can be improved for the case of high aspect ratio particles such as platelets and rods.

**H2** Particle size measurements can be made more reliable for high aspect ratio particles by a carefully reviewed choice of method.

**H3** Equations for aspect ratios based surface area measurements are invalid for particles which **(a)** agglomerate or **(b)** are porous.

**H4** The adsorption capacity of minerals for dissolved and colloidal substances from wood processing is proportional to the specific surface area of the minerals.

**H5** The adsorption mechanism of dissolved and colloidal substances from wood processing onto minerals is controlled mainly by hydrophobic interactions, and hence, hydrophobic materials preferably adsorb these substances.

**H6** Process conditions such as **(a)** pH and **(b)** temperature can negatively influence the adsorption of dissolved and colloidal substances.

**H7** On the basis of **H4** and **H5**, tailored mineral particulates can be developed which optimise pitch adsorption while coping with modern trends in paper making.

### **1.3 Structure of the thesis**

The thesis is split into 8 chapters. Chapter 1 puts the thesis in the context of the research field of the mineral, forest and paper industry by describing the fundamental processes of paper manufacturing. Chapter 2 is a review of the relevant literature in the field of papermaking and mineral characterisation. In order to encompass with the techniques applied in the thesis. Chapter 3 describes relevant experimental procedures and techniques.

The novel findings of this study are described in Chapter 4-7. Chapter 4 describes an improved model for the calculation of the aspect ratios of disc- and rod-like particles. This topic is relevant for following chapters that deal with irregularly shaped mineral

particles. The next chapters concentrate on the adsorption properties of various minerals under different conditions for the adsorption of dissolved and colloidal substances (DCS) in paper making process water. In Chapter 5 chlorite and pyrophyllite, typical ancillary minerals present in talc ores, are compared in their pitch adsorption efficiency against talc. Chapter 6 covers the effects of process conditions such as pH and temperature on the adsorption efficiency of talc for dissolved and colloidal substances in paper mill water streams. The development of calcium carbonate based modified mineral particles for the efficient adsorption of dissolved and colloidal substances is described in Chapter 7. In Chapter 8 the project is summarised and conclusions are drawn which lead to an outlook for future work.

#### **1.4 The collaborative basis of this research project**

The study has been performed as a collaboration project between Omya Development AG, supervised by Prof. Dr. Patrick A.C. Gane and Dr. Joachim Schoelkopf and the Environmental and Fluid Modelling Group at the University of Plymouth with Prof. G. Peter Matthews as the Director of Studies. This study was made in a part-time programme in parallel with several other research projects of high relevance for Omya Development AG, that are not described in this thesis. One of these was carried out by Dr. Chris Gribble who investigated the ‘Surface Adsorption and Pore-Level Properties of Mineral and Related Systems of Relevance to the Recycling of Paper’. Both studies investigated the interactions of mineral surfaces with colloidal organic contaminants in papermaking water streams. However, the main difference was in the origin of these contaminants, being either from recycled fibre (stickies) as in the case of the related project or as in the case of the current thesis from virgin fibres (pitch).

## **2 Theory and literature review**

This chapter reviews fundamental knowledge of the paper making process which allows the reader to place the study in the context of the research field. After an overview of the papermaking process, a more detailed background is given for the fibre processing with a special focus on wood resin and its composition. A second part covers the use of mineral in papermaking, some aspects of mineral characterisation, and finally the current understanding of their use to control unwanted deposits of pitch.

### **2.1 Paper and Papermaking**

Papermaking has developed from a rather simple technique to an automated and highly complex process. This introduction cannot cover all of the speciality topics involved but attempts to provide a summary of the manufacturing principles and to highlight the scientific fields of most relevance to this study. General overviews are to be found in textbooks such as that of Bos et al. (2006).

Paper satisfies many human needs. We use it to store and communicate information (newspapers, books, documents and writing paper), for cultural and artistic purposes, to transport and protect food (packaging, sacks, tetra<sup>®</sup> packs), for personal hygiene (tissues, napkins, diapers etc.) and in medicine (hospital uses). Whether not only are to the practical applications of importance, but also environmental concerns.

The manufacturing of paper is an involved process, from the forest, to the production of paper, to the use and final recovery of the product. Paper and board differ in specialised ways from other materials. The fibres from which the paper is formed can be recycled again and again, and when no longer useful for paper making, due to loss of strength or brightness form an excellent biofuel resource or compost.

### ***2.1.1 History***

The word paper is derived from the papyrus plant. This plant grows mainly on the edges of rivers in the Middle East and Egypt. Real paper produced by the filtration of plant fibres from water was invented in 105 AD by a Chinese imperial appointee, called Ts'ai Lun. Relatively quickly, a paper grade was developed by Chinese papermakers which was resistant to insect attack. It was then already possible to gain plant fibres from bamboo to produce paper. Nevertheless, old textiles were the main raw material for the production of paper until the 19th century. The technology of papermaking was adopted by the Arabs around 700 AD, and was imported to Europe via Spain and Italy in the 13th century. During the 14th century (Nürnberg 1390, Ravensburg 1392 and Chemnitz 1398), the first mills in Germany were developing. The first mill in Switzerland, where the work of this thesis was mainly performed, was opened in 1410 in Basel. The Dutch paper industry developed the pulp beater in the 17th century (1672). It allowed for more exact and reproducible refining of the fibres, which led to a higher sheet quality. This technology was state of the art for over 200 years. The invention of the paper machine in 1798 was a breakthrough in terms of automation of the paper production process. The technology was brought to England during the French revolution where it was further developed by the Fourdrinier brothers. In 1820 the drying section with steam heated cylinders was patented. There followed several major inventions, like the sizing with resin to prevent the paper from weakening when water-based ink was used. The production efficiency and quality continually increased, such that the production capacity of an automated paper factory was 5 – 8 times higher than a manually operated paper production. Social questions arose with the introduction of the new technologies (Bos et al. 2006).

## 2.1.2 The papermaking process

While papermaking has advanced during the last two thousand years, the basic steps of the process remain essentially unchanged. The basis for every paper sheet is a matt of fibres. The fibre source can vary but today typically up to 94% of the natural fibre in paper is from wood. Other sources can be straw, sugar cane, bamboo and esparto or textile fibre sources like cotton, flax, hemp or wool.

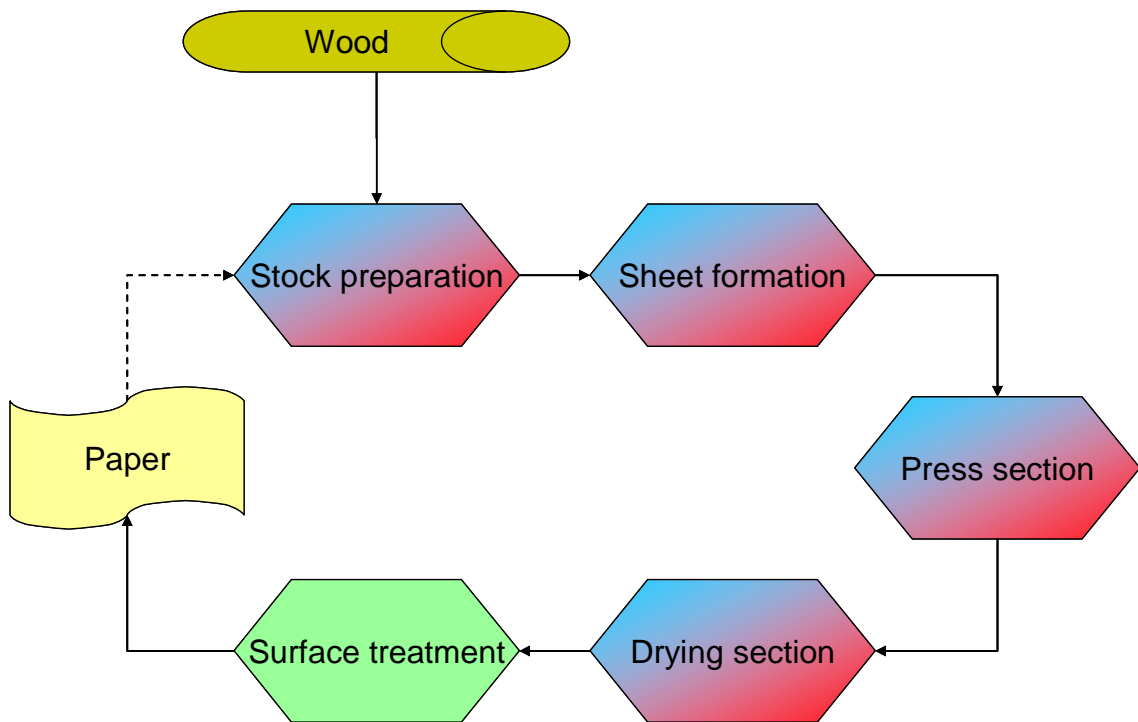


Figure 2-1: Schematic of the papermaking process.

### 2.1.2.1 Wood

In the context of this thesis only wood will be discussed as the fibre source, as it is the natural resinous material in wood that is the focus of the interactions studied here. Typically, the papermaker uses the terms softwood and hardwood to describe the type and properties. Softwood refers to needle-leaved trees, such as pine and spruce. The fibres are considered to be long, 2-5 mm, and relatively dense. Due to their length they can form stronger networks and therefore provide additional strength in the final paper, and are thus often found in board and packaging grades such as grocery bags or boxes.



Hardwoods belong to the families of oak, beech, birch and eucalyptus. The fibres are shorter, 1-2mm. As a result they feature as a preferred raw material for smoothness and bulk, and are often found in writing and printing paper qualities, as well as tissue papers. The structural polymeric constituents of wood, i.e. cellulose, hemicellulose and lignin, are much the same in various pulp woods. Certain differences, however, do occur, especially between hardwoods and softwoods. The extractable lipophilic and phenolic components differ greatly among the genera or within tree families. This fact is related to the role of the extractives in nature, associated with protection against insects and fungi, wounding or entry of air during aging.

### ***2.1.2.2 Fibre and stock preparation***

In a first step selected trees are harvested. The trees are brought to the pulping plant where they first are debarked. A next step involves chipping to wood chips with a defined size. The chips are then reduced to fibres. This can be done with several methods. The methods include grinding, supported by heat and steam or the addition of chemicals, or the wood is cooked in a digester with the aid of chemicals. During this process wood resin is released into the process water. Depending on the method which is used, the problems caused by the wood resin can be more or less harmful since some methods modify the wood resin by chemical reactions or use intensive washing to remove the chemicals, and in parallel also wash out the wood resin. It is possible that a next step may include a further chemical treatment, in the form of bleaching, to increase the brightness of the pulp.

The simplest process adopts stone grinders to release the fibrous material from the wood. Following the logic of this process method, the resulting pulp is called ground wood. Other processes based on refining are thermo mechanical pulping (TMP) and the chemical thermo mechanical pulp (CTMP). Refiners act like knives that cut fibres

mainly in their longitudinal direction. A major difference is also the partial dissolution of the lignin by the aid of heat and chemicals in these processes. Sodium sulphite is added in the CTMP process which sulphonates the lignin and increases its solubility. The resulting lignosulphonates can be found in the water phase and may act as stabiliser of wood resin droplets (Back, Allen 2000). All these fibre qualities, however, still contain lignin, and are, therefore, referred to as wood containing pulps. Bleaching steps are often required to control the brightness. TMP is the relevant process for fibre preparation in the case of the current study.

To obtain so-called wood free fibres, i.e. lignin-free pulp, two widespread processes are usually applied: the acidic sulphite process and the alkaline sulphate process. By cooking the wood in the corresponding chemical, the lignin is transformed to a water soluble form which allows separation from the wood fibres. Especially in the sulphite process, the lignosulphonates develop as a by-product.

### ***2.1.2.3 Sheet formation***

The fibre stock, including fibres, fillers and chemicals, is pumped to the head box. The head box feeds the stock evenly onto a screen or mesh. The water is drained by vacuum and a fibre mat is left on the screen or mesh. During this mat formation a substantial amount of water is removed. The thin mat of wet fibres forming the paper sheet is still very weak and has a water content of approx. 25%. In this process step, pitch and other lyophobic particles may form agglomerates and deposit on or in the mesh, thus reducing machine efficiency. These deposits may cause further problems further down the process, particularly in the drying section.

### ***2.1.2.4 Press and dryer section***

The press section provides filtration through permeable felts mounted on heavy cylinders by contact pressure under partial vacuum. This is then followed by hot

cylinder driers. In the drier section a large number of steam-heated cylinders, which have a temperature over 100 °C, dry the paper. These two sections bring the paper to the desired moisture (~3-5%), but not completely dry as that would cause the paper to become brittle. Pitch may block the felts in the press section. Especially in the dryer section, the pitch deposits are very detrimental. Due to the heat, they can melt and create adhesive contact between the paper web and the machinery equipment. The induced strain may then lead to a web break or tear in the paper or create holes in the paper. Even if the deposits do not get in contact with the machinery equipment they can form translucent spots in the paper, which may darken and severely reduce the paper quality.

#### ***2.1.2.5 Surface treatment***

After the dryer section, a surface sizing agent like starch can be applied to the paper. The sizing improves the printing properties. A means to smoothen the surface of the paper is provided by the use of an on-machine calender. Pair-wise mounted hot polished metal rollers act to soften the fibres by heating and then under pressure to compact them.

High-quality printing papers are coated by a formulation known as a coating colour. This usually consists of a water-based pigment suspension or blend of pigments, such as fine ground calcium carbonate, clay or talc, or, on occasions, other speciality pigments may be added, such as calcined clay or plastic hollow spheres, to enhance coverage or brightness. Coatings can be formed from multiple layers adopting, say a precoat and a topcoat. Today's digital printing paper production applies, for example, highly absorbent coatings for inkjet, thermally sensitive coatings and the like. The coating formulation also contains a binder or blend of binders. These are usually synthetic latex in the case of the highest quality coatings, whereas starch and protein are frequently used for lower quality wood containing light weight papers. Additionally, thickeners are

used to provide static water retention to the coating, and these may also be based on synthetic chemistry, such as polyacrylate derivatives or are derived from natural polymers, such as carboxymethyl cellulose.

Some of the above mentioned components together with the pigments can cause further problems in terms of deposition of detrimental material in the paper machine when they come back into the paper making circuit in the form of recycled paper or coated broke (waste paper resulting from machine breaks, cutting procedures, reel winding etc.). Coated papers are often very smooth and glossy, and this is achieved by using either super calenders consisting of alternate metal rolls, or an on-line polymer covered, so-called hot soft nip, calender.

#### ***2.1.2.6 Paper recycling***

Paper recycling is not really a new trend. Due to the high paper demand and the rather low availability of virgin fibres it was obvious to reuse the fibres derived from waste paper and board. The real interest, however, for recycled fibres developed in 1950 (Bos et al. 2006). Whereas in a first step mostly packaging paper was considered for recycled fibres, the development of the deinking process also allowed the use of the deinked material in printing and tissue grades. The recovery of fibres from recycled paper consumes around 1 000 kWh<sup>-1</sup> less energy than the processing of wood towards virgin fibres (Bos et al. 2006). Together with the perception that 1 tonne of recycled paper replaces 10-12 grown trees the use of recycled paper was further stimulated and in 1996 up to 70% of the converted fibres in England originated from recycled paper (Bos et al. 2006). As previously mentioned, problems arising with agglomerates and deposits from paper recycling are not the main focus of this study and were a part of a second PhD thesis performed in parallel (Section 1.4).

When considering recycled material we need to consider the history of its prior use. Printing and writing grades, as the name suggests, are printed, glued or stapled or may contain plastic foils like those used in some envelope types. Packaging boxes are mounted with adhesives tape. All these paper grades including the various contaminants from the prior use are part of the recycle portfolio. A certain pre-selection of the recycled paper quality may be part of the process in order to fit the final paper qualities to the targeted re-use, and also to match the recycling technology available in the mill. A typical paper recycling process then prepares the raw material so that it can be fed to a pulper, in which the paper is disintegrated by a combination of chemical and mechanical impact. In this preparation, large contaminants like staples, plastic shreds or more exotic material like PET bottles can be sorted out. This is done by a combination of screens, sorters and cyclones. This is followed by a deinking process. Today, flotation deinking is the main technology used in mills. However, also wash deinking might be needed to remove water soluble inks or inks that form very small particles. Sodium hydroxide, hydrogen peroxide, water glass and some form of metal complexation agent are added. In addition sodium-soaps are also added, which help to remove the hydrophobic ink particles from the fibres. These hydrophobic particles become attached to the air bubbles present in the flotation deinking and are removed with the foam. A second sorting step follows the deinking in order to remove a certain fraction of stickies. This is again done by either screening or the use of cyclones. None of these process steps has an efficiency of 100% and thus some contaminants are still present. In order to minimise their effect a dispersing step reduces their size and disperses them favourably into a non-harmful form. Additionally, the dispersing step also leads to the development of the mechanical strength of the fibres. If desired the fibres can be further bleached to increase their brightness and finally the circuit is closed and the fibres can be used again in the papermaking process.

An important aim of the described process is not only to remove inks but also to remove so-called “stickies”. Stickies develop from hot melt glues and binders and other thermoplastic materials, for example from book-backs and adhesive tapes or from silicone based defoamers (Ackermann et al. 1996; Capozzi 1995; Cathie et al. 1992; Cathie 1994). Stickies are described as tacky, hydrophobic, pliable organic materials found in recycled paper systems. Their composition ranges across a variety of materials such as adhesives, styrene-butadiene and styrene acrylic latex binders, polystyrene in general, rubber, vinyl acrylates, polyisoprene, polybutadiene, hot melts etc. Stickies can be classified based on their size as either macrostickies, the reject or retains on a 0.15 mm or 0.10 mm laboratory slotted screen, or microstickies, the accept through the same screen (Doshi 1991; Douek, Guo 1997; Hayes, Kauffman 1993; Keller, Trojna 2001; Patel, Banerjee 1999). Macrostickies are considered removable from pulp by the application of fine slotted screens or hydrocyclones, while microstickies may be removed to some degree by washing and flotation. Problems occur, however, with weakly to non hydrophobic microstickies (Menke 1998). A further classification of stickies describes primary and secondary stickies. Primary stickies are those resulting from the disintegration of adhesives during pulping and subsequent stock preparation sequences. Secondary stickies result from soluble and water-dispersible substances dispersed during stock preparation. Therefore, the solid stickies in a given pulp are considered primary stickies and secondary stickies, the latter deriving from the change in the physico-chemical environment of the pulp sample (Carre et al. 1998).

A further form or subgroup of sticky is white pitch. White pitch is generally associated with the re-use of coated broke, i.e. coated paper manufacturing waste, such as reel trims, splice breaks, out of specification paper or faulty product, and consists mainly of the binders used in the paper coating formulation. These include primarily synthetic latex, incorporating styrene, butadiene, acrylic and/or nitrile groups.

## **2.2 Wood components**

Polysaccharides, i.e. cellulose, hemicellulose and pectins are together with lignin the main constituents of wood and wood pulps (Willför et al. 2008). Lignin contributes to about 20-35% of the wood components. Extractables such as wood resin contribute around 3-10%. After having removed the fibrous material by centrifugation and/or filtration the remainder is often referred to as dissolved and colloidal substances (DCS), and contain hemicelluloses, pectins as well as soluble lignin in the dissolved fraction and lipophilic extractives (wood resin) and lignans. Depending on the wood source and history of the wood a typical composition of DSC from thermo mechanical pulp may contain 19 mg g<sup>-1</sup> (based on dry pulp) carbohydrates, 4 mg g<sup>-1</sup> lignin and 4 mg g<sup>-1</sup> wood resin (Holmbom, Sundberg 2003).

This section will give an introduction to wood resin and pitch. The section mainly refers to the book of Back and Allen (2000) who compiled hundreds of publications. Wood resin is released during the pulping process into the process water. Naturally stabilised the wood resin is present as colloidal droplets with an average size of 0.1 – 2 µm (Holmbom, Sundberg 2003; Parmentier 1973). These droplets often referred to as pitch can be destabilised and consequently cause serious problems in the paper machine. Destabilised pitch can agglomerate or deposit on paper machine equipment such as felts, wire and cylinders in the paper machine. These deposits can break loose and appear as visible spots in the paper sheet. Pitch deposits can also cause holes and breaks in the paper sheet. A mill with serious pitch problems can have long downtimes of the machine and rapidly loses production efficiency.

### ***2.2.1 Origin and composition of Wood resin***

The structural polymeric constituents of wood, i.e. cellulose, hemicellulose and lignin, are much the same in the various types of pulp woods. Certain differences in respect to

extractives, however, certainly occur, especially between hardwoods and softwoods. The composition of wood resin as occurring in the wet-end of a paper mill can be summarised as:

- fats and fatty acids
- steryl esters and sterols
- terpenoids including terpenes and polyisoprenes
- waxes, i.e. long-chain alcohols and their (commonly fatty) acid esters

Wood resin refers to lipophilic components, mainly of lower molecular mass (usually below  $1\ 000\ \text{g mol}^{-1}$ ), which in sapwood are extraneous to the lignocellulosic cell wall. Wood resin occurs in parenchyma cells and in resin canals or resin pockets only. Resin canals are the most important type of secretory tissue in wood. Often vertical and radial resin canals occur together and then form an intercommunicating system of ducts in the stem. Canal resin in softwoods is generally an amorphous mixture of cyclic terpenes and terpenoids (e.g. resin acids), all biosynthesised from the isoprene unit by various cyclase enzymes (Figure 2-2) (Back, Allen 2000).

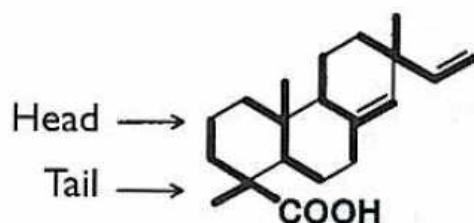


**Figure 2-2: Dissection of the cyclic carbon skeleton of primaric acid into isoprene units linked tail to head (Back, Allen 2000).**

The tricyclic carbon ring of the resin acids is obviously very stable since such terpenoids have been found in fossil wood, soil, lignite and amber. Common examples are pimaric acid, abietic and dehydroabietic acid (Figure 2-3). In addition to the



common resin acids, nonvolatile neutral diterpenoids such as methyl esters, oxides, aldehydes, alcohols, and hydrocarbons are present in minor quantities in the softwood canal resin.

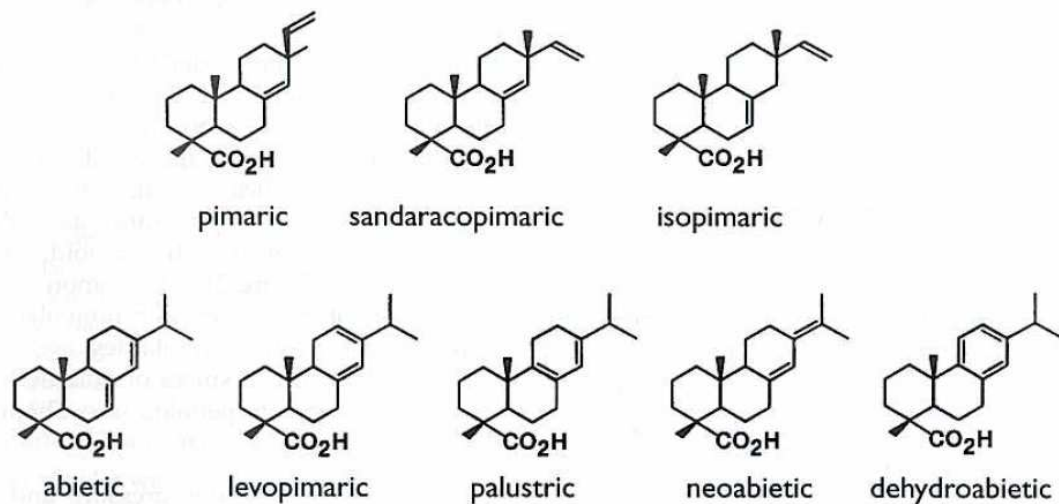
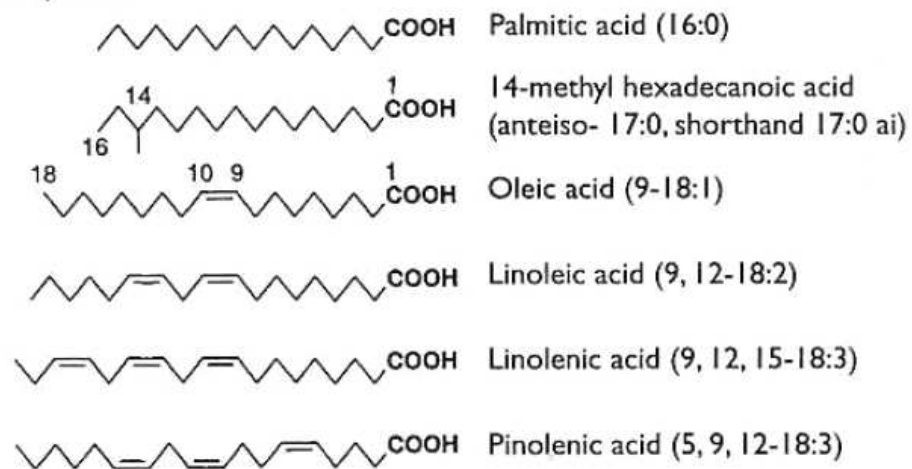


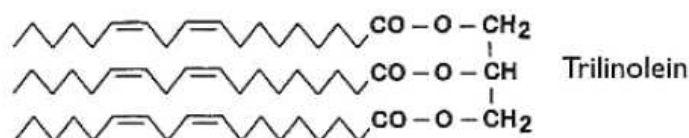
Figure 2-3: Common resin acids in softwood canal resin (Back, Allen 2000).

The chemical composition of the softwood parenchyma resin is entirely different from that of canal resin of the same wood. The parenchyma resin is predominantly composed of fatty acids, triglycerides and fatty acid esters with higher polycyclic alcohols such as sterols (Figure 2-5) and nonsteroidal triterpenyl alcohols. The term fatty acid fits for chemicals with a long lipophilic hydrocarbon chain and a hydrophilic acid head. This group includes saturated hydrocarbons like palmitic acid (16:0), as well as unsaturated, like oleic acid (9-18:1) or linoleic acid (9, 12-18:2).

### Fatty Acids



### Triglycerides (triacylglycerols):



### Fatty acid esters:

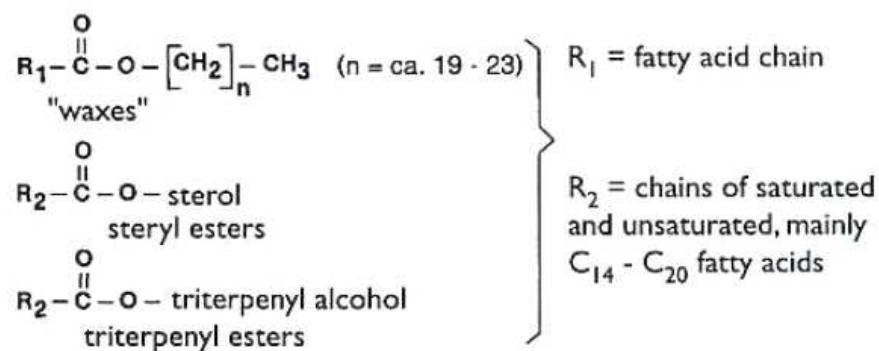


Figure 2-4: Characteristic parenchyma wood resin constituents (Back, Allen 2000).

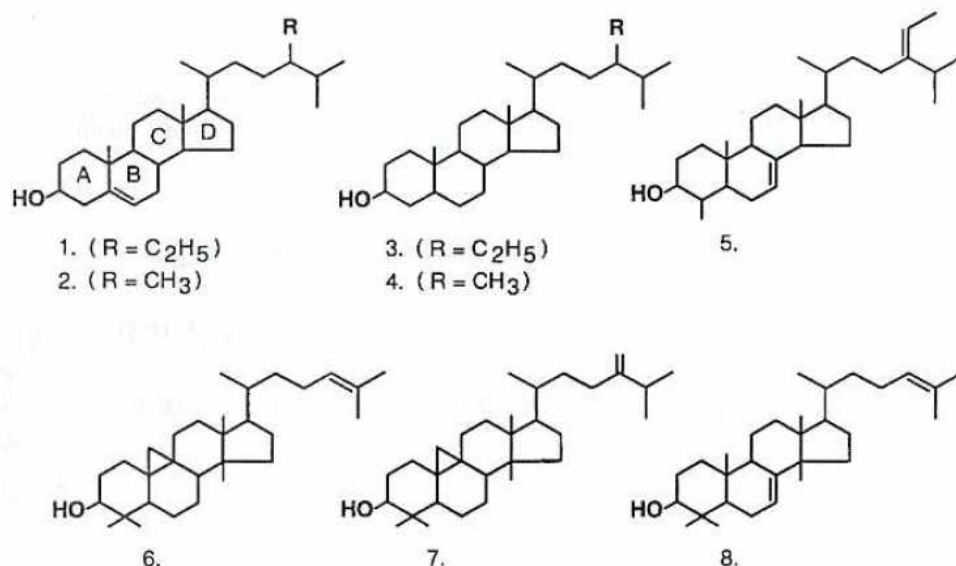


Figure 2-5: Chemical structure of some common sterols in wood resin: (1) sitosterol, (2) campesterol, (3) sitostanol, (4) campestanol and (5) citrostadienol, (6) cycloartenol, (7) 24-methylene cycloartanol, and (8) butyrospermol (Back, Allen 2000)

### 2.2.2 Lignin

Lignin (lat. *lignum* “wood”) is a major constituent of wood fibres. The hydrophobic amorphous heteropolymer acts as glue, and provides stiffness to the fibres. Papermakers distinguish between wood containing and wood free paper, and refer by this categorisation to the content of lignin in the fibre. The lignin is a co-polymer that is based on several phenylpropanoids like cumaryl alcohol, coniferyl alcohol and sinapyl alcohol.

### 2.2.3 Polysaccharides

The relevant polysaccharides in papermaking are cellulose, hemicellulose, pectins, and often starch as a wet-end additive. Cellulose, as well as starch, is irrelevant for this study, since neither belong to the dissolved and colloidal fraction (DCS) as defined earlier. A major part of the DCS is hemicellulose, especially in the form of galactoglucomannans (GGM) (Holmbom, Sundberg 2003). Hemicellulose differs from cellulose in their degree of polymerisation, which is typically lower for hemicellulose,

and composition. Cellulose consists of only  $\beta(1\rightarrow4)$ linked D-glucose units whereas hemicellulose is a hetero polysaccharide which consists of glucose, mannose, galactose, xylose and arabinose. They are water soluble but maintain a certain affinity to hydrophobic surfaces as a result of their methylene backbone (Jenkins, Ralston 1998). They can be, thus, regarded as surface active components and have been shown to act as stabiliser of colloidal wood resin (Holmbom, Sundberg 2003; Otero et al. 2000; Saarimaa et al. 2006; Sihvonen et al. 1998; Sundberg et al. 1996d). These hemicellulose species may also be oxidised partially to uronic acids, carrying thus anionic charge (Sundberg et al. 2000). A typical hemicellulose present in Norwegian spruce is acetylated galactoglucomannan (GGM) (Figure 2-6) (Willför et al. 2008). GGMs consist of a backbone of randomly distributed (1 $\rightarrow$ 4) linked mannose and glucose units which at the mannose are (1 $\rightarrow$ 6) linked to galactose. Some of the hydroxyl groups in the mannose units can be acetylated. The degree of acetylation strongly depends on the treatment history of the pulp.

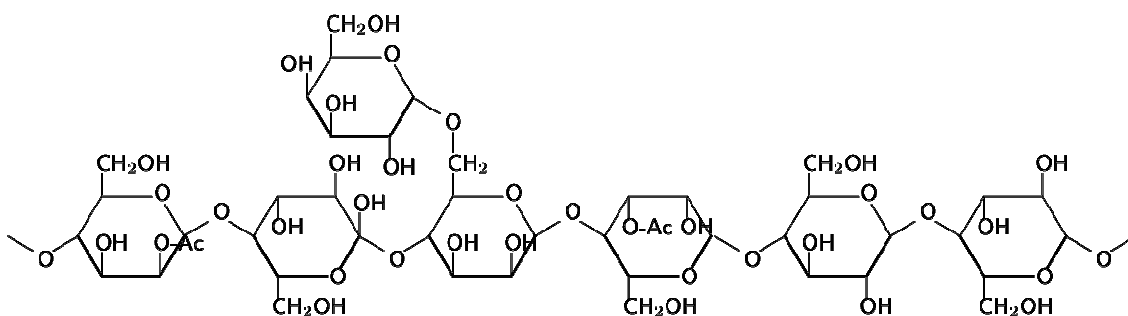


Figure 2-6: Possible structure of *O*-acetylgalactoglucomannan.

#### 2.2.4 Wood resin in aqueous environment

In the previous sections the fundamental chemistry of dissolved and colloidal substances has been explored. The important understanding, however, lies in the nature of the physical appearance of the wood resin components in an aqueous system which defines subsequently their interaction with their environment. Most of the components in wood resin have rather bad water solubility and may thus be referred to as

hydrophobic. Resin and fatty acids and especially their soaps can be regarded as amphiphiles and can form micelles in water through self assembly (Back, Allen 2000). Pitch droplets, however, should not be considered as micelles but rather as a liquid crystal-like phase which can solubilise other hydrophobes. No sufficient knowledge exists about the development of homogeneous colloidal dispersions of resin droplets. The resin diffuses out of parenchyma cells or may be squeezed out from broken cells. Due to the high temperature and high ionic strength, a lamellar liquid crystalline structure phase is formed, which further goes on to form separate droplets at the pulping temperature, i.e. 150-180 °C (Back, Allen 2000). Typically, the appearance of wood resin droplets from TMP form a unimodal, lipophilic colloidal system (Swerin et al. 1993; Wagberg, Ödberg 1991) shown schematically in Figure 2-7. The hydrophobic part of the wood resin components like triglycerides, steryl esters, waxes as well as the hydrophobic backbones of resin and fatty acids, sterols and fatty alcohols preferably assemble in the centre of the colloid (orange). Hydrophilic uncharged groups (light blue circles) like alcohols as in the case of sterols and fatty alcohols can form hydrogen bonds and may also be found on the surface of the colloid. They can be considered as co-surfactants. The hydrophilic head groups (green circles) of the resin and fatty acids and especially of their soaps, determine the outer surface of the colloid and hence its electrostatic stabilisation (Back, Allen 2000; Garver, Yuan 2002). These compounds are in equilibrium with the bulk solution and may dissolve as a result of pH, temperature or ionic strength change (indicated by the dark grey arrows in Figure 2-7 which point to and from the colloid). Finally, hydrophilic water soluble polymers (blue chains), like the hemicelluloses or lignosulphonates (Back, Allen 2000; Lindström et al. 1988) adsorb onto the wood resin droplets and add to their colloidal stabilisation by steric or electrostatic interactions (Otero et al. 2000; Qin et al. 2004; Saarimaa et al. 2006; Sundberg et al. 1994a; Sundberg et al. 1994b; Sundberg et al. 1996c; Willför et al.

2008). The sorption mechanism of these polymers may be explained by their partially hydrophobic nature (see section 2.2.3) and their ability to form hydrogen bonds. Compared to the wood resin content, these polymers are in excess and occur in equilibrium between the surface and bulk solution (indicated by the light grey arrows pointing to and from the surface in Figure 2-7). Typically, a wood resin droplet without polymer layer can be considered as still very hydrophobic (Wallqvist et al. 2007) due to a rather low charge density (Sundberg et al. 2000).

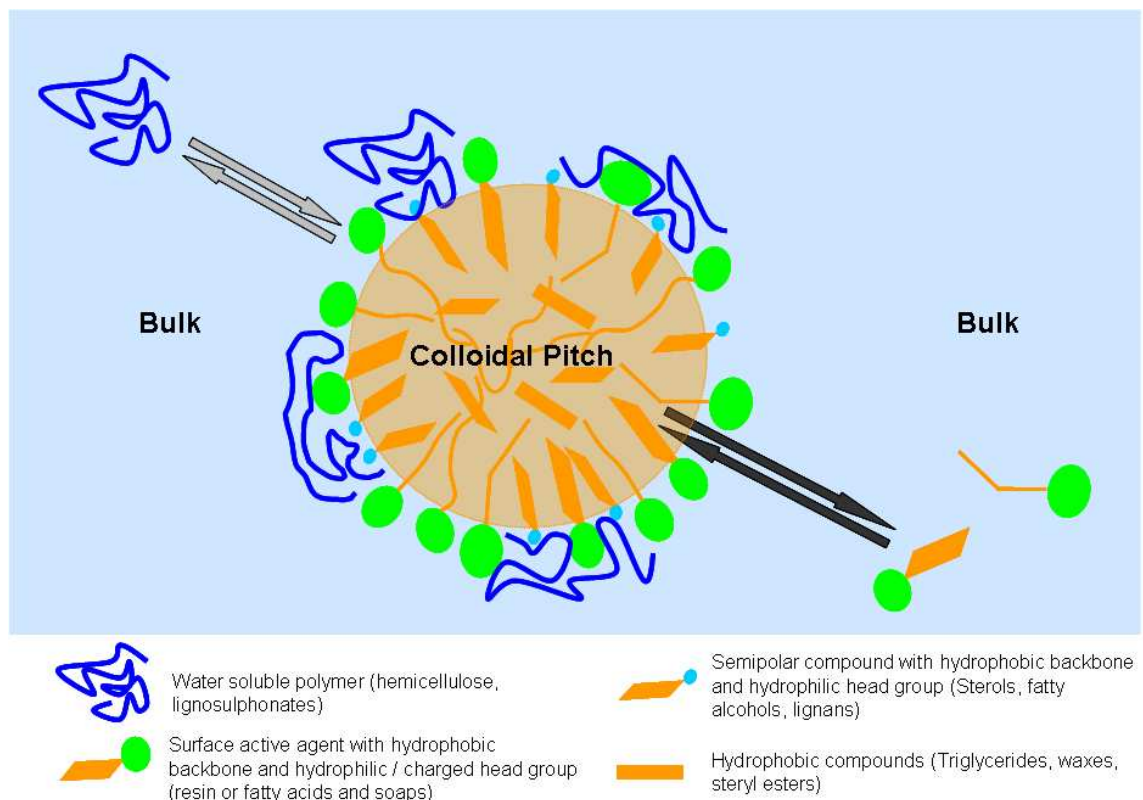


**Figure 2-7: Tentative illustration of pitch globules and their equilibrium with the surrounding bulk solution.**

This system is often referred to as dissolved and colloidal substances (DCS). A colloid can be defined as a particle that has some linear dimensions between 1 and 1 000 nm (Hiemenz, Rajagopalan 1997). This may of course also include polymers such as polysaccharides. The distinction in papermaking science is rather done based on a separation step. As described above the hydrophobic wood resin forms colloidal droplets which are in the size range of 10 to 2 000 nm (Mosbye et al. 2003). A

separation is typically obtained by membrane filtration using 0.1 or 0.2  $\mu\text{m}$  filters (Holmbom, Sundberg 2003). Everything retained by the filter is part of the colloidal substances and everything passing through the filter is dissolved material. In the current thesis the distinction is based on turbidity measurements, as well as extraction with a non-polar solvent. Substances that cause turbidity are considered as part of the colloidal fraction and include mainly hydrophobic wood resin with adsorbed hemicellulose (Figure 2-7). Furthermore, in some cases (sections 7.1.3.3 and 7.2.3.2) the colloidal fraction is quantified by solvent extraction at acidic pH. Dissolved substances are either quantified indirectly by subtracting the amount of colloidal material from the total organic material or directly by quantification of the carbohydrate monomers after hydrolysis plus the UV absorption of dissolved lignin.

### ***2.2.5 Environmental aspects of wood resinous compounds***

This section shortly discusses the environmental aspects of wood resinous compounds. It is based on the book of Back and Allen (2000) and the reader is referred to the various publications about that topic in the cited text book.

*Resin acids* are known to be toxic to fish.  $\text{LC}_{50}$  values, which is the concentration at which 50% of the organisms in the experiment die, of some resin acids are lower than  $1 \text{ mgdm}^{-3}$ . Furthermore, toxicity was also observed for fish exposed to sub-lethal doses. Resin acids and metabolites have been detected in fish captured in receiving waters of mill effluents. The bioaccumulation not only occurs in vertebrate fish but also in invertebrate molluscs, such as mussels. The data, however, suggest that the bioaccumulation can be excreted when exposure is stopped. Neoabietic acid (Figure 2-3) has been identified as a potential mutagen, whereas the other resin acids did not show a positive response in the Salmonella/mammalian-microsome assay.

*Fatty acids* originate from triglycerides through saponification. They, too, have been found to cause toxic effects in fish, but the acute lethal toxicity is, however, less than that of resin acids. Unsaturated fatty acids (Figure 2-4) appear to be more toxic to fish than saturated. Chlorinated fatty acids may accumulate in fish muscle lipids.

*Neutral terpenes and terpenoids* can have acute fish toxicity and chlorinate derivatives show mutagenic and genotoxic activities. LC<sub>50</sub> values for pimarol and dehydroabietol were found to be 0.3 and 0.8 mgdm<sup>-3</sup>, respectively.

*Sterols*, often with sitosterol (Figure 2-5) as the main component, are present in softwood and hardwood species. Some unidentified compounds in pulp mill effluents act similarly to hormones and affect functions of the endocrine glands in fish. Plant sterols can be one group of compounds that exhibit such properties. Especially sitosterol and stigmasterol, and/or their bacterial metabolites, are suspected to cause “masculinisation” of female fish. Sitosterol may also mimic oestrogen in fish and subsequently reduce the reproductive steroid hormone levels in fish.

Paper mills try to close their water circuits more and more, and thereby also reduce the amounts of effluents. Nevertheless, undiluted mechanical pulping effluents are often acutely lethal to aquatic organisms and need to be treated before discharging. Anaerobic and/or aerobic microbiological treatments are applied. The fact that the compounds present in mill effluents can be toxic has driven the development of methods for their efficient removal. Adsorption on a mineral surface, on the one hand, reduces the reactivity of the compounds in bleaching steps, and, on the other hand, removes them efficiently from the aqueous circuits and effluent streams. Furthermore, the solubility of resin and fatty acids increase under today’s neutral to alkaline paper making conditions (Lehmonen et al. 2009; Nyren, Back 1958a; Nyren, Back 1958b), and so improved



mineral particles for effective adsorption under these circumstances are highly sought after.

## ***2.2.6 Analysis and quantification of dissolved and colloidal substances, and of pitch control measures***

The methods of pitch analysis either focus on the dissolved and colloidal fractions of the wood pulps in a direct or indirect way, or they focus on the deposition tendency of the wood pitch by so-called deposition tests. This chapter will not cover the technical details of the applied methods, but will rather give a short overview of the different possibilities and methods available in the literature and consider briefly their respective merits and practical limitations.

### ***2.2.6.1 Analysis of dissolved and colloidal substances***

The methods to quantify dissolved and colloidal substances are wide ranging. Typically, sophisticated methods are in use to quantify the wood resin constituents directly by extraction followed by gas chromatography (GC) (Ekman, Holmbom 1989; Holmbom 1977; Orsa, Holmbom 1994; Saltsman, Kuiken 1959; Wagberg, Ödberg 1991). Differences often appear in the selection of the solvent for extraction (Salvador et al. 1992). Rogan (1994) used HPLC to quantify oleic acid and triolein in his experiments. The dissolved lignin and carbohydrates are analysed by UV/Vis photometry or also by gas or ion exchange chromatography; chromatography allows a quantification of the single carbohydrate monomer units (Asselman, Garnier 2000; Ekman, Holmbom 1989; Orsa, Holmbom 1994; Sundberg et al. 1996a; Thornton et al. 1994; Wagberg, Ödberg 1991). The use of sulphuric acid to hydrolyse the polysaccharides results in a decomposition of charged uronic acids, which will then not be included in the analysis, and thus remain overlooked. Only methylation of the carbohydrates will result in both charged and uncharged carbohydrates. Another direct measurement of the colloidal

resin fraction includes the use of microscopy (Baak, Gill 1971; Parmentier 1973) and quantification can be achieved via a haemocytometer (Allen 1977), or more recent developments include flow cytometers (Kerman et al. 2006; Kröhl et al. 1994; Lindberg et al. 2004; Saarimaa et al. 2006; Vahasalo et al. 2005; Yu et al. 2003). Besides the particle count, flow cytometers also report the size of the counted particles. For a more accurate particle size measurement, static and dynamic light scattering measurements are available (Sundberg et al. 1996b; Wagberg, Ödberg 1991). Turbidity is an indirect measure for the content of colloidal particles (Ravnjak et al. 2003; Sihvonen et al. 1998; Sundberg et al. 1994b). Turbidity measurements are simple to perform in contrast to sophisticated extraction with subsequent GC analysis, but nevertheless correlate well with the concentration of colloidal extractives in an idealised water system that does not contain fillers or fibres. Oxidation with chromic acid with subsequent photometry not only quantifies colloidal substances but all components which are oxidised under the applied conditions (Hamilton, Lloyd 1984; Lloyd, Stratton 1986). Usually, this mainly involves organic materials, dissolved and colloidal. Others used acetic anhydride and sulphuric acid to colour the pitch with subsequent photometry (Hughes 1977). Staining pitch particles with dyes or direct photometry can also be applied (Asselman, Garnier 2000; Chang 1985).

A combination of these methods was presented by Guera et al. (2005) in which turbidity, chemical oxygen demand and a gravimetric residue was compared. This allowed a comparison between adsorption of colloidal and dissolved substances onto talc. This method forms one of the fundamental assessment techniques in this thesis, and will be further explained in the chapter 3.

### ***2.2.6.2 Deposition tests***

Papermaking furnish can contain up to 5% of depositable material like pitch and stickies (Hubbe et al. 2006) but only a minor fraction of it may be involved in deposition. Since the mass flow in paper mills is very high even these tiny amounts of material with deposition potential can be enough to require a shutdown of the machine. Therefore it is very difficult to simulate in lab scale the real deposition behaviour of pitch. For monitoring the deposition potential in paper mills collector plates are placed in the water circuit and evaluated after a defined time to determine the deposited material (Dreisbach, Michalopoulos 1989; Pelton, Lawrence 1991).

Gustafsson et al. (1952) reviewed the pre- 1952 work, focusing on the circumstances under which pitch adheres to surfaces. They reported a method in which the pitch is adsorbed on to the surface of a metal vessel. This general procedure was subsequently known and used in the paper industry as the “Gustafsson-method” even though Gustafsson et al. (1952) only reported the method and were not the inventors, though they suggested certain modifications. Originally, the method was developed by Gavelin (1949) in which he used a British Standard Disintegrator, made out of chromium, and a chromium vessel. Due to the chromium surfaces, the pitch deposits were comparatively small, which might possibly have an adverse effect on the reproducibility. Gustafsson et al. (1952) compared stirrers made from different materials and altered the conditions under which the test was performed (pH, temperature and stirring time). It was observed that the pH value of the system is an important factor. In alkaline domains more pitch deposition is seen. Different metal surfaces of the stirrers were investigated by measuring the resin deposition from sulphite pulps at pH 6. Copper had the highest amount of deposition followed by zinc, stainless steel, aluminium and chromium, which had the smallest amount of deposits. Therefore, to obtain a maximum pitch deposition a copper vessel and a copper disc attached to a stirrer were used. Strong stirring of the

pulp suspension over 2 hours at 50 °C led to pitch being deposited on the copper surfaces. The pitch deposited on the walls of the vessel and on the propeller was collected by means of cotton wool soaked with ether. The solution in ether was evaporated and the remainder was dried in vacuum after which the pitch was re-weighed. The copper surface, however, undergoes an ageing effect. An aged copper (> 2 month, > 40 runs) surface adsorbed three times the amount of pitch than did a fresh surface, at constant pulp composition.

A number of variations on this method has since been reported following on with the idea of pitch adsorption onto a surface. Hamilton and Lloyd (1984) found that the extraction and adsorption of pitch onto XAD-2, a non-ionic polystyrene divinylbenzene resin, was not entirely satisfactory because the quantitative recovery was difficult to achieve due to emulsion formation and pH effects. Studies by Douek and Allen (1983) showed that calcium carbonate and calcium soaps were major components of brown stock pitch deposits. They, therefore, tried to find a process that involved the adsorption of soap anions onto plates of calcium carbonate. Their results show that a measurable quantity of deposits can be obtained by this method. But the background lignin concentration has a big influence on the quantity of deposits and the plates cannot be used in the presence of fibres, which could then detach the particles of calcium carbonate from the support. Furthermore, the conditions of the tests carried out are not representative of those prevailing in a mill.

Hassler (1988) induced deposition by applying a high shear forces using a Vibromixer<sup>1</sup> consisting of a stainless steel disc attached to a rod.

---

<sup>1</sup> TAPPI Routine Control Method No. RC-324, TAPPI Press, Atlanta

The Hydro-Pulsed Colloidal Deposition (HPCD) test (Figure 2-8), or impinging jet principle, was developed to investigate the deposition tendency of industrial pulp samples (McGregor, Philippaerts 1998). Pitch or stickies can be detected. It was possible to detect deposits, but also a filmy layer. These results led to a possible mechanism in which a filmy layer is first built up upon which deposits can later form. The pulp sample is pumped from a vessel to a glass tube where the pulp is deflected repeatedly around a transparent collector film. The outlet side of the tube returns to the reservoir that contains the pulp sample. The detection is made by UV-VIS spectroscopy. Depositions are measured at a wavelength of 400 nm and the filmy layer itself is measured at a wavelength of 228 nm. Problems occur when using too high a flow rate as deposits become detached. Also some problems occur with the detection, because some deposits cannot be seen either in the visible wavelength or in the ultraviolet regions.

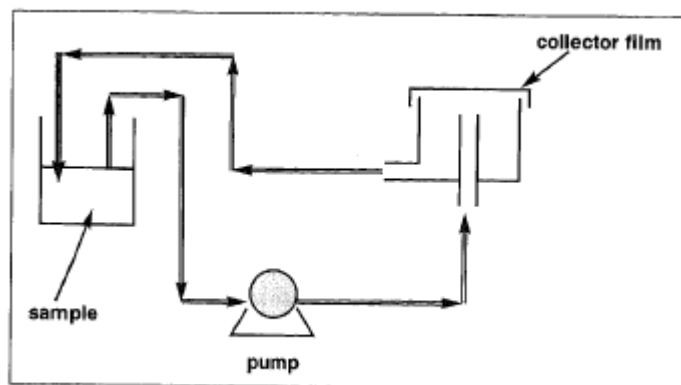


**Figure 2-8: Flowsheet of the apparatus used for the Hydro-Pulsed Colloidal Deposition (HPCD) test (McGregor, Philippaerts 1998).**

More fundamental methods use wettability gradients on silica wavers to investigate the stability of pitch particles (Kekkonen, Stenius 2001).

## **2.3 Pitch Control**

Generally, three different techniques are considered for pitch control. Deresination refers to the term which includes process steps like storage of the wood and wash steps of the pulp. The two other techniques are directly related with specific additives, the dispersing of wood resin and its retention.

### ***2.3.1 Retention***

The term retention includes a variety of measures to control pitch problems. In fact all these measures aim to retain the wood resin in the final paper sheet and remove it from the water circuit in the final product. Since today's paper mills, for environmental reasons, tend to close their water circuits more and more, such an approach is clearly beneficial by avoiding the concentration of detrimental compounds in the water circuit (Biza 2001). The wood resinous fraction in paper mills can be retained by the use of adsorbents, multivalent inorganic cations, and polyelectrolytes (Hubbe et al. 2006). Typically, talc was the benchmark for deposit-control as an adsorbent mineral (Hubbe et al. 2006). A vast collection of publications can be found about the use of talc in pitch control (Allen, Douek 1993; Allen et al. 1993; Allen 1977; Allen 1980; Baak, Gill 1971; Boardman 1996; Biza 2001; Chang 1985; Douek, Allen 1991b; Dunlop-Jones et al. 1987; Gill 1974; Guera et al. 2005; Hamilton, Lloyd 1984; Hassler 1988; Holton, Moebus 1982; Hughes 1977; Kiser 1976; Kallio et al. 2004; Lee, Sumimoto 1991; Mosbye et al. 2003; Pereira 1990; Parmentier 1973; Parmentier 1979; Reynolds, Yordan 2002; Rogan 1994; Tijero et al. 2009; Willför et al. 2000; Yordan, Maat 1997). Also other minerals like bentonite (Asselman, Garnier 2000; Boardman 1996; Kallio et al. 2004; Kerman et al. 2006; Moebius 1978; Stockwell 1997), clay (Mosbye et al. 2003; Rogan 1994; Willför et al. 2000), asbestos (Williams 1987) or calcium carbonate were also described (Rogan 1994; Whiting 1997; Willför et al. 2000). The idea is to adsorb

the pitch onto the mineral surface and retain this composite in the fibre matt or if already agglomerated pitch is present to adsorb the mineral onto the pitch agglomerate rendering it less tacky and removing it as a powdered agglomerate within the fibre matt. Since this topic is the main focus of the whole study it will be discussed in section 2.5 about the use of mineral in pitch control.

Multi-valent inorganic cations present in the system are mainly aluminium, and more specifically papermaker's alum (aluminium sulphate) or poly-aluminium chloride (Allen 1980; Dreisbach, Michalopoulos 1989; Glazer 1991; Hubbe et al. 2006). The aluminium cationises the pitch surfaces and enhances the adsorption of the pitch droplets onto the fibres. The use of alum is only possible under acidic pH conditions which today are changing towards neutral or slightly alkaline, where other more hydroxylated aluminium formulations based on aluminium chloride are more efficient (Hubbe et al. 2006).

Finally, retention aids like acrylamide based polyelectrolytes as well as high charge cationic polymers as fixation aids are often applied as a second means for pitch control. Their use is summarised in various review articles (Hubbe et al. 2006; Wagberg 2000).

### ***2.3.2 Dispersion***

Various types of additives that stabilise the colloidal stability by either electrostatic or steric interactions can act to disperse the pitch droplets. They may include partially hydrophobic polymers that have a high affinity for hydrophobic pitch particles, polyacrylates or phosphates and also surfactants that reduced the hydrophobicity of the pitch droplets (Hubbe et al. 2006).

### **2.3.3 Deresination**

One major part of an efficient pitch control strategy is deresination. Two chapters are dedicated to deresination in the book of Back and Allen (2000). As this is not the major focus of the current work it will here be mentioned just for completeness. Deresination starts with storage of the wood prior to its use (Opedal et al. 2011). It can be done chemically or mechanically, i.e. resin removal during pulping and pulp washing. The wood preparation process starts with debarking and chip screening and continues with kraft pulping and kraft pulp washing. Deresination can also be performed by the sulphite process and during the production of Chemo Thermo Mechanical Pulp (CTMP). Mechanical deresination is also possible. Nowadays, with closed water circuits white water treatment is also required.

Furthermore pulp can be bleached. The principal aim of bleaching is, however, to brighten or whiten, but purification and deresination of the pulp can also be achieved during this step. Bleaching of chemical pulp is closely integrated with the cooking and washing process (Back, Allen 2000).

## **2.4 Minerals in paper making**

An artificial extension of the fibre with cheaper minerals has historically almost been regarded as “cheating” on paper quality. This changed in the 19<sup>th</sup> century after considering the positive impact of minerals on brightness, opacity and smoothness of the paper. Today, the most common fillers and pigments are (Bos et al. 2006; Paltakari 2009):

- Carbonates
  - Natural ground calcium carbonate (GCC) in the form of chalk, limestone or marble



- Synthetic precipitated calcium carbonate (PCC)
- Silicates
  - Kaolin clay or China-clay
  - Talc and related minerals
  - Bentonite
- Sulphates
  - Gypsum (Annaline)
  - Satinwhite (Calcium-aluminiumsulphate)
- Oxides
  - Titanium dioxide

Before 1970 mainly gypsum, china-clay, satinwhite and barite were in use, and by changing the acidic papermaking process towards neutral or even alkaline the use of high brightness calcium carbonate allowed a revolution in paper making.

Today, paper may contain up to 50 % of its weight of minerals in the case of multi-coated woodfree grades.

But minerals are not only added as fillers and coating pigments. Some minerals are also added for pitch control, like talc and Bentonite, the latter being frequently used also as part of a microparticle retention system (Dixit et al. 1991), used to retain filler in the fibre matrix during the draining phase of the wet paper stock on the paper machine wire bed.

### ***2.4.1 Talc and related minerals***

In everyday language, the word "talc" is used to describe the mineral, rock, or powder form of the soft layered silicate, talcum. Many different types of talc are used in paper making. Their properties differ according to the end-use requirements and are defined by the selected ore, milling and classification process and, finally, by the specific slurring technology used to bring the material into water suspension (Likitalo, Gantenbein 2009).

Often talc is associated with chlorite and in some countries talc and chlorite are substituted by its closest structural relative, pyrophyllite. Therefore, in chapter 5 focus is laid on the differences in pitch adsorption between these three related minerals.

#### ***2.4.1.1 History of talc in paper***

The use of talc in the paper industry has a long history: talc as a filler appeared for the first time in the beginning of the 20th century in France, Italy, Spain, Finland, and Japan, though its use in these countries may be predated in China. In pitch applications, Maurice Warner (Cyprus Minerals) launched the use of talc in 1960 (Likitalo, Gantenbein 2009). Following the technological evolution in paper production, talc as a coating pigment was introduced industrially in Finland and France in 1982. Since then, talc has become widely used in lightweight coated (LWC) rotogravure and coated wood free (WF) offset formulations applied mainly in matt and silk grades to aid primarily print rub resistance. Recently, another use has been found for talc in the coating of speciality papers, such as for barrier coatings for siliconised tape backing (release paper) or other water repellent and impermeable coatings (Likitalo, Gantenbein 2009).

#### ***2.4.1.2 Mineralogy of phyllosilicates***

Effectively, talc-bearing rocks contain a variety of different ores, of which the most abundant are chlorite - hence its importance for testing in the pitch control context,

calcium carbonate ( $\text{CaCO}_3$ ), dolomite ( $\text{CaMg}(\text{CO}_3)_2$ ), magnesite ( $\text{MgCO}_3$ ), and quartz ( $\text{SiO}_2$ ). The presence of these ancillary minerals may to some varying degree influence the effectiveness in pitch control. Consequently, the application efficiency of commercially available talc grades may not only be defined by the mineral talc alone but can also be influenced to some extent by the other minerals, either separately or in combination. Comparing the application efficiency of commercially available mineral grades needs, therefore, careful consideration of the mineralogical composition of the materials used.

The minerals talc, chlorite and pyrophyllite belong to the group of hydrous phyllosilicates. They typically display a platy habit, a perfect basal cleavage and are soft, with Mohs hardness of 1-2 for talc, chlorite and pyrophyllite.

Besides the many similarities, the three minerals also display important differences (Table 2-1) with respect to crystal structure and chemical composition in particular, that may influence many of their surface properties and, hence, their performance in a particular application.

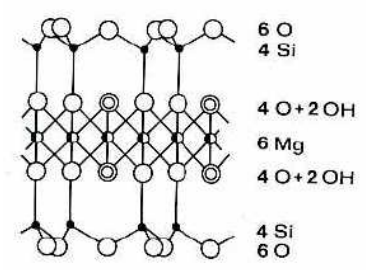
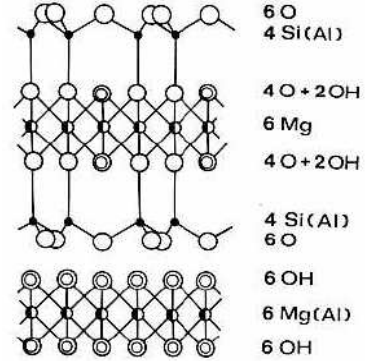
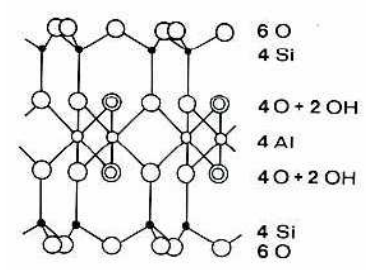
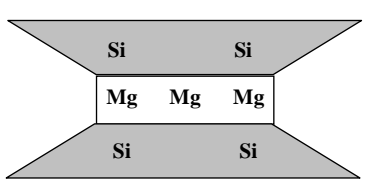
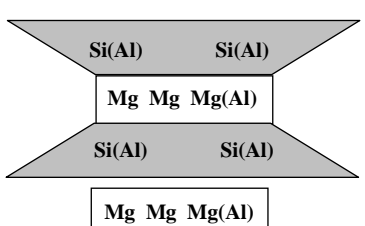
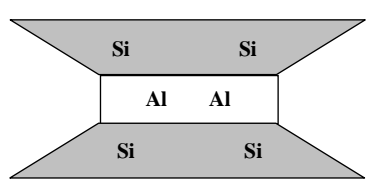
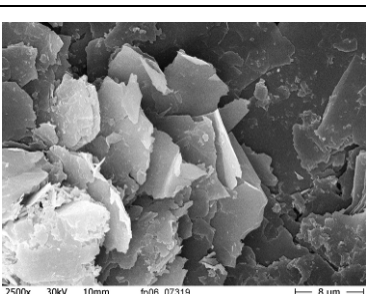
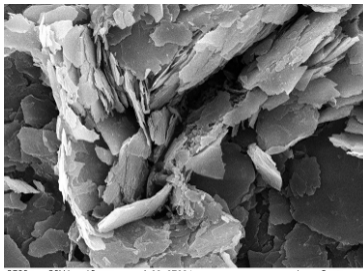
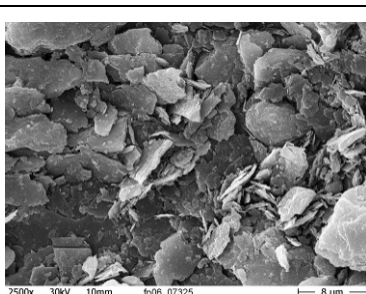
The mineral talc is the tri-octahedral form of the hydrous phyllosilicate group that consists of simple 2:1 layers, i.e. its crystal structure is composed of a layer of octahedrally coordinated cations embedded in a framework of oxygen atoms and hydroxyl groups. This “talc-like” layer is sandwiched between two layers of tetrahedrally coordinated cations coordinated to oxygen atoms alone (Evans, Guggenheim 1988). The chemical composition of most natural talc can be described, to a good approximation, by  $\text{Mg}_3\text{Si}_4\text{O}_{10}(\text{OH})_2$ . In theoretical terms talc contains 31.9 % MgO, 63.4 %  $\text{SiO}_2$  and 4.7 %  $\text{H}_2\text{O}$ . In naturally occurring crystals, Mg may be partially replaced by Al, Ni, Fe or Cr. Talc is a tri-octahedral layered mineral with a unit cell thickness of 0.92 nm (Bergaya et al. 2006). The talc lamellae are stacked on top of each

other and are composed of two tetrahedral layers of SiO<sub>2</sub> on either side of an octahedral central layer of Mg-OH (brucite). The hydrophobic and chemically inert character of talc comes from the SiO<sub>2</sub> layers on the basal surfaces of each lamella.

The mineral pyrophyllite may be regarded as the di-octahedral analogue of talc, i.e. its structure is also composed of a layer of octahedrally coordinated cations sandwiched between two sheets of linked SiO<sub>4</sub> tetrahedra. In contrast to talc, two-thirds of the octahedral sites are occupied by Al and the remainder are empty. Like talc, pyrophyllites show little deviation from their ideal chemical formula, which can be described by Al<sub>2</sub>Si<sub>4</sub>O<sub>10</sub>(OH)<sub>2</sub> (Bergaya et al. 2006).

The chlorite group of minerals comprise a large sub-group of hydrous phyllosilicates that consist of 2:1:1 layers, i.e. of negatively charged 2:1-layers of ideal composition (R<sup>2+</sup>, R<sup>3+</sup>)<sub>3</sub>(Si, Al)<sub>4</sub>O<sub>10</sub>(OH)<sub>2</sub> and of positively charged interlayers ((R<sup>2+</sup>, R<sup>3+</sup>)<sub>3</sub>(OH)<sub>6</sub>) that alternate along the crystallographic z-direction. Most natural chlorite samples are tri-octahedral and incorporate mainly Fe<sup>2+</sup>, Mg<sup>2+</sup>, Si<sup>4+</sup> and Al<sup>3+</sup> (Bailey 1988). Unlike talc and pyrophyllite, natural chlorite samples typically display a variable chemical composition that can be best described by the general mineral formula (Mg<sub>6-x-y</sub>Fe<sub>y</sub>Al<sub>y</sub>)(Si<sub>4-x</sub>Al<sub>x</sub>)O<sub>10</sub>(OH)<sub>8</sub>.

**Table 2-1: Overview of the three phyllosilicates: talc, chlorite and pyrophyllite.<sup>2</sup>**

Talc	Chlorite	Pyrophyllite
 <p>6 O 4 Si 4 O + 2 OH 6 Mg 4 O + 2 OH 4 Si 6 O</p>	 <p>6 O 4 Si(Al) 4 O + 2 OH 6 Mg 4 O + 2 OH 4 Si(Al) 6 O 6 OH 6 Mg(Al) 6 OH</p>	 <p>6 O 4 Si 4 O + 2 OH 4 Al 4 O + 2 OH 4 Si 6 O</p>
$Mg_3Si_4O_{10}(OH)_2$	$(Mg,Al)_6(Si,Al)_4O_{10}(OH)_8$	$Al_2Si_4O_{10}(OH)_2$
 <p>2:1 Layer</p>	 <p>2:1:1 Layer</p>	 <p>2:1 Layer</p>
 <p>2500x 30kV 10mm fp06_07319 8 μm</p>	 <p>2500x 30kV 10mm fp06_07331 8 μm</p>	 <p>2500x 30kV 10mm fp06_07325 8 μm</p>
Finland	France	South Africa

**2.4.1.2.1 Occurrence of talc and chlorite**

Talc deposits are formed as the result of transformations of existing rocks, carrying one or more of the building-block components (MgO, SiO<sub>2</sub>, and CO<sub>2</sub>) needed to form the mineral, under the effect of hydrothermal activity, which acts to combine the components and/or to introduce the complementary/missing components in solubilised

<sup>2</sup> Structure diagrams taken from Mineralogie 4th edition, Siegfried Matthes, Springer-Verlag, 1993.

form. As the mineral composition resulting from this process is naturally determined by the parent rock, each ore has its own geological signature formed many millions of years ago. As a natural ore, talc has always been found in combination with at least one other mineral. The most common of these is chlorite. Other associated minerals often found in talc include dolomite and magnesite. All types of talc are lamellar, the platelet size differing from one deposit to another. Large crystals occur in layers, often referred to as booklets, as they resemble the stacked pages of a small book, whilst small crystals provide a compact dense ore. The unique morphology and mineralogy of each talc source specifies its individual properties concerning specific functions for a particular application (Likitalo, Gantenbein 2009).

#### ***2.4.1.2.1.1 (A) Magnesium carbonate derivative ore bodies***

One kind of talc ore is known to evolve from the transformation of carbonates (dolomite and magnesite) in the presence of silica (Figure 2-9). The carbonates fix in-situ the magnesium component, whereas the silica is provided by hydrothermal circulation. This reaction results in talc which is either mineralogically pure or structurally associated with minerals such as carbonates, quartz and chlorite.

Deposits of this type represent about 70 % of world production and provide the whitest and purest talc ores. Examples are the deposits in Yellowstone (Montana, USA) and Respina (North-West Spain).

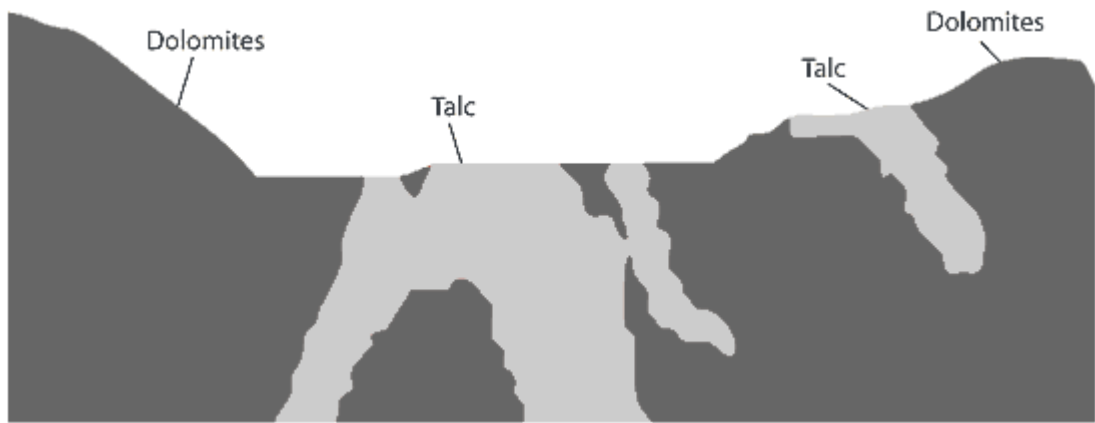


Figure 2-9: Simplified geological cross section through a magnesium carbonate ore. (<http://www.luzenac.com/geology.htm>)

#### 2.4.1.2.1.2 (B) Serpentine derivative ore bodies

About 20 % of the present world production comes from the transformation of serpentine into a mixture of talc and magnesium carbonate (Figure 2-11). This ore is commonly called “soapstone”. The crude ore is nearly always grey and as such would not be pure enough to be used directly as an industrial coating pigment. Flotation of the mineral is therefore applied to reduce the ancillary contaminants and so increase the talc content and consequently its whiteness (Figure 2-10).

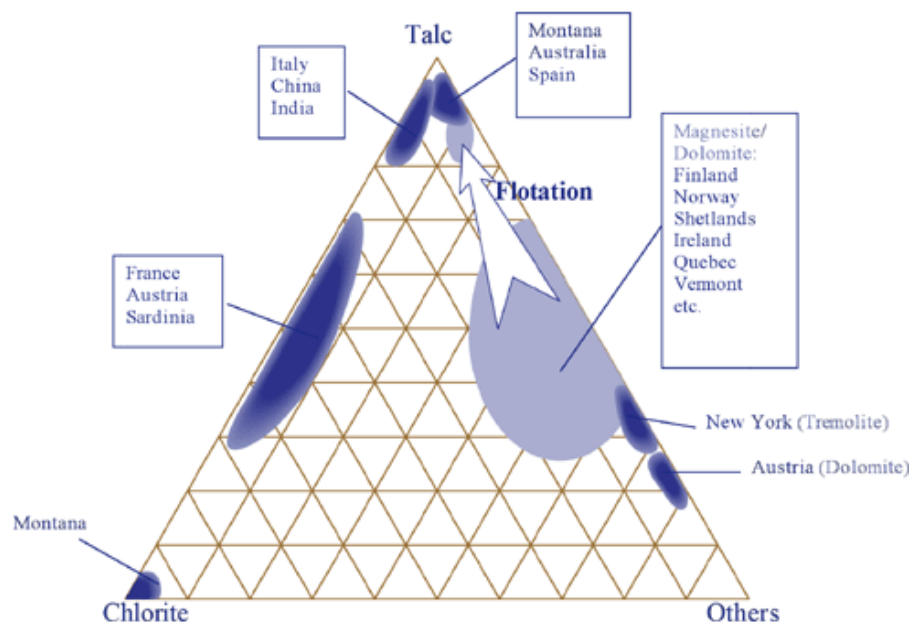


Figure 2-10: Schematic illustration of the different talc ore origins. Serpentine derivative ore bodies are upgraded by flotation to reach a high talc content and high whiteness. (<http://www.mondominerals.com/geology.asp>)

Soapstone deposits are relatively common and widely distributed along ultramafic rock belts. The term mafic is a shortening of the constituents, magnesium and iron (ferric). Ultramafic rocks are igneous rocks with silica content less than 45 %, generally greater than 18 % magnesium oxide and high iron oxide content. A significant proportion of coating talc grades in Europe and North America are developed from this type of ore, e.g. Vermont in the USA, Québec and Ontario in Canada and in Finland.

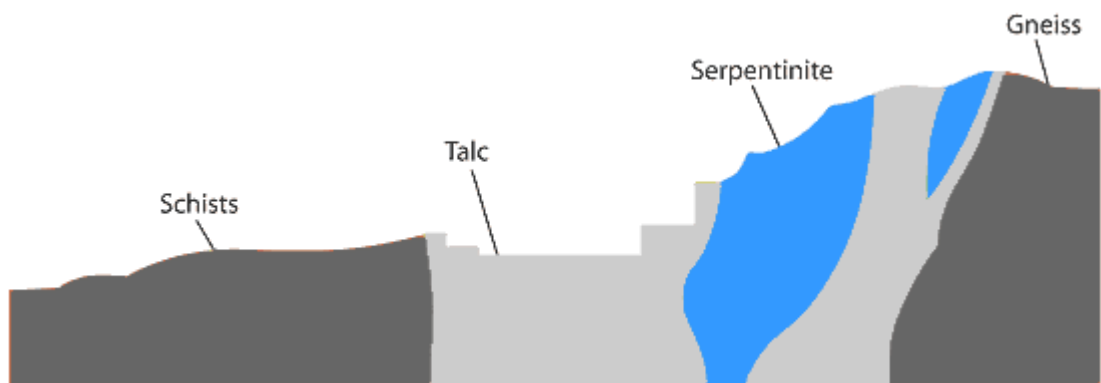


Figure 2-11: Simplified geological cross section through a serpentine derivative ore. (<http://www.luzenac.com/geology.htm>)

#### **2.4.1.2.1.3 (C) Silica aluminous rock derivative ore bodies**

Silica aluminous rock derivatives can often be found in association with deposits of type (A), described in section 2.4.1.2.1.1, for example linked to magnesium carbonate derivative ore, e.g. as can be found in the French Pyrénées. The crude ore is also generally grey due to the presence of associated minerals. The talc in these ore bodies is associated with chlorite, a mineral with quite similar characteristics containing brucite (Figure 2-12). Chlorite is used together with talc to obtain specific end-use properties. Ten percent of the world's talc production comes from these deposits.



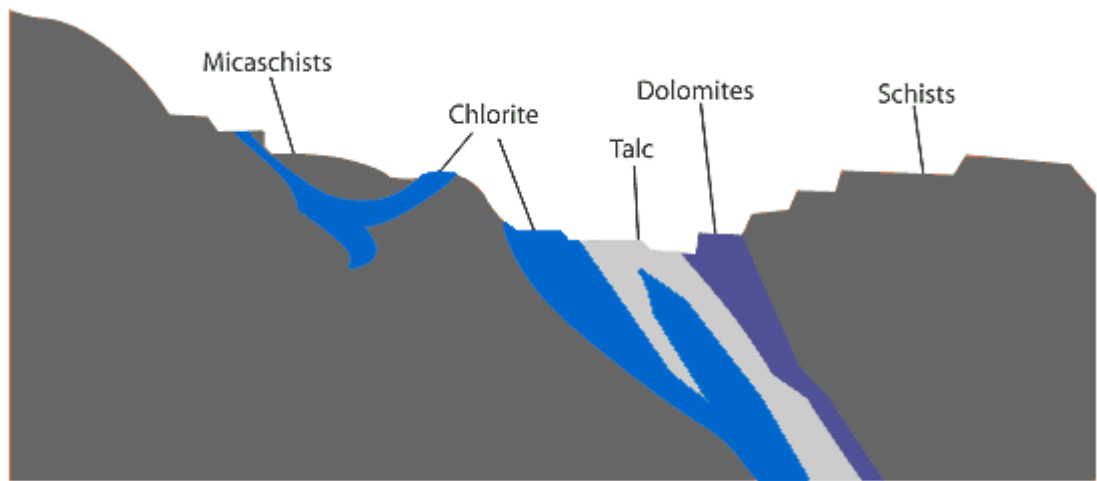


Figure 2-12; Simplified geological cross section through a siliceous derivative ore. (<http://www.luzenac.com/geology.htm>)

#### **2.4.1.2.1.4 (D) Magnesium sedimentary deposit derivative ore bodies**

The sedimentary ore type is only mentioned here for the sake of completeness. Currently, none of these deposits is exploited. The ore is generally a mixture of talc and quartz, sometimes associated with mica, clay, iron oxides and organic materials.

#### **2.4.1.3 Surface properties of talc, chlorite and pyrophyllite**

The bulk crystal structure of talc, chlorite and pyrophyllite is terminated by two different kinds of surfaces usually denoted as basal and edge-face, respectively. Whereas the structure and composition of the edge surfaces are comparable, important differences are observed with regard to the respective basal planes. Briefly, the edge surface of the three phyllosilicates is terminated by metal cations (primarily Fe, Mg, Si and Al), the charges of which are largely pH dependent, that can bind different ionic species. Owing to these similarities, comparable interaction between the edge surfaces of talc, chlorite and pyrophyllite with their local environment may be expected. In contrast to the edge surface, large differences can exist between the basal surface of talc and pyrophyllite on the one hand, and chlorite on the other hand.

Qualitatively, the two different types of surface can be described as being hydrophobic for the basal surface and hydrophilic for the edge surface, and the hydrophilic brucite

layer being additionally present in the case of chlorite. However, the terms hydrophobic and hydrophilic describe only the behaviour of a phase against water. Following the suggestion of Fowkes (1963) the two terms can be written in a more quantitative form dividing the surface energy into an apolar component and a polar component. Therefore, the surface energy  $\gamma^{\text{Tot}}$  of a phase  $i$  can be written as,

$$\gamma_i^{\text{Tot}} = \gamma_i^{\text{LW}} + \gamma_i^{\text{AB}}$$

**Equation 2-1**

in which the designation LW stands for Lifshitz-van der Waals and summarises London, Keesom and Debye components (van Oss et al. 1988), and the polar component is best described by the Lewis acid-base (AB) theory. Values found in the literature for talc and pyrophyllite are reported in Table 2-2, in which  $\gamma^{\text{A}}$  is the acid component and  $\gamma^{\text{B}}$  is the basic component out of which  $\gamma^{\text{AB}}$  is formed by the geometric mean of the two.

**Table 2-2: Values of the interfacial surface free energy components of talc and pyrophyllite (Giese et al. 1991).**

<b>Mineral</b>	$\gamma^{\text{Tot}} / \text{mJm}^{-2}$	$\gamma^{\text{LW}} / \text{mJm}^{-2}$	$\gamma^{\text{A}} / \text{mJm}^{-2}$	$\gamma^{\text{B}} / \text{mJm}^{-2}$
Talc	36.6	31.5	2.4	2.7
Pyrophyllite	39.1	34.4	1.7	3.2

Alternative values are given by Schrader and Yariv (1990) such as a Lifshitz-van der Waals component  $\gamma^{\text{LW}}$  of 35.5 mJm<sup>-2</sup> for talc, and they separate the total surface interaction into a dispersive and non-dispersive component having the ratio 7 : 3, respectively. The remarkably low values for the Lewis acid-base components explain the observed hydrophobicity of the two minerals in the presence of highly polar water molecules (Giese et al. 1991).

The above mentioned values are measured for samples in environmental atmosphere and are therefore suitable to be considered in an aqueous environment. Values on the other hand for outgassed samples of talc and talc-chlorite mixtures are reported by Douillard et al. (1994) and Malandrini et al. (1997). Higher values for the apolar component  $\gamma^{LW}$ , but also for the polar components  $\gamma^A$  and  $\gamma^B$ , were measured, concluding therefore that outgassed talcs are highly polar compounds essentially because of their high surface acidity. This is explained by open hexagonal cavities in the ring-like SiO surface structure where the underlying O-atoms of the brucite layer are accessible for hydrogen bonding. When these activities are blocked by adsorbed molecules (mainly gas) under ambient conditions, the whole layer is rendered hydrophobic (Michot et al. 1994). What remains unclear is why this is also suggested for adsorbed water vapour by some authors (Malandrini et al. 1997) who assume that, in the presence of ambient moisture, the acid sites are rendered inactive.

Another approach tried to define the different types of surface by adsorption in aqueous environment (Charnay et al. 2001). Four different species were used, namely

1. highly water soluble organic anionic molecule → benzene sulphonate
2. highly water soluble organic cationic molecule → benzyltrimethylammonium bromide
3. amphiphilic organic anionic surfactant → sodium dodecylsulphate
4. amphiphilic organic cationic surfactant → benzyldimethyldodecylammonium bromide

The four types of molecules were adsorbed independently on different talc / chlorite blends, containing between 3 and 53 % (w/w%) chlorite. The adsorption of the highly soluble charged molecules showed that the hydrophilic surface area is only adsorbing

positively charged species and the density of positively charged surface sites on the minerals is very low. The adsorption of the anionic surfactant essentially occurs through dispersive interactions. The amphilic cationic surfactant adsorbed on both types of surface, hydrophobic and hydrophilic, and subtraction of the hydrophilic surface area determined by the adsorption of the highly water soluble cationic molecule gave the same hydrophobic surface areas as determined by the adsorption of the anionic surfactant. With increasing chlorite content the hydrophilic surface area not accessible for anionic species linearly increased (Figure 2-13).

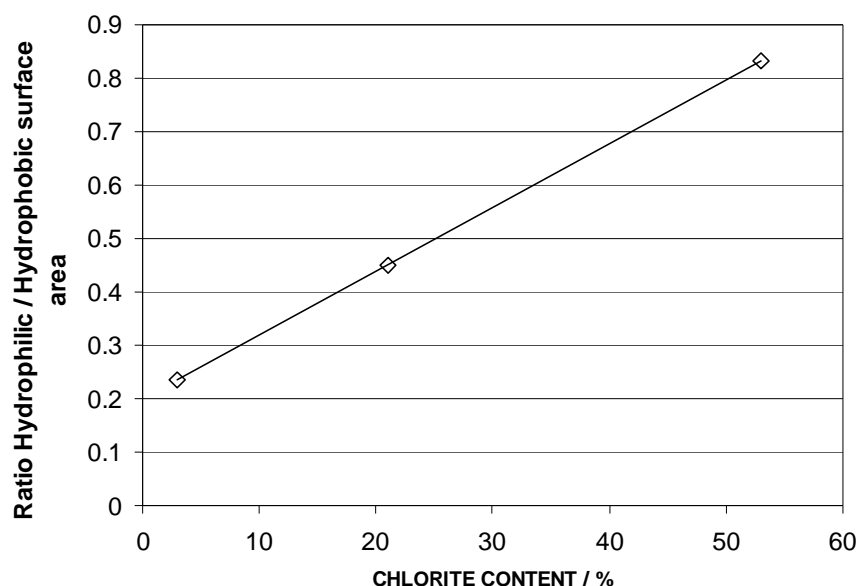
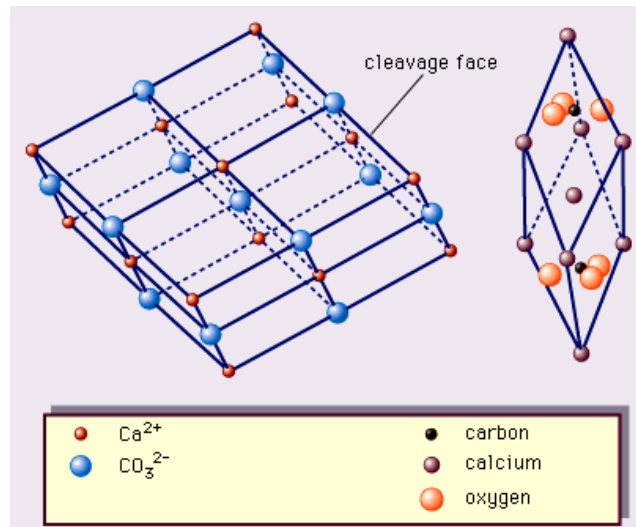


Figure 2-13: Ratio between hydrophilic and hydrophobic surface area for different talc / chlorite mixtures with approximately  $10 \text{ m}^2\text{g}^{-1}$  specific surface area (Charnay et al. 2001).

### 2.4.2 Calcium carbonate

Calcium Carbonate ( $\text{CaCO}_3$ ) can be found in a vast myriad of types and forms. It is a structural component of most skeletal creatures and is part of an unbroken cycle and so, in principle, is inexhaustible. The majority of deposits were formed by the capture of  $\text{CO}_2$  from the atmosphere by microorganisms which combined the dissolved gas with calcium ions to form their exo-skeleton providing protection and structural support. Consumption by higher vertebrates also captured the mineral in their bone skeletal

structures. Deposits of coccoliths formed chalk beds at the sea bottom, which, with the inclusion of snail and mussel deposits later became transformed under pressure to form limestone, and in some cases combining high pressure and temperature to promote recrystallisation into marble, the hardest and brightest form of calcite (Gane 2001).



**Figure 2-14: Crystal structure of calcite<sup>3</sup>.** The schematic shows both (left) the true unit cell the calcite rhombohedron, which contains 2[CaCO<sub>3</sub>] and (right) an alternative cell based on the cleavage rhombohedron.

The Ca atoms (red) (Figure 2-14) are at the corners and body centre position of a trigonal lattice with  $\alpha = 46^\circ$  and a lattice parameter of 0.06361 nm. The planar CO<sub>3</sub> (blue) radicals are at about  $\frac{1}{4}$  and  $\frac{3}{4}$  the distance along the major diagonal. Each Ca atom has 6 closest oxygen atoms. The CO<sub>3</sub> groups are arranged in a flat triangle with the C in the middle (Gane 2001).

The calcium carbonates used in this study were of calcitic type (Figure 2-15), ground from natural rock deposits. The surface free energy of calcite has been extensively studied in the past, with widely differing results. Holysz and Chibowski (1994) used a wicking technique and the Lucas-Washburn (LW) equation (Lucas 1918; Washburn 1921) to determine the surface free energy of CaCO<sub>3</sub>. They calculated a Lifshitz-van der

<sup>3</sup> Encyclopaedia Britannica

Waals interaction of  $48 \text{ mJm}^{-2}$  and an acid-base electron donor parameter of  $79.0 \text{ mJm}^{-2}$ . Papierer et al. (1984) found  $58 \pm 6 \text{ mJm}^{-2}$  for the dispersive component of the surface energy of  $\text{CaCO}_3$  using inverse gas chromatography. Using the same technique, Keller and Luner (2000) found surface energy values for ground chalk samples of 140-180  $\text{mJm}^{-2}$ , for marble and precipitated (pcc)  $\text{CaCO}_3$ , 55  $\text{mJm}^{-2}$  and for thermally treated pcc, 250  $\text{mJm}^{-2}$ . Janczuk et al. (1987) used contact angle measurement (static sessile drop) on prepared marble surfaces, and calculated a dispersive interaction component of  $64 \text{ mJm}^{-2}$  and polar component  $106.6 \text{ mJm}^{-2}$ . Adamson (1990) summarised a number of crystal cleavage experiments, among which, for  $\text{CaCO}_3$ , the value of  $230 \text{ mJm}^{-2}$  is given for the 001 plane. Schoelkopf (2002) reviewed all these earlier approaches and came to the conclusion that the effective surface energy of calcite is largely influenced by crystallographic rearrangement of the crystallite surface layers and immediate adsorption of other species out of the surrounding environment (mainly water) following the generation of freshly cleaved surfaces. Furthermore, all the approaches based on wetting experiments have to be treated carefully, either because of assumed values of parameters or the formation of surface layers due to film flow. The results suggest that the high values approach those of the intrinsic values of the material, while the lower values report the surface free energy as it is reduced towards the value of the adsorbate present, probably water or other airborne contaminants.

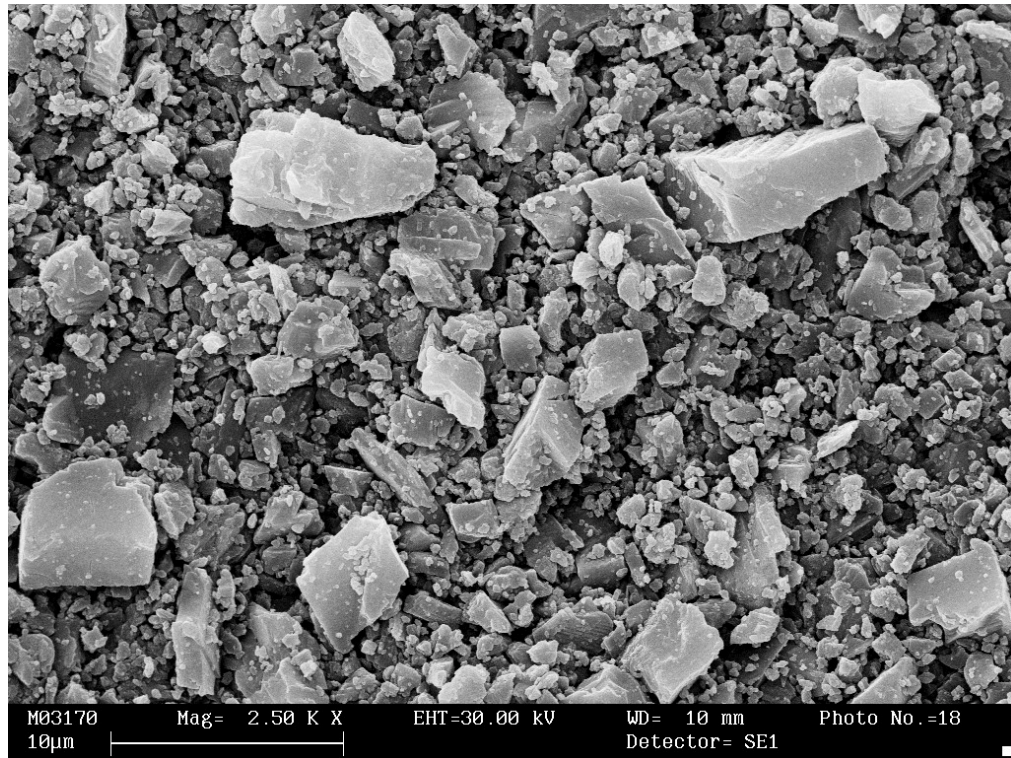


Figure 2-15: SEM image of a ground natural calcium carbonate (marble) [Omya].

Fatty acid treatment of calcite was investigated previously (Compton, Brown 1995; Fenter, Sturchio 1999; Osman, Suter 2002; Papirer et al. 1984). The overall view is that fatty acid molecules such as stearic acid self-assemble on the terminal faces of the calcite crystals by chemisorption, forming a layer of calcium stearate with the carboxylic groups attaching to the calcite lattice and the aliphatic chains forming a kind of molecular “bristle” or “brush”. For the estimation of the surface coverage, Equation 2-2 was used in which  $m_{SA}$  is the mass of stearic acid (SA) that has to be added to treat the calcite with a surface coverage fraction by stearic acid  $X_{SA}$ . This is calculated with the specific surface area of the mineral  $\epsilon_{BET}$  obtained via nitrogen adsorption, the molecular weight of stearic acid  $M_{wSA}$ , the Avogadro constant  $N_A$  and the surface area that is covered by one stearic acid molecule  $A_{SA}$  which is  $0.26 \text{ nm}^2$  (Papirer et al. 1984).

$$m_{SA} = \frac{\epsilon_{BET} \cdot M_{wSA} \cdot X_{SA}}{A_{SA} \cdot N_A}$$

Equation 2-2

Synthetic  $\text{CaCO}_3$  (PCC) is made by firstly reversing the natural process endothermically, driving off the  $\text{CO}_2$  once more, subsequently slaking in water exothermically followed by reprecipitation of the carbonate by bubbling through  $\text{CO}_2$ . This can be made under carefully controlled concentration and temperature conditions to form any of the commonly useful crystal habits of  $\text{CaCO}_3$ : rhombohedral calcite (as found in marble), prismatic, spherically agglomerated and scalenohedral (“cigar”-shaped crystals occurring frequently in a clustered form) (Figure 2-16a). The aragonitic (needle form) habit is more difficult to produce and is generally reserved for specialised coating applications (Gane 2001; Schoelkopf 2002) (Figure 2-16b).

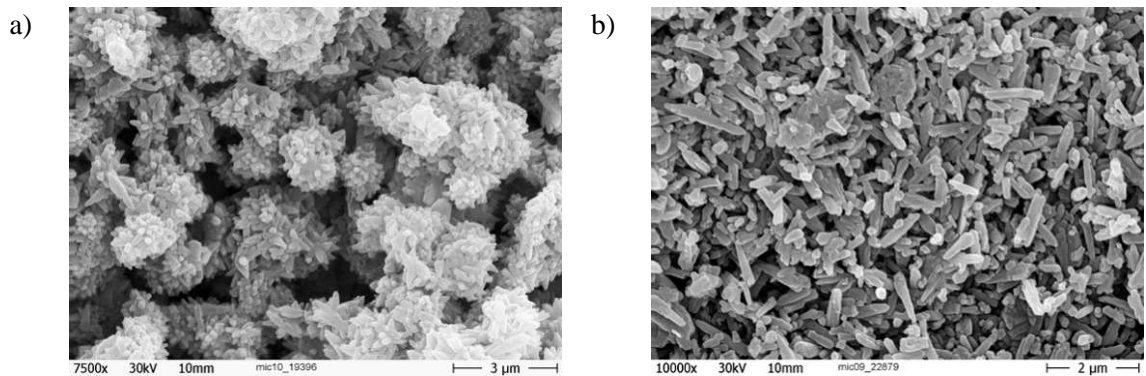


**Figure 2-16: a) SEM image of a scalenohedral precipitated calcium carbonate (S-PCC) and b) a aragonitic precipitated calcium carbonate A-PCC [Omya].**

Modified calcium carbonate (MCC) is formed from calcium carbonate and phosphate via an in-situ surface re-precipitation (Beuleke, Burri 1999; Gane et al. 1999; Gane 2001; Ridgway et al. 2004). MCCs have hydrophilic surfaces and exhibit both calcium phosphate and carbonate crystalline structure. MCC is a porous material with a discretely bimodal pore size distribution when formed into a packed bed (Figure 2-17).



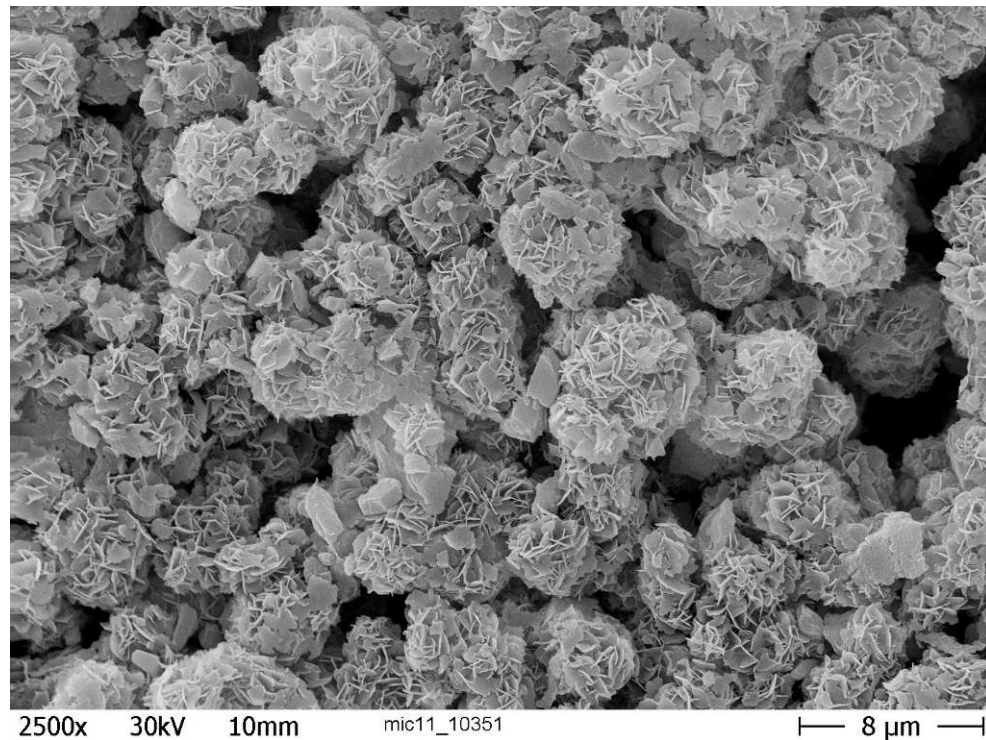


Figure 2-17: SEM image of a modified calcium carbonate with a rosy structure [Omya].

### ***2.4.3 Particle size and aspect ratio***

#### ***2.4.3.1 Importance and definitions of aspect ratio***

Mineral particles are used as fillers in a range of applications, including paper, decorative and functional coatings, plastics and ceramics (Baudet et al. 1993; Ferrage et al. 2003; Gane et al. 1995; Gane 2001; Lohmander 2000; Murray, Kogel 2005; Naito et al. 1998). Frequently, the morphology of the particles constituting the mineral within a desired particle size distribution can be a key factor in determining the functionality of the end use. Mineral particles such as talc are found in paper coatings and as paper fillers in the bulk of the fibrous sheet. They are also applied as filtration aids or as a component in fixed bed reactors (Aris 1957; Casal et al. 1985), and found in cosmetic products (Papirer et al. 1992). In all these application fields, the particle shape is of great importance. For example, in paper, platy talc or acicular aragonite provide for coating coverage and internal bulk, respectively. Minerals may also expose different surface properties, depending on the orientation of the particulate in respect to its

morphology. The ratio of anisometric surfaces may control properties such as wettability to certain liquids, which can affect mineral processing and end-use function or the rheological behaviour of a particle suspension (Gane, Coggon 1987; Gane, Watters 1989; Gane et al. 1997; Kroon et al. 1998; Morris et al. 1965; Mourchid et al. 1995; Mourchid, Levitz 1998). A typical example was given by Yekeler et al. (2004) and Yildirim (2001) in respect to the specific adsorption potential of a mineral in relation to its surface differential properties. Similarly, minerals used as catalysts owe their functionality to the exposure of the required reactive surface. Thus, for simple planar and longitudinal geometries, it is crucial for assessing particle-related performance to ascertain a representation of the aspect ratio (Li et al. 2002). Aspect ratio,  $\rho$ , expresses the relative abundance of the two characteristic surfaces of platy particles (Figure 2-18), and is defined generally as the ratio of the major axis dimension to that of the minor dimension. In the case of platy particles this is given by the ratio of the major diameter,  $d_d$ , of the planar platelet to its laminar thickness,  $t_d$  (Equation 2-3). The thickness of a platy particle may for some minerals be in the region of a few nanometres, having thus an effectively very high localised curvature and thus a very high surface free energy.

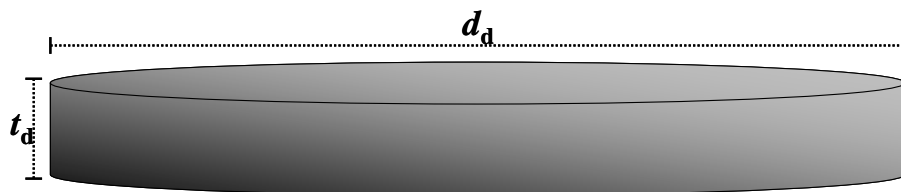


**Figure 2-18: Definition of the disc-like approximation for a high aspect ratio platelet.**

The particle size and shape are not only important for disc-like particles but also for rod-like and fibrous particles (Figure 2-19). These parameters, for example, control the rheological properties of dispersions (Baltar et al. 2009; Pabst et al. 2006b; Yin et al. 2009). Properties of particulate materials in other applications, like catalysis,

environmental control or drug delivery, may also be affected by the particle shape (Yang et al. 2010). The aspect ratio of a rod-like particle is defined by the ratio of its length,  $l$ , divided by its width,  $w$  (Equation 2-4), and is, thus, the reciprocal pendant to the aspect ratio of a platy particle.

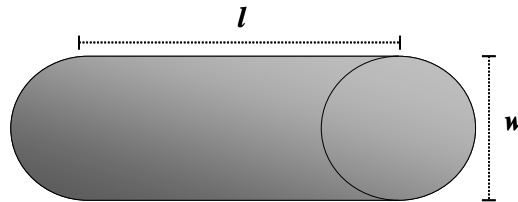


Figure 2-19: Definition of the aspect ratio of a rod.

$$\rho = \frac{d_d}{t_d}$$

Equation 2-3

$$\rho = \frac{l}{w}$$

Equation 2-4

Besides these definitions above other terms may be used to describe the nature of particles and particle shapes (Table 2-3, Figure 2-20).

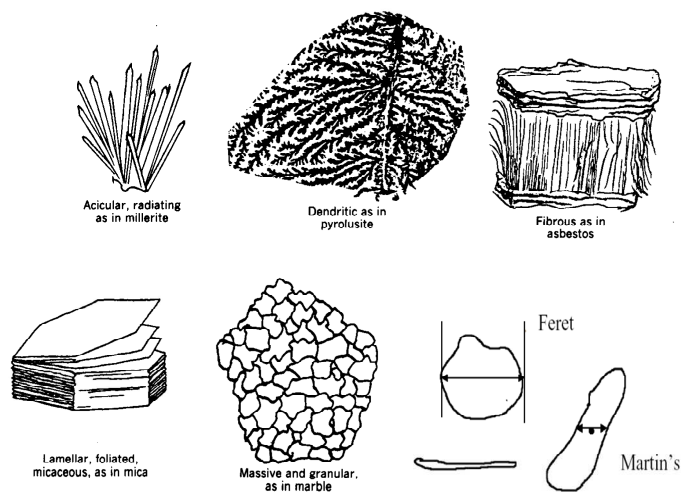


Figure 2-20: Definitions of particles and particle shape (Allen 1990).

**Table 2-3: Definitions of particles and particle shapes (Allen 1990).**

<b>Name</b>	<b>Definition of particle shape</b>
Acicular	Needle-shaped
Angular	Sharp edged or having roughly polyhedral shape
Crystalline	Of geometric shape, freely developed in a fluid medium
Dentritic	Having a branched crystalline shape
Fibrous	Regularly or irregularly thread-like
Flaky	Plate-like
Granular	Having approximately an equidimensional irregular shape
Irregular	Lacking any symmetry
Modular	Having a rounded, irregular shape
Spherical	Globule shaped

### ***2.4.3.2 Methods to evaluate the aspect ratio***

Different techniques to measure or determine aspect ratios were reported in the literature. A vast number of studies (Baudet et al. 1993; Jennings, Parslow 1988; Lohmander 2000; Pabst et al. 2000; Pabst et al. 2001; Pabst et al. 2006a; Pabst et al. 2006b; Pabst, Berthold 2007; Pabst et al. 2007; Slepety, Cleland 1993) described how laser ensemble diffraction and single particle light scattering (static and dynamic) offer an opportunity to measure aspect ratios. The same authors also referred to gravitational sedimentation, which is effective for particles greater than the suspension-maintained Brownian motion limit. Many of the above quoted methods had their basis in the work published by Jennings and Parslow (1988). They derived the transformation of an equivalent spherical diameter (*esd*), as manifest by the various sizing techniques, into the major particle dimension, i.e. platelet diameter for the cases studied here (Table 2-4).

**Table 2-4: Formulae to calculate the disc diameter,  $d_d$ , and rod length,  $l$ , based on the  $esd$  ( $d_s$ ,  $d_a$ ,  $d_v$  and  $d_T$ ) response from the corresponding particle sizing method.**

Particle sizing method	Disc	Rod
Sedimentation	$d_s = d_d \sqrt{\frac{3}{2 \cdot \rho} \tan^{-1}(\rho)}$	$d_s = \frac{l}{\rho} \sqrt{\frac{3}{2} \ln \rho}$
Laser light scattering / Projected area (Fraunhofer)	$d_a = d_d \sqrt{\frac{1}{2} + \frac{1}{\rho}}$	$d_a = l \sqrt{\frac{1}{\rho} + \frac{1}{2\rho^2}}$
Laser light scattering / Particle volume (Mie theory)	$d_v = d_d \sqrt[3]{\frac{3}{2 \cdot \rho}}$	$d_v = l \cdot \sqrt[3]{\frac{3}{2\rho^2}}$
Photon correlation spectroscopy / Translational diffusion	$d_T = \frac{d_d}{\tan^{-1}(\rho)}$	$d_T = \frac{l}{\ln(2\rho)}$

$\rho$  : aspect ratio

$d_s$  : particle diameter based on sedimentation

$d_a$  : particle diameter based on projected area / static laser light scattering  
with Fraunhofer optics

$d_v$  : particle diameter based on particle volume / static laser light scattering  
with Mie theory

$d_T$  : particle diameter based on translatory diffusion / photon correlation  
spectroscopy (PCS)

By combining two of the particle size measurement methods, e.g. sedimentation and projected area, Jennings and Parslow (1988) extracted an aspect ratio defined purely at one given particle size (Equation 2-5), or, depending on the light scattering technique, an ensemble average value of a distribution of particles, which is derived for oblate spheroids, and can, thus, be adopted to calculate the aspect ratio of platy minerals. In the

limit of extremely high aspect ratio, the formula reduces to that for a circular disc (Equation 2-6).

$$\frac{d_S}{d_a} = \sqrt{\frac{2 \cdot \rho \cdot \tan^{-1}(\sqrt{\rho^2 - 1})}{\rho \cdot \sqrt{\rho^2 - 1} + \ln(\rho + \sqrt{\rho^2 - 1})}}$$

**Equation 2-5**

$$\frac{d_S}{d_a} = \sqrt{\frac{3 \cdot \tan^{-1}(\rho)}{\rho + 2}}$$

**Equation 2-6**

A similar approach was presented by Pabst and Berthold (2007) (Equation 2-7). However, the model of Pabst and Berthold (2007) overestimates the aspect ratio. In the case of high aspect ratios  $\tan^{-1}(\rho)$  becomes  $\pi/2$  and so Equation 2-6 can be solved for  $\rho$  (Equation 2-8) which shows that the approximation of Pabst and Berthold (2007) differs from the Jennings and Parslow (1988) model by an addition of 2.

$$\rho = \frac{3\pi}{2} \cdot \left(\frac{d_a}{d_S}\right)^2$$

**Equation 2-7**

$$\rho + 2 = \frac{3\pi}{2} \cdot \left(\frac{d_a}{d_S}\right)^2$$

**Equation 2-8**

For rods, the Jennings-Parslow solution (Jennings, Parslow 1988) as the limit of prolate spheroids (Equation 2-9) was considered, too. This reduces in the limit for extremely thin rods to Equation 2-10. However, image analysis from micrographs is the typical tool to obtain a number based aspect ratio distribution for rod-like minerals (Pabst et al. 2007).

$$\frac{d_s}{d_a} = \sqrt{\frac{2 \cdot \rho \cdot \ln(\rho + \sqrt{\rho^2 - 1})}{\sqrt{\rho^2 - 1} + \rho^2 \cdot \tan^{-1}(\sqrt{\rho^2 - 1})}}$$

**Equation 2-9**

$$\frac{d_s}{d_a} = \sqrt{\frac{\frac{3}{2} \cdot \ln(\rho)}{\rho + 2}}$$

**Equation 2-10**

Another method including the turbidity of colloidal kaolinite particles as a function of random or shear flow orientation was used to extract shape information as presented by Champion et al. (1979). Champion et al. (1978) also published a magneto-optical method to determine the particle shape via the particle area (permanent magnetic moment) and the particle volume (magnetic susceptibility anisotropy). Another possibility identified, was to use scanning and transmission electron microscopy together with image analysis, employing such techniques as particle shadowing (Conley 1966; Morris et al. 1965; Podczeck 1997; Yekeler et al. 2004). Further literature exemplified methods including FTIR measurements made from deuterium structure-exchanged particles (Ferrage et al. 2003) or calorimetric measurements (Groszek, Partyka 1993; Yildirim 2001).

X-ray diffraction (XRD) was also regularly used to describe surface texture of compacted powders, and particle orientation, but the technique also delivered information related rather to crystallite size than to particle size or relative anisotropy. The correlation of crystallite size and peak width was first described by Scherrer (1918). Also small angle X-ray scattering measurements were reported by some authors to estimate the aspect ratio of disc-like particles like Laponite (Kroon et al. 1996; Kroon et al. 1998).

## **2.5 Minerals in Pitch control**

As touched upon earlier the use of mineral in pitch control is well known. Minerals like talc, kaolin, bentonite, asbestos and calcium carbonate have been reported in the literature, and, especially in the case of talc, are widely used in the industry to control the tacky materials from wood and recycled fibre processing.

### ***2.5.1 Talc***

The use of talc as a pitch control agent is well accepted in the papermaking industry and it has been the benchmark for many studies. The surface properties of talc allow preferential interactions between hydrophobic groups of molecules, polymers or colloids, and the hydrophobic basal surface of talc. In that way talc may either adsorb amphiphilic molecules, polymers and colloids, or it may be adsorbed on to microscopic aggregates of such materials (Figure 2-21) (Allen 1980; Allen et al. 1993; Holton, Moebus 1982; Hubbe et al. 2006). Up to 50% of the talc was found to be retained in such aggregates (Dunlop-Jones et al. 1987). In this way the detrimental substances are retained in the paper sheet, and so removed from the papermaking system. Allen (1980) quantified that 14 pitch particles were adsorbed per talc platelet. Furthermore, also dissolved fatty- and resin acid soaps can adsorb onto talc (Allen 1980; Allen et al. 1993; Willför et al. 2000). Dissolved hemicellulose (Jenkins, Ralston 1998; Mosbye et al. 2003), lignin and its derivatives (Allen et al. 1993; Allen, Douek 1993; Willför et al. 2000) as well as defoamers (Allen et al. 1993; Benecke et al. 2009; Douek, Allen 1991a; Gribble et al. 2010) show a high affinity for the talc surface and compete with the colloidal wood resin, which may lead to a decreased efficiency of the added talc or, conversely, reduce deposition problems connected with defoamers.

The influence of the resin composition has only partially been investigated, most work being confined to either the use of pure model compounds or blends thereof. Some



authors found that fatty acids are preferably adsorbed over fats and over resin acids (Hamilton, Lloyd 1984; Hughes 1977), whereas others found the opposite - a preferred adsorption of fats over fatty acids (Rogan 1994). It was also found that the composition of the wood resin prior and after the adsorption did not change and, thus, that the wood resin droplets are adsorbed as one unit without a preferred selection of single components (Tijero et al. 2009; Willför et al. 2000). That, however, might be different at increased pH levels where substantial amounts of the fatty- and resin acids are dissolved and compete with the colloidal wood resin (Allen, Douek 1993).

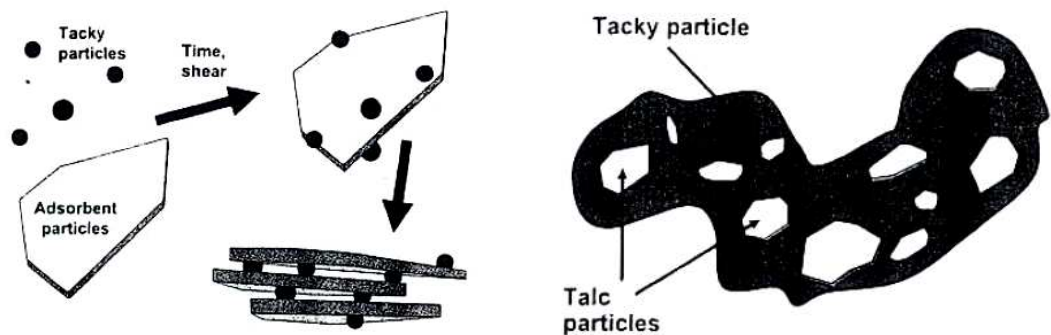


Figure 2-21: Model of talc as an adsorbent for tacky particles (left) and adsorbed onto tacky aggregates (right) (Hubbe et al. 2006).

Whereas the observations discussed above mainly covered adsorption phenomena, the action of talc is often also described as one of detackification (Allen et al. 1993). Such a mechanism involves, of course, adsorption in either direction (organic onto mineral or mineral onto organic). Only a small portion of the total wood resin was found to be adsorbed onto talc in the presence of fibres (Allen, Douek 1993; Allen 1980). Thus, the conclusion was drawn that only destabilised pitch particles are adsorbed, whereas those particles that are stabilised are either bound to the fibres or remain stable in colloidal suspension (Garver, Yuan 2002; Gill 1974). Further, in the case of destabilised pitch droplets, which either had started to agglomerate or already had agglomerated, the incorporation of talc in these composites led to a change in the pitch rheology and therefore to a reduced tackiness and hence to a detackification (Allen et al. 1993; Douek, Allen 1991a; Holton, Moebus 1982; Hubbe et al. 2006). In this manner talc has

shown itself to be an efficient tool in the task of reducing deposits related to wood resin as well as a general reduction in the content of dissolved and colloidal substances as determined by the various reported techniques.

Depending on the source of wood and the specific pulping process the composition of the dissolved and colloidal substances can vary. For example, the wood resin from Aspen was found to have a higher affinity for the talc surface than that from softwood (Allen et al. 1993). Also, differences between bleached and unbleached TMP were observed. In particular, hemicellulose types, which were deacetylated during bleaching, did not adsorb onto talc but preferably did so onto the fibres (Willför et al. 2000). Allen and co-workers (Allen, Douek 1993; Allen et al. 1993) as well as Parmentier (1979) made studies on Kraft pulp samples with special focus on the black liquor, i.e. the liquor arising after cooking the fibres in the Kraft process. The presence of fibres is crucial since they naturally adsorb dissolved and colloidal substances depending on various parameters like pH, temperature or on the additives present. In some studies, therefore, samples have been filtered (Guera et al. 2005) or centrifuged (Willför et al. 2000) prior to the adsorption experiments, or taken directly from the white water system. Others have used model pitch, which was previously extracted from a pulp sample (Mosbye et al. 2003; Otero et al. 2000). In other cases artificial blends of typical compounds found in wood resin were used (Chang 1985; Hughes 1977). In the most idealised cases single compounds found in wood resin like oleic acid, abietic acid or triolein have been studied in isolation (Hamilton, Lloyd 1984; Rogan 1994).

Process parameters which might influence the adsorption, such as pH and temperature were also investigated. Both impact on the solubility of the resin components and hence their appearance in the aqueous phase. The temperature has a direct influence on the thermodynamic equilibrium of the adsorption. Furthermore, the pH also affects the

colloidal stability of the wood resin droplets. Under acidic pH the fatty- and resin acid soaps become protonated and the electrostatic repulsion decreases. This leads to a preferred adsorption of wood resin droplets onto the talc surface but in the presence of fibres, for example, the wood resin droplets preferably adsorb onto the fibres. Alkaline pH leads on one hand to saponification of fatty acid ester, and a resulting deprotonation of the fatty- and resin acids. Both mechanisms result in a higher anionic charge with a resulting increased electrostatic stability of the wood resin droplets (see section 3.2.6), and this strong influence of the pH on the adsorption efficiency of wood resin onto talc was reported (Allen et al. 1993; Hamilton, Lloyd 1984; Trafford 1988). The higher the pH, the lower is the adsorption efficiency. An influence of the temperature on the adsorption of wood resin *per se* onto talc was, however, not identified (Douek, Allen 1991a; Hamilton, Lloyd 1984) but temperature was seen to affect the adsorption of hemicellulosic materials, like guar-gum onto talc was identified. This observation was attributed to the entropically driven preference of hydrophobic interactions of the methylene groups within the carbohydrates monomers and the siloxane ( $\text{R}_2\text{Si}(\text{O}^-)_2$ ) groups in the hydrophobic basal surface of the talc particles (Jenkins, Ralston 1998). All these quoted studies were thus either performed in the presence of fibres, which is clearly relevant for the paper making environment, performed using only model compounds or wood resin extractives without the presence of natural stabiliser like hemicelluloses and lignin derivatives, or the studies only reported a very narrow pH range. Therefore, a detailed evaluation of the impact of these two process parameters pH and temperature is still required, and forms one experimental facet of this thesis.

Mineralogical and morphological properties were also determined as playing an important role. The most commonly occurring impurity in talc is chlorite. The opinions in the literature differ in respect to the impact of chlorite on the performance of talc as a pitch control agent. Some have found a reduced adsorption capacity of chlorite

compared to talc (Chang 1985; Baak, Gill 1971), and generally it was suggested to use talc in as pure a form as possible (Holton, Moebus 1982). Others, however, did not see a reduced adsorption capacity of talc containing high amounts of chlorite (Guera et al. 2005). These inconclusive findings require, therefore, a more thorough evaluation. A common opinion was that an increase in surface area is beneficial for an increased adsorption of wood resin materials onto talc (Allen et al. 1993; Allen, Douek 1993; Baak, Gill 1971; Chang 1985; Hamilton, Lloyd 1984; Holton, Moebus 1982) and even a linear proportionality was described between surface area of the talc and the pitch adsorption capacity (Guera et al. 2005). The surface area increase can be obtained by delamination of the talc platelets which can be induced by high shear in a mill or even in a fibre stock (Allen, Douek 1993).

Several mechanisms have been proposed to explain the adsorption of dissolved and colloidal substances from wood processing onto talc. Some authors considered the surface free energy of talc and wood resin to be the driving force, and calculated that the wetting of wood resin on talc is thermodynamically favoured (Baak, Gill 1971; Mosbye et al. 2003). This consideration is of course not false as soon as two particles have made contact, but in an aqueous environment the barrier to obtain full contact between two particles is influenced strongly by other factors, such as electrostatic repulsion of the double layers and steric interactions between polymers (Napper 1983). A perfect example of that discrepancy was even shown by Mosybe et al. (2003), who calculated that the wetting of wood resin is thermodynamically favoured also for kaolin. As we will see later kaolin is known and was described to be much less efficient than talc in the adsorption of wood resin (Hughes 1977). The inability of the DLVO theory (Derjaguin, Landau 1941; Verwey, Overbeek 1948) to describe the interaction between two hydrophobic particles like talc and wood resin led some authors to consider another mechanism which was considered as belonging to the general phenomenon known as

hydrophobic interaction force (Wallqvist et al. 2006; Wallqvist et al. 2007). The force was identified to be a long-range attractive one induced by gas/vapour cavities as a result of either gas/vapour layers already surrounding the hydrophobic particles or an induced vaporisation under the pressure drop arising from the establishment of gas-liquid menisci. It can be visualised in terms of the fluid air, i.e. gas in this case, “wetting” the hydrophobic surface to the exclusion of the liquid water at the air-water meniscus interface boundary. This force was first shown acting between talc and silanised silica, and thiolised gold, using atomic force probe microscopy (AFM), and later on also between abietic acid colloids and talc. As described above, however, a lot of surface active components are also present in typical paper mill water. Amphiphilic compounds such as fatty and resin acids will act to reduce the surface tension of the water, and, hence, diminish this effect. Further, adsorbed hemicellulose or lignosulphonates on the pitch particles substantially decrease the hydrophobic character of the pitch and with it the possibility of gas entrapment on the particles. Nevertheless, Willför et al. (2000) have shown that for bleached TMP samples hemicellulosic materials are not involved in the pitch adsorption and preferably adsorb onto the wood fibres, and in such cases the hydrophobic force remains and plays a crucial role. The same authors have shown that hemicellulosic materials are involved in the adsorption of dissolved and colloidal substances from unbleached TMP and proposed that these surface-active hetero polysaccharides can play a key role in the adsorption mechanism. Due to the high affinity of the acetylated galactoglucomannans (Ac-GGMs) to both the talc and the pitch, they may establish a bridging contact between the two particles.

Once the pitch is adsorbed, the adsorption process was typically described as being irreversible (Baak, Gill 1971; Holton, Moebus 1982; Kiser 1976; Tijero et al. 2009). This is, however, contradicting the observations of others who investigated the adsorption behaviour by means of adsorption isotherms. In some cases the adsorption

isotherms could be modelled with Langmuir (1916) and/or Freundlich (1907) isotherms. These models, by definition, only apply, as we will see in section 2.6, for reversible adsorption systems (Rogan 1994; Tijero et al. 2009). Other workers applied the principle of adsorption isotherms but did not fit any specific model, but found that not all the pitch, even with excess of free talc surface area, adsorbed onto the talc (Douek, Allen 1991a; Hamilton, Lloyd 1984; Hughes 1977).

The addition of the talc should be as early as possible in the process, and definitely has to be dosed before problems occur. Due to the chemical inertness the effectiveness of the talc surface is not altered throughout the various acidic, alkaline or bleaching steps during the fibre processing (Baak, Gill 1971). In order to find the right talc dosage, the suggestion was to overdose the talc since under-dosing can even deteriorate the situation (Hassler 1988). After the deposition problem has been eliminated, the talc dosage can be stepwise reduced until the point where pitch deposition starts again and subsequently the talc dosage can be slightly increased until the problems disappear.

In other studies and product developments the talc was modified. The idea was to collect anionic trash with cationic talc (Biza 2001; Reynolds, Yordan 2002). While some authors found promising results with such talcs, others could not identify any efficiency difference from that of normal talc (Guera et al. 2005).

Although talc is well accepted for pitch control, its use in the control of stickies and white pitch is, however, not so unanimously accepted. Nevertheless, some positive results were found for talc in sticky control (Gruber et al. 2001; Maat, Yordan 1998; Putz et al. 2003; Williams 1987; Yordan, Maat 1997). These authors mainly focussed on the reduction of depositable material caused by the addition of talc rather than on the adsorption of the sticky components themselves onto the talc.

### **2.5.2 Bentonite**

The use of bentonite in paper making is well known, especially as a retention system in combination with cationic polymers (Allen, Lapointe 2005; Hubbe et al. 2006). Its use as a pitch and sticky control agent is also often quoted and some studies have investigated this in detail. In general bentonite was found to reduce the chemical oxygen demand in fibrous suspensions, a measure for the amount of organic material, and also the overall amount of colloidal substances (Auhorn, Melzer 1979; Boardman 1996; Moebius 1978; Stockwell 1997; Williams 1987). Some studies even found a higher *pro rata* efficiency for bentonite than for talc as an adsorbent. This is not surprising given the huge differences in typical specific surface area of the two minerals.

A more detailed study of the action of bentonite used model compounds to represent the components of dissolved and colloidal substances. Dextran was used as the model compound for hemicellulose. Lignin was also included and a model colloidal suspension of abietic acid (Asselman, Garnier 2000). The authors found that the polymeric materials, dextran and lignin, adsorb in a monolayer as random coils. The affinity of the bentonite surface was higher for the dextran than for the lignin. The abietic acid was adsorbed with extremely high loadings, this being attributed to a monolayer formation of colloidal droplets. This is in contrast to the adsorption of oleic acid which was found to form a molecular monolayer on bentonite (Rogan 1994). This effect is most probably related to the different melting points of abietic (173.5 °C) and oleic (13 °C) acid.

### **2.5.3 Kaolin**

Despite its lack of hydrophobicity, kaolin has also been considered as a pitch and sticky control agent, since it is part of the inorganic fraction of a paper mill and often present in immense quantities in comparison to wood resin components.

Chang (1985) did not find any activity of kaolin in adsorbing pitch from a synthetic model suspension. In the review of Hubbe et al. (2006) kaolin is described to work only in combination with cationic polymers. Some authors calculated that wood resin will wet a kaolin surface based on the surface free energy of the two materials (Mosbye et al. 2003). Rogan (1994) determined a Langmuir adsorption isotherm for oleic acid onto kaolin. Also Willför et al. (2000) identified a potential for kaolin in pitch adsorption. The observation was attributed to the amphoteric property of kaolin having cationic and anionic sites on its platy structure.

#### ***2.5.4 Calcium carbonate***

The list of publications that investigated the action of calcium carbonate in pitch and stickies control is rather short. Rogan (1994) quantified the adsorption potential of calcite, silicate treated calcite, and stearic acid treated calcite for oleic acid. Only for the case of stearic acid treated calcite was a Freundlich isotherm applied to the data. The idea of hydrophobisation, and therefore the opportunity to mimic the properties of talc is striking. Unfortunately, the author was not very clear about the degree of hydrophobising. The direct quantification of the isotherm for the untreated calcite and the silicate treated calcite failed due to Ca-soap precipitation. Willför et al. (2000) found that ground and precipitated calcium carbonate mainly adsorbed lipophilic extractives from unbleached TMP. The problem with this detailed study is that the authors did not properly describe the calcium carbonates used for the study and it appears that the products were all of anionically dispersed nature. The anionic dispersing system of the calcium carbonates are known to corrupt its adsorption potential (Whiting 1997).

Finally, Gruber et al. (2001) identified the potential of natural and precipitated calcium carbonate to reduce tacky deposits that originate from sticky contaminants like ethylene vinyl acetate (EVA) hot melts. The minerals, however, were also seen to be



incorporated in deposits together with polyacrylic latex, and hence even increased the amount of deposits.

### **2.5.5 Other minerals**

Besides the many known minerals used in paper making, only a few others than those described above have been tested for their potential in pitch and stickies control. Materials like amorphous SiO<sub>2</sub> showed no activity in pitch control (Chang 1985). Others like TiO<sub>2</sub> were seen to have only a weak affinity for pitch or sticky materials (Gruber et al. 2001; Willför et al. 2000). Also materials from the family of asbestos have been studied and shown to have some potential in pitch and sticky control. Their amphoteric nature with cationic and anionic sites allowed adsorption of anionic trash (Moebius 1978; Williams 1987). Needless to say, the rather old studies in this case did not consider the health issues related to the material!

## **2.6 Adsorption**

A process in which a substance (sorbate) becomes associated with a solid phase (sorber) is generally termed sorption. If the substance attaches to a locally described two-dimensional surface, the term *adsorption* is used (Figure 2-22). *Absorption* on the other hand, refers to a penetration by positive attraction of a substance into a three-dimensional porous matrix (Schwarzenbach et al. 2003).

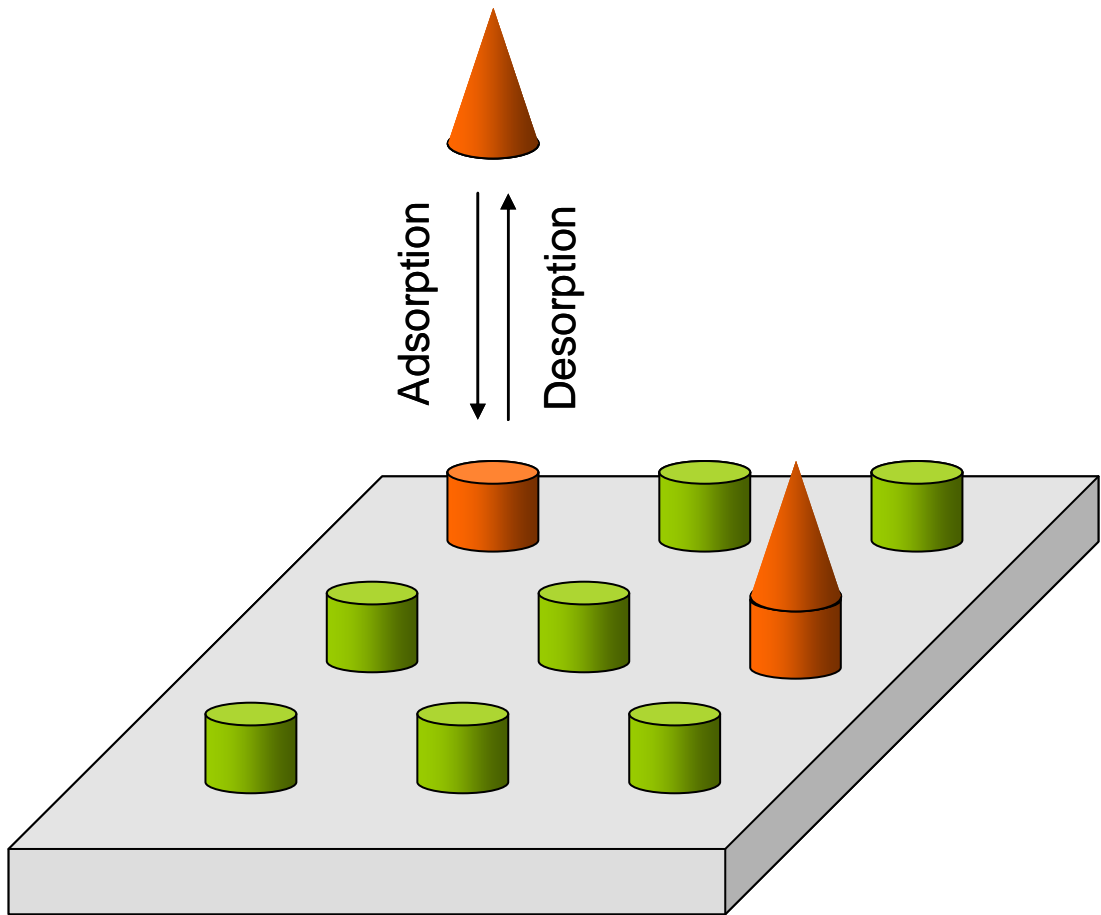


**Figure 2-22: General scheme of adsorption on a two-dimensional surface (grey) with various adsorption sites (green and orange cylinders) and the adsorbate that adsorbs onto available surface sites (orange cones).**

Physisorption refers to interactions between the adsorbate and the surface via one or more of van der Waals forces, acid-base interactions, and ionic interactions. Chemisorption involves the formation of a new co-valent bonding between surface and substrate. The adsorption can be formulated as a reaction (Figure 2-23). The reaction speed of the adsorption,  $v_{\text{ads}}$ , is defined by the concentration of the adsorbate in solution,  $c_{\text{sol}}$ , the available surface sites,  $(1-\Gamma)$  and the adsorption rate,  $k_{\text{ads}}$ . The desorption reaction speed,  $v_{\text{des}}$ , is only defined by the concentration of the adsorbate on the adsorbent which is defined by the fractional covered surface sites,  $\Gamma$ .

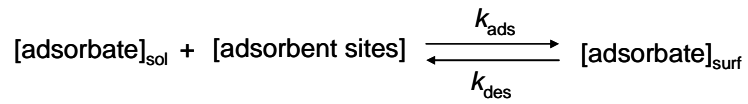


Figure 2-23: Adsorption reaction scheme.

$$v_{\text{ads}} = \frac{dc_{\text{sol}}}{dt} = k_{\text{ads}} \cdot c_{\text{sol}} \cdot (1 - \Gamma)$$

Equation 2-11

$$v_{\text{des}} = \frac{dc_{\text{sol}}}{dt} = k_{\text{des}} \cdot \Gamma$$

Equation 2-12

In equilibrium,

$$v_{\text{ads}} = v_{\text{des}}$$

Equation 2-13

and so

$$k_{\text{ads}} \cdot c_{\text{sol}} \cdot (1 - \Gamma) = k_{\text{des}} \cdot \Gamma$$

Equation 2-14

with

$$K_{\text{eq}} = \frac{k_{\text{ads}}}{k_{\text{des}}}$$

Equation 2-15

we can write then

$$\Gamma = \frac{K_{\text{eq}} \cdot c_{\text{sol}}}{1 + K_{\text{eq}} \cdot c_{\text{sol}}}$$

Equation 2-16

By defining the total surface sites per unit adsorbent surface the classical Langmuir (1916) isotherm can be written as

$$\Gamma_{eq} = \frac{K_L \cdot \Gamma_{max} \cdot c_{eq}}{1 + K_L \cdot c_{eq}}$$

Equation 2-17

with  $c_{eq}$  as the equilibrium concentration of the adsorbate in solution, the equilibrium concentration of the adsorbate on the adsorbent,  $\Gamma_{eq}$ , the equilibrium constant for the adsorption reaction often quoted as Langmuir constant,  $K_L$ , and  $\Gamma_{max}$  as the total surface sites on the adsorbent.

### **2.6.1 Langmuir isotherm**

The Langmuir isotherm (Equation 2-17) has been derived above based on the adsorption process described in Figure 2-23. While carefully considering the reaction it becomes apparent the model is only applicable if two conditions apply:

- i. Constant adsorption energies throughout the whole adsorption process. This implies that the adsorbates on the surface do not affect the further adsorption process. Furthermore, also the surface is considered homogeneous.
- ii. The surface contains a defined amount of total adsorption sites and if they have been covered no further adsorption takes place, resulting in an adsorbate monolayer.

The isotherm was originally developed for the adsorption of gases and later modified for the adsorption from solution. The isotherm was applied in many studies where the adsorption of wood resin constituents onto mineral particles was investigated (Asselman, Garnier 2000; Hamilton, Lloyd 1984; Hughes 1977; Rogan 1994; Tijero et al. 2009).

### 2.6.2 Freundlich isotherm

The Freundlich isotherm (1907) is an empirical relationship to describe adsorption processes (Equation 2-18). It has been derived to explain the solubility of gases in liquids or on surfaces, that did not follow Henry's law (Henry 1803).

$$\Gamma_{\text{eq}} = (K_{\text{F}} \cdot c_{\text{eq}})^n$$

Equation 2-18

$\Gamma_{\text{eq}}$  and  $c_{\text{eq}}$  are the equilibrium concentrations of the adsorbate on the adsorbent and in solution, respectively, and  $K_{\text{F}}$  is the Freundlich constant.  $n$  is the Freundlich exponent and if  $n = 1$  the Freundlich isotherm is equivalent to Henry's law. The case where the adsorption energy increases during the process of adsorption is indicated by an exponent  $n > 1$ , and in the case where the adsorption energy decreases over the process of adsorption the exponent is  $0 < n < 1$ . Also the Freundlich isotherm was applied to describe the adsorption process of wood resin constituents onto minerals as shown by Rogan (Rogan 1994) for the adsorption of oleic acid onto a stearic acid treated calcite.

### 2.6.3 Other useful isotherms

Various combinations of Langmuir and Freundlich type isotherms have been reported (Kinniburgh 1986). All these empirical isotherms account for changing adsorption energies by modifying the equilibrium constant over the adsorption process. These are the Langmuir-Freundlich isotherm (Equation 2-19), the Redlich-Peterson (1959) isotherm (Equation 2-20) and the Tóth (1971) isotherm (Equation 2-21) with the corresponding equilibrium constants  $K_{\text{LF}}$ ,  $K_{\text{RP}}$  and  $K_{\text{T}}$ , respectively.

$$\Gamma = \frac{(K_{\text{LF}} \cdot c_{\text{eq}})^n \cdot \Gamma_{\text{max}}}{1 + (K_{\text{LF}} \cdot c_{\text{eq}})^n}$$

Equation 2-19

$$\Gamma = \frac{K_{RP} \cdot c_{eq} \cdot \Gamma_{max}}{1 + (K_{RP} \cdot c_{eq})^n}$$

Equation 2-20

$$\Gamma = \frac{K_T \cdot c_{eq} \cdot \Gamma_{max}}{1 + (K_T \cdot c_{eq})^{1/n}}$$

Equation 2-21

These isotherms are not relevant in the current study but are mentioned for completeness. Additionally, other adsorption models are also known such as the Frumkin model, Temkin model, Dubinin-Radushkevich or the Flory-Huggins isotherm.

#### **2.6.4 Brunauer, Emmett, Teller isotherm**

Gas adsorption instruments typically use nitrogen as adsorbate for the determination of surface area. The most common surface area equation used is the BET equation shown in Equation 2-22. The BET theory is an extension of the Langmuir theory for monolayer molecular adsorption. The following hypotheses are made by BET theory: (a) gas molecules physically adsorb on a solid in layers infinitely; (b) there is no chemical interaction between each adsorption layer and (c) the Langmuir theory can be applied to each layer (Brunauer et al. 1938).

$$\frac{1}{v \left( \frac{P_0}{P} - 1 \right)} = \frac{K_{BET} - 1}{v_m \cdot K_{BET}} \cdot \left( \frac{P}{P_0} \right) + \frac{1}{v_m \cdot K_{BET}}$$

Equation 2-22

$P$  and  $P_0$  are the equilibrium and saturation pressure, respectively, of the adsorbates at the temperature of adsorption,  $K_{BET}$  is the BET constant,  $v$  the volume of gas adsorbed and  $v_m$  the monolayer adsorbed gas quantity. The BET constant can be expressed by Equation 2-23.

$$K_{\text{BET}} = e^{\left(\frac{E_1 - E_L}{RT}\right)}$$

Equation 2-23

where  $R$  is the universal gas constant,  $T$  is the absolute temperature, and  $E_1$  and  $E_L$  are the energy of adsorption for the first layer and for the second and higher layers respectively. Equation 2-22 can be plotted as a straight line, with a linear relationship maintained in the range of  $0.05 < P/P_0 < 0.35$ . A typical BET plot is illustrated in Figure 2-24 with  $P/P_0$  plotted on the  $x$ -axis and  $P/(v(P_0 - P))$  plotted on the  $y$ -axis.

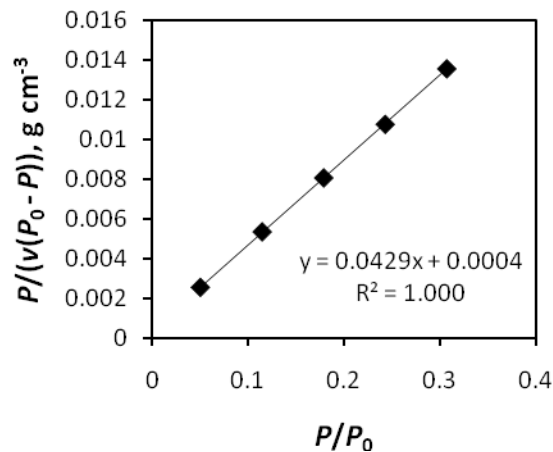


Figure 2-24: BET plot for a modified calcium carbonate [Omya].

The slope  $a$  and the intercept  $b$  of the best fit line are used to calculate the BET constant  $K_{\text{BET}}$  and the monolayer adsorbed gas quantity  $v_m$ :

$$v_m = \frac{1}{a + b}$$

Equation 2-24

$$K_{\text{BET}} = 1 + \frac{a}{b}$$

Equation 2-25

The monolayer adsorbed gas quantity is then used to calculate the surface area of the skeletal material in the porous matrix as shown in Equation 2-26.

$$\varepsilon_{\text{BET}} = \frac{V_m \cdot N_A \cdot \varepsilon_{\text{gas}}}{V_m}$$

**Equation 2-26**

where  $\varepsilon_{\text{BET}}$  is the surface area,  $N_A$  Avogadro's number,  $\varepsilon_{\text{gas}}$  the cross sectional area of adsorbent gas, and  $V_m$  the molar volume of adsorbate gas. All gas adsorption experiments are carried out under isothermal conditions, so the molar volume of adsorbate gas does not change (Gribble 2011).

The form of the BET equation for a system with a solute as adsorbate is given in Equation 2-27.  $\Gamma_{\text{Mono}}$  is the monolayer of adsorbate on the adsorbent and  $c_{\text{sat}}$  is the maximum solubility of the adsorbate in the solvent.

$$\Gamma = \frac{K_{\text{BET}} \cdot \Gamma_{\text{Mono}} \cdot c_{\text{eq}}}{(c_{\text{sat}} - c_{\text{eq}}) \cdot \left( 1 + \frac{(K_{\text{BET}} - 1) \cdot c_{\text{eq}}}{c_{\text{sat}}} \right)}$$

**Equation 2-27**

Figure 2-25 a) – d) illustrate some exemplified isotherms as discussed above. The linear isotherm with its Freundlich deviation is shown in Figure 2-25 a), the Langmuir isotherm in Figure 2-25 b), the Langmuir-Freundlich (LF) isotherm, the Redlich-Peterson (RP) isotherm and the Tóth (T) isotherm in Figure 2-25 c) together with a Langmuir isotherm as comparison. Whenever the constant  $n$  in these three isotherms is 1 they are identical with the Langmuir isotherm. Finally, in Figure 2-25 d) the BET isotherm can be seen.



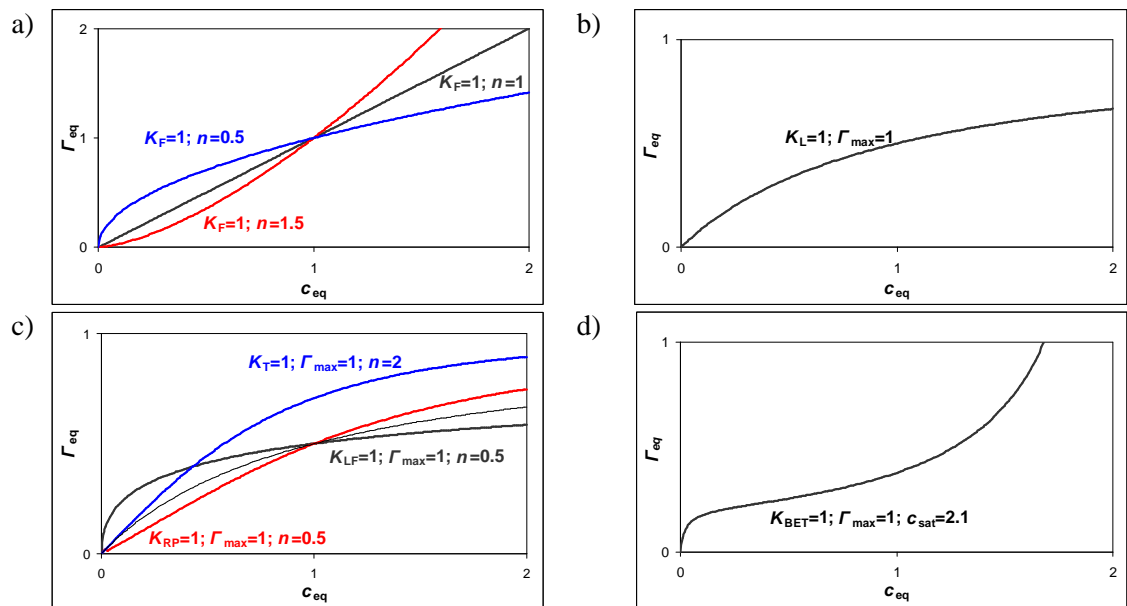


Figure 2-25: Overview of the different adsorption isotherms. a) Freundlich isotherms with  $K_F=1$  and  $n=0.5$  (blue),  $n=1.0$  (black), and  $n=1.5$  (red). b) Langmuir isotherm with  $K_L=1$  and  $\Gamma_{\max}=1$ . c) Langmuir-Freundlich (black) with  $K_{LF}=1$ ,  $\Gamma_{\max}=1$  and  $n=0.5$ ; Redlich-Peterson isotherm (red) with  $K_{RP}=1$ ,  $\Gamma_{\max}=1$  and  $n=0.5$ ; and Tóth isotherm (blue) with  $K_T=1$ ,  $\Gamma_{\max}=1$  and  $n=2.0$ . d) BET isotherm with  $K_{BET}=1$ ,  $\Gamma_{\max}=1$  and  $c_{\text{sat}}=2.1$ . The equilibrium concentration in solution,  $c_{\text{eq}}$ , and on the surface,  $\Gamma_{\text{eq}}$ , are both dimensionless.

### 2.6.5 Colloidal Deposition

The isotherms above were derived either for the adsorption of gas onto solid substrates or for solutes from solution onto a solid substrate. The colloidal substances from the wood pitch fraction behave differently from either gases or dissolved molecules. The sorption process of colloids on solid substrates is also often referred to as irreversible adsorption or colloidal deposition. Such processes are often described by the Random Sequential Adsorption (RSA) model (Hinrichsen et al. 1986). Much work has been published in this area and the literature given here is far from complete, but does provide some of the main background to the topic (Adamczyk et al. 1990; Adamczyk et al. 2002; Adamczyk et al. 2009; Schaaf, Talbot 1989; Semmler et al. 1998; Semmler et al. 2000; Senger et al. 2000). Colloidal particles adhere on a solid substrate by non specific interactions. These interactions are based on van der Waals, hydrophobic and electrostatic forces, and hydrogen bonding. All these interactions lead either to reversible or irreversible attachment. In the case of the reversible attachment, the colloid can explore the whole collector surface through diffusion and repeated desorption. This process can be studied using equilibrium mechanics. Irreversible attachment implies

that, once fixed on a surface, the colloids neither desorb nor diffuse on the collector surface. This latter process can not be studied, therefore, by equilibrium mechanics (Senger et al. 2000). Since all the adsorption studies are based on adsorption isotherms, it is assumed that the adsorption process of wood components onto minerals is reversible. If it was observed otherwise it is discussed in the respective chapter.

## 3 Techniques

All experimental techniques used during the PhD project are summarized in this chapter, with some background information. If not mentioned otherwise deionised water (18.3 MΩ) was used and the experiments run at room temperature (21-24 °C). All chemicals used were of analytical grade supplied by Sigma Aldrich.

### 3.1 Preparation of the mineral particles

In most of the experiments mineral particles are involved. This section gives a short overview of how the minerals were prepared.

#### *3.1.1 Talc, chlorite and pyrophyllite*

This family of lamellar phyllosilicate minerals are typically available as dry powders and have to be dispersed in water. A convenient way to prepare an aqueous suspension of these minerals is to place water in a beaker and add the mineral under stirring to form a 10 wt% solids suspension. Typical stirrers employed for this suspension makedown are of the so-called dissolver type, having saw-tooth disks. Often, for such hydrophobic materials, this shear force is not sufficient to properly deagglomerate and wet the particles properly. Wetting and proper dispersing are, however, key to access the complete surface area of the minerals. Therefore, in a second step, the aqueous mineral dispersion is treated with high shear mixers like Polytron or Megatron from Kinematica AG<sup>4</sup>.

One aim of the study is to understand the effect of surface area of the mineral particles on the adsorption efficiency for pitch. In order to fulfil this, mineral particles of the

---

<sup>4</sup> Kinematica AG, Luzernerstrasse 147a, 6014 Luzern, Switzerland

same origin but with increasing specific surface areas are required. In section 2.4.1.3 the surface properties of the phyllosilicates has been described as hydrophobic on the basal surface (crystallographic *001* plane). The resulting weak hydrophobic interactions between the individual platelets allow them to be quite readily exfoliated (delaminated) to create additional surface area (Figure 3-1). The delamination process can be run in a glass beaker using a stirrer and glass beads with a size range of 1.0 – 1.6 mm. An aqueous dispersion of 10 wt% of the mineral is added and the mixture with the beads stirred vigorously. The result is a combination of slight grinding and delamination. The course of grinding can be followed by analysing the particle size, and the delamination in relation to grinding by the specific surface area.

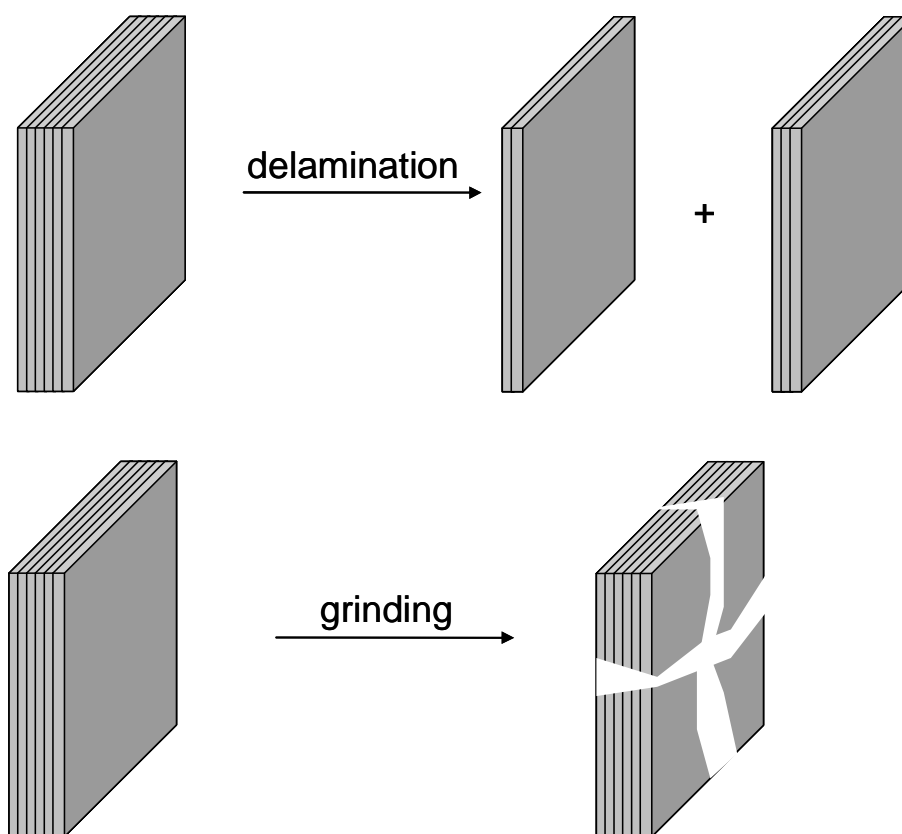


Figure 3-1: Schematic drawing of the grinding and exfoliation/delamination of a platelet shaped material.

### ***3.1.2 Hydrophobised calcium carbonate***

Calcium carbonate, either ground or precipitated form, can be treated in aqueous suspension or as a dry powder with fatty acid to render the surface oleophilic. In this

study a dry treatment was chosen to establish comparable hydrophobicity of that of talc. The powder is filled into the working chamber of an MTI<sup>5</sup> mixer (Type M3/1.5). The mixing chamber can be heated, and during the treatment the temperature has to be kept above the melting point of the fatty acid. Stearic acid has a melting point of 342 K and so the temperature during the process is always 80 °C. The amount of stearic acid to provide the desired degree of surface coverage is calculated according to Equation 2-2.

These products are partially hydrophobic and may cause the same dispersion problems as talc and other hydrophobic minerals. A possibility to obtain well dispersed aqueous dispersion is explained in section 3.1.1.

### ***3.1.3 Modified calcium carbonate***

Modified calcium carbonate, as used in this study, is formed from calcium carbonate and phosphate via an in-situ surface re-precipitation (Ridgway et al. 2004).

## **3.2 Particle characterisation**

The minerals of interest have to be characterised in term of their size, shape, electrical properties and interactions with their environment. Also the colloidal fraction of the dissolved and colloidal substances (DCS) can be characterised partially by these parameters.

### ***3.2.1 Particle size***

Particle size analyses in this study were either performed using sedimentation techniques or laser light scattering. In all cases the samples have to be properly dispersed prior to analysis. This is done using a solution of 0.1% sodium diphosphate ( $\text{Na}_2\text{P}_2\text{O}_7$ ) in deionised water (18.3 M $\Omega$ ). The concentration of the particles to be

---

<sup>5</sup> MIT Mischtechnik International GmbH, Ohmstrasse 8, 32758 Detmold, Germany

analysed is for sedimentation measurements around 5 wt% and in the case of laser light scattering measurements 0.1 wt%.

### **3.2.1.1 Sedimentation**

In the sedimentation method the cumulative mass distribution over the defined range of particle size (= volume at known density) is measured and expressed as an equivalent Stokes settling diameter. The concentration within a given sedimentation range is normalised to the whole, and measured in respect to mass conveniently by considering radiation decay passing through the sample at the given sedimentation depth via the Beer-Lambert law (path length). Sedimentation particle size measurements were performed in a Sedigraph® 5120 from Micromeritics<sup>6</sup>.

The method of sedimentation is well known in particle processing technology. It relies on the resistance proportionality to particulate cross-sectional area as the constituent particles of a dispersed material pass through a liquid, which in mineral processing is usually water. That proportionality is given by the Stokes equation,

$$v_P = \frac{2(\delta_p - \delta_l) \cdot \mathbf{g} \cdot r^2}{9 \cdot \eta}$$

**Equation 3-1**

which applies for dilute suspensions (no particle-particle interactions) under Reynolds number  $< 0.1$ , and predicts the settling velocity  $v_p$ , of a particle of radius  $r$  as a function of the density difference between the particle and the liquid ( $\delta_p - \delta_l$ ) of dynamic viscosity  $\eta$ , settling under the action of gravity  $\mathbf{g}$ .

---

<sup>6</sup> Micromeritics NV/SA, Eugene Plasky laan 140, 1030 Brussels, Belgium.

Once terminal settling velocity has been reached, particles of differing size will separate in distance,  $h$ , after a given time  $t$ ,

$$r = \sqrt{\frac{9 \cdot \eta}{2(\delta_p - \delta_l) \cdot g \cdot t}} \cdot h$$

**Equation 3-2**

Thus, by scanning the concentration of particles  $c'$  over a range of heights at known time,  $c'(h(t))$ , a particle size distribution according to hydrodynamic radius can be constructed.

The common method used today of determining the particle concentration is by effective volume concentration using the attenuation of X-rays, or another penetrating radiation, applying the Beer-Lambert decay function. This gives a relative logarithmic attenuation distribution as a function of fractional volume (% weight distribution) and particle size, resulting in the typical cumulative size distribution expressed as weight% finer than a given size. Commonly, the weight median particle size is quoted as that size corresponding to the 50 wt% less than point on the distribution curve,  $d_{50}$ .

### ***3.2.1.2 Laser light scattering***

Scattering of a light beam by random particles forms a diffraction intensity distribution as a function of scattering angle. The individual contribution from each particle to the interfering scattered light intensity is related to the projected area of the particulate scatterer, known as the scattering cross-section if Fraunhofer optics are used (Jennings 1993). Alternatively, Mie theory applied to the angular scattering intensity distribution (Mie 1908) expresses the particle in terms of optical path length, and hence particle volume under random orientation (Jennings 1993; Schmidt 2000). The drawback of both methods is that laser scattering as a technique only detects the particles according to the respective theory limitations. For example, concentration of the constituent

particle sizes in a distribution of sizes is not known, and so particle size distributions, normalised to the observed particles only, tend to ignore either the ultrafine and/or ultracoarse particles depending on the respective light scattering theory adopted. The normalisation is then, per force, restricted to within the assumed observed range. For the present studies laser light diffraction measurements were made on a Malvern Mastersizer 2000<sup>7</sup>. Particles having refractive indices that contrast to their surroundings scatter light. Very fine particles less than or approximately equal to the wavelength of the illuminating light scatter equally in all directions (Rayleigh scattering) according to their scattering cross-section (Brownsey, Jennings 1978). An assembly of such particles in random motion, such as in a suspension undergoing a Brownian random walk, will lead to a scattering pattern having a variation of intensity in the plane of scatter as a function of scattering angle  $2\theta$ . To account for larger particles, which display a form factor, Mie theory provides probably the best compromise in describing the light interaction with the particles (Mie 1908), in that it is sensitive to the smaller dimension in the respective form factor.

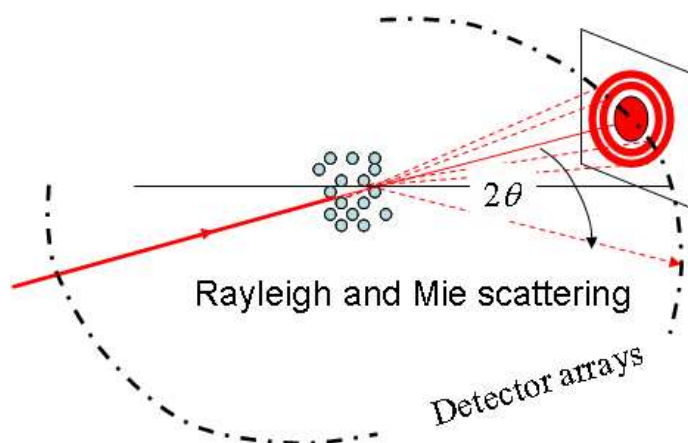


Figure 3-2: Geometry and laser light scattering detection as used for particle sizing (Schoelkopf et al. 2008a).

<sup>7</sup> Malvern Instruments Ltd., Enigma Business Park, Grovewood Road, Malvern, Worcestershire WR14 1XZ, United Kingdom.



Mie theory is based on Maxwell's electromagnetic field equations accounting for refractive index contrast (primary scattering) and absorption of transmitted light through the particles (secondary scattering/refraction). Assumptions are made including the spherical approximation for the particle morphology (Jennings, Parslow 1988; Inoue 1998), the use of dilute suspensions to minimize particle-particle effects, thus eliminating multi-particle scatter, complete knowledge of the optical properties of the particles and that of the surrounding medium, and that the particles are all of the same type, i.e. homogeneous. The theory holds well for particles having a representative diameter,  $d$ ,  $< 50 \mu\text{m}$ , which is the dominant region for coating and paper filling pigments. However, Mie is very problematic in the case where  $d \sim \lambda$ . The connection between scattered light and particle diameter may vary strongly in this region (approaching Rayleigh scattering) and can lead to problems in practical applications (Schmidt 2000).

Fraunhofer diffraction is also frequently used in which the particles are approximated by opaque discs, collecting the scattering intensity distribution from low angles only (Barber, Hill 1990). The major limitations to this approach are the need to consider the refractive index contrast to be infinite and that all the particles scatter light equally. Fraunhofer gives a first scattering maximum at  $9^\circ$  for particles with  $d \approx 5\lambda$  (Schmidt 2000), and is thus rather more suitable for particles  $> 50 \mu\text{m}$ .

Thus, either method alone may not be adequate for the particles investigated, especially if they exhibit a broad particle size distribution, in that a portion of them may be too small, too big or have a diameter near the wavelength of the illuminating laser light.

### ***3.2.1.3 Dynamic light scattering – photon correlation spectroscopy***

By way of contrast, dynamic light scattering (DLS), based on photon correlation spectroscopy (PCS), expresses an equivalent Stokes-Einstein translational diffusion

diameter including the mineral core and any associated layer of adsorbate, such as dispersant and water. In this method, the ensemble distributed translatory diffusion coefficient is the influential particle parameter. In this work, dynamic laser light scattering analyses were performed on a Malvern<sup>7</sup> Zetasizer ZS.

Colloidal particles with a sufficient refractive index contrast to the surrounding liquid scatter light. Monochromatic laser light, of wavelength  $\lambda$ , provides for a defined scatter having an intensity distribution defined by the scattering cross-section of the particles in a refractive medium of index  $n$  over scattering vector,  $q$ , or scattering angle  $2\theta$ , as measured relative to the direction of incidence.

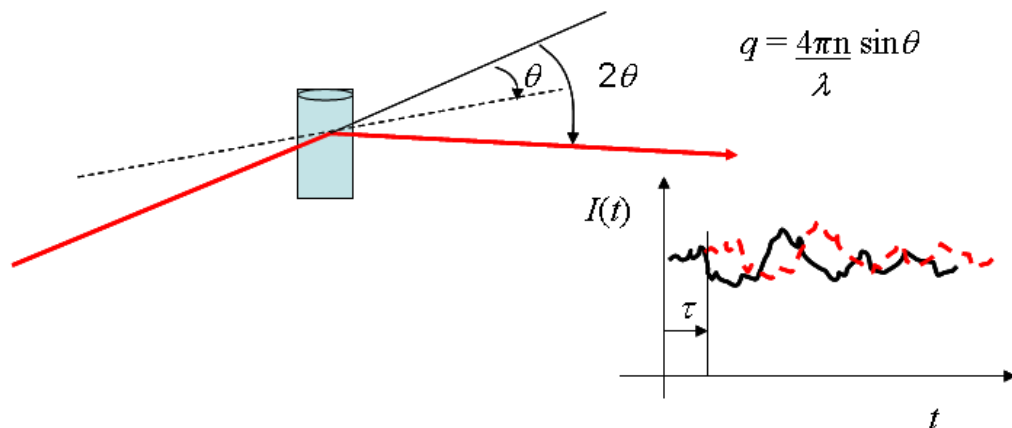


**Figure 3-3: Dynamic light scattering geometry and principle of autocorrelation (Schoelkopf et al. 2008a).**

The decay or e-folding parameter,  $\Lambda$ , at which the autocorrelation function, derived from the time varying scattered intensity,  $I(t)$  in Figure 3-3, has reached  $1/e$ , after a time delay of  $\tau$ , of its initial normalised value of 1, depends on the diffusion coefficient  $D_T$  of the particle,

$$D_T = q^2 \cdot \Lambda$$

**Equation 3-3**

In turn, the diffusion coefficient is related to the Stokes radius,  $r$ , of the particle by the Stokes-Einstein thermodynamic relation

$$D_T = \frac{k_B \cdot T}{6 \cdot \pi \cdot \eta \cdot r}$$

Equation 3-4

where  $k_B$  is the Boltzmann constant,  $T$  the absolute temperature, and,  $\eta$  represents the viscosity of the liquid.

Since we are generally dealing with a distribution of particles, each particle size fraction will result in its own correlation decay constant, such that the complete correlation function will be an ensemble average of a multiple of exponential functions. This leaves us with the well-known multi-inverse problem, which cannot be analytically deconvoluted (Koppel 1972), and methods, such as considering a two-parameter model particle size distribution are applied.

### ***3.2.2 Specific surface area***

Gas adsorption has been used to determine the specific surface area of the minerals following the BET equation as described in section 2.6.4. For gas adsorption data also the pore size and volume can be derived by using the BJH algorithm (Barret et al. 1951).

The samples were outgassed at 250 °C for 30 minutes under nitrogen in a Micromeritics<sup>6</sup> Flow Prep 060.

The experiments were run on a Gemini 2360 from Micromeritics<sup>6</sup>. In the case of a powder with a specific surface area of 1-5 m<sup>2</sup>g<sup>-1</sup> around 4.0 g were weighed and in the case of a powder with 40 m<sup>2</sup>g<sup>-1</sup> around 0.5 g were weighed on a Mettler Toledo<sup>12</sup> AB 304-S with an accuracy of ± 0.1mg. A five point measurements isotherm was recorded using nitrogen. As a reference a carbon black reference material (Part Number 004-16833-00, Lot D-7) from Micromeritics<sup>6</sup> was used with 21.0 ± 0.75 m<sup>2</sup>g<sup>-1</sup>. 0.2-0.3 g of

the material was weighed in and outgassed at 300 °C for 10 minutes before the measurement.

### ***3.2.3 Scanning electron microscopy (SEM) and image analysis***

In a scanning electron microscope, electrons are emitted from a cathode filament and drawn towards an anode. Electron emitting sources can be either thermionic emitters or field emitters. An example of a thermionic emitter is a tungsten filament cathode (2 800 K) or mono-crystalline lanthanum hexaboride sources (1 800 K). The emitted electrons are held back in a cloud by a negative potential in a Wehnelt control grid. The accumulated electrons are then accelerated by a high voltage field towards the anode. Field emitters emit the electrons under high voltage fields instead of high temperatures. The electron beam is directly accelerated towards the anode. The electron beam is focused by successive magnetic lenses into a very fine spot (from 0.5 – 5 nm in diameter). As electrons strike the surface of a material where they are scattered by atoms in the sample. The sample density, atomic number and electron energy affect the scattering event. Interactions in this region lead to the subsequent emission of electrons and x-rays, which are then detected. There are various collection methods of the sample-emitted electrons used to generate images; secondary electron and backscattered electron capture are two commonly used methods.

Secondary electrons are electrons generated by the process of ionization; they are called secondary electrons as they are generated from the interaction with the primary electron beam. Secondary electrons are low energy electrons and can be detected using an Everhart-Thornley scintillator photomultiplier detector positioned to the side of the sample. An Everhart-Thornly detector, together with a field emitting source (Zeiss-

Gemini<sup>8</sup> DSM982) was used for the field emission (FE-SEM) images of aragonite in chapter 4.

Backscattered electrons are primary electrons, i.e. originating from the incident beam, which have been reflected or backscattered from the material being analysed. The contrast in backscatter electron images is dependent on the atomic number of the element(s) constituting sample. The higher the atomic number of the element the more the backscattered electrons will be scattered, and the more the electrons have been scattered, the brighter is the image. So, heavier elements appear brighter in backscatter images than lighter elements. Backscatter electrons are detected from a position above the sample in the form of a doughnut shaped detector array. The primary use of backscatter electrons is to generate atomic number mapping, and provide information about the topography of the sample. The palygorskite images in chapter 4 were made using also a field emitting source and an energy selective backscattered electron (ESB) detector. The images were made on a Zeiss<sup>8</sup> Ultra 55.

Image analysis as a technique is limited by the quality of the images analysed. To ensure a fair comparison between different samples, the images need to be acquired using the same technique, under identical conditions, and preferably with the same equipment. The images acquired then need to be analysed using equivalent parameters in the image analysis software. To consider the image analysis data quantitatively, the number of images analysed needs to be representative of the entire structure. Image analysis was performed with the digital imaging system of the Voyager software from Noran<sup>9</sup> Instruments. The software calculates the aspect ratio based on Equation 2-4.

---

<sup>8</sup> Carl Zeiss NTS GmbH, Carl-Zeiss-Str. 56, 73447 Oberkochen, Germany.

<sup>9</sup> Noran Instruments Inc., 2551 West Beltline Highway, Middleton, WI, United States.

### **3.2.4 Mineral analysis**

#### **3.2.4.1 X-ray fluorescence**

If a material is exposed to high energy radiation, such as X-rays, ionisation of the atoms may take place. Ionisation will occur only if the energy of the irradiating beam is higher than the ionisation potential of the electron in the atom. X-rays can have sufficient energy to ionise the inner electron orbitals of the atoms. Electrons from outer orbitals fall back into vacancy generated and release a photon. The energy difference between the orbitals defines the energy of the emitted photons. The content of each element in the material is directly related to the relative intensity of each characteristic radiation. The method thus allows the elemental analysis of all elements above atomic number 5 (boron).

X-ray fluorescence (XRF) analysis in this study was made on a Thermo<sup>10</sup> ARL 9400 Sequential XRF spectrometer.

#### **3.2.4.2 Loss on ignition LOI**

In addition to the elemental analysis by X-ray fluorescence the loss on ignition (LOI) is also measured by a Thermogravimetric analysis (TGA). Loss on ignition quantifies the amount of material that is combusted when a sample is heated up to a certain temperature. In the case of calcium carbonate or phyllosilicates this is mainly related to calcination of the mineral, i.e. release of CO<sub>2</sub> and formation of CaO or release of H<sub>2</sub>O, respectively. The measurements were done on a Mettler Toledo<sup>12</sup> SDTA 851e. The sample (50 – 100 mg ± 0.01 mg) is heated from 20 °C to 1 000 °C with a heating rate of 25 °Cmin<sup>-1</sup> and further kept at 1 000 °C for another 10 minutes in order to guarantee complete conversion. The weight loss is then expressed in % or mg of the total sample

---

<sup>10</sup> Thermo Fisher Scientific Inc., 81 Wyman Street, Waltham, MA, United States.

weight. If, for example, calcination has to be avoided the temperature has to be kept below a certain temperature (570 °C for calcium carbonate) in order to quantify only adsorbed moisture or organic material (see also section 3.4.7).

### **3.2.4.3 X-ray diffraction**

Electrons are emitted, typically from a heated tungsten filament similar to the thermionic emitter described in section 3.2.3, and accelerated in a high voltage field (40-80 kV) so as to impact on a chosen anode material. The anode is water cooled, and often consists of Mo, Cu, Fe or Cr. The high energy electrons lose their kinetic energy while entering the surface of the anode and remove another electron from one of the orbitals. Similar to the X-ray fluorescence (section 3.2.4.1), the electron is replaced by an electron from another orbital and a photon with a defined energy level is radiated. If, for example, an electron is removed from the K-orbital of a copper atom and replaced by an electron from the L-orbital the  $K_{\alpha}$  line is radiated. Filters can be installed to eliminate other radiation lines, such as a Ni filter to eliminate the  $K_{\beta}$ -line which originates from an electron replacement in the K-orbital by an electron from the M-orbital.

The geometrical conditions for diffraction of X-rays by a crystal are given by Bragg's law (Equation 3-5). Bragg coherent diffraction assumes that X-rays are reflected by the atoms populating a set of parallel lattice planes such that each plane acts as a semi-transparent mirror. Bragg's law describes the condition for constructive interference of the reflected X-rays.

$$n \cdot \lambda = 2d_L \cdot \sin(\theta)$$

**Equation 3-5**

Two beams of parallel X-rays are reflected from adjacent lattice planes, which are separated by the distance  $d_L$ , at a certain angle  $\theta$ . The lower beam has to travel an extra

distance as compared to the upper beam. Constructive interference of the reflected beams only occurs if the extra path length of the second beam corresponds to a whole number of wavelengths,  $n\lambda$ . In real crystals, which contain thousands of planes, Bragg's law imposes a stringent condition on the angles of diffraction. If the angle is other than that which creates constructive interference, by more than a few tenths of a degree, cancellation of the refracted beam by destructive interference is usually complete.

The mineral powders of the present study were analysed by X-ray diffraction (XRD) from 5-100°  $2\theta$  Bragg diffraction using a Bruker AXS D8 advanced XRD system with  $\text{CuK}_\alpha$  radiation, automated divergence slits and a linear position-sensitive detector. The tube current and voltage were 50 mA and 35 kV, respectively: the step size was 0.02°  $2\theta$  and the counting residence time 0.5 s  $\text{step}^{-1}$ .

### **3.2.5 Pore size**

A porous system in contact with non-wetting liquid (contact angle is greater than 90°) resists penetration of the liquid into the pores of the solid according to the Young-Laplace equation (Equation 3-6) (Swanson 2003).

$$D = -\frac{4 \cdot \gamma_{LV} \cdot \cos(\theta)}{P}$$

**Equation 3-6**

where  $\gamma_{LV}$  is the surface tension of the liquid-vapour interface,  $\theta$  is the contact angle between liquid and solid, and  $D$  is the diameter of the equivalent cylindrical capillary that fills with liquid at applied pressure,  $P$ . Mercury is most frequently used because of its high contact angle and high surface tension. Mercury intrusion porosimetry, however, renders the sample non-reusable.

As pressure increases, the mercury fills all accessible pores having a diameter greater than those calculated by Equation 3-6. The cumulative volume thus intruded can be



measured at each interval of increasing pressure. A pressure-volume curve can be derived, which can be transformed into a cumulative volume as a function of equivalent capillary pore diameter. Differentiation of this cumulative curve with respect to diameter yields a volume frequency - pore diameter distribution curve. The sample is therefore represented by a bundle of parallel capillaries, distributed in diameter size according to the volume distribution curve. Inevitably, a drawback of this method is that larger pores may be shielded by smaller entry pores in such a way that the volume associated with such shielded pore is attributed to the finer entry pore size. To achieve greater realism in describing complex pore network structures, fitted models may be applied, such as that of the 3D array model PoreCor/PoreXpert<sup>11</sup>.

The mercury intrusion measurements are corrected further for the compression of mercury, expansion of the glass sample chamber, and compressibility of the solid phase of the sample (Gane et al. 1996).

The porosimetric analysis of the samples has been made using a Micromeritics<sup>6</sup> Autopore IV mercury porosimeter.

### ***3.2.6 Zeta potential and electrophoretic mobility***

When solids contact liquids they often acquire an electrical charge that becomes quite significant if the solid is dispersed in small particles. The surface charge develops through ionisation of surface groups or adsorption of charged species. On the surface of an anionic surface potential a layer of counter charged particles adsorb and form the Stern layer in distance  $\delta$  (Figure 3-4). The Stern surface is drawn through the ions that are assumed to be adsorbed on the charged wall. This surface is also known as the *inner*

---

<sup>11</sup> PoreCor and PoreXpert are software packages developed by the Fluid Modelling Group, University of Plymouth, PL4 8AA, UK.

*Helmholtz plane* (IHP). The surface running parallel to the IHP, through the surface of shear shown in Figure 3-4, is called the outer Helmholtz plan (OHP). It should be noticed that the diffuse part of the ionic cloud beyond the OHP is the diffuse double layer. It is the mutual repulsion of these double layers, commonly known as DLVO (Derjaguin, Landau 1941; Verwey, Overbeek 1948) repulsion, that provides colloidal dispersion via electrostatic stabilisation. The repulsion is mainly caused by the osmotic pressure other than the often quoted electrostatic repulsion. The thickness of the electrical double layer is a sensitive function of the ionic strength of the dispersion medium. The thickness is normally characterised by the Debye length  $\kappa^{-1}$ , given in Equation 3-7 (Napper 1983),

$$\kappa = \sqrt{\frac{q^2 \cdot N_A}{\epsilon_0 \cdot \epsilon_r \cdot k_B \cdot T} \cdot \sum_i z_i^2 c_i}$$

**Equation 3-7**

with  $q$  as the elementary charge ( $1.602 \cdot 10^{-19}$  C),  $N_A$  the Avogadro constant,  $\epsilon_0$  is the permittivity of free space ( $8.85 \cdot 10^{-12}$  C<sup>2</sup>J<sup>-1</sup>m<sup>-1</sup>),  $\epsilon_r$  is the dielectric constant of the medium (water at 298 K; 78.64),  $z_i$  is the valency of the ion, and  $c_i$  is the molar concentration of the ion in molm<sup>-3</sup> (Hiemenz, Rajagopalan 1997).

A common measurement technique to obtain zeta potential is the electrophoretic mobility measurement. An electric field is applied and the particles within the dispersion migrate toward the electrode of opposite charge. The velocity is measured by laser Doppler anemometry in which the frequency shift of a laser beam caused by the moving particles is measured. The velocity is the resultant of the balance of the force of electrical attraction and the flow resistance (Stokes) related the effective size of the particle, including the attached double layer. The mobility can be converted into zeta potential values by either the Helmholtz-Smoluchowski (1903) or the Hückel (1924)

theories. In the current study, electrophoretic mobility measurements were run on a Malvern<sup>7</sup> Zetasizer Nano ZS.

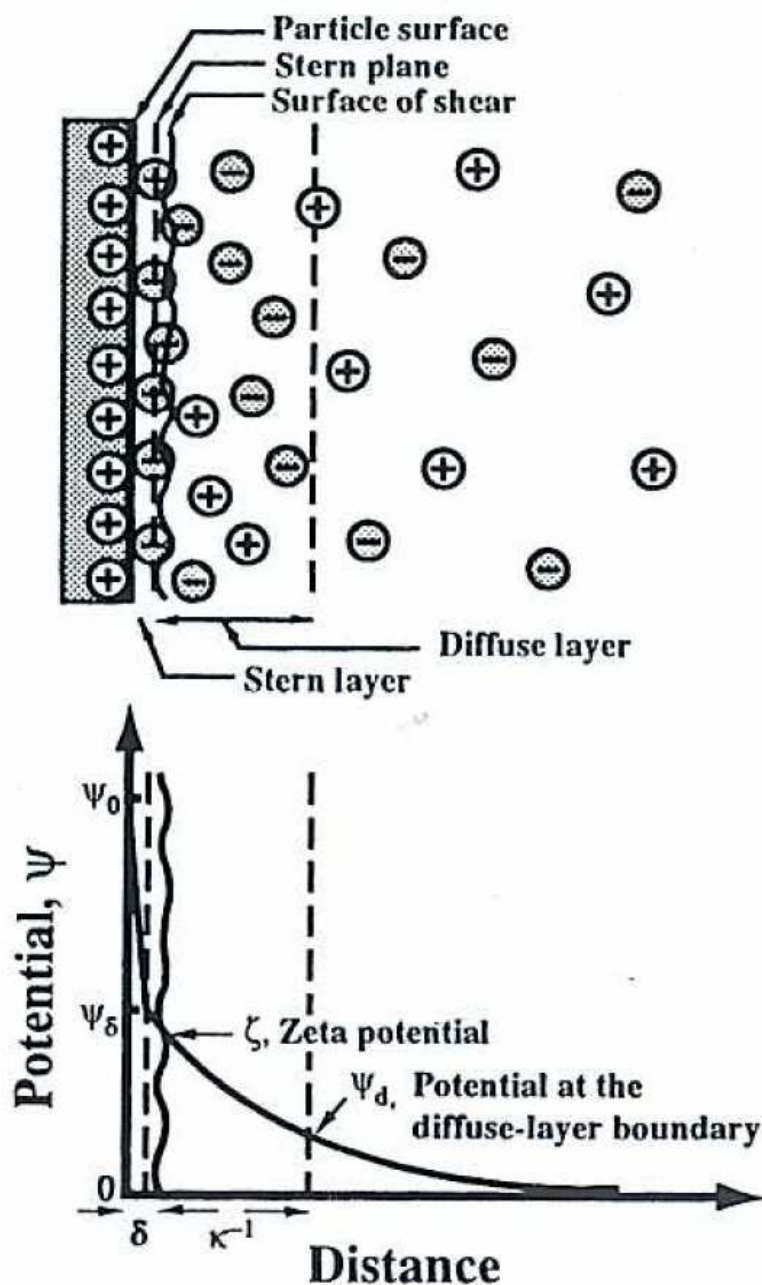


Figure 3-4: Schematic representation of zeta potential (Hiemenz, Rajagopalan 1997).

The Helmholtz-Smoluchowski theory holds for particles with a much larger radius ( $R_S$ ) than double layer thickness ( $\kappa R_S > 100$ ) and the Hückel theory holds for systems with  $\kappa R_S < 0.1$ . The dependency of the electrophoretic mobility ( $u$ ) on the zeta potential ( $\zeta$ )

can be expressed in one general formula via the constant  $C$  in Equation 3-8, where  $\eta$  is the viscosity of the liquid.

$$u = C \cdot \frac{\epsilon_0 \cdot \epsilon_r \cdot \zeta}{\eta}$$

**Equation 3-8**

If  $\kappa R_S > 100$  then  $C = 1$ , and if  $\kappa R_S < 0.1$  then  $C = 2/3$ .

It becomes apparent that there is a window of  $\kappa R_S$  that is not defined by these two inequalities. A more general theory was formulated by Henry (1931). The Henry equation requires the knowledge of all ions in solution and the exact size of the particles in question. In many cases for the studied pitch particles and the ionic environment in this study, the values lie within the range  $0.1 < \kappa R_S < 100$ . It was therefore decided to report only electrophoretic mobilities which are independent from any theoretical conversion, and are thus the direct results as read from the apparatus.

As an implication, the thickness of the double layer diminishes with increasing ionic strength significantly. At ionic strengths greater than 0.1 M the thickness of the double layer is less than 1 nm. Electrostatic repulsion is then usually of insufficient range to outweigh the van der Waals attraction. This explains why most electrostatically stabilised dispersion coagulate when the ionic strength is increased (Napper 1983). At large distances of separation, the total interaction energy is obtained from the superposition of the van der Waals attraction and the electrostatic double layer repulsion (Figure 3-5).

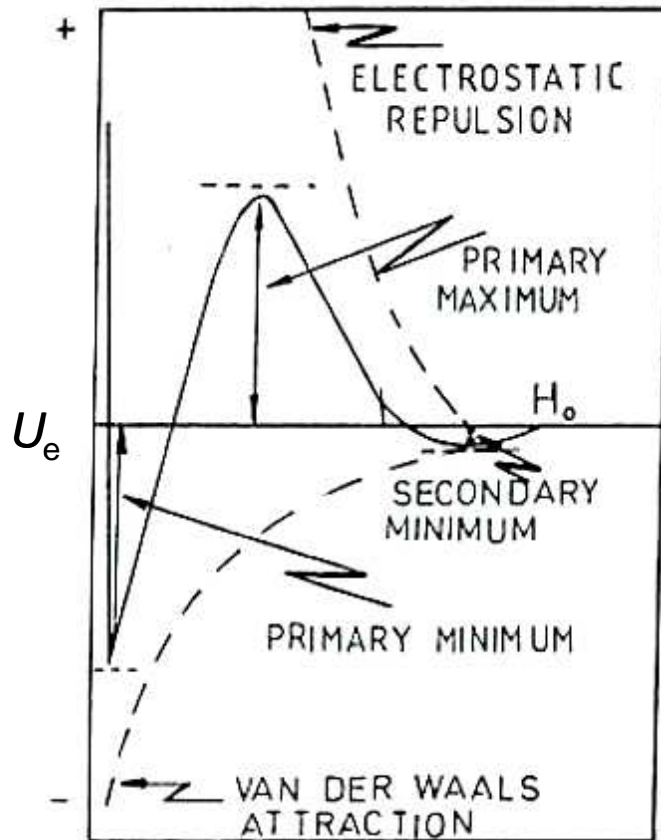


Figure 3-5: Schematic representation of the total potential energy ( $U_e$ ) against the distance of separation for a pair of electrostatically stabilised particles according to the DLVO theory (Napper 1983).

One maximum and two minima in the potential energy curve (Figure 3-5) are frequently identified. The height of the primary maximum, if sufficiently large, will ensure that the rate of coagulation is so slow that the system displays long-term stability. In that respect the system is kinetically stabilised but exhibits a thermodynamic metastability (Napper 1983).

### 3.2.7 Polyelectrolyte titration and streaming current detector

The charge of a colloidal particle or a polymer may not only be quantified in terms of zeta potential or electrophoretic mobility but also via charge titration using an oppositely charged polymer, i.e. polyelectrolyte titration (PET). Electrostatic interactions are important for the adsorption of polyelectrolytes onto oppositely charged surfaces and can be strongly affected by electrolyte concentration and pH. The direct polyelectrolyte titration of a cationic polyelectrolyte with an anionic polyelectrolyte

using a cationic indicator, orthotoluidine blue (OTB), was first developed by Terayama (1952). The PET is independent of molecular mass (Horn 1978) and the polyelectrolyte complex is stoichiometric with respect to charge if the charge densities of the polyelectrolytes are sufficiently high (Horn 1979). The 1:1 stoichiometry, however, is only given for low ionic strength (Horvath 2003). The polyelectrolyte titration is not reporting the total charge of a system but rather a response to the added cationic polymer. If the 1:1 stoichiometry applies then the PET is a measure for the total charge that is accessible for the cationic polymer. For example anionic charge sites within fibres or other particles may not be included that way. Due to the size of the cationic polymer the reaction is clearly diffusion controlled and depending on the time scale during the titration different values can be obtained. A better way to determine the total charge of a system could be potentiometric titration in which pH is varied. However, wood resinous systems are highly sensitive to pH and alkaline medium may lead to saponification or dissolution of certain compounds. Therefore, PET is a tool for papermakers to quantify the anionic charge in a system and indicate the consumption of cationic additives in the wet-end of a paper machine in order to induce flocculation.

PET is typically run indirectly. An anionic sample is overdosed with a cationic polyelectrolyte, e.g. poly-DADMAC (poly diallyldimethylammonium chloride) or poly-PDDPC (poly N,N-dimethyl-3,5-dimethylene-piperidinium chloride). After a given time to allow sufficient reaction time, the sample is filtered. The obtained filtrate is then, often under pH buffering, titrated with an anionic polyelectrolyte, e.g. KPVS (potassium polyvinylsulphate), to determine the excess of cationic polyelectrolyte and thus the anionic charge of the sample. The end point of the titration can be indicated with the indicator orthotoluidine or today more commonly with photocells (Phototrode

dp 660 from Mettler Toledo<sup>12</sup>) that measure the cloud point, which indicates the complete neutralisation, and thus, the end point of the titration.

Approximately 5 g of the aqueous sample ( $\pm 0.1$  mg) are weighed. The sample is diluted with 40 cm<sup>3</sup> deionised water and 10.00 cm<sup>3</sup> of the PDDPC solution (0.01 M) is dosed. After 20 minute agitation at room temperature the sample is filtered through a 0.2  $\mu$ m Milipore filter and washed with some deionised water. 5 cm<sup>3</sup> of Phosphate buffer pH 7.00 (Riedel-de-Haen) is added. The remaining PDDPC or poly-DADMAC is titrated with the KPVS solution (0.01 M).

The streaming current detector is another way for following the poly electrolyte titration. It is based on the opposite effect of electrophoresis. It occurs when a particle is mechanically moved through the fluid, or the fluid is moved past the particle. The shear results in a separation of charges causing a potential to exist. For example, negatively charged particles are forced through a filter. The particles retain on the filter and the positively charged ions are washed through the filter. In that way an electrical potential develops. A typical detector consists of a cylinder and a piston that oscillates within the cylinder. A small gap exists between the piston and the cylinder. The colloidal particles are assumed to adsorb on the cylinder and piston wall. The oscillation is then causing the separation between the adsorbed particles and their counterions. An oppositely charged polymer can be titrated and the potential within the detector cell can be monitored until 0. This is then the point of complete neutralisation and the charge can be calculated. Streaming current detection is not very accurate and is a very rough tool for papermakers to estimate the anionic charge in a fibrous system. Factors like cylinder

---

<sup>12</sup> Mettler-Toledo GmbH, Im Langacher 44, 8606 Griefensee, Switzerland.

and piston surfaces, and the affinity of the substances for these surfaces are not known and highly influence the outcome. The time scale in this method is very short and diffusion into porous media might not take place. In the case of TMP filtrate samples huge differences can be expected between PET and SCD measurements. SCD results are expected to be lower because mainly measuring the charge of the pitch droplets. The reason for that is the affinity of the hydrophobic pitch particles and their affinity to deposit on the equipment walls in comparison to the water soluble charge carriers, such as pectin and other charged polysaccharides.

Approximately 5 g ( $\pm 0.1$  mg) of the aqueous sample are filled into the titration chamber of the PCD-02 from Müttek<sup>13</sup>. The sample is titrated with 0.01 M PDDPC solution until the streaming potential is 0.

### ***3.2.8 Wetting properties of minerals***

The wetting behaviour of mineral powders is difficult to determine since not only the surface tensions control the wetting but, additionally, geometrical effects and surface rugosity. Therefore, a rather simple and semi-quantitative test was used in this study to evaluate the wetting potential of surface treated minerals and talc against water. As explained in the section 2.4.1.3, talc has a surface tension of 35-60 mJ m<sup>-2</sup> and fatty acid treatment of calcite can reduce the surface tension of ground calcium carbonate (gcc).

Mixtures of water and ethanol were prepared in volume ratios of 100:0, 90:10, 80:20, 70:30, 60:40, 50:50, 40:60, 30:70, 20:80, 10:90 and 0:100. 50 cm<sup>3</sup> of each of these mixtures were placed in a 100 cm<sup>3</sup> beaker. About 0.5 – 1.0 g of the powder in question was carefully put on top of the liquid. The wetting behaviour was quantified by the time needed for the powder to be wetted according to the following judgement:

---

<sup>13</sup> BTG Instruments GmbH, Arzbergerstrasse 10, D-82211 Herrsching, Germany



- 0 → immediate wetting of the powder (sinks within 30 seconds)
- 0.25 → within 5 minutes all of the powder is wetted
- 0.5 → after 5 minutes more than 50% of the powder is wetted
- 0.75 → after 5 minutes less than 25% of the powder is wetted
- 1 → the powder is not wetted within 5 minutes

Figure 3-6 shows the surface tension of various water / ethanol mixtures. The ethanol content is given here in mass and not in volume as described for the wetting test above.

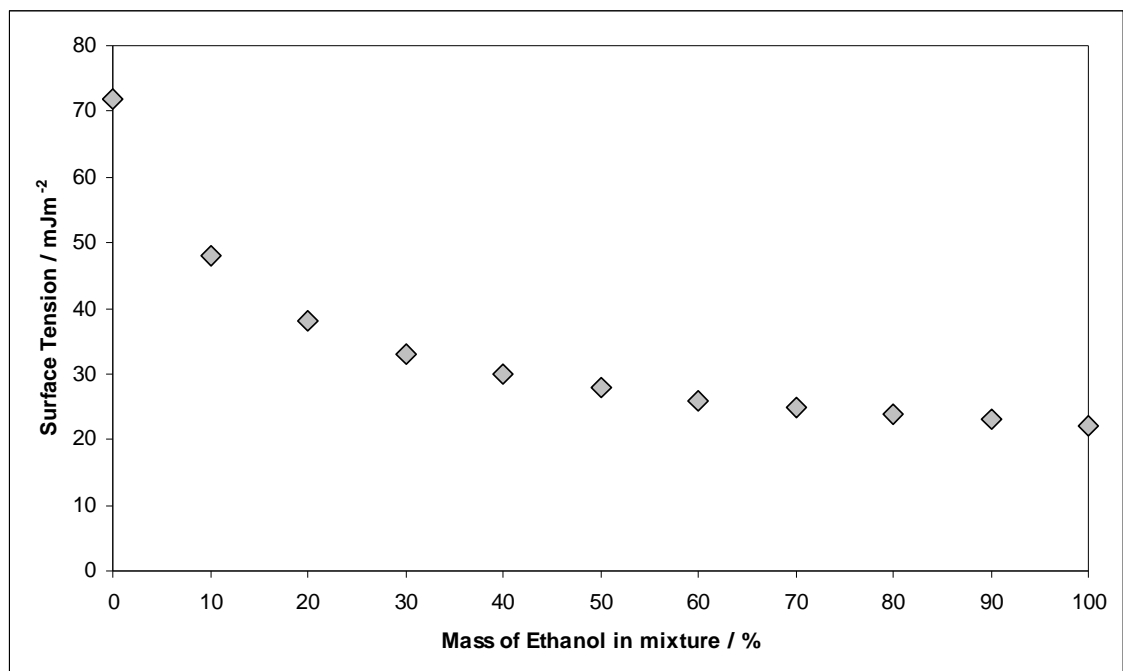


Figure 3-6: Surface tension of aqueous ethanol mixtures (Lide 2002).

### 3.3 Preparation of the dissolved and colloidal substances and the adsorption experiments

In order to study the potential at laboratory scale for the potential use of minerals to control unwanted deposits in paper mills, a defined system of colloidal and dissolved substances is required. A part of the applied method bases itself on the method published by Guera et al. (2005). A sample of an unbleached thermo mechanical pulp

was collected in a paper mill in Switzerland. The mill uses 100 % fresh water in their TMP plant. The TMP consists of 70 % spruce (*Picea abies*), the rest being composed of fir (*Abies alba*) and a small part of pine (*Pinus sylvestris*). The TMP is collected at 90 °C from the accept of the classifier after the TMP refiner and has a consistency of 3-4 wt%. The TMP is cooled to room temperature and directly used. Any storage may alter the properties due to microbiological activities.

The TMP is vacuum (~50 mbar) filtered in a first step through a filter with rather coarse pores (Whatman lack ribbon) to remove the main part of the fibres. In a second step a finer filter (pore size < 2 µm → Whatman blue ribbon) is applied (vacuum filtration ~50 mbar) in order to remove all fines and fibrils which might distort later analyses and to collect the dissolved and colloidal fractions of the TMP. The colloidal nature of the filtrate is checked with a light microscope for the absence of fibres and fibrils. Filtration of the TMP is discussed somewhat controversially in the literature (Orsa, Holmbom 1994). The built-up fibre matt during filtration is supposed to retain selectively certain parts of the colloidal and dissolved substances. Centrifugation is quoted as being more suitable and more reproducible. However, since this study does not focus on the exact composition of the DCS in the TMP but rather on adsorption properties of minerals, this selective screening is accepted, bearing also in mind that every study used fresh TMP samples which, in any case, denies the direct comparison between the trials. Furthermore, the isolated DCS fraction is defined in respect to its state by the various techniques. One characterisation technique is to determine the electrophoretic mobility of the particles in the TMP filtrate, more precisely the change of it with varying pH. Another method measures the particle size of the colloidal fraction in the TMP filtrate with dynamic laser light scattering. Others are highlighted in the following sections.

After isolation of the DCS from the TMP, the pH is usually adjusted to 7.0-7.5 to represent the neutral to alkaline conditions in modern paper mills. The TMP filtrate can now be distributed into glass bottles and the mineral can be added as an aqueous dispersion. An already prepared aqueous dispersion, which has undergone deagglomeration and dispersing (section 3.1) by various means, is preferred in order to guarantee exposure of the maximum surface of the minerals. It is important to control the amount of added water. The amount of water in a series of experiments should be constant. The bottles are air-tight when closed, to avoid further uptake of CO<sub>2</sub>, and sufficiently agitated for at least 2 hours. Even though the adsorption process is described as instantaneous (Chang 1985) sufficient time is given to reach equilibrium. After this the dispersions are filled into centrifuge tubes and centrifuged. Applying 2 600 |g| allows the separation of the mineral fraction including also adsorbed organic material without separating the non-adsorbed dissolved and colloidal substances. Both requirements have to be checked carefully in blank runs in every experiment, namely: does the mineral settle and is the colloidal material in the TMP filtrate not settling under the applied conditions? This, however, does not exclude possible interactions of the two which may result in destabilisation of the pitch or stabilisation of the mineral.

### **3.4 Quantification of dissolved and colloidal substances**

After the mineral has been separated from the TMP filtrate, the two phases can be analysed. Most of the analysis techniques are indirect measurements of the dissolved and colloidal substances.

As explained in section 2.2.4 colloidal species are defined as particles < 2 µm that cause turbidity and are hence determined by the analysis of turbidity. As dissolved substances everything is included that does not cause turbidity and can be filtered by a 0.2 µm

membrane filter. Dissolved substances mainly include inorganic ions, polysaccharides, lignin and lignosulphonate, as well as some dissolved fatty and resin acids.

### **3.4.1 Turbidity**

The turbidity of the sticky suspensions, mineral suspensions, and sticky and mineral suspensions, were measured either on a Hach DR/890 Colorimeter (Hach Company, USA) or a Novasina 155 Model NTM-S. Turbidity is a measure of light scattering by particles in suspension, assessed by the drop in light transmission through a given sample length. The Novasina 155 Model NTM-S instrument transmits light in the near infrared spectrum through an optical fibre probe where the emerging beam is scattered by small particles in suspension. Light scattered back at 180° to the incident beam is collected by parallel optical fibres in the probe and focused onto a photo-diode. The resulting signal is amplified and displayed directly in Nephelometric Turbidity Units (NTU), defined as the intensity of light at a specified wavelength scattered, attenuated or absorbed by suspended particles at a method-specified angle from the path of the incident light, compared to a synthetic chemically prepared standard. Since optical properties depend on suspended particle size, a stable synthetic material Formazin, having uniform particle size, is used as the standard for calibration and reproducibility. Nephelometric Turbidity Units (NTU), as specified by the United States Environmental Protection Agency, adopts a white light source combined with defined geometrical properties of the measurement apparatus. Interference from ambient light is eliminated by using a modulated transmitting signal, removing the need for light-tight sample handling systems.

The particle size distribution and concentration of the scattering particles are key factors in altering the turbidity of the suspension (Lawler 1995). The turbidity,  $\tau$ , is

proportionally related to the volume occupied by each individual scattering particle,  $V_p$ , and the numerical particle concentration  $c'$ .

$$\tau \propto V_p^2 \cdot c'$$

Equation 3-9

If the particles do not aggregate then the turbidity is directly proportional to the numerical particle concentration  $c'$ .

Turbidity offers an opportunity to quantify the total amount of colloidal particles in a system and thus the colloidal fraction in a TMP filtrate.

### **3.4.2 Chemical oxygen demand (COD)**

The COD is a property commonly used as an indirect measure of the amount of organic compounds in water. The COD indicates the amount of oxygen required to oxidise organic compounds completely into carbon dioxide. It is a useful measure of water quality. The organic compounds are fully oxidised into carbon dioxide using potassium dichromate. On oxidising the organic compounds, the chromium ion is reduced from  $[\text{Cr}_2\text{O}_7]^{2-}$  to  $\text{Cr}^{3+}$ . The  $\text{Cr}^{3+}$  concentration is then determined spectrophotometrically. The concentration of  $\text{Cr}^{3+}$  indicates the COD of the sample.

The COD is therefore a measure for the total organic material in a TMP filtrate including dissolved and colloidal substances.

### **3.4.3 Gravimetric analysis**

Gravimetric analysis is a basic analytical technique that has a wide applicability to various chemical systems, and is one of the most precise and accurate methods of macro-quantitative analysis. Gravimetric analysis involves converting the analyte to an insoluble form, and the separated precipitate is then dried and accurately weighed. From

the weight of the precipitate, and knowledge of the chemical composition, one can calculate the weight of analyte in the desired form.

Gravimetry, finally, quantifies the total amount of material in a TMP filtrate, including organic and inorganic dissolved and colloidal substances.

#### ***3.4.4 Analysis of extractives***

Another tool to quantify the colloidal part of paper mill water is to extract the samples with an organic solvent with low dielectric constant. Various solvents can be used such as petroleum ether, methyl tertiary butylether (MTBE), chloroform, acetone and others (Back, Allen 2000). The choice is made according to the nature of the sample. Wood chips and also fibrous samples need a solvent that is able to penetrate into the wood whilst aqueous dissolved samples do not have this requirement. In this study petroleum ether was used following the method of Saltsman and Kuiken (1959). Prior to extraction, the water sample was acidified (pH 3) in order to protonate all acid groups. This was to guarantee a complete extraction of all wood resin components. Simply drying the extracts would yield a gravimetric amount of wood resin. The extract can, however, be further analysed for its composition either for individual components or for component groups. The groups cover fatty acids (FA), resin acids (RA), lignans, sterols, sterol esters and triglycerides. The wood resin groups can be separated and determined by several chromatographic techniques, including gas chromatography (GC) or high performance liquid chromatography (HPLC). In the current study the analysis was done by GC using a flame ionisation detector (FID). Prior to analysis a part of the compounds (acids) have to be derivatised into a form that allows evaporation. This is typically done by the formation of trimethylsilyl esters of the fatty and resin acids. Internal standards are added in order to identify and quantify the different groups (Orsa, Holmbom 1994).

In a typical procedure 50 cm<sup>3</sup> of the aqueous sample (TMP filtrate) are transferred into a 250 cm<sup>3</sup> separation funnel. The flask which contained the water sample is rinsed with a small aliquote of deionised water heated to 60 °C. With a micro pipette 100 mm<sup>3</sup> of the internal standard solution (containing 0.02 mgcm<sup>-3</sup> of heneicosanoic acid (21:0), betulinol, cholesteryl heptadecanoate and 1,3-dipalmitoyl-2-oleoyl-glycerol, all available from Sigma Aldrich in analytical grades) is pipetted to the aqueous sample. The pH of the aqueous sample in the separation funnel is adjusted to 2 with 1M sulphuric acid. 50 cm<sup>3</sup> of acetone, 15 cm<sup>3</sup> methanol and 50 cm<sup>3</sup> petroleum ether are added to the separation funnel. The securely sealed separation funnel is shaken for 10 minutes (let out the gas evolved) and the phases are left to separate. Drain the water phase. Wash the petroleum ether phase with 15 cm<sup>3</sup> of a solution containing acetone / methanol / water in a ratio 2:1:1. After phase separation the water phase is drained again and combined with the previously removed water phase. The collected water phases are extracted twice with 25 cm<sup>3</sup> for another 10 minutes of shaking. The petroleum ether phases are combined and dried over sodium sulphate (approx. 10 g). After removal of the sodium sulphate the organic phase is evaporated to a volume of 2 cm<sup>3</sup>. Transfer the sample into a GC vial and evaporate the remaining solvent under a nitrogen stream at 60 °C. Add 100 mm<sup>3</sup> N,O-Bis(trimethylsilyl)-trifluoro-acetamide and 50 mm<sup>3</sup> Trimethylchlorosilane (both available from Sigma Aldrich in analytical grade). Shake the test vial gently and heat to 70 °C for 30 minutes. A small amount of Pyridine can be added to guarantee complete silylation. The sample is now ready to be analysed by GC-FID. 0.5 mm<sup>3</sup> of the solution is injected to the gas chromatograph. The GC method is shown in Table 3-1.

The analyses were performed at Innventia<sup>14</sup>. For that purpose the samples were frozen and shipped by courier. According to Innventia the method had the following reproducibility determined in six different laboratories on the same TMP effluent sample (Table 3-2).

**Table 3-1: GC-FID method settings for the analysis of wood extractive groups.**

Column	100 % dimethyl polysiloxane, length 6-8 m, inner diameter 0.53 mm, 0.15 µm phase thickness
Temperature program	100 °C for 1.5 min, 12 °Cmin <sup>-1</sup> to 340 °C, 340 °C for 5 minutes
Injector	On-column injection
Injector temperature	80 °C for 0.5 min
Detector type	FID at 340 °C

**Table 3-2: Reproducibility of the TMP effluent extraction and quantification by GC-FID. *n* refers to the amount of data points used for the calculation of the mean and the standard deviation**

Group (Internal standard)	Mean ( <i>n</i> =6) / mgdm <sup>-3</sup>	Standard deviation ( <i>n</i> =6) / mgdm <sup>-3</sup>
Fatty acids (heneicosanoic acid)	4.2	1.8
Resin acids (heneicosanoic acid)	9.3	1.9
Lignans (betulinol)	164.7	35.8
Sterols (betulinol)	6.5	3.1
Sterylesters (cholesteryl heptadecanoate)	18.9	4.5
Triglycerides (1,3-dipalmitoyl-2-oleoyl-glycerol)	20.5	8.7
Sum	224.0	36.6

<sup>14</sup> Innventia AB, Drottning Kristinas väg 61, 11486 Stockholm, Sweden.



### ***3.4.5 Analysis of carbohydrates and lignin***

Carbohydrates and lignin, as defined here, are both part of the soluble fraction of the TMP filtrate. The analysis quantifies the five principal, neutral monosaccharides: arabinose, galactose, glucose, mannose and xylose. Therefore, in a first step the polysaccharides have to be hydrolysed. This is made by the use of sulphuric acid in an autoclave (120 °C). This hydrolysis condition, however, acts to decompose uronic acids, and does not include charged carbohydrates. In unbleached TMP samples mainly uronic acids of xylan and galactose are present and also in these polysaccharides not every monomer unit carries a carboxyl group (Sundberg et al. 2000). After hydrolysis with sulphuric acid the sample is run over a high performance anion exchange chromatograph with a pulsed amperometric detector (HPAEC-PAD) subsequently referred to as ion chromatography (IC).

After having removed the acid insoluble fraction by filtration, which includes, for example, the lipophilic extractives, the lignin content is measured in a UV-spectrophotometer at 205 nm. The extinction coefficient is  $110 \text{ dm}^3 \text{ g}^{-1} \text{ cm}^{-1}$ .

$400 \text{ cm}^3$  of the aqueous sample are dried in a glass beaker in an oven at 100 °C. To the dried sample  $3 \text{ cm}^3$  of sulphuric acid (73 wt%) are added and stirred at 30 °C for one hour and further  $84 \text{ cm}^3$  of deionised water is added. The beaker is covered with aluminium foil and placed in an autoclave at 120 °C for another hour. After that the hydrolysed sample is allowed to cool to room temperature. An aliquote of the sample is used for UV-spectroscopy to quantify the acid soluble lignin (see above). Another  $50.00 \text{ cm}^3$  is filtered through a  $0.2 \text{ }\mu\text{m}$  nylon membrane filter. The residue is washed with 1M sulphuric acid, dried and weighed to obtain the acid insoluble residue.

The rest of the acidic sample containing the hydrolysed monosaccharides is filled into a  $250 \text{ cm}^3$  volumetric flask and filled to the mark with deionised water. The sample can

be injected to the ion chromatograph. Arabinose, galactose, glucose, mannose and xylose were supplied by Sigma Aldrich in analytical grade and served as monosaccharide standards.

The analyses were performed externally at Innventia.

The reproducibility of the monosacchride content in a bleached softwood pulp determined in five different laboratories is shown in Table 3-3 (Innventia). It has to be noted that this analysis was made for a pulp sample, thus containing fibres, and hence, also a high glucose content originating from cellulose. The mean values and standard deviations are given in mg monosaccharide per g dry pulp. Nevertheless, the data shown in Table 3-3 gives some idea about the accuracy of the method.

**Table 3-3: Reproducibility of the method to determine the monosaccharide composition of the same bleached softwood pulp sample determined in five different laboratories.**

Group	Mean ( $n=5$ ) / $\text{mgg}^{-1}$	Standard deviation ( $n=5$ ) / $\text{mgg}^{-1}$
Arabinose	7.8	0.9
Galactose	93.0	15.8
Glucose	825.8	57.8
Xylose	86.6	7.8
Mannose	66.3	4.6
Sum	989.4	69.3

### ***3.4.6 Analysis of inorganic ions***

Ion chromatography is an ideal tool to determine anions and cations over a wide concentration range. The measurements were done on an ion chromatograph type 882

Compact IC from Metrohm<sup>15</sup>. The unit consists of two Compact devices (one for anions and one for cations), an autosampler and a dialysis unit.



**Figure 3-7: Ion chromatograph 882 Compact IC plus with autosampler (left), dialysis unit (middle) and the two 882 Compact IC plus units for anions (second from right) and cations (right).**

**Table 3-4: Method parameter for anion and cation analysis on the ion chromatograph.**

	Anions	Cations
Column	Metrosep A SUPP 5 150/0.4	Metrosep C 4-150/4.0
Pre-column	Metrosep A Supp 4/5 Guard	Metrosep C 4 Guard/4.0
Eluent	3.2 mM Na <sub>2</sub> CO <sub>3</sub> / 1 mM NaHCO <sub>3</sub> in deion. water (18.3 MΩ)	1.7 mM HNO <sub>3</sub> / 0.7 mM Dipidcolinic acid in deion. water (18.3 MΩ)
Flow / cm <sup>3</sup> min <sup>-1</sup>	0.7	0.9
Temperature / °C	23 ± 2	23 ± 2
Dialysis time / min	13	13
Analysis time / min	23	23
Pressure / MPa	6.9	6.8
Sample cvolume / mm <sup>3</sup>	20	10
Suppression solution	50 mM H <sub>2</sub> SO <sub>4</sub> in deion. water (18.3 MΩ)	none

<sup>15</sup> Metrohm Schweiz AG, Bleiche West, 4800 Zofingen, Switzerland

In order to removed undesired matrix components the samples are dialysed in the dialysis unit. The dialysis filter has a pore size of 0.2  $\mu\text{m}$  and is made out of celluloseacetate and nylon.

Chemical suppression was used in the analysis of the anions. Suppression improves the sensitivity by reducing the background conductivity. Detection is achieved with a conductivity detector. The detection range is 0 to 15 000  $\mu\text{Scm}^{-1}$ .

Figure 3-8 shows example calibration curves for chloride (left) and calcium (right) ions. The regression coefficient  $R^2$  is in both cases  $> 0.999$ . The steepness of the calibration curve is in both cases significant ( $p$ -value  $< 0.01$ , whereas the intercept is not significant ( $p$ -value  $> 0.05$ ).

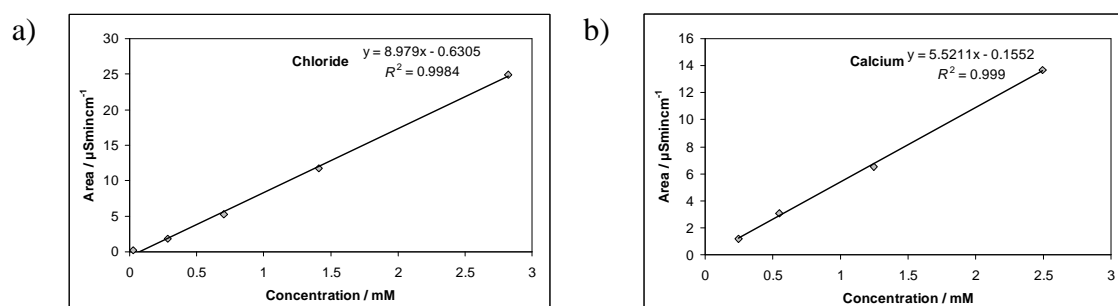


Figure 3-8: Calibration curves for a) chloride ions and b) calcium ions. Only the steepness is significant according to the  $t$ -test resulting in a  $p$ -value of 0.00 in both cases. The intercept is not significantly different from 0 having a  $p$ -value of 0.13 in the chloride calibration curve and 0.47 in the calcium calibration curve.

Table 3-5 includes the product number of the various ions supplied by Sigma Aldrich.

Calibration solutions are obtained from Sigma Aldrich. They have an ion concentration of  $1\,000 \pm 4\text{ mgdm}^{-3}$  (except  $\text{NH}_4^+$  and  $\text{Ca}^{2+}$  with  $\pm 5\text{ mgdm}^{-3}$ ) and are diluted with deionised water (18.3  $\text{M}\Omega$ ) using  $100.00 \pm 0.10\text{ cm}^3$  volumetric flasks and volumetric pipettes ( $1.00 \pm 0.01\text{ cm}^3$ ,  $2.50 \pm 0.01\text{ cm}^3$ ,  $5.00 \pm 0.02\text{ cm}^3$  and  $10.00 \pm 0.02\text{ cm}^3$ ). Furthermore, also the values for the limit of detection (LOD) are shown. The values are taken from the user manual of the IC 882 Compact IC plus measured by applying the same method settings as shown in Table 3-4.

**Table 3-5: Limit of detection according to the user manual of Metrohm and Sigma Aldrich order number of the various ions.**

Ion	Sigma Aldrich	Concentration / mM	Limit of detection <sup>1</sup> / mM
Fluorid F <sup>-</sup>	ICS010	52.6 ± 0.2	0.013
Chlorid Cl <sup>-</sup>	ICS005	28.2 ± 0.1	0.010
Nitrit NO <sub>2</sub> <sup>-</sup>	ICS016	21.7 ± 0.1	0.008
Bromid Br <sup>-</sup>	ICS003	12.5 ± 0.1	0.004
Nitrate NO <sub>3</sub> <sup>-</sup>	ICS014	16.1 ± 0.1	0.021
Phosphate PO <sub>4</sub> <sup>3-</sup>	ICS020	10.5 ± 0.0	0.010
Sulphate SO <sub>4</sub> <sup>2-</sup>	ICS022	10.4 ± 0.0	0.003
Lithium Li <sup>+</sup>	ICS029	144.1 ± 0.6	0.022
Sodium Na <sup>+</sup>	ICS032	43.5 ± 0.2	0.032
Ammonium NH <sub>4</sub> <sup>+</sup>	ICS027	55.4 ± 0.3	0.028
Potassium K <sup>+</sup>	ICS031	25.6 ± 0.1	0.080
Magnesium Mg <sup>2+</sup>	ICS030	41.1 ± 0.2	0.050
Calcium Ca <sup>2+</sup>	ICS028	25.0 ± 0.1	0.021

<sup>1</sup> According to the user manual of Metrohm – IC Application Work AW CH6-1001-072009 “Detection limits of the 882 Compact IC plus”

### ***3.4.7 Thermo gravimetric analysis***

The methods so far quoted to follow the adsorption process have focused on the liquid phase after centrifugation. A complementary view on the adsorption process can be achieved by analysing the sediment phase, for example with thermo gravimetric analysis (TGA). A defined amount of a material is weighed and heated. The loss of weight is recorded over the temperature profile. This method permits one to follow evaporation and decomposition processes and to determine the amount of volatile and/or decomposing material in the sample. In this thesis, the mineral / pitch composites were heated from 20 °C to 1 000 °C and the weight loss between 200 °C and 1 000 °C was recorded. As a reference also the mineral alone was measured, and the weight loss

from the mineral subtracted from the weight loss of a mineral / pitch composite related to the pitch alone. In addition, the applied scanning differential thermal analysis (SDTA) provides, in combination with the TGA, an evaluation of the volatility, thermal degradation and melting point, as well as physical and chemical transitions. The measurements were done on a Mettler Toledo<sup>12</sup> SDTA 851e.

The example TGA (black) and SDTA (violet) curves (Figure 3-9), for a talc that has been used for pitch adsorption in a TMP filtrate, show three important features. First is the endothermic process below 100 °C. While a part of that process is related to water evaporation, a certain portion can also be related to the glass transition /melting of the wood resin in the composite. The second feature is the exothermal process between 300 °C and 400 °C, which is related to the decomposition of wood resinous material. Finally, the third feature is related to dehydration, or, more specifically, dehydroxylation, of the mineral around 900 °C, i.e. calcination.

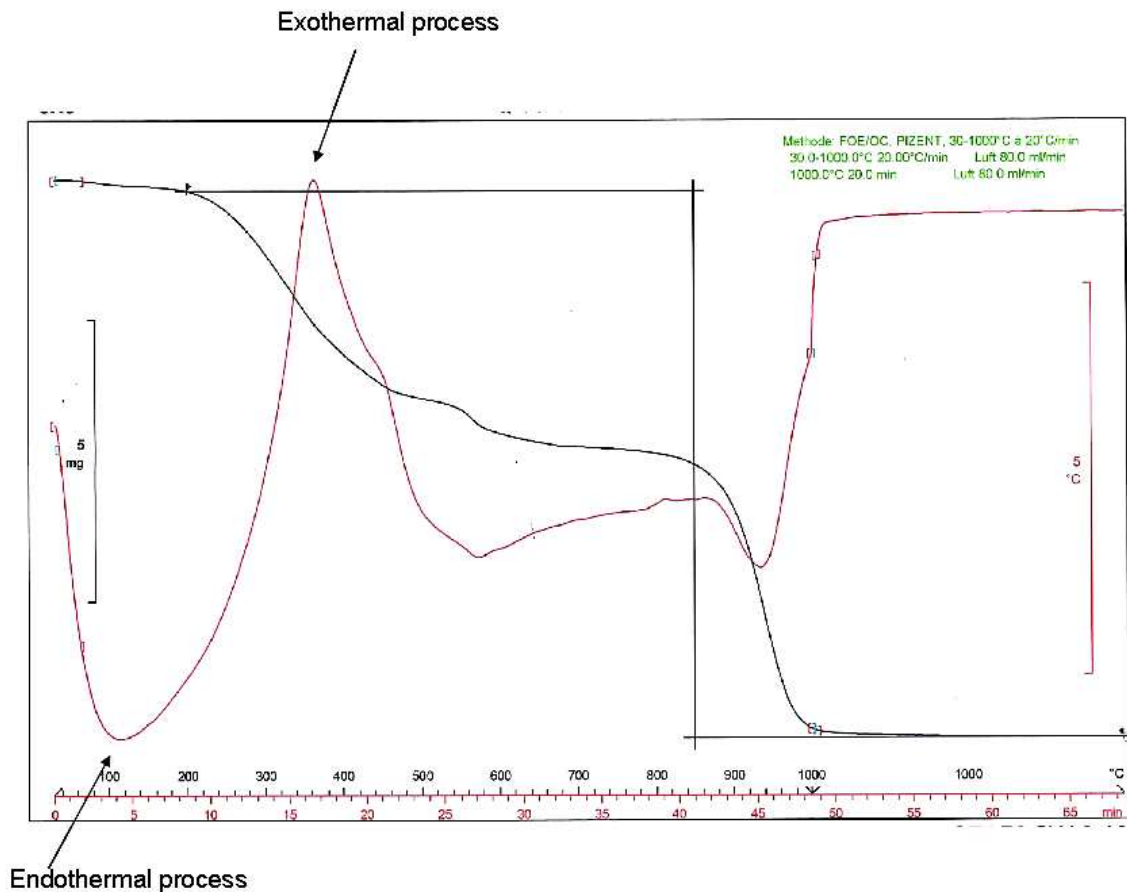


Figure 3-9: Example of a TGA (black)/SDTA (violet) curves for a talc/pitch composite.

### 3.4.8 Equilibrium

The term equilibrium is defined through the situation at which the reaction speed of adsorption and desorption is equal and hence the Gibbs free energy of the adsorption reaction,  $\Delta_r G$ , is equal  $= 0 \text{ kJmol}^{-1}$ . In order to verify if the adsorption isotherms were in equilibrium the turbidity change of a TMP filtrate with a starting turbidity of 425 NTU was measured over time (Figure 3-10). The filtrate was treated with 10 and 20  $\text{gdm}^{-3}$  of HSA-talc (see section 6.1.2.1). It can be seen that the adsorption takes place within a few minutes and that the employed 120 min for an adsorption experiment can be considered as equilibrium condition. It must, however, be recognised that kinetic studies with this method always suffers from a time delay of 15 min due to the necessary separation step. Therefore, kinetical interpretations should not be followed. Other authors (Chang 1985) described the adsorption process to be instantenous.

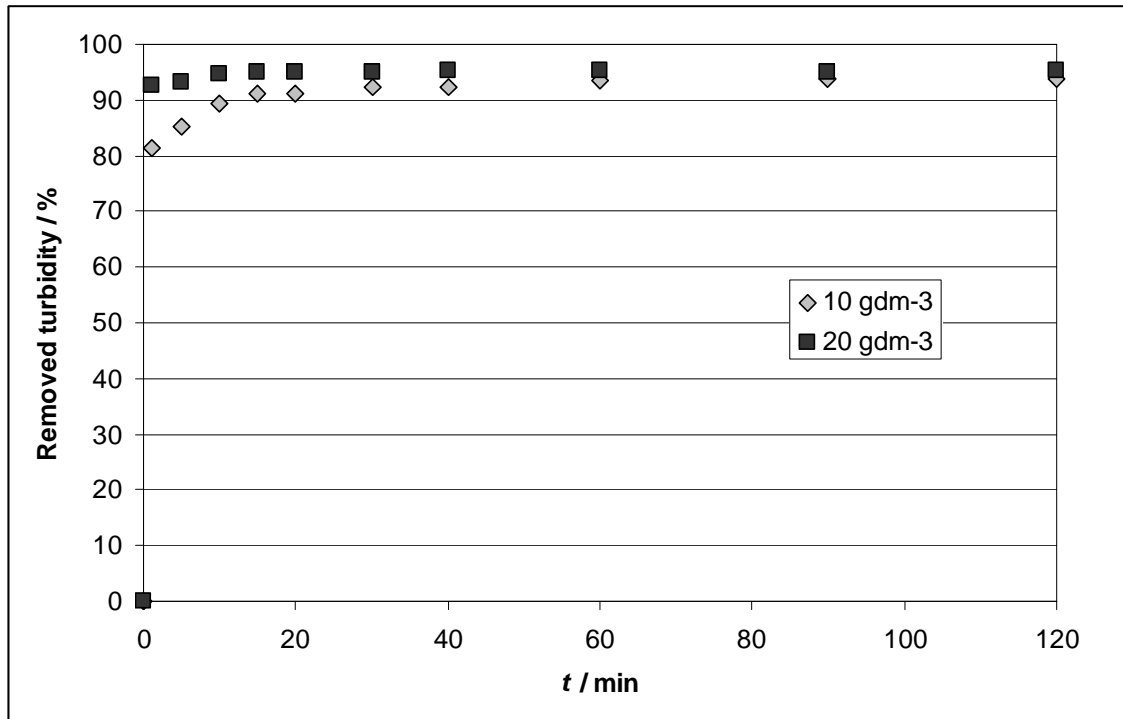


Figure 3-10: Adsorption kinetic of colloidal pitch onto HSA-talc. The starting turbidity was 425 NTU. Talc dosage was 10 (grey diamonds) and 20 (dark squares)  $\text{gdm}^{-3}$ .

### 3.4.9 Statistical considerations

Some mention needs to be made about statistics in this thesis. The scope of this section, is however, only to give the reader some idea about the experimental procedures by which the later presented data was obtained and to give some fundamental information about the statistical significance of the data and fits.

The presented particle size data, specific surface areas and densities of the minerals are typically double determinations. A specific sample was, however, measured until the difference between two measurements was not bigger than 1 %. From these two measurements the average is shown in the thesis.

Electrophoretic mobility measurements are single point measurements if not indicated otherwise.



Typical adsorption measurements are based on three independent data points and the shown error bars represent the standard deviation of the triplicate. The adsorption isotherms are single point measurements. This makes it difficult to draw significant conclusions between the adsorption behaviour of two different minerals. Nevertheless, trends can be observed and discussed. The reason for not including more replicates was to keep the work effort on a reasonable level. For example, in section 6.1 isotherms at seven different pH levels were recorded. With only eight or nine data points per isotherm this yields already in 60 measurements. Including triplicates would expand the experimental matrix hugely. 60 measurements can be handled in one day. It is absolutely crucial to run a set of experiments within one day and with the same pulp sample. TMP samples, especially after removal of the fibres, alter very fast and start to coagulate. Because the filtration step in the procedure is hard difficult to reproduce it is also no alternative to use different filtrate batches of the same TMP sample. Finally, using different TMP samples would only show the natural fluctuation of the wood composition.

#### ***3.4.9.1 Linear and non-linear regression***

In the following chapters linear and non-linear regression were made to fit the data. The common form of the linear regression is  $y=mx+b$  with the parameters  $m$  as the steepness and  $b$  as the intercept. For these fits the regression coefficient or goodness of fit  $R^2$  is given in the figures and tables or in the corresponding text. The regression coefficient contains no information about the statistical significance of the fitted parameters. The regression coefficient only explains how well the variation of  $x$  explains the variation of  $y$ , e.g. if  $R^2=0.75$ , the variation of  $x$  explains 75 % of the variation of  $y$ . The regression coefficient also serves to decide between different models to fit the data. For example, if one wants to decide whether a set of adsorption isotherm data is preferably fitted with a Langmuir (Equation 2-17) or a Freundlich (Equation 2-18) isotherm. In this case both

isotherms are plotted in their linear form and fitted with the adsorption data. The fit with the better goodness of fit describes the adsorption isotherm best.

In order to answer the question of statistical significance of the fitted parameters one can either use the confidence intervals of each parameter or the hypothesis test. The null hypothesis  $H_0$  is that the fitted parameter is equal to zero. The alternative hypothesis  $H_A$  is that the fitted parameter can have every other value except 0. Obviously, if the parameter  $m$  is 0 no significant relation between  $y$  and  $x$  is possible. Instead of the confidence interval the  $p$ -value of the fitted parameter can be used to decide upon statistical significance. Since in this thesis in all cases the confidence interval was chosen to be 95%, statistical significance is given with  $p$  is equal or smaller than 0.05. Therefore, the  $p$ -value allows deciding about significance of the fitted parameter. Additionally, the  $p$ -value quantifies how significant an alternative hypothesis is (i.e. how strong the evidence to reject  $H_0$  is). This may be expressed as follows:

- $p$ -value  $\sim 0.05$  : weakly significant
- $p$ -value  $\sim 0.01$  : significant
- $p$ -value  $\sim 0.001$  : strongly significant
- $p$ -value  $< 10^{-4}$  : highly significant

Besides the linear regression applied in this thesis also non-linear regressions were performed. This was typically done to fit the parameters for the Langmuir isotherm or to fit log-normal distribution functions through particle size distribution data. It is here not intended to explain how non-linear least squares regressions are performed. The fits were computed with TableCurve<sup>®</sup> 2D<sup>16</sup>. In the case of the fitted Langmuir parameters,

---

<sup>16</sup> SYSTAT Software Inc., 501 Canal Boulevard, Suite F, 94804-2028 Richmond, Canada

$K_L$  and  $I_{\max}$ , the  $p$ -value ( $P > |t|$ ) is given as a measure for the statistical significance similar to the linear regression explained above.  $P$  stands for the probability ( $p$ -value) and  $|t|$  is referring to the  $t$ - or students-test which assumes a normal or student distribution of the parameter value and its probability of appearance. In addition also the regression coefficient is given, which again does not contain any information about statistical significance.

It is also important to mention here that the discussed statistical significance only describes if the outcome of a parameter fit is significant. It does, however, not describe, if this parameter is statistically significant from the same parameter of another set of data.

## **4 Determining the size distribution-defined aspect ratio of platy and rod-like particles**

In this chapter the practical determination of aspect ratio for mineral particles based on knowledge of surface area and a carefully defined particle size distribution is explored.

The following hypotheses are tested:

**H1** The traditional (Hohenberger) equation relating the aspect ratio of a particle to its diameter and surface area contains false assumptions and can be improved for the case of high aspect ratio particles such as platelets and rods.

**H2** Particle size measurements can be made more reliable for high aspect ratio particles by a carefully reviewed choice of method.

**H3** Equations for aspect ratios based surface area measurements are invalid for particles which **(a)** agglomerate or **(b)** are porous.

The work reported here has also been published as part of the thesis activities (Gantenbein et al. 2011a; Gantenbein et al. 2011b).

### **4.1 Introduction**

This study focuses on the Hohenberger model (Hohenberger 2001) for the determination of aspect ratios of platy- and rod-like particles. The advantage of this model is the fact that it has two independent parameters, namely the specific surface area and the particle size. Methods for the determination of both parameters are readily available and are routinely measured in the analysis of mineral particles. The model assumes either a disc or rod-like geometry, and a resulting aspect ratio from the specific

surface area by BET combined with a necessarily well-defined particle size measurement. Despite the reasonable results usually obtained by the Hohenberger approach, some significantly false assumptions in respect to parameter input have been frequently presented in the literature. This study set out to clarify these issues, improve the application and definition of the model and further apply it by way of illustration for platy particles (talc and Laponite (Laponite® RD)), which represent materials having typical particle size distributions to be found in many industrially relevant applications. The results are compared with other methods that are based on particle size analysis. Additionally, by contrasting talc particles with Laponite particles swelling in water, the sensitivity to the input parameters in respect to their physical interpretation is illustrated. Aragonite and palygorskite are used as models for rod-like particles. Comparison is made with image analysis results and other methods based on various methods of particle sizing. Sensitivity with respect to the physical and geometrical interpretation of the specific surface area as measured by nitrogen adsorption is illustrated by comparing non-porous (aragonite) and porous (palygorskite) particles.

#### ***4.1.1 Hohenberger model (2001)***

According to Hohenberger (2001) the representative aspect ratio of platy particles like talc or kaolin can be calculated by

$$\rho = \frac{\varepsilon_{\text{BET}} \cdot d_{50} \cdot e^{-\ln^2\left(\frac{d_{84}}{d_{50}}\right)} \cdot \delta_{\text{P}} - 4}{2}$$

**Equation 4-1**

and similarly for rod like particles by

$$\rho = \frac{\varepsilon_{\text{BET}} \cdot d_{50} \cdot e^{-\ln^2\left(\frac{d_{84}}{d_{50}}\right)} \cdot \delta_{\text{P}} - 2}{4}$$

Equation 4-2

in which the measured variables are defined as,

$\varepsilon_{\text{BET}}$  : specific surface area by nitrogen adsorption (BET)

$d_{84}$  : particle size at 84 % of the sample having less than this size, originally,  
by Hohenberger, arbitrarily defined

$d_{50}$  : particle size at 50 % of the sample having less than this size, originally,  
by Hohenberger arbitrarily defined

$\delta_{\text{P}}$  : density of the particle

Hohenberger (2001) did not define the particle size measurement method. Following the manuscript, sieving for coarse particles or sedimentation for fine particles could be the methods of choice for particle size analysis. Applying Stoke's law for particle size measurements results in an equivalent spherical diameter (*esd*), which is not corresponding to the disc diameter *d*, needed for the rigorous application of Hohenberger's equations, Equation 4-1 and Equation 4-2. Furthermore, it is very unclear from the literature whether the cumulative particle size curve should be used in number, volume or mass (for which the latter two are the same if a constant density applies for all particles in the system).

The aspect ratio  $\rho$  of a circular disc-like particle, was given in Equation 2-3. The surface area *s* of one such particle (Figure 2-18) is given by

$$s = 2\left(\frac{\pi \cdot d_d^2}{4}\right) + \pi \cdot d_d \cdot t_d$$

**Equation 4-3**

and so, we can express the aspect ratio  $\rho$  as

$$\frac{1}{\rho} = \frac{s}{\pi \cdot d_d^2} - \frac{1}{2}$$

**Equation 4-4**

The specific surface area (ssa)  $\varepsilon$  for a single particle is defined as

$$\varepsilon = \frac{s}{m}$$

**Equation 4-5**

where  $m$  is the mass of the particle having the surface area  $s$ . If the density of the particle is  $\delta$ , then

$$\varepsilon = \frac{s}{\left(\frac{\pi \cdot d_d^2 \cdot t_d}{4}\right) \delta}$$

**Equation 4-6**

which gives

$$s = \varepsilon \left(\frac{\pi \cdot d_d^2 \cdot t_d}{4}\right) \delta$$

**Equation 4-7**

Substituting in Equation 4-4 provides

$$\frac{1}{\rho} = \frac{\varepsilon \left( \frac{\pi \cdot d_d^2 \cdot t_d}{4} \right) \delta}{\pi \cdot d_d^2} - \frac{1}{2} = \frac{\varepsilon \cdot \delta \cdot t_d - 2}{4}$$

**Equation 4-8**

and

$$\rho = \frac{4}{\varepsilon \cdot \delta \cdot t_d - 2}$$

**Equation 4-9**

By eliminating the particle thickness  $t$  by substituting with the expression for  $\rho$  from Equation 2-3, we obtain

$$\rho = \frac{4}{\frac{\varepsilon \cdot \delta \cdot d_d}{\rho} - 2}$$

**Equation 4-10**

such that

$$\rho = \frac{\varepsilon \cdot \delta \cdot d_d - 4}{2}$$

**Equation 4-11**

With the knowledge of the specific surface area determined by the BET method  $\varepsilon_{\text{BET}}$ , the aspect ratio can be written as

$$\rho = \frac{\varepsilon_{\text{BET}} \cdot \delta_P \cdot d_d - 4}{2}$$

**Equation 4-12**

In most cases, particle size distributions were described statistically by using the log-normal distribution (Randall 1989). In a log-normal distribution the particle with the most occurrence probability is given by the mode value,



$$\bar{d}_N = e^{\mu - \sigma^2}$$

**Equation 4-13**

where  $\mu$  and  $\sigma$  are the natural log geometric mean and natural log standard deviation respectively, such that the median (midpoint or 50% value) is expressed by

$$d_{50} = e^{\mu}$$

**Equation 4-14**

The geometric standard deviation  $\sigma$  of a log-normal distribution is determined either by dividing the number median particle diameter (which is the particle size where 50% of the particles are finer than this size) by the particle size at 15.87 % or by dividing the particle size at 84.13% by the number median particle diameter (Aitchison, Brown 1957).

$$\sigma = \frac{d_{N50}}{d_{N15.87}} = \frac{d_{N84.13}}{d_{N50}}$$

**Equation 4-15**

Thus, dealing with a number distribution, and not the commonly used mass (volume) percent, results in

$$\bar{d}_N = d_{N50} \cdot e^{-\ln^2\left(\frac{d_{N84.13}}{d_{N50}}\right)}$$

**Equation 4-16**

Combining Equation 4-12 with Equation 4-16 leads to Equation 4-17, which is very similar to the one proposed by Hohenberger (Equation 4-1).

$$\rho = \frac{\varepsilon_{\text{BET}} \cdot d_{N50} \cdot e^{-\ln^2\left(\frac{d_{N84.13}}{d_{N50}}\right)} \cdot \delta_{\text{P}} - 4}{2}$$

**Equation 4-17**

Similarly, for rod like particles the aspect ratio can be written as

$$\rho = \frac{\varepsilon_{\text{BET}} \cdot d_{N50} \cdot e^{-\ln^2\left(\frac{d_{N84.13}}{d_{N50}}\right)} \cdot \delta_{\text{P}} - 2}{4}$$

**Equation 4-18**

In Equation 2-3 and Equation 4-12, the disc diameter  $d$  was used to calculate the aspect ratio and consequently in the whole derivation of Equation 4-17. It is, thus, necessary to transform the equivalent spherical diameter ( $esd$ ) into the platelet diameter  $d$ . A proposed answer to this was given by Jennings and Parslow (1988) and Jennings (1993) in Table 2-4. Similarly, in Equation 2-4 the rod length was used to calculate the aspect ratio of the rod and hence,  $esd$  needs to be converted into the rod length via the formulae in Table 2-4.

The platelet diameter  $d$  is a function of the equivalent spherical diameter ( $esd$ ) and the aspect ratio  $\rho$  as shown in Equation 4-19.

$$\rho = \frac{\varepsilon_{\text{BET}} \cdot d_{N50}(esd_{N50}, \rho) \cdot e^{-\ln^2\left(\frac{esd_{N84.13}}{esd_{N50}}\right)} \cdot \delta_{\text{P}} - 4}{2}$$

**Equation 4-19**

In the case of rod-like particles the rod length  $l$  is a function of the  $esd$  and the aspect ratio  $\rho$  resulting in Equation 4-20.

$$\rho = \frac{\varepsilon_{\text{BET}} \cdot l_{N50}(\text{esd}_{N50}, \rho) \cdot e^{-\ln^2\left(\frac{\text{esd}_{N84.13}}{\text{esd}_{N50}}\right)} \cdot \delta_p - 2}{4}$$

**Equation 4-20**

These equations may then be solved by iteration until convergence of  $\rho$  is achieved.

In the case where the aspect ratio of coarse and fine particles in a sample can differ, the variables  $\text{esd}_{N84}$  and  $\text{esd}_{N50}$  in the exponent would require a modification in respect to the conversion factor expressing the platelet diameter. In the case described here, this information was not known *a priori*, and thus, a constant aspect ratio throughout the whole particle size distribution was assumed. Furthermore, the definition of an aspect ratio distribution spanning a particle size distribution is a highly complex topic (Pabst, Berthold 2007) and would not go hand in hand with the intended fast and simple solution.

Thus, all the open questions and incomplete assumptions made by Hohenberger could be answered by following the proposed model in this study.

## **4.2 Platy particles**

### **4.2.1 Material and Methods**

#### **4.2.1.1 Minerals**

Finnish talc (FT) was sourced from Mondo Minerals B.V., originating from the region of Sotkamo, Finland, available as Finntalc P05. It had a specific surface area determined by nitrogen adsorption, of  $9 \text{ m}^2\text{g}^{-1}$ .

Australian talc (AT) was also sourced from Mondo Minerals B.V., available as Westmin PCS. It had a specific surface area of  $19 \text{ m}^2\text{g}^{-1}$ .

The high surface area talc grade (HSA) was specially manufactured by comminuting the coarser Finnish talc grade described above. It had a specific surface area of  $45 \text{ m}^2\text{g}^{-1}$ .

XRD analysis of all talc samples similarly indicated talc and associated chlorite.

The sample of Laponite, having the formula  $\text{Si}_8\text{Mg}_{5.45}\text{Li}_{0.4}\text{H}_4\text{O}_{24}\text{Na}_{0.7}$  (Mourchid et al. 1995), was provided by Rockwood additives, available as Laponite<sup>®</sup> RD. It had a specific surface area of  $330 \text{ m}^2\text{g}^{-1}$ .

SEM pictures of the various minerals are shown in Figure 4-1. The Laponite<sup>®</sup> RD appears as rather big lumps. That is due to the swelling property of the synthetic hectorite such that in the dry state the individual platelets aggregate.

#### **4.2.1.2 Methods**

The samples were analysed with a Bruker D8 Advanced powder diffractometer (2.2 kW X-ray tube, a sample holder, a  $\theta$ - $\theta$  goniometer, and a point scintillator, Ni-filtered  $\text{Cu K}_\alpha$  radiation). The profiles were chart recorded automatically using a scan speed of  $0.7^\circ$  in  $2\theta$  per minute. The mineral content was estimated by the DIFFRACplus software packages EVA and SEARCH, based on reference patterns of the ICDD PDF 2 database.

The density of the mineral powders was determined with the AccuPyc<sup>®</sup> 1330 pycnometer from Micromeritics.

The specific surface area was determined with the Gemini 2360 from Micromeritics. The samples were outgassed at  $250^\circ\text{C}$  for 30 minutes under nitrogen in a Micromeritics Flow Prep 060.

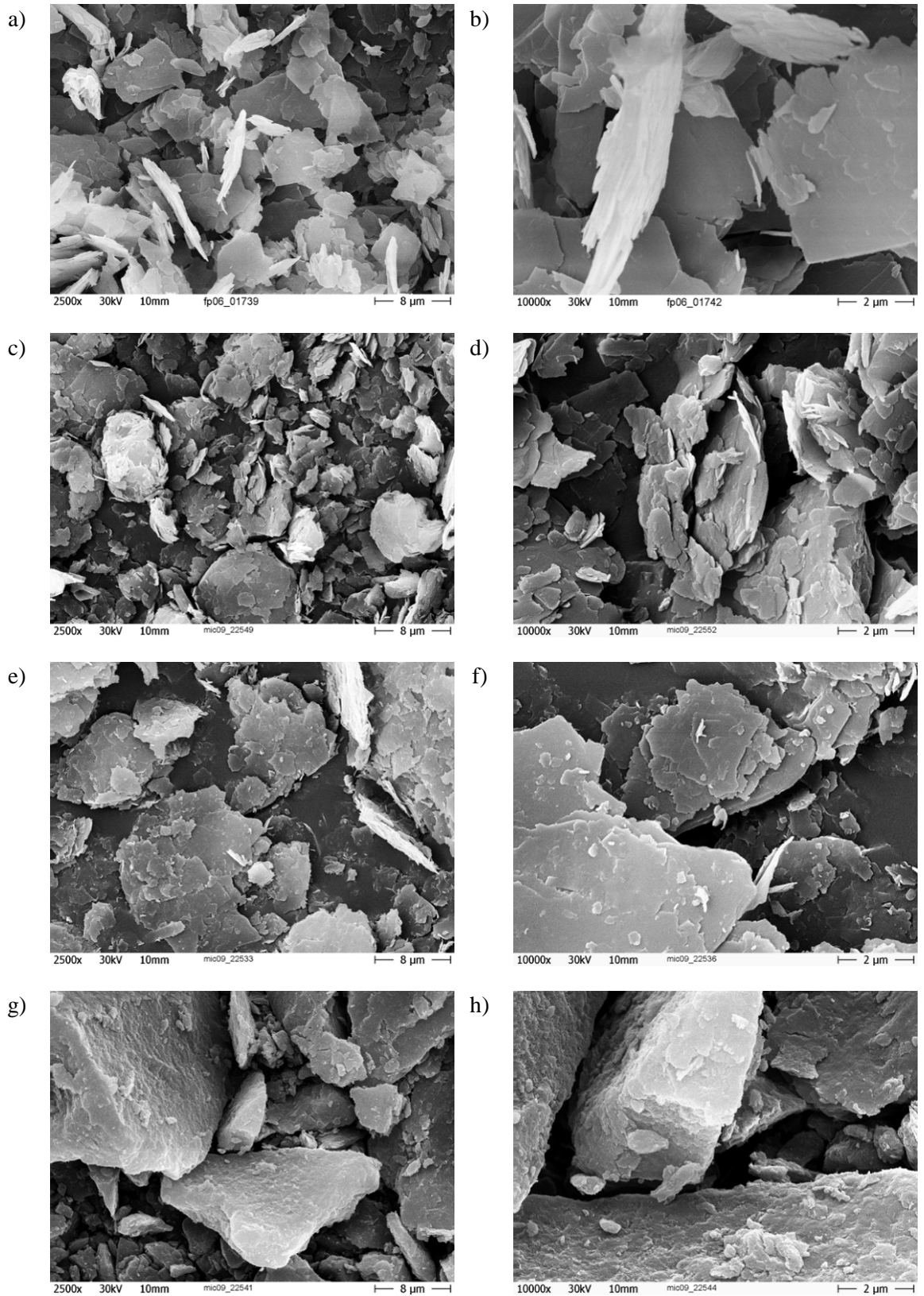


Figure 4-1: SEM pictures of the four investigated minerals Finntalc P05 (a + b), Westmin PCS (c + d), Comminuted high surface area talc (e + f) and Laponite<sup>®</sup> RD (g + h).

The samples were measured on the Sedigraph® 5120 from Micromeritics. All samples were dispersed with a 0.1 % solution of sodium diphosphate ( $\text{Na}_4\text{P}_2\text{O}_7$ ). Samples of 10 g dry talc were dispersed in  $100 \text{ cm}^3$  of the diphosphate solution with a high speed blender (Polytron PT 3100 from Kinematica) for 15 min at  $15\,000 \text{ min}^{-1}$  followed by ultrasonication for 10 minutes in a 130 W ultrasonic bath.

A few drops of the dispersions were diluted further with 0.1 % solution of sodium diphosphate. The samples were measured with the Malvern Mastersizer 2000. The laser obscuration was set to be between 10 and 20 %.

A few drops of the dispersions were also diluted with the 0.1 % solution of sodium diphosphate and measured on the Malvern Zetasizer Nano ZS.

#### ***4.2.2 Results and Discussion***

The specific surface areas of the investigated materials lay between 9 and  $330 \text{ m}^2\text{g}^{-1}$  and the density between  $2\,570$  and  $2\,750 \text{ kgm}^{-3}$  (Table 4-1). The specific surface area of a dispersed product may differ from the one measured by nitrogen adsorption in the dry state. For the investigated model it is crucial to apply the specific surface area of the dispersed particle. This was valid for the talc particles but not for laponite.

**Table 4-1: Specific surface area determined by nitrogen adsorption and density of the investigated minerals.**

	<b>FT</b>	<b>AT</b>	<b>HSA</b>	<b>Laponite</b>
Specific surface area (BET) / $\text{m}^2\text{g}^{-1}$	9	19	45	330
Density / $\text{kgm}^{-3}$	2 750	2 750	2 750	2 570

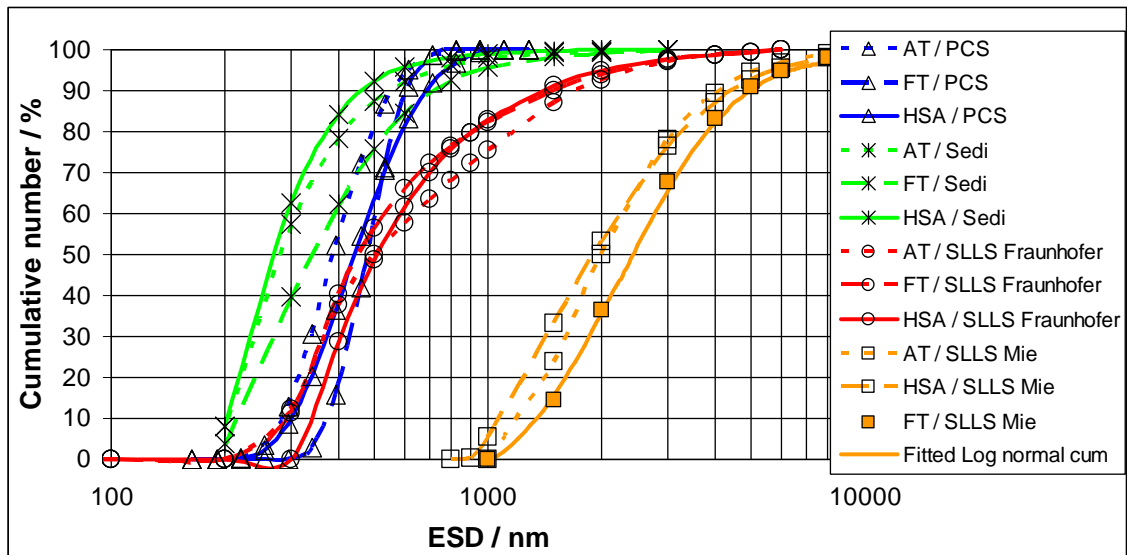


Figure 4-2: Particle size distribution by photon correlation spectroscopy (PCS), static laser light scattering (SLLS) and sedimentation for the three talc grades (number based).

The particle size data obtained by sedimentation suggested the presence of finer particles (Figure 4-2). Disc-like particles will not settle like a sphere following the direct and shortest path but rather will float and oscillate like a falling leaf, moving also side-ways. The photon correlation spectroscopy data showed a step log-normal distribution (Figure 4-2). The static laser light scattering with Fraunhofer optics did not yield a log-normal size distribution and showed an increased amount of coarse material (Figure 4-2). Static laser light scattering using Mie theory only detected the very coarse fraction of talc particles (Figure 4-2). The  $d_{N50}$  and  $d_{N84}$  values (Table 4-2) were used to calculate the mode values, which were consequently converted into the corresponding aspect ratios (Table 4-3).

Each particle size method has its optimal size region for analysis and some of the methods are affected more strongly by anisometric shapes than others. These facts also influenced the determination of the aspect ratio. PCS measurements are not so strongly affected by anisometric shapes than are the others (Jennings and Parslow, 1988) since the detection in PCS excludes particles that do not undergo random Brownian motion and, thus, there is no preferred orientation for the particles as there is for sedimentation.

The particle size was already at the upper limit for PCS measurements. The Fraunhofer model is, in theory, only valid for particles with a diameter five times larger than the illuminating wavelength (Schmidt 2000). Sedimentation by Stokes' law for anisometric disc-like particles is perturbed due to the falling leaf effect, which becomes more and more significant the more the aspect ratio increases, and, thus, the method is not reliable for high aspect ratio particles.

**Table 4-2:  $d_{N50}$  and  $d_{N84}$  based on a fitted logarithmic cumulative distribution performed with TableCurve 2D.**

<b>Method</b>		<b>FT</b>	<b>AT</b>	<b>HSA</b>
PCS	$d_{N50}$ / nm	480	390	450
	$d_{N84}$ / nm	570	510	620
SLLS / Fraunhofer	$d_{N50}$ / nm	500	550	530
	$d_{N84}$ / nm	920	1 170	830
SLLS /Mie	$d_{N50}$ / nm	2 400	2 030	1 930
	$d_{N84}$ / nm	4 040	3 420	3 600
Sedigraph®	$d_{N50}$ / nm	340	280	270
	$d_{N84}$ / nm	600	450	400

Also the other models of Jennings and Parslow (1988) and Pabst and Berthold (2007) depend on the sedimentation result and suffer from the same root problem. However, the opposite was observed for the HSA talc particles. The number based sedimentation particle size data suggested the presence of too coarse particles and thus the resulting aspect ratio was higher than the one calculated by the other methods. The same effect also led to an underestimation of the aspect ratio by the model of Jennings and Parslow (1988) and Pabst and Berthold (2007). Finally, the laser diffraction based on the true Mie theory was overestimating the coarse fraction of the talc samples, although, from a purely physical point of view of equivalent size, interpretation by the Mie theory seems more appropriate. Assumptions like isotropic spheres, for which the Mie theory is valid,



may lead to erroneous deconvolution for systems with anisotropic particles (Pabst et al. 2000). It is, therefore, suggested to apply either PCS or static laser light scattering with Fraunhofer optics. PCS showed the least number of drawbacks compared to the other methods when considering the whole particle size range investigated in this paper, though the upper size limit of Brownian motion is restrictive. Static laser light scattering with Fraunhofer optics is limited in respect to the fine particle analysis, though in the exemplified cases it did reach the lower limit of the particle size. The models of Jennings and Parslow (1988) and Pabst and Berthold (2007) could not clearly distinguish the aspect ratios of the different talc particles based on the number based distribution data.

**Table 4-3: Calculated aspect ratio for the three talc particles. The aspect ratios were calculated by Equation 4-19. In addition the aspect ratios were calculated based on the model of Pabst and Berthold (2007) (Equation 2-8) and on the model of Jennings and Parslow (1988) for oblate spheroids (Equation 2-5) and discs (Equation 2-6). All calculations were based on the mode value from the corresponding  $d_{N50}$  and  $d_{N84}$  values in Table 4-2.**

Model	Method	FT	AT	HSA	Comment
Gantenbein <i>et al.</i> (Equation 4-19)	PCS	6	12	37	Upper limit of the particle size range
	SLLS / Fraunhofer	2	8	35	Only log-normal in a certain region
	Sedigraph®	2	11	84	Mass to number transformation
	SLLS / Mie	85	207	590	Over estimating the coarse fraction
Jennings and Parslow for oblate spheroids (Equation 2-5)	Sedigraph® / SLLS Fraunhofer	5	5	7	Falling leaf effect
Jennings and Parslow for discs (Equation 2-6)	Sedigraph® / SLLS Fraunhofer	6	6	9	Falling leaf effect
Pabst and Berthold (Equation 2-8)	Sedigraph® / SLLS Fraunhofer	9	9	12	Falling leaf effect

Based on the values calculated above, together with Equation 2-3 and the equations in Table 2-4, the particle dimensions diameter  $d_d$  and thickness  $t_d$  were calculated (Table 4-4). The different particle size measurement methods indicated similar particle thickness values. The thickness of the low surface area Finnish talc (FT) varied between 80 and 180 nm. The thickness of the Australian talc particles was  $\sim 40 - 50$  nm and of the highly delaminated talc particles  $\sim 17$  nm. The crystallographically defined talc layer is 0.92 nm thick (Bergaya et al. 2006). The thickness mainly controls the specific surface area of the particles, and, thus, the surface area determination is a sensitive method. Of course, for lower surface area materials this influence becomes smaller, and the particle thickness is then also affected by the disc diameter. The disc diameter varied strongly for the different talc grades and measurement methods, mainly as a result of the different responses of the particle size measurement methods. Nevertheless, the results for the FT and AT talc particles with PCS, Fraunhofer light scattering and Sedigraph<sup>®</sup> particle size data gave similar results, whereas the results for the HSA grade were only similar for the PCS and Fraunhofer model particle size data.

**Table 4-4: Particle disc diameter  $d_d$  and disc thickness  $t_d$  in nm.**

Method	FT		AT		HSA	
	$d_d$ / nm	$t_d$ / nm	$d_d$ / nm	$t_d$ / nm	$d_d$ / nm	$t_d$ / nm
PCS	660	110	540	45	630	17
SLLS / Fraunhofer	360	150	390	48	600	17
Sedigraph <sup>®</sup>	260	180	500	45	1 390	17
SLLS / Mie	7 030	80	8 000	39	9 600	16

Besides the calculations quoted above, which were based on the number particle size distribution, it is also possible to use the mass or volume based particle size distribution data (Table 4-5). Similar particle sizes were found only for the PCS measurements. This

is because of the steep distribution of the data in the PCS measurement. Since the PCS measurements are restricted to the Brownian motion limit, they tend to underestimate the aspect ratio. Similar aspect ratios were calculated for the Finnish and Australian talc particles with the particle size data from the static laser light scattering using Fraunhofer optics and the sedimentation technique. These aspect ratios compare also well with the aspect ratios calculated by the model of Jennings and Parslow (1988) and Pabst and Berthold (2007). In the case of the HSA talc the falling leaf effect for very fine platelets perturbed the aspect ratio values for all models based on the sedimentation technique.

The current model underestimates the aspect ratio if the particles are too fine to be measured in the Sedigraph<sup>®</sup> whereas the models of Jennings and Parslow (1988) and Pabst and Berthold (2007) overestimate the aspect ratio if the particles are too fine. The sedimentation data allowed us to consider the contrast between mass/volume and number probability distribution of particle size. When using mass/volume distribution, the aspect ratios appear much greater, as the distribution mass median is shifted to larger particle size than the number median. The exception to this finding is the HSA talc grade, for which the aspect ratio reduces to 22. This effect, at first sight unexpected, clearly relates to the inappropriate method of sedimentation of highly delaminated platy particles. The falling leaf effect suggests much finer particles than are found in reality. Sedimentation data were also used for the models of Pabst et al. (2000) and Jennings and Parslow (1988). It is, therefore, questionable to use these models for platy particles with large diameters and very thin thickness, whereas fine particles undergoing strong Brownian rotation are better suited.

**Table 4-5: Aspect ratio of the three different talc particles based on the various models. The values were obtained by inserting the mode value of the volume or mass based distribution data.**

<b>Model</b>	<b>Method</b>	<b>FT</b>	<b>AT</b>	<b>HSA</b>
	PCS	7	15	50
Gantenbein et al. (Equation 4-19)	SLLS / Fraunhofer	63	114	330
	SLLS / Mie	345	840	4380
	Sedigraph®	62	108	22
Jennings and Parslow for oblate spheroids (Equation 2-5)	Sedigraph® / SLLS Fraunhofer	50	80	2800
Jennings and Parslow for discs (Equation 2-6)	Sedigraph® / SLLS Fraunhofer	75	120	4300
Pabst et al. (Equation 2-8)	Sedigraph® / SLLS Fraunhofer	78	121	4300

**Table 4-6: Aspect ratio calculated with the original Hohenberger model (Equation 4-1) based on number and volume or mass based distribution data.**

<b>Method</b>	<b>FT</b>		<b>AT</b>		<b>HSA</b>	
	<b>Number</b>	<b>Volume</b>	<b>Number</b>	<b>Volume</b>	<b>Number</b>	<b>Volume</b>
PCS	4	4	7	9	22	31
SLLS / Fraunhofer	2	44	8	80	25	230
SLLS / Mie	20	56	37	100	70	300
Sedigraph	1	11	3	11	12	6

For completeness, the aspect ratios based on the original Hohenberger equation (Equation 4-1) (Table 4-6) were also calculated based on number distribution and volume or mass distribution data for comparison.

To illustrate the sensitivity of the specific surface area, dispersions of laponite particles were studied. They could only be measured by PCS (Figure 4-3), due to the nanosized dimensions. The curve showed a log-normal distribution with a  $d_{N50}$  of 13 nm and a  $d_{N84}$  of 17 nm. The resulting aspect ratio was 5.2 (Equation 4-19). For comparison, the

following references are considered (Bonn et al. 1999; Kroon et al. 1996; Kroon et al. 1998; Mal et al. 2008; Mouchid, Levitz 1998; Mouchid et al. 1995; Thompson, Butterworth 1992). The particle disc diameters were around 20 - 30 nm and the thickness 1 nm. Thus the aspect ratio would vary between 20 and 30. These values clearly differed from the value of 5.2 obtained in this study. This is related to the inappropriate value of the specific surface area determined by nitrogen adsorption. The surface area exposed by the laponite particles in water is manifestly higher than in the dry state due to swelling and delamination of the particles. Thus, the available specific surface area of the dispersed particles was approximated as follows.

Based on Equation 4-21, the particle thickness  $t_d$  was calculated as a function of the aspect ratio  $\rho$  with the  $d_{N50}$  of 13 nm and  $d_{N84}$  of 17 nm and plotted in Figure 4-4.

$$t_d = \frac{\tan^{-1}(\rho) \cdot esd_{N50} \cdot e^{-\ln^2\left(\frac{esd_{N84}}{esd_{N50}}\right)}}{\rho}$$

Equation 4-21

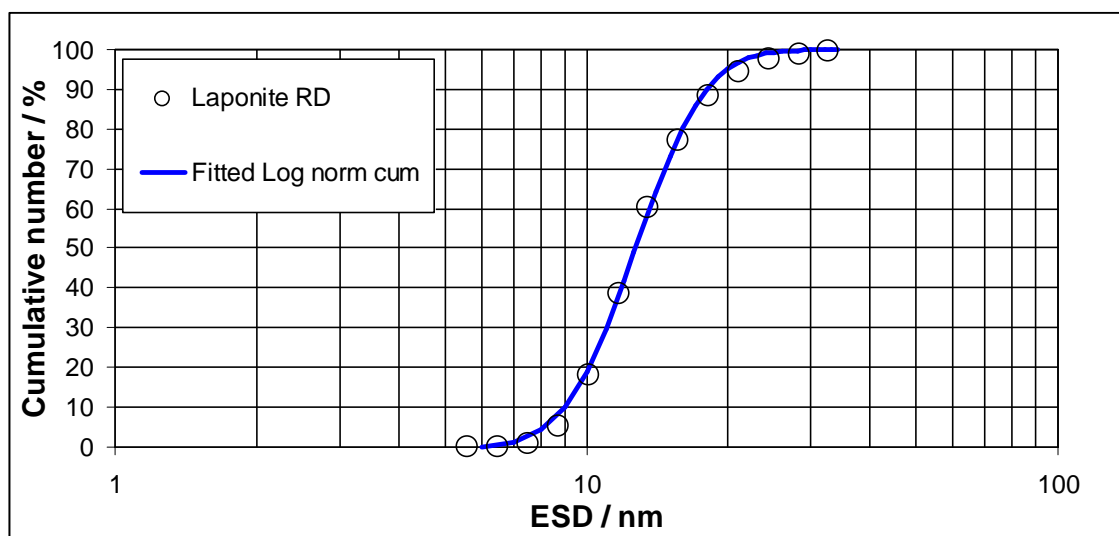


Figure 4-3: Particle size distribution measured by photon correlation spectroscopy for the Laponite® RD.

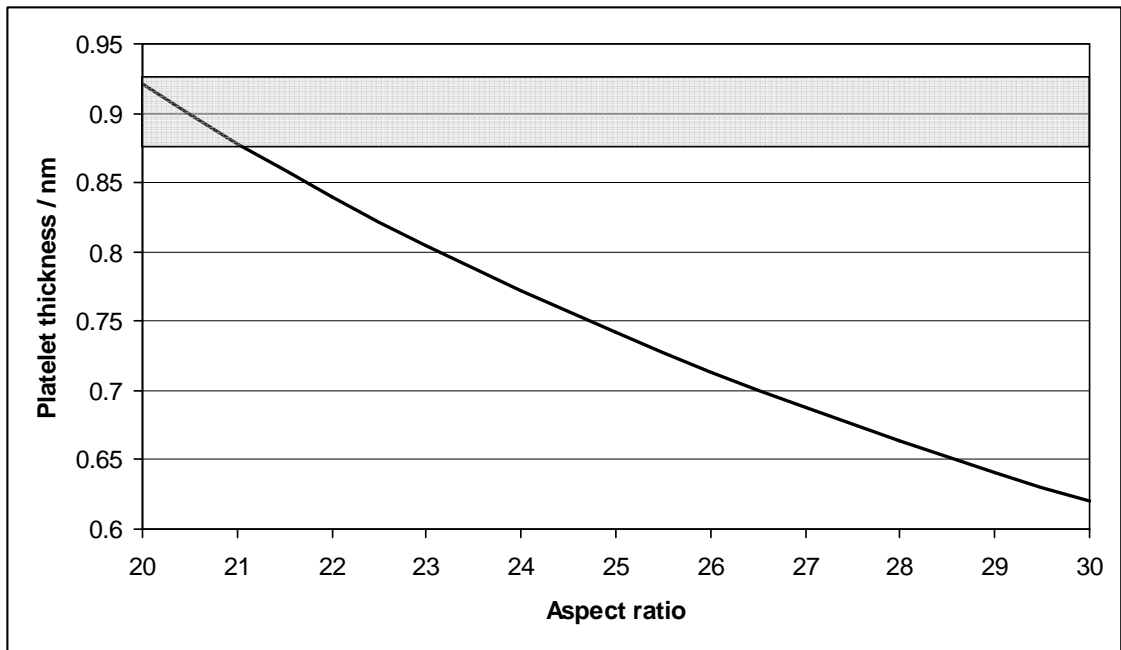


Figure 4-4: Platelet thickness of Laponite® RD calculated with Equation 4-21 and with the  $d_{N50} = 13$  nm and  $d_{N84} = 17$  nm.

The grey area in Figure 4-4 marks the layer thickness of 0.88 – 0.92 nm. The aspect ratio is in the range of 20 – 21, which, according to the equation for PCS given in Table 2-4, resulted in a particle diameter  $d_d$  of ~ 18.4 nm. The surface area must therefore be of the order of 930 – 970  $\text{m}^2\text{g}^{-1}$ . Calculating the surface area of a disc with  $d_d = 18.4$  nm,  $t_d = 0.9$  nm and a density of 2 570  $\text{kgm}^{-3}$  results in ~ 970  $\text{m}^2\text{g}^{-1}$ .

## 4.3 Rod-like particles

### 4.3.1 Material and Methods

#### 4.3.1.1 Minerals

The sample of aragonite (Figure 4-5 a+b), a precipitated calcium carbonate, was used here as an example of needle-like particles. It had a specific surface area of 14  $\text{m}^2\text{g}^{-1}$ . X-ray diffraction (XRD) showed the minerals present in the sample to be predominantly aragonite, with calcite and quartz. Semi-quantitative analysis by XRD showed an aragonite content of 70% and 25% calcite.

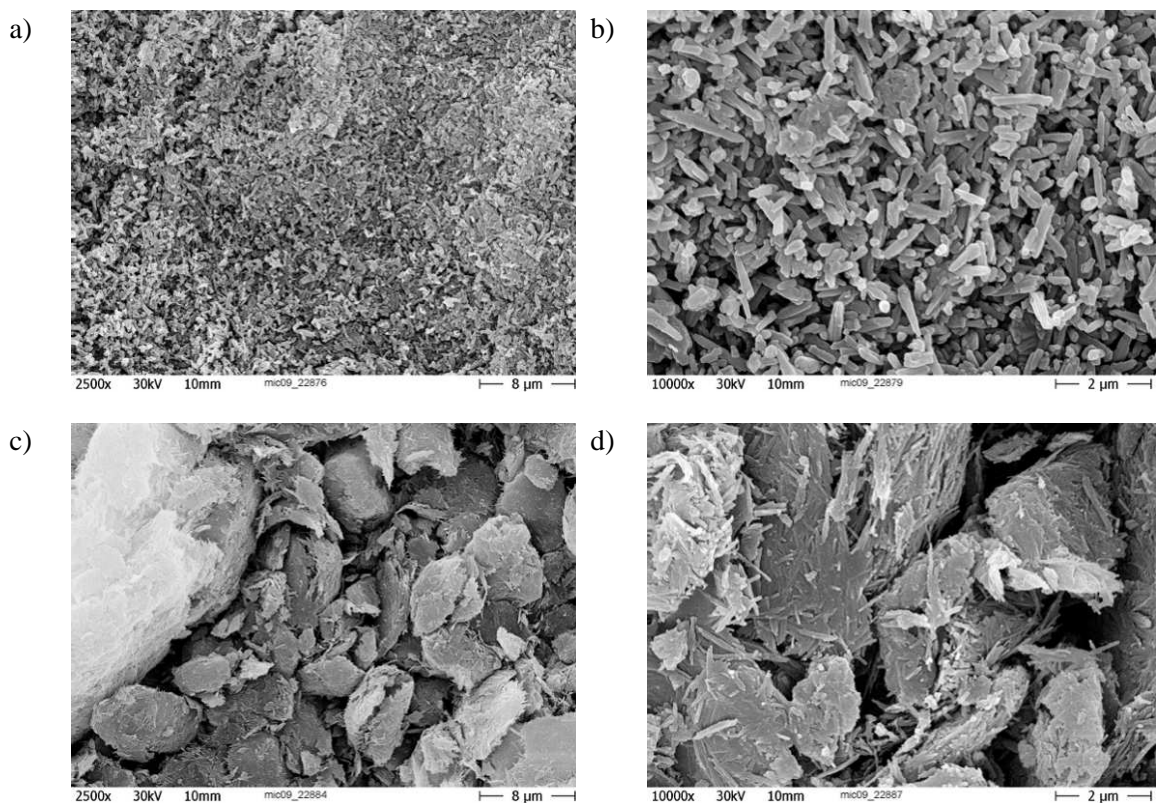


**Figure 4-5: SEM pictures of aragonite (a + b) and palygorskite (c + d). The palygorskite needles aggregate in dry state.**

The sample of palygorskite (Figure 4-5 c+d) was obtained from BASF<sup>17</sup>, available as Attagel<sup>®</sup> 50. It had a specific surface area of  $175 \text{ m}^2\text{g}^{-1}$ . XRD analysis indicated the minerals palygorskite (75%), quartz (10%), montmorillonite (9%), calcite (4%) and brookite (2%).

#### **4.3.1.2 Methods**

For sedimentation particle size measurements, the Sedigraph<sup>®</sup> 5120 from Micromeritics was used. Static laser light scattering (SLLS) particle size data were recorded on the Malvern Mastersizer 2000. Dynamic laser light scattering measurements were performed using the Malvern Zetasizer Nano ZS.

<sup>17</sup> BASF Corporation, 100 Campus Drive, Florham Park, NJ 07932, United States.

#### **4.3.1.2.1 Image analysis**

Samples of 5 mg dried mineral were dispersed in 5 cm<sup>3</sup> ethanol by means of an ultrasonic bath. The dispersion was diluted in a ratio of 1:40 with ethanol. The samples were prepared for microscopy as follows.

*Aragonite*: one drop of the above described dispersion was put on a membrane filter with a pore size of 0.1 µm. The membrane was fixed on the microscope sample holder and coated with carbon. The sample was studied with the Zeiss-Gemini DSM982 electron microscope applying 5 kV acceleration voltage using an Everhart Thornley detector. Image acquisition was made by the Voyager Software from Noran Instruments having a pixel size of 22 nm.

*Palygorskite*: the membrane filter (pore size 0.1 µm) was coated with carbon. One drop of the palygorskite dispersion was put on the coated membrane, which was fixed on the microscope sample holder. The analysis was made on the Zeiss Ultra 55 with 1 kV acceleration voltage and an EsB-detector, also from Zeiss. Image acquisition was made again using the Voyager Software, having a pixel size of 7.4 nm.

For both samples, image analysis was performed with the digital imaging system of the Voyager software. The software calculates the aspect ratio according to Equation 2-4. In the case of aragonite, 1 600 particles, and in the case of palygorskite, 270 particles were automatically analysed, resulting in a number aspect ratio distribution. Micrographs and binary images are shown in Figure 4-6.



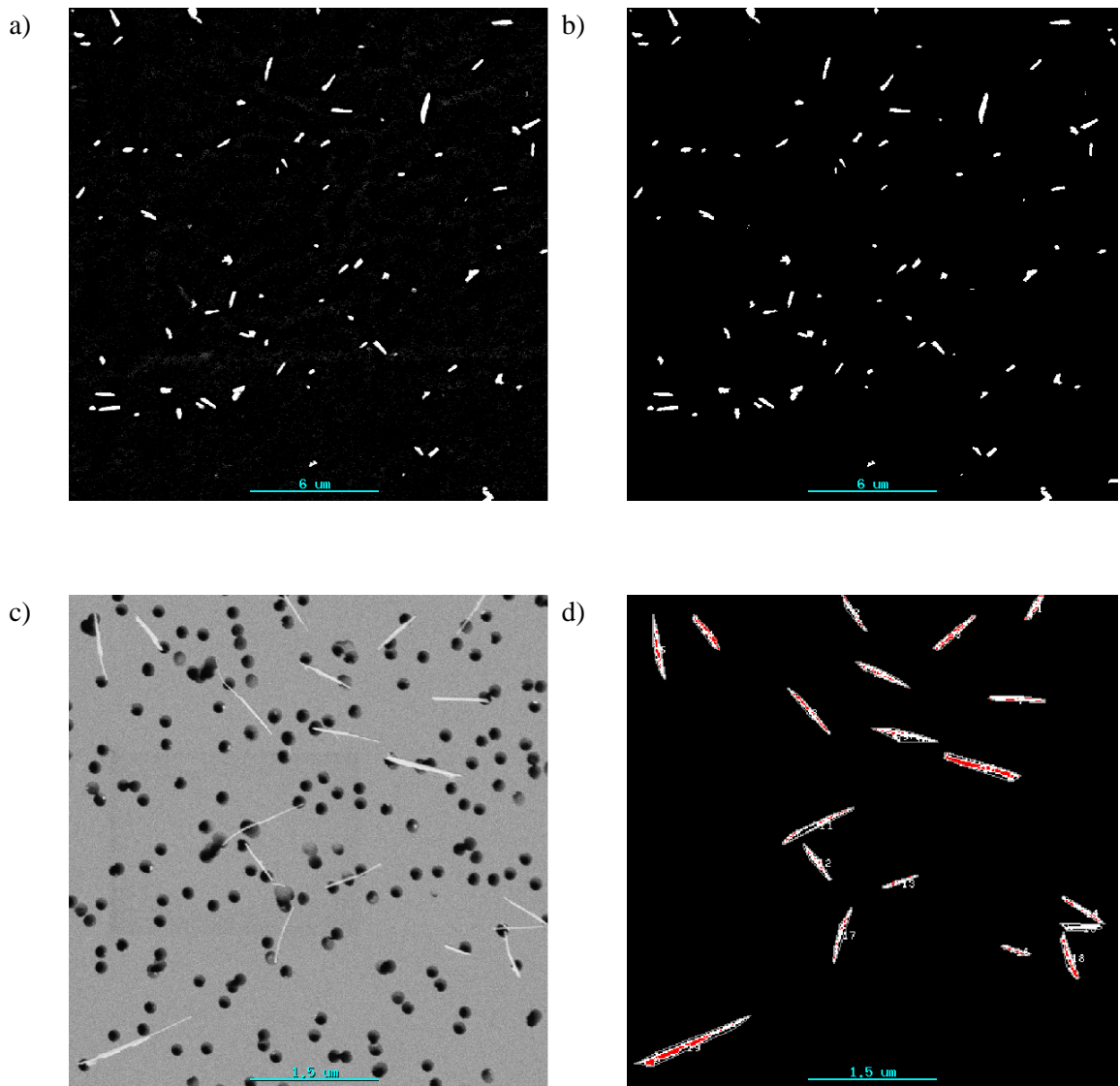


Figure 4-6: a) SEM micrograph with very high contrast of aragonite used for image analysis. Image width corresponds to 22.9  $\mu\text{m}$ . b) Binary image of the SEM micrograph for aragonite used for image analysis. Image width corresponds to 22.9  $\mu\text{m}$ . c) SEM micrograph of palygorskite used for image analysis. Image width corresponds to 5.7  $\mu\text{m}$ . d) Binary image of palygorskite used for image analysis. Image width corresponds to 5.7  $\mu\text{m}$ .

### 4.3.2 Results and Discussion

The specific surface area of aragonite was  $14 \text{ m}^2\text{g}^{-1}$  and the density was  $2750 \text{ kgm}^{-3}$ . The surface area of palygorskite was found to be  $175 \text{ m}^2\text{g}^{-1}$  having a density of  $2310 \text{ kgm}^{-3}$ . For the investigated model it is crucial to apply the outer surface area of the dispersed particles, as exemplified in the case of aragonite. Minerals like palygorskite, having a porous structure (Bergaya et al. 2006; Helmy et al. 2007; Yang et al. 2010) display an inner surface area, thus not representing the external surface  $s$  of the

representative cylinder. Figure 4-7 shows the nitrogen adsorption and desorption isotherms of palygorskite, giving a total pore volume of  $0.35 \text{ cm}^3 \text{ g}^{-1}$  (Barret et al. 1951).

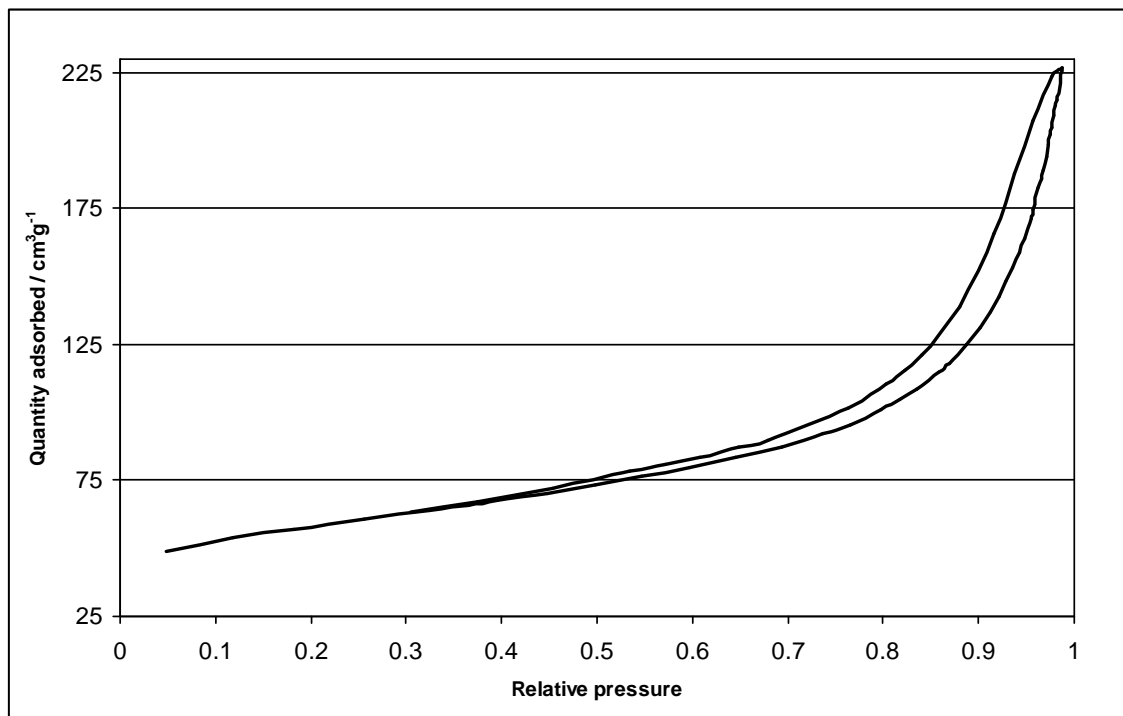


Figure 4-7: Nitrogen adsorption and desorption isotherm on palygorskite.

The number based particle size distributions for the aragonite, derived from the various measurement techniques, are presented in Figure 4-8. The distribution data deviate only slightly from the log normal behaviour. The fitted log normal distribution is based on  $d_{N50}$  and  $d_{N84}$  or  $d_{N16}$ , and all fits had an  $R^2 > 0.99$ .

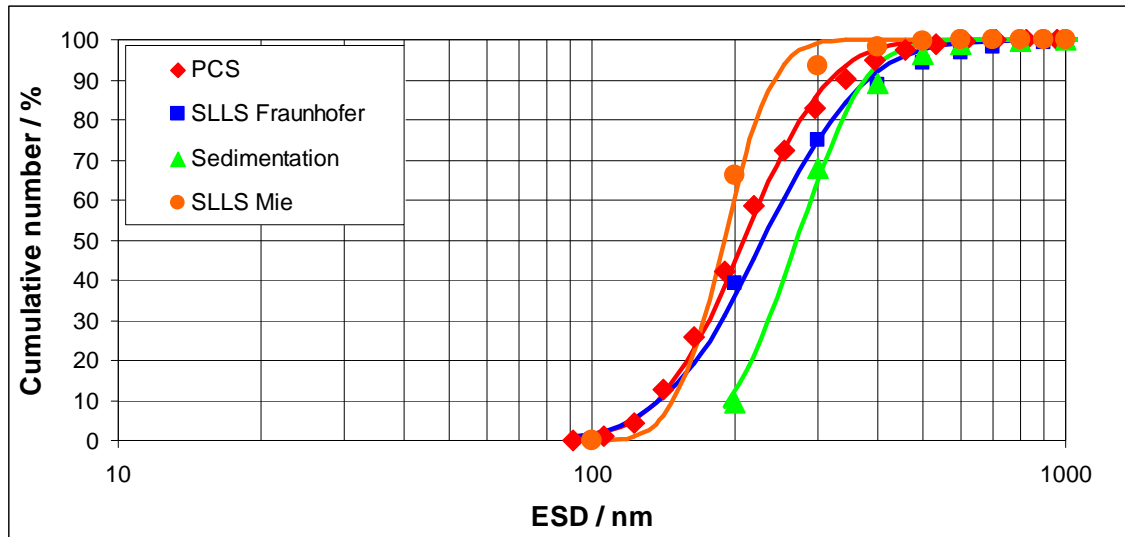


Figure 4-8: Particle size distribution measured by photon correlation spectroscopy (PCS), static laser light scattering (SLLS) (Fraunhofer and Mie optics) and sedimentation of aragonite. The corresponding lines are based on a cumulative log normal distribution calculated by the  $d_{N50}$ ,  $d_{N84}$  or  $d_{N16}$  giving an  $R^2 > 0.99$ .

Table 4-7: Measured  $d_{N50}$  and  $d_{N84}$  or  $d_{N16}$  for aragonite particles.

Method		Aragonite
PCS	$d_{N50}$ / nm	210
	$d_{N84}$ / nm	290
SLLS / Fraunhofer	$d_{N50}$ / nm	240
	$d_{N84}$ / nm	360
SLLS /Mie	$d_{N50}$ / nm	190
	$d_{N16}$ / nm	160
Sedimentation	$d_{N50}$ / nm	270
	$d_{N84}$ / nm	350

A small deviation from a log normal distribution was observed especially in the coarse region, suggesting either a slight aggregation or the presence of oversize material passing through the refining process.  $d_{N50}$  and  $d_{N84}$  or  $d_{N16}$  values, relevant for the aspect ratio calculation, are summarised in Table 4-7.

The calculated aspect ratios are presented in Table 4-8. To generate a ranking, the aspect ratios were compared with the value from the image analysis (Figure 4-9). The image analysis showed a median aspect ratio of 2.1 and a mode value of 1.8.

**Table 4-8: Calculated aspect ratios, determined by the different particle size and specific surface area measurements, compared with calculated values based on the model of Jennings and Parslow (1988) and those measured by image analysis.**

Rank	Model	Method	$\rho$	Comment
1		SLLS / Mie	1.8	Minimum that can be determined
2		SLLS / Fraunhofer	1.9	Minimum that can be determined
3	Gantenbein <i>et al.</i>	PCS	2.2	Very sensitive to small changes in particle size data
4		Sedimentation	21.0	Inappropriate transformation from mass to number distribution
	Jennings and Parslow Equation 2-9	Sedimentation / SLLS Fraunhofer	21.0 <sup>a</sup>	Only applicable with volume/mass distribution data
		Image analysis	1.8	Given as the mode value

<sup>a</sup>) Volume based

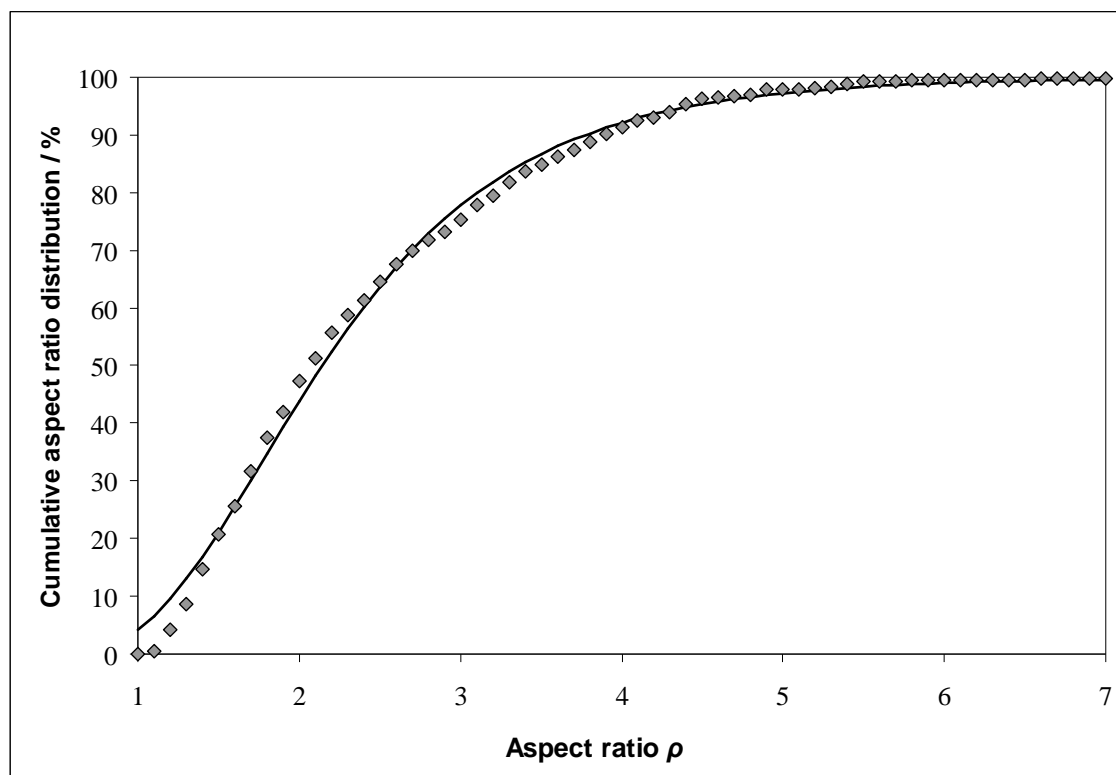


**Figure 4-9: Cumulative aspect ratio distribution based on the image analysis. The line corresponds to a fitted log normal distribution with  $\rho_{N50}$  of 2.14 and  $\rho_{N84}$  of 3.33.**

Laser scattering methods gave results best comparable with the data from image analysis, whereas sedimentation results deviated significantly from the image analysis result. This can be mainly related to the inappropriate transformation of the mass-based sedimentation result into the number-based distribution. The transform used to convert from the mass to the number distribution assumed a spherical particle and a size-invariant aspect ratio. The effect of a varying aspect ratio over the size distribution has the strongest effect for sedimentation-based data because rod-like particles tend to settle faster than the equivalent spheres. This is especially important when considering coarse particles with high aspect ratios, which exceed the Brownian domain for random orientation, in contrast to fine particles with low aspect ratios, as is often the case due to the breakage of rod-like particles. It is also interesting to see that the Jennings and Parslow solution (1988) could not be solved for number-based results from the sedimentation method, as the left side of Equation 2-9 resulted in a value of  $d_s/d_a > 1$ . Also, this can be related to the effect of the size-variant aspect ratio. As a result, the aspect ratio obtained by the Jennings and Parslow method was calculated directly via the mass/volume distribution data. Interestingly, the results found for the model of Jennings and Parslow (1988), and calculated on the basis of the mass (and volume) distribution, provided a similar aspect ratio to that of the models considering sedimentation number distribution based data, i.e. the equivalent spherical assumption ignores the preferential sedimentation velocity of larger rods.

After obtaining the aspect ratios, the apparent particle dimensions, rod length  $l$  and rod width  $w$  were calculated for aragonite using the following procedure:

- i) Calculate the aspect ratio with Equation 4-20.
- ii) Calculate the mode value similar to Equation 4-16 using  $esd$  instead of  $d$ .

- iii) Insert the mode value and the calculated aspect ratio  $\rho$  using the appropriate equation from Table 2-4 to calculate the rod length  $l$ .
- iv) Calculate the rod width  $w$  by dividing the rod length  $l$  by the aspect ratio  $\rho$ .

The result of this procedure is shown in Table 4-9. The laser scattering techniques provided very similar values for the length (240 – 280 nm) and width (~ 130 nm). The sedimentation technique gave a width of 120 nm and a length of 2.5  $\mu\text{m}$ .

**Table 4-9: Rod dimensions for the rod-like particles: rod length  $l$  and rod width  $w$  for the aragonite.**

Method	$l$ / nm	$w$ / nm
PCS	280	130
SLLS / Fraunhofer	240	130
SLLS / Mie	240	130
Sedimentation	2480	120

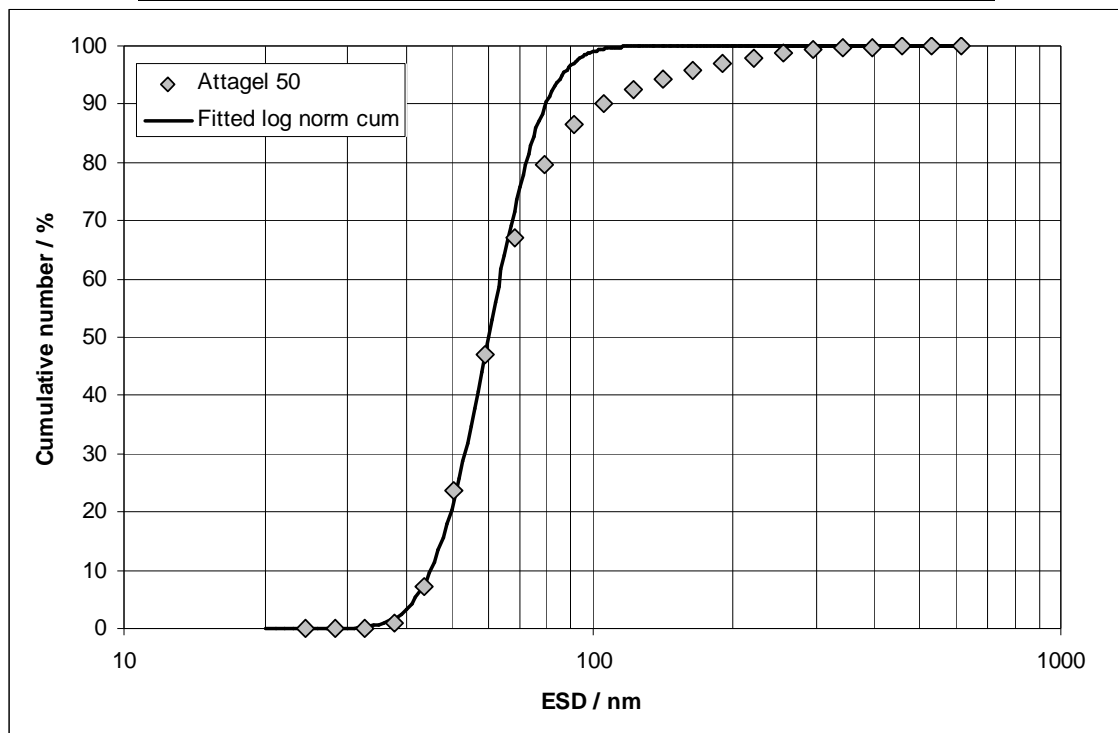


**Figure 4-10: Particle size distribution measured by photon correlation spectroscopy for the rod-like palygorskite particles, Attagel 50. The fitted log normal distribution is based on  $d_{N50}$  and  $d_{N16}$ .**

The particle size distribution of palygorskite could only be recorded by PCS (Figure 4-10) due to the nano dimension of the particles. The curve was slightly bimodal with

some coarse material between 100 and 300 nm. It was tried to deagglomerate by ultrasonic treatment, but without success. Therefore, it was decided to use  $d_{N50}$  (60 nm) and  $d_{N16}$  (47 nm) to describe the log normal distribution of the data, where the fit was clearly more representative.

Based on the particle size data, the aspect ratio was calculated to be 21, giving for the rod length 210 nm and width 10 nm. These dimensions corresponded with other data published (Stoylov, Petkanch 1972), but the image analysis revealed an aspect ratio of 7. Other authors described that the particle length of palygorskite can vary from 10 nm up to 5  $\mu\text{m}$ , and its width and thickness from 5 to 30 nm (Bergaya et al. 2006; Helmy et al. 2007). This difference between the image analysis and the presented method is caused by two factors. First of all, the image analysis showed aggregated palygorskite needles, thus underestimating the aspect ratio. Initially, the palygorskite was dispersed by following the instructions of the supplier. This procedure yielded the formation of some aggregates (Figure 4-10). They formed at the drying front of the palygorskite dispersion droplets when dried on the microscope sample holder. Ethanol was selected to try to minimise this phenomenon, but was no more effective than water alone. Secondly, and most importantly, palygorskite is a highly porous mineral. The determined surface area was clearly too high in respect to the geometrically representative solid rod, and consequently the calculated aspect ratio was overestimated. This showed the limits of the model presented here, which requires that the specific surface area be determined only by the external surface of the particles.

#### **4.4 Conclusions**

The equations of Jennings and Parslow (1988) for the application of equivalent spherical diameters and their relation to real particle dimensions were discussed. Furthermore, the model of Hohenberger was derived and further developed by clearly

defining which parameters have to be inserted for an appropriate use in support of hypothesis **H1**.

Practical examples for different talc particles varying in their specific surface area and geological origin were presented, using different particle size determination methods like photon correlation spectroscopy (PCS), static laser light scattering interpreted with different theories (Fraunhofer and Mie) as well as the sedimentation technique. An aspect ratio of  $\sim 6$  for a Finnish talc (FT) grade with low specific surface area,  $\sim 12$  for an Australian talc (AT) grade with medium specific surface area and an aspect ratio of  $\sim 37$  for a Finnish talc grade with high specific surface area (HSA) were found based on PCS particle size data. The results were also compared with other models, based on the particle size distribution data as proposed by Pabst and Berthold (2007) and Jennings and Parslow (1988). The use of laponite clearly revealed a weakness of the model presented here. The specific surface area determined in the dry state by nitrogen adsorption is for some minerals not representing the geometrically defined exterior available surface area in water. However, this drawback was shown to be an opportunity to approximate the total specific surface area of the delaminated laponite particles, which in the current study was determined to be  $930 - 970 \text{ m}^2\text{g}^{-1}$ . This finding supports hypothesis **H3(a)**. However, other materials which agglomerate in the dry state may nevertheless retain their wet-state surface area, whereupon **H3(a)** is not valid.

Based on the aspect ratios derived by adopting the presented model, the particle diameter  $d$  and thickness  $t$  were able to be calculated. Despite the sometimes different responses for the diameter  $d$ , comparable values for the particle thickness  $t$  were found. This is not surprising. According to the assumed model, the particle thickness mainly determines the specific surface area. The average particle thicknesses lay for the low surface area Finnish talc (FT) between 80 and 180 nm, for the medium surface area



Australian talc (AT) between 40 and 50 nm and was for the highly exfoliated Finnish talc (HSA) around 17 nm.

The particle size measurement method has to be chosen carefully. The method should be applicable over the relevant size range of the particles in question and it should not be affected by the anisotropy of the particles, such as the falling leaf analogy observed for the sedimentation technique. With reference to hypothesis **H2**, for the talc and laponite particles tested in this study, photon correlation spectroscopy is suggested as preferable. If not available or not relevant in respect to the particle size (considering materials larger than 100 nm diameter) static laser light scattering with Fraunhofer optics can be used.

A review of the work of Jennings and Parslow (1988) explained the use of formulae that allow transformation from the equivalent spherical diameter into the rod length  $l$  as a function of the aspect ratio  $\rho$ . The newly more fully defined method for the determination of the aspect ratio related to the particle size and surface area for rod-like materials was tested for aragonite and for palygorskite particles adopting different particle size measurement methods. All laser scattering-based methods produced results comparable to those of image analysis. The investigated aragonite particles returned an aspect ratio of 1.8. The aragonite length  $l$  was determined to be between 240 and 280 nm with a rod width  $w$  of about 130 nm. Sedimentation particle size data indicated a too high aspect ratio of 21. The reason is related partly to the transformation of particle size from the mass distribution to the number distribution, data assuming a size-invariant aspect ratio. Nevertheless, the sedimentation-based aspect ratio gave a comparable rod width  $w$  of 120 nm.

Applying the model for porous minerals, like palygorskite, illustrated the drawback of using the surface area determination by nitrogen adsorption. It is only possible to

receive a correct aspect ratio if the geometrically appropriate outer surface only is used, and not the total surface area including internal pores. Hypothesis **H3(b)** is thus confirmed.

## **5 Efficiency of colloidal pitch adsorption onto phyllosilicates: comparing talc, chlorite and pyrophyllite**

Having defined the nature, and especially the surface area and shape of the mineral particles, we now proceed to establish the efficiency of adsorption amongst platy, variously hydrophobic family of phyllosilicates minerals. The hypotheses tested in this chapter are:

**H4** The adsorption capacity of minerals for dissolved and colloidal substances from wood processing is proportional to the specific surface area of the minerals.

**H5** The adsorption mechanism of dissolved and colloidal substances from wood processing onto minerals is controlled mainly by hydrophobic interactions, and hence, hydrophobic materials preferably adsorb these substances.

During the activities of the thesis, the work has been published (Gantenbein et al. 2009).

### **5.1 Introduction**

The objective of this chapter is to compare talc with its closest structural relatives in the phyllosilicate family, namely its di-octahedral counterpart pyrophyllite and the magnesium-rich chlorite, which is often present in significant ancillary quantities in talc ores. In some countries, chlorite and pyrophyllite are more easily available than talc, and papermakers raise the question about how these minerals compare with the performance of talc. Furthermore, it is not clear how the different surface chemistries of the minerals affect the pitch adsorption efficiency. A range of commercially available

naturally occurring minerals have been used, namely a chlorite from France, containing limited quantities of talc, effectively as contaminant, a pyrophyllite from South Africa, contaminated with several other minerals, like muscovite and/or other micas, and a talc from Finland. The minerals were wet ground in a chemical-free environment to achieve a range of comparable surface areas.

The mineralogical comparison of the three phyllosilicates is presented in the sections 2.4.1.2 and 2.4.1.3.

## **5.2 Materials and Methods**

### ***5.2.1 Materials***

The experiments have been performed using a pulp sample taken in January 2006 (see detailed description in section 3.3). The sample was cooled to room temperature after sampling and directly used without any further storage. The pH of the pulp sample was between 6.7 – 6.8 at 25 °C. The pulp was wet pressed through a filter of 2 µm pore size (filter paper, circular 602 EH). A sample taken from the 5.0 dm<sup>3</sup> of filtrate/liquor thus obtained was examined under a light microscope (Olympus AX-70) to check for the absence of fibrils which might act to distort the measurements (Figure 5-1). The zeta potential of the particles in suspension was measured with a PenKem 500 device giving a value of -15 mV. The anionic charge was determined by a streaming current detector (SCD) titration (Mütek PCD-02) and was found to be -0.56 µEqg<sup>-1</sup> and the polyelectrolyte titration of the pulp filtrate gave -2.6 µEqg<sup>-1</sup>. Ion chromatography (Dionex DX 120 Ion-Chromatograph) of the TMP sample of January 2006 showed the following anions present in the TMP filtrate: SO<sub>4</sub><sup>2-</sup> = 2.08 mM, PO<sub>4</sub><sup>3-</sup> = 0.35 mM and Cl<sup>-</sup> = 0.62 mM.

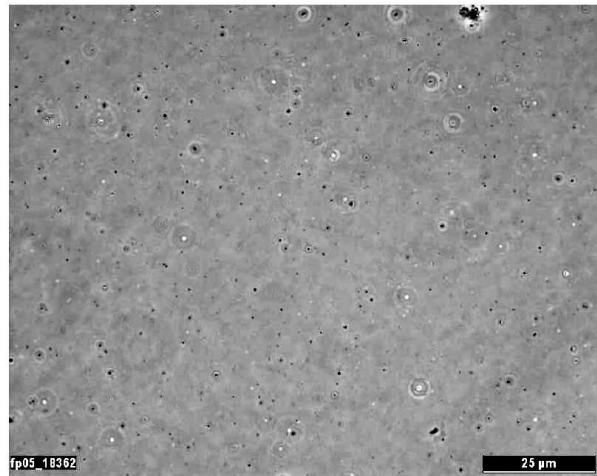


**Figure 5-1:** Light microscope picture of the TMP filtrate used showing colloidal pitch doplets and the elimination of disturbing fibrils.

**Table 5-1:** Loss on ignition and XRF analyses for raw talc, chlorite and pyrophyllite samples (before grinding). Error range for the LOI values is based on the standard deviation of three measurements. XRF values were measured only once.

	<b>Talc</b> / w/w %	<b>Chlorite</b> / w/w %	<b>Pyrophyllite</b> / w/w %
Loss on ignition at 1 000 °C	6.48 ± 0.02	12.64 ± 0.05	6.19 ± 0.05
Al <sub>2</sub> O <sub>3</sub>	0.71	18.26	33.60
CaO	0.15	0.33	0.13
Fe <sub>2</sub> O <sub>3</sub>	2.28	0.23	0.08
K <sub>2</sub> O	---	0.20	2.32
MgO	30.90	32.95	0.07
Na <sub>2</sub> O	0.46	0.65	1.23
P <sub>2</sub> O <sub>5</sub>	0.02	0.03	0.13
SO <sub>3</sub>	0.13	0.07	0.07
SiO <sub>2</sub>	58.80	34.52	54.79
TiO <sub>2</sub>	0.02	0.12	1.39

The mineral powders of the present study were analysed both by X-ray fluorescence (XRF) and X-ray diffraction (XRD). The talc grade used was shown to contain the minerals talc, chlorite and magnesite, which was confirmed also by FTIR [Perkin Elmer

Spectrum One Spectrometer] analysis, and XRF gave a talc content of ~ 94 %. Chlorite, talc and quartz were identified in the chlorite sample, which was also confirmed with FTIR. The calculation of the chlorite content in the chlorite is very difficult because of the frequently changing elemental composition found in chlorites. Naturally occurring chlorite grades show mostly the composition  $(Mg_5Al)(Si_3Al)O_{10}(OH)_8$ . By assuming this formula for chlorite, the chlorite content in the investigated sample is ~ 83 % and contains ~ 14 % talc. For Pyrophyllite the XRD analysis found pyrophyllite, muscovite, kaolinite, quartz, diaspore and rutile. XRF analysis showed a pyrophyllite content of > 80 % with an  $Al_2O_3$  excess of ~ 8 % (Table 5-1).

**Table 5-2: Physical properties of the mineral samples, characterised according to origin and specific surface area.**

<b>Sample abbrev.</b>	<b>Specific Surface Area / <math>m^2g^{-1}</math> (BET Tristar)</b>	<b><math>d_{50}</math> / <math>\mu m</math> (MasterSizer S)</b>	<b><math>d_{50}</math> / <math>\mu m</math> (Sedigraph® 5100)</b>	<b>Surface Charge Density / <math>\mu Eqg^{-1}</math> (Mütek PCD-02)</b>
FT-LSSA	13.6	15.2	3.0	-1.4
FT-MSSA	19.7	14.7	2.6	-6.0
FT-HSSA	24.0	14.1	2.0	-10.0
C-LSSA	16.5	7.4	1.4	-6.3
C-MSSA	19.0	6.8	1.1	-13.8
C-HSSA	25.2	5.8	0.8	-20.0
P-LSSA	15.8	4.7	2.9	-4.4
P-MSSA	19.6	4.7	1.4	-12.0
P-HSSA	25.1	4.4	0.7	-26.1

Each mineral family was ground under attrition to provide a range of specific surface areas. The specific surface area is defined by BET analysis. The respective particle size distributions were also analysed with two different devices, namely a static laser light scattering-based Malvern MasterSizer and a sedimentation method using a

Micromeritics Sedigraph 5100. To evaluate the total charge of each sample by electrolytic titration, a streaming current detector was used [together with N-methylglycol-chitosan, concentration  $c = 0.005 \text{ mol dm}^{-3}$ , as cationic agent, and K-polyvinylsulphate (KPVS),  $c = 0.0025 \text{ mol dm}^{-3}$  as anionic agent, both from WACO-chemicals]. These analyses are summarised in Table 5-2 and characterised, according to the abbreviations, in terms of origin (FT = Finnish talc, C = chlorite, P = pyrophyllite), and specific surface area (SSA), i.e. LSSA = low SSA, MSSA = medium SSA and HSSA = high SSA.

### **5.2.2 Methods**

The filtrate was distributed into glass bottles immediately after filtration; 200 g of filtrate in each bottle and 1 w/w % of the mineral (chemical-free slurry of 10 w/w %) was added to each. Then the bottles were closed and agitated for 2 hours. The suspension was then centrifuged for 30 minutes in a centrifuge (Jouan C 312 , by IG Instruments) at a centrifugal force of  $2\ 600 \text{ |g|}$ . Two phases are collected; an upper aqueous phase and a lower sedimented mineral-containing phase. A reference sample without mineral addition was used as a comparison. Furthermore, mineral alone was centrifuged to confirm whether the process removed mineral particles from the upper phase. The upper liquid and the lower solid phase obtained after the centrifugation were separated and analysed according to the following procedures.

A  $100 \text{ cm}^3$  sample of the upper aqueous phase, obtained after centrifugation, was placed into a pre-weighed aluminium beaker and dried in an oven ( $90 \text{ }^\circ\text{C}$ , 24 hours) to get a total amount of non-volatile residue in the aqueous phase.

The total charge was determined by a streaming current detector (SCD) titration (Mütek PCD-02).

Ion chromatography was measured on a Dionex DX 120 Ion-Chromatograph.

A further 45 cm<sup>3</sup> sample was taken to analyse for turbidity by means of a NOVASINA 155 Modell NTM-S (152).

A yet further 2 cm<sup>3</sup> sample was taken for chemical oxygen demand (COD) analysis, providing a value for the total organic content. The COD analysis expresses the quantity of oxygen necessary for the oxidation of organic materials into CO<sub>2</sub> and was measured using a Lange CSB LCK 014, range 1 000-10 000 mg dm<sup>-3</sup> with a LASA 1/Plus cuvette.

Thermogravimetric analysis (TGA) of the sedimented mineral containing phase was made with a scanning differential thermal analyser (SDTA) 851e by Mettler Toledo, under constant heating rate of 20 °C min<sup>-1</sup> from 30 °C up to 1 000 °C.

## **5.3 Results and Discussion**

### ***5.3.1 Effect of mineral on pH – correction for turbidity***

Table 5-3 shows the effect of added minerals on the pH of the upper liquid phase, relative to added water. The progressively comminuted talc samples (FT-LSSA, FT-MSSA and FT-HSSA) are seen to increase pH from 7.1 to a constant value of 7.4. Chlorite, with an initial specific surface area of 17 m<sup>2</sup>g<sup>-1</sup> (C-LSSA), increased pH from 7.1 to 7.8. Chlorite, with increasing surface area (C-MSSA with 19 m<sup>2</sup>g<sup>-1</sup> and C-HSSA with 25 m<sup>2</sup>g<sup>-1</sup>), increased the pH slightly further to 8.1. The degree of increasing surface area of chlorite has, therefore, only a small influence on the pH. The pH of the pyrophyllite treated samples, however, is strongly dependent on the degree of grinding. The more surface area is liberated, the more alkaline the solution becomes. For the pyrophyllite with the low surface area (P-LSSA) of 16 m<sup>2</sup>g<sup>-1</sup> the pH was the same as the untreated reference sample (pH 7.0), but for the pyrophyllite with 20 m<sup>2</sup>g<sup>-1</sup> (P-MSSA) the pH is already 7.6, and finally the high surface area pyrophyllite (P-HSSA) with 25 m<sup>2</sup>g<sup>-1</sup> has a pH of 8.3. Additionally, in Table 5-2 an increase of the anionic charge of



the minerals with increasing specific surface area can be observed. This increase in anionicity can be related to the grinding process in which, on one hand, more of the basal surface is liberated. Lattice errors may, thus, expose anionic charge. On the other hand, and far more relevant, the increased anionic charge is connected to the exposure of the edge surface. This finding indicates that during the grinding process the phyllosilicates are not only exfoliated but also strongly broken as demonstrated in Figure 3-1. This observation, of course, questions the assumption of similar surface properties of a mineral with increasing specific surface area and might also affect the Langmuir parameters *A* and *B*.

**Table 5-3: pH values of the upper liquid phase after the treatment with the respective mineral, each as a function of increasing specific surface area.**

<b>TMP filtrate treated with</b>	<b>pH</b>
deionised water	7.1
FT-LSSA	7.4
FT-MSSA	7.4
FT-HSSA	7.4
C-LSSA	7.8
C-MSSA	8.1
C-HSSA	8.1
P-LSSA	7.0
P-MSSA	7.6
P-HSSA	8.3

The impact of both pH and temperature on the collection of colloidal pitch will be the subject of chapter 6. The effect, however, in this work is most marked in terms of the turbidity of the colloidal TMP pitch being used. In this analysis a procedure was adopted whereby the impact of pH increase on turbidity was taken into account.

Turbidity was measured over a range of pH (Figure 5-2). This procedure was made on the pure TMP filtrate, prior to mineral addition, using either dilute hydrochloric acid or sodium hydroxide, respectively, and the turbidity measured online. The turbidity response was then used to correct subsequent adsorption results to pH 7.4, i.e. to that value seen after talc treatment in order to have a fair comparison. The measured turbidity  $\tau$  value was corrected according to Equation 5-1. The function  $f(pH)$  is the linear regression (Equation 5-2) of the turbidity-pH response curve between pH 6.8 and 8.2. It was assumed to be linear in this range.  $R^2$  was found to be 0.996 and both fitted parameters were significant with a  $p$ -value  $<0.01$ . The impact of pH arising from the mineral itself during pitch adsorption was assumed to be a part of the mineral function, and in this work no corrections for this were made during adsorption.

$$\tau_{\text{corrected}} = \tau_{\text{measured}} \cdot \frac{f(pH)}{f(7.4)}$$

**Equation 5-1**

$\tau_{\text{corrected}}$  : absolute turbidity value in NTU corrected to pH 7.4

$\tau_{\text{corrected}}$  : absolute turbidity value in NTU measured at the resulting pH  
after mineral treatment

with

$$f(pH) = -5.8 \cdot pH + 139.5$$

**Equation 5-2**

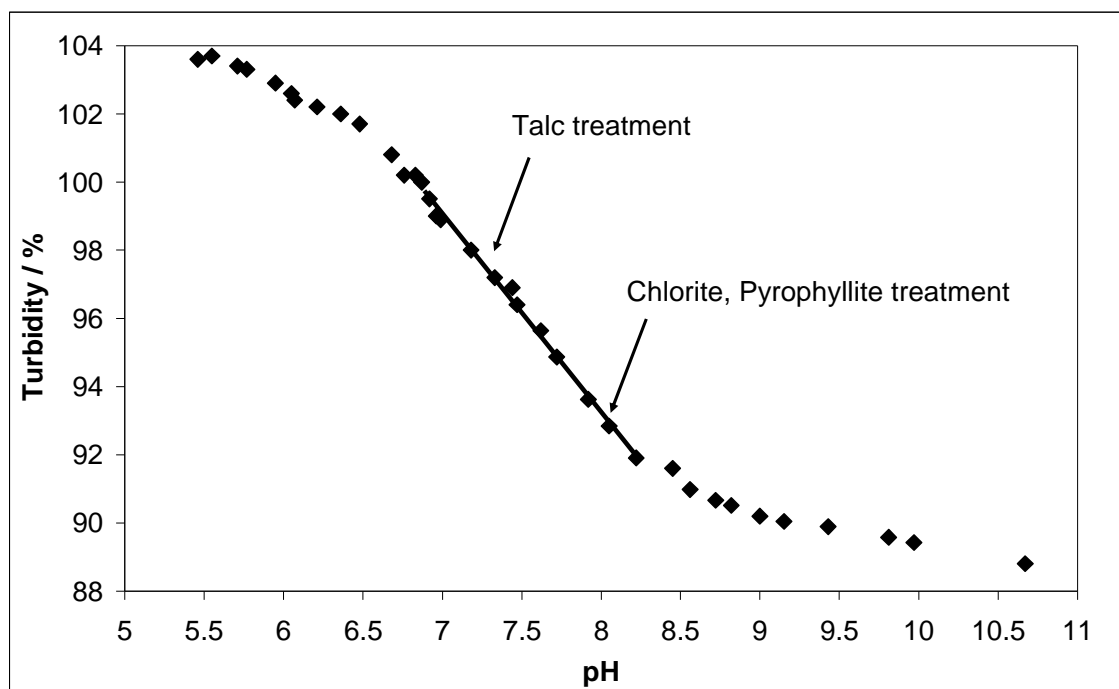


Figure 5-2: Turbidity as a function of the pH in the range of pH 5.5 to 10.8. The pH reached after treatment with each of the high surface area minerals is also shown on the plot. The TMP filtrate has an incoming pH of 6.8 and a turbidity of 577 NTU, which here corresponds to a relative turbidity of 100 %.

### 5.3.2 Modelling the adsorption

This present study reveals a profile of pitch compound adsorption on talc, chlorite and pyrophyllite over a mineral specific surface area regime of  $14 < \epsilon_{\text{BET}} < 25 \text{ m}^2\text{g}^{-1}$ . Values of the analysis are given in percent normalised with the untreated TMP filtrate as the reference, corresponding to 100 %.

In Figure 5-3, Figure 5-4, Figure 5-5, and Figure 5-6, the adsorption data are expressed following lines inserted to help the reader's eye to follow the data points (Equation 5-3). As a model behaviour, a Langmuir-like approach was chosen to fit the data, in which the usual species concentration ratio is replaced with the specific surface area  $\epsilon_{\text{BET}}$  of the mineral presented for adsorption. The normalised value of turbidity, COD or gravimetry in % is denoted as  $y$ . Constant A is describing the affinity of the mineral for the pitch particles, whereas constant B is a measure for the removal capacity of a mineral per applied surface area.

$$y = 100 - \frac{A \cdot B \cdot \varepsilon_{\text{BET}}}{1 + B \cdot \varepsilon_{\text{BET}}}$$

**Equation 5-3**

Rearrangement leads to Equation 5-4, for which a linear regression can be made with  $\varepsilon_{\text{BET}}/(100-y)$  against  $\varepsilon_{\text{BET}}$ . With the resulting steepness and intercept,  $A$  and  $B$  can be calculated. This method is called the Langmuir linear regression (Langmuir 1916). This linear form is biased toward fitting the data in the middle and large  $\varepsilon_{\text{BET}}$  region of the function. Alternative fits were attempted, including the Lineweaver-Burk (1934), Eadie-Hofstee (1942; Hofstee 1959) or Scatchard (1949), but the results were less than satisfactory, having poor regression coefficient.

$$\frac{\varepsilon_{\text{BET}}}{100 - y} = \frac{\varepsilon_{\text{BET}}}{A} + \frac{1}{A \cdot B}$$

**Equation 5-4**

Based on the limited available data range, it is not possible to extrapolate the fitted curve with any degree of confidence, and so drawing firm conclusions about affinity constant ( $A$ ) and saturation constant ( $B$ ) has been avoided. Due to the fact that the adsorbent amount (surface area) is changed and not the adsorbate concentration (pitch particles) an inversed situation compared to the normal Langmuir isotherm is given. In the standard isotherm an excess of adsorbent is present in the low concentration region, changing into an excess of adsorbate (surface saturation). In the current case an excess of adsorbate is present in the low surface area region of the curve, changing into an excess of adsorbent in the high surface area region.

### ***5.3.3 Application to data***

In a first step the results of the upper liquid phase for the talc and chlorite treatment are compared. In a second step the TGA analysis of the lower sedimented phase of the talc, chlorite and pyrophyllite treatment are discussed. Finally, in a third step the analysis of

the liquid phase of the pyrophyllite treatment is presented. The separation of the data is necessary for an appropriate discussion, because talc and chlorite are high purity minerals and are only contaminated, in effect, with each other. Pyrophyllite shows a lot of other impurities. Furthermore, the analysis of the upper liquid phase of the pyrophyllite treatment shows unexpected results which will be discussed separately.

Figure 5-3 shows the turbidity results after treatment with talc and chlorite, respectively. The absolute values for talc and chlorite differ only a little and can not be taken alone as being significant (100 % corresponds to 577 NTU). After correction of the turbidity values with Equation 5-1 it is concluded that the values are similar and proposed to arise from the same mechanism and magnitude of adsorption. From Equation 5-4, constant  $A$  was determined to be 94 % and constant  $B$  being  $0.15 \text{ \% m}^2 \text{ g}^{-1}$ , with linearised Langmuir regression (Equation 5-4) of  $R^2 = 0.9532$ . Both fitted parameters in the linearised Langmuir plot are significant with  $p < 0.01$ .

Figure 5-4 confirms the trend suggested in the turbidity analysis, and shows the reduction of the oxidisable compounds after the TMP filtrate was treated with talc and chlorite, respectively. Both minerals act to reduce the COD value. 100 % corresponds to  $4\,914 \text{ mg O}_2 \text{ per dm}^{-3}$  of the upper liquid phase. Also for COD the data were considered to be of the same origin. Due to the greater statistical scatter of the COD data, the linearised Langmuir regression (Equation 5-4) gave only regression coefficient of  $R^2 = 0.5292$ . The value of the constant  $B$  is  $0.17 \text{ \% m}^2 \text{ g}^{-1}$  and  $A$  is 17 % in this measurement technique. Only  $1/A$  (steepness) in the linearised Langmuir plot is significant ( $p < 0.01$ ). The intercept ( $1/A \cdot B$ ) is not significant ( $p > 0.05$ )

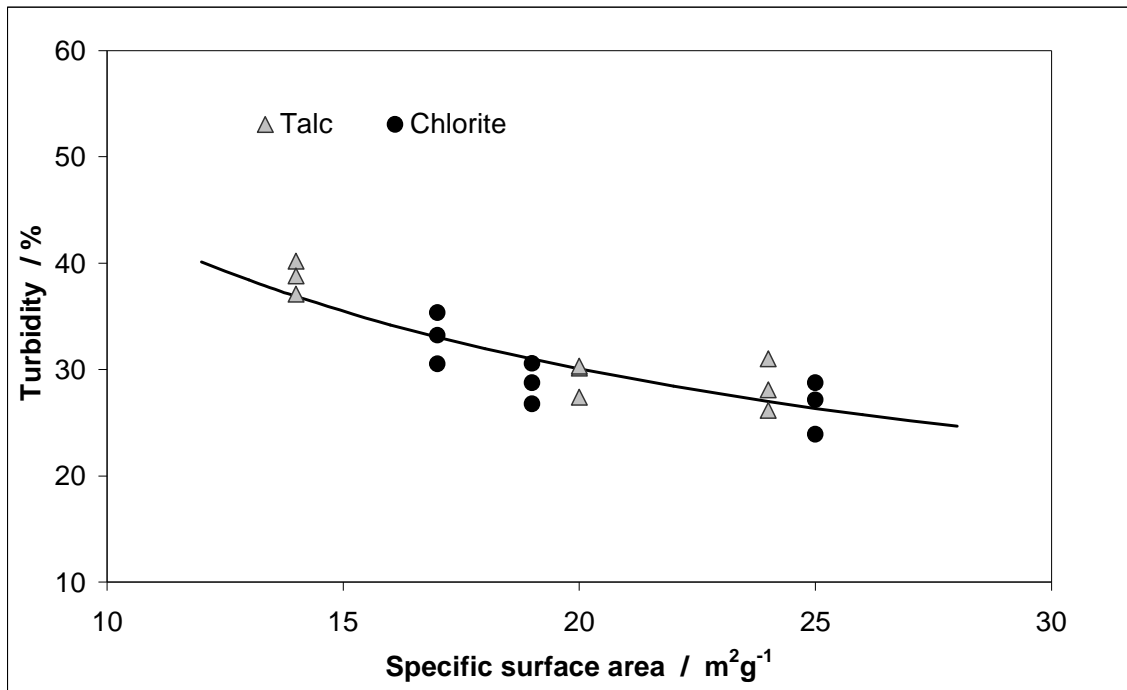


Figure 5-3: Influence of talc and chlorite on the turbidity of a TMP filtrate normalised with the untreated reference TMP filtrate. 100 % corresponds to 577 NTU in the upper liquid phase at pH 7.0. Values have been corrected to those expected at pH 7.4.

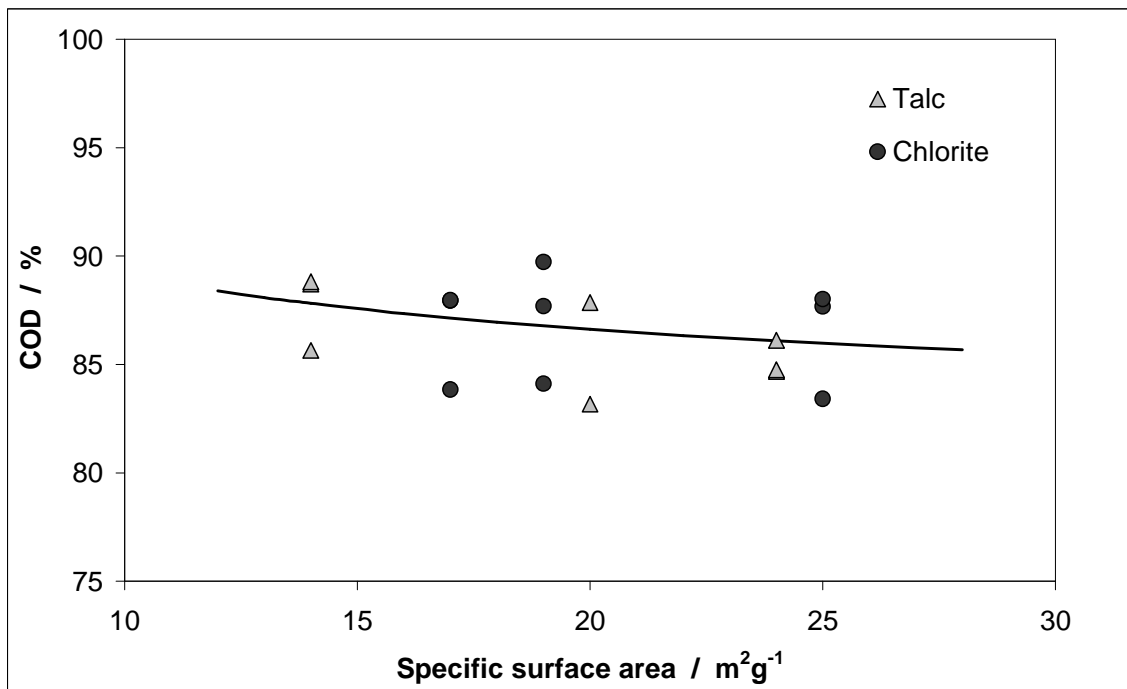


Figure 5-4: Influence of talc and chlorite on Chemical Oxygen Demand (COD) of a TMP filtrate normalised with the untreated reference TMP filtrate. 100 % corresponds to 4 914 mg O<sub>2</sub> per dm<sup>3</sup> of the upper liquid phase.

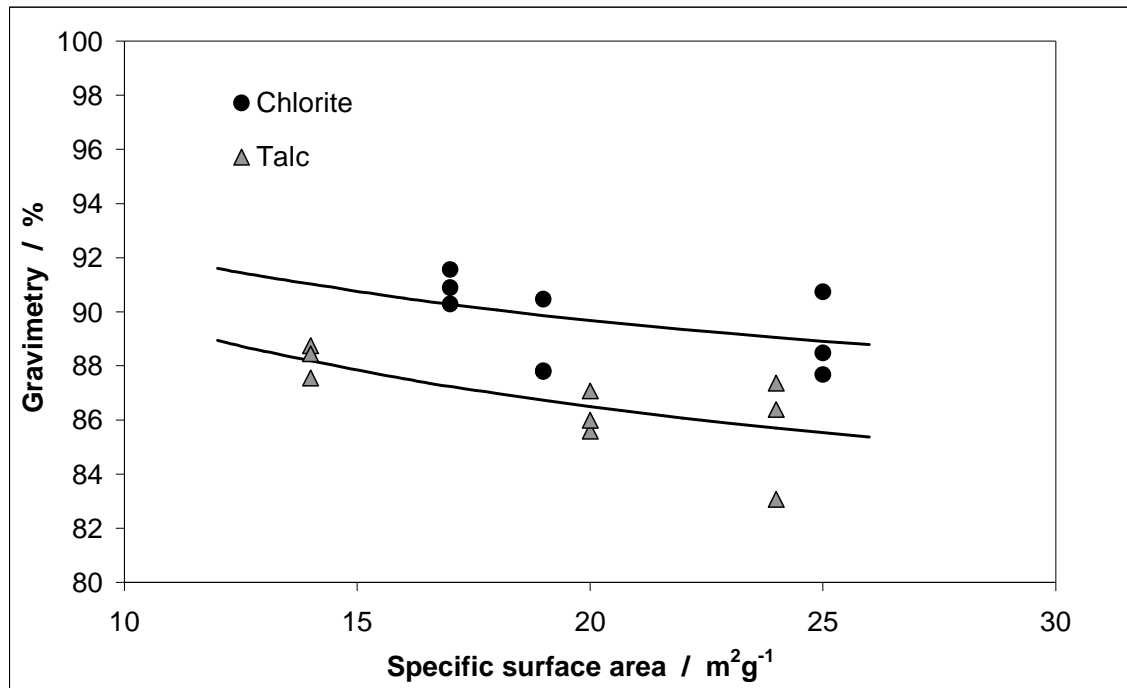


Figure 5-5: Influence of talc and chlorite on gravimetric analysis of the remaining material in a TMP filtrate treated with mineral, normalised to the untreated reference TMP filtrate and with the dissolved fraction of minerals subtracted. 100 % corresponds to 3.52 gdm<sup>-3</sup> residue in the upper liquid phase.

In Figure 5-5, the gravimetric analysis is presented. The soluble parts of each mineral in water were measured as a reference sample for gravimetric subtraction, with the same dilution at the same pH and the same conductivity as the pulp liquor. Approximately 30 mg were found to be dissolved when 10 000 mg mineral were suspended in 1 dm<sup>3</sup> water. The values are also normalised to 100 % with respect to the untreated reference sample: 100 % corresponds to 3.52 g residue in 1 dm<sup>3</sup> of the upper liquid phase. In contrast to the already discussed analyses of turbidity and COD, the gravimetric analysis shows a clear difference between talc and chlorite. The difference is around 4 %. Based on this, in gravimetry the two minerals were treated separately for finding the corresponding Langmuir equation (Equation 5-3). Table 5-4 shows the constants *A* and *B* and the regression coefficients *R*<sup>2</sup> of the linearised Langmuir equation for both series of data. The data were split in order to calculate the constants *A* and *B* for talc and chlorite separately. There are insufficient data to separate the potentially different particle morphologies within each mineral type, though the wide spread of results

(relatively low  $R^2$  value) may well reflect differences in binding energy (constant  $A$ ) and its combination with total adsorbed amount per unit area (constant  $B$ ) for each of the different comminution conditions assuming true Langmuir behaviour. The best that can be proposed here is a curve that can be described as Langmuir-like. Additionally, we note that the gravimetry results are strongly affected by release in some cases of soluble material from the minerals (Table 5-5), rendering potential deconvolution of the constants  $A$  and  $B$  for the various morphologies tenuous at best. We see, then, that the major difference occurs only in the constant  $A$ , whereas  $B$  follows the values obtained previously for both turbidity and COD. To consider possible factors affecting this result as well as the poor regression coefficient, i.e. differentiation between talc and chlorite as an experimental artefact, a study was undertaken to determine the soluble species present during the application of the mineral in suspension.

**Table 5-4: Constants  $A$  and  $B$  and regression coefficient for the gravimetric analysis of the talc and chlorite treated TMP samples. Only constant  $A$  for talc is significant ( $p < 0.01$ ). The other fitted parameters are not significant ( $p > 0.05$ ).**

	Constant A	Constant B	$R^2$
Talc	20	0.10	0.7163
Chlorite	16	0.01	0.4298

Dissociated soluble species generally affect electrolyte concentration. Table 5-5 compares the electrolyte balance typical ions in the supernatant in the reference sample and the mineral treated samples.

After the talc treatment, conductivity and SCD are seen to increase slightly (Table 5-5). A slight increase in sodium and potassium concentration as well as magnesium concentration can be observed. The calcium concentration slightly decreased. However,



after the chlorite treatment, the conductivity increased even more than in the case of the talc treatment. The sodium and potassium concentrations also increased more than was observed after the talc treatment. The magnesium concentration was not affected, but the calcium concentration decreased a little bit more than after the talc treatment.

**Table 5-5: Comparison of the electrolyte balance of the supernatant in the reference sample, the talc treated samples and the chlorite treated samples.**

	Reference	Talc			Chlorite		
		LSSA	MSSA	HSSA	LSSA	MSSA	HSSA
pH	7.1	7.4	7.4	7.4	7.8	8.1	8.1
Conductivity / $\mu\text{Scm}^{-1}$	1 200	1 215	1 211	1 222	1 252	1 260	1 264
SCD / $\mu\text{Eqg}^{-1}$	-0.47	-0.50	-0.49	-0.48	-0.54	-0.53	-0.56
Sodium / mM	9.3	9.6	9.6	9.7	10.2	10.3	10.3
Potassium / mM	1.3	1.3	1.3	1.4	1.6	1.7	1.6
Magnesium / mM	0.3	0.4	0.5	0.4	0.3	0.3	0.3
Calcium / mM	1.6	1.4	1.4	1.4	1.3	1.2	1.3
Chloride / mM	0.7	0.8	0.8	0.8	0.8	0.8	0.8
Sulphate / mM	1.9	1.9	1.9	1.9	1.9	1.9	1.9

From the two phases, resulting after centrifugation of the TMP mineral-treated filtrate, the lower phase is seen to contain the mineral and adsorbed pitch, as expected. The reference pitch suspension was also centrifuged to determine if there are solid particles that sediment which could be confused for mineral-sorbed compounds. The use of a special cone-shaped centrifuge glass revealed no such deposits.

TGA provides the complementary trend to the results from the residue in the upper centrifuged liquid phase. The organic compounds being removed from the liquid phase should be found as the mass balance adsorbed on the lower mineral phase.

The TGA results (Figure 5-6) show that talc has a higher net loss than chlorite. In these data, the pyrophyllite is now included for comparison. Pyrophyllite has a lower net loss than talc and is comparable to chlorite.

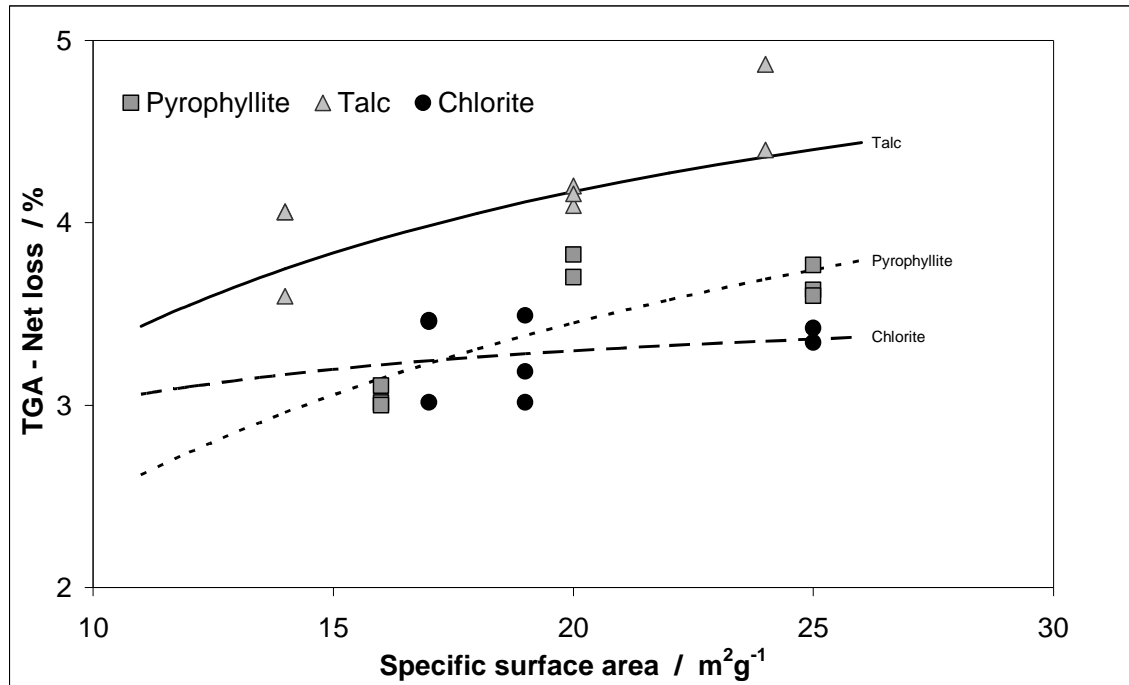


Figure 5-6: TGA analysis from 200 °C to 1 000 °C on the talc-, chlorite- and pyrophyllite-containing residues in the lower centrifuged phase, showing the cumulative weight loss.

We see from Figure 5-6 that TGA results, like gravimetry, also diverge from those of turbidity and COD. Talc shows with increasing surface area an increasing release of material between 200 °C and 1 000 °C, whereas chlorite releases the same amount of material for all three surface areas.

Thus, despite the theoretically different ratios of hydrophobic to hydrophilic surface area, we conclude that talc and chlorite show a comparable adsorption efficiency for colloidal pitch shown by turbidity and COD measurements under the applied conditions (specific surface area, amount of added mineral, temperature, pH, ...). The gravimetric analysis, however, does not show this equivalence in respect to absolute levels. The main difference in response between gravimetry and the other analyses of the liquid phase can be explained by considering the ion balance of the mineral treated TMP

filtrate. Ions, especially sodium and potassium are released/desorbed from chlorite and affect the gravimetric residue. Most probably, then, this release of inorganic material correlates with the effects seen also in the TGA results.

By comparing, therefore, the reduction in turbidity, COD and gravimetry it can be concluded whether the minerals adsorbed preferably dissolved or colloidal material. For example, the low surface area talc (FT-LSSA) showed a remaining turbidity of 38.7 %, a remaining COD of 87.7 % and a gravimetric residue of 86.6 %. The total removed material given by the remaining gravimetric residue can be interpreted as mainly consisting of organic species due to its linear proportionality to the removed COD amount (Figure 5-7). From the available organic material (given by COD), which is split into dissolved and colloidal materials (given by turbidity), mainly colloidal material was removed. The ratio between the removed colloidal particles and removed organic matter is about 5 to 1. In the case of chlorite the same trend can be observed, even though the regression lines are shifted towards higher COD and gravimetry values. The comparable steepness for talc and chlorite in Figure 5-7 indicates that both minerals mainly adsorb wood resin droplets. For chlorite the ratio between removed colloidal particles and removed organics is even higher with 5.5 to 1. This increase can be related to either a preferred adsorption of colloidal substances or to an increased amount of soluble substances that did not adsorb during the adsorption process. The increased pH of the chlorite treated TMP filtrates will clearly favour the dissolution of fatty and resin acids. This will on one hand reduce the measured turbidity and suggest an increased adsorption efficiency and on the other hand increase the amount of dissolved substances and hence increase COD and subsequently suggest a reduced adsorption efficiency for dissolved species. However, the effect of pH on reduced turbidity was accounted for in the performed pH corrections (Equation 5-2). It is, therefore, suggested that the increased ratio of removed colloidal substances to removed dissolved substances is

mainly due to the increased amount of dissolved resin and fatty acids in the aqueous phase. The shift of gravimetry can again be explained by considering the ion balance.

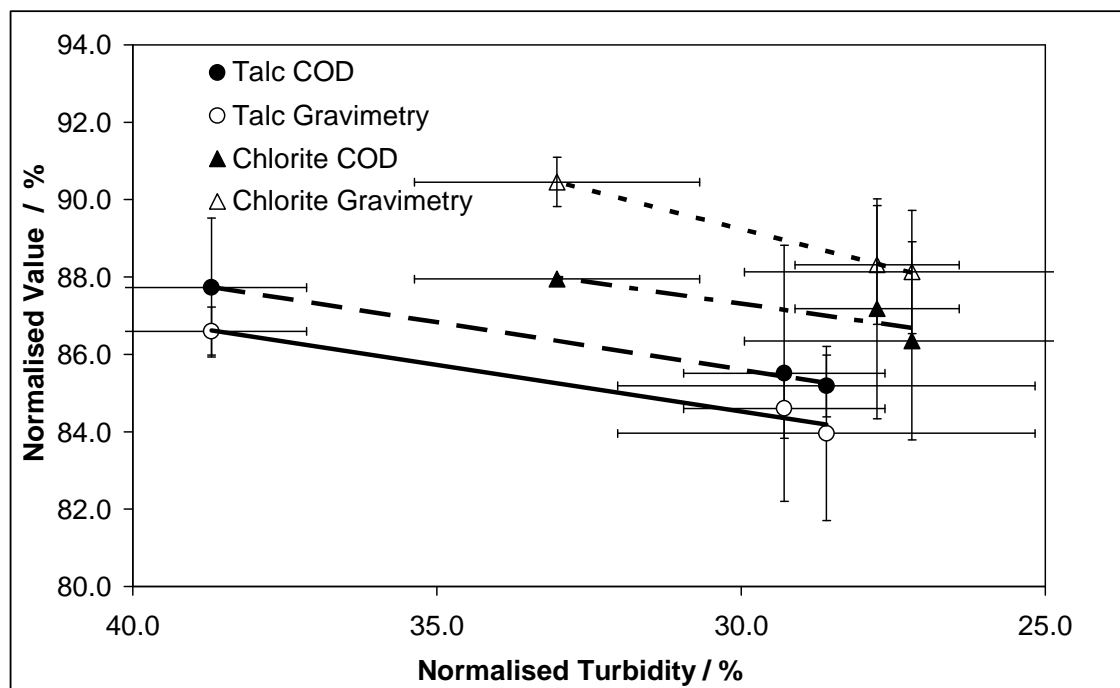


Figure 5-7: Normalised Gravimetry and COD against normalised turbidity for talc and chlorite. Each point is the average of three measurements and the error bars represent the standard deviation of the three measurements.

The ion balance for the pyrophyllite treated TMP filtrate in Table 5-6 shows comparable trends as found for the chlorite treated TMP filtrate. The more the pyrophyllite is delaminated the higher becomes the pH, conductivity and SCD. As a consequence, the sodium and potassium concentration increases, whereas the calcium concentration decreases. Overall more matter is dissolved/desorbed than recovered in centrifugation for these measured inorganic species.

The trend shown by TGA (Figure 5-6) on the lower mineral-rich phase of increasing adsorption as a function of pyrophyllite surface area could not, however, be confirmed by analysis of the liquid phase (Figure 5-8). The gravimetric analysis of the pyrophyllite treated TMP filtrate is given as grey squares and with a dotted regression line. The corresponding talc values are given as unfilled squares. The COD analysis is drawn as

black circles and the regression line is dashed, and, finally, the turbidity values are given as grey triangles with the continuous regression line.

**Table 5-6: Electrolytic balance of the pyrophyllite treated samples (supernatant).**

	Reference	Pyrophyllite		
		LSSA	MSSA	HSSA
pH	7.1	7.0	7.6	8.3
Conductivity / $\mu\text{Scm}^{-1}$	1 200	1 175	1 220	1 268
SCD / $\mu\text{Eqg}^{-1}$	-0.47	-0.50	-0.52	-0.58
Sodium / mM	9.3	9.4	10.1	10.6
Potassium / mM	1.3	1.2	1.5	1.6
Magnesium / mM	0.3	0.3	0.3	0.3
Calcium / mM	1.6	1.4	1.3	1.3
Chloride / mM	0.7	0.8	0.8	0.8
Sulphate / mM	1.9	1.9	1.9	1.9

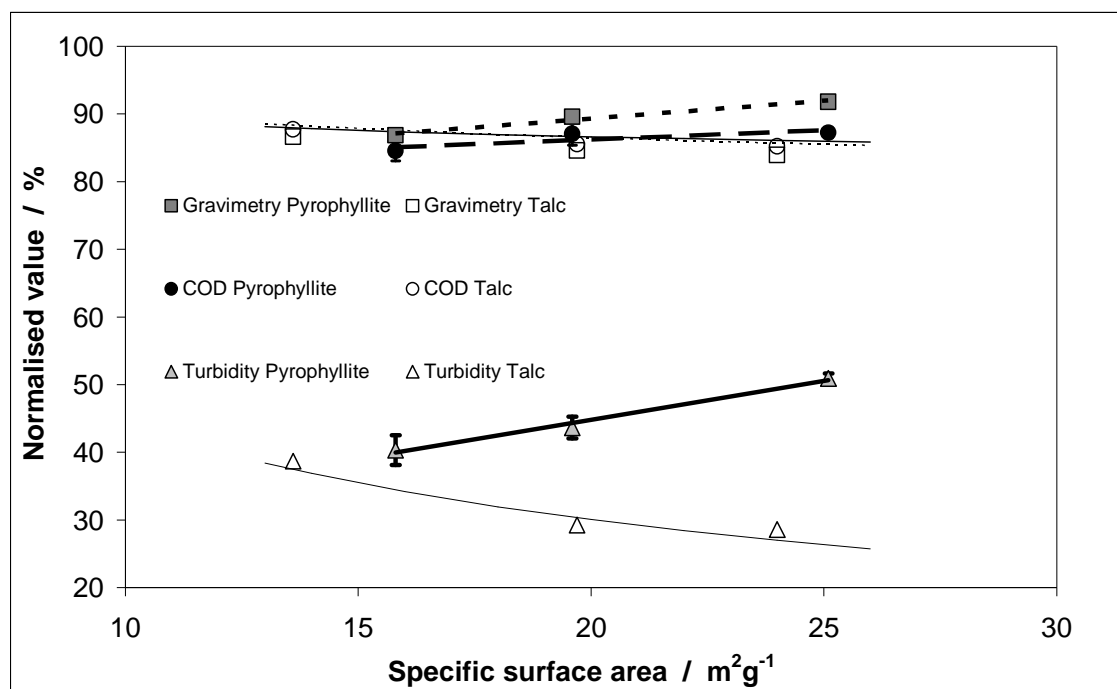


**Figure 5-8: Analysis of the upper liquid phase after the treatment with pyrophyllite. The analyses of the talc treatment are given as references for each method, having the corresponding unfilled symbols.**

The COD values (Figure 5-8) for pyrophyllite are in the same range as the values found for talc and chlorite, but the pyrophyllite seems to decrease its removal efficiency from the upper phase with increasing surface area. This observation was also shown by the turbidity and gravimetry (Figure 5-8) of the upper liquid phase. This unexpected trend most probably fails to show the adsorption efficiency of pyrophyllite *per se*. A test was made to evaluate whether very fine particles, present in the ground pyrophyllite samples, and unable to be centrifuged, changed the apparent values. The particle size distributions of the pyrophyllite samples (PSD), shown in Figure 5-9, demonstrate that about 20 w/w% of the particles are smaller than 0.2  $\mu\text{m}$  for the finest material (P-HSSA), whereas the talc sample with 24  $\text{m}^2\text{g}^{-1}$  (FT-HSSA) shows only 8.5 w/w% of the particles smaller than 0.2  $\mu\text{m}$ . However, in a separate centrifugation of the pure mineral in water it was confirmed that only a clear upper phase (0 NTU) remained, and that the ultrafines were successfully separated during the centrifugation. So, the observed effect happens only when pitch and fine pyrophyllite grades are brought together. In this case, material from the pulp, and the mineral, remains in the upper phase after the centrifugation of the pitch suspension. This leads with increasing amount of fines to the increased turbidity values, higher COD values and of course to higher gravimetric values (Figure 5-8). Such fines, it is assumed therefore, can be further stabilised with dissolved substances in TMP, such as carbohydrates as described previously (Mosbye et al. 2003; Willför et al. 2000).

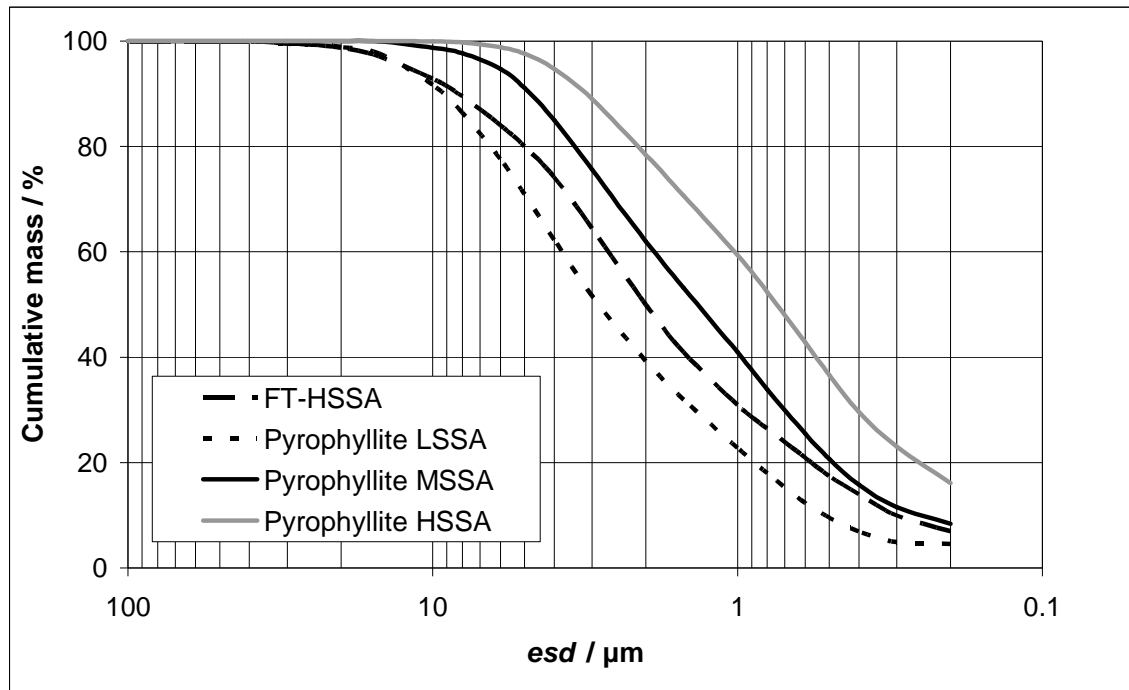


Figure 5-9: Particle size distributions (PSD) for the investigated pyrophyllite samples P-LSSA, P-MSSA and P-HSSA compared with the FT-HSSA talc. The particle size is given as an Equivalent Spherical Diameter (*esd*). The data were measured on a Micromeritics Sedigraph® 5100. P-HSSA is seen to have significantly more ultrafines than the finest talc, which are suspected to become dispersion stabilised during adsorption of pitch.

## 5.4 Conclusions

All three minerals, talc, chlorite and pyrophyllite, act to reduce the colloidal pitch compounds in suspension taken from a TMP-filtrate. Comparisons between the removal efficiency were made using gravimetry, chemical oxygen demand, turbidity and thermo gravimetric analyses.

A Langmuir adsorption model approach, in which the more usual isotherm parameter of adsorbate to adsorbent concentration was replaced with specific surface area of the mineral presented at constant addition weight, gave reasonable regression, partially supporting hypothesis **H4**. It would be necessary, however, to have a broader statistical range of data to confirm just one single mechanism of adsorption, for example over all available parameters of relative mineral and pitch particle size etc.

Against expectation from a mineralogical point of view, which would suggest that talc exposes approximately twice the hydrophobic surface compared to chlorite, and

assuming that the hydrophobic attraction force dominates the adsorption of pitch, talc and chlorite showed similar adsorption behaviour for colloidal pitch with only a slight indication of preference for talc. Hypothesis **H5** is therefore incorrect, and a more advanced explanation is required. It has been shown that the effectively presented hydrophobic attraction force does not match the crystallographically expected one, and that other factors play a role, including either heterogeneity of the chlorite platelet surface, geometry/association of talc particles and/or the nature of pitch. We assume, taking into account the measured zeta potential, that the colloidal pitch particles exhibit also an electro-steric stabilisation in the presence of naturally occurring hemi-cellulose (Sundberg et al. 1994a). Alongside the more expected lipophilic properties, this stabilisation promotes adsorption on a variety of amphiphilic surfaces. The influence of impurities in the minerals are effectively complementary between talc and chlorite, i.e. talc is often contaminated with chlorite and vice versa, though impurities in pyrophyllite, being more wide ranging, most probably influence the performance of pyrophyllite more specifically.

The development of more advanced explanations for hypothesis **H5** were hampered by differences in the findings from gravimetry, TGA, and from the methods of turbidity and COD. These differences could in part be explained by the combination of progressive increase in conductivity between talc, chlorite and pyrophyllite in respect to soluble ionic strength, and, in the case of pyrophyllite, by colloidal stabilisation of mineral fines in the presence of the natural pitch components.



## **6 Influence of pH and temperature on the adsorption of dissolved and colloidal substances from thermo mechanical pulp filtrates onto talc**

The move toward neutral or alkaline papermaking is making ever greater demands on the closed water circuit of paper mills. The need to control contaminants in the form of calcium-containing species, for example soaps, and pitch and stickies, which can be strongly dependent in respect to their surface chemistry under different pH conditions, requires that the mineral response to pitch contaminants under varied pH be studied to understand the potential for adsorption. In this part of the investigation, the following hypothesis was tested:

**H6** Process conditions such as **(a)** pH and **(b)** temperature can negatively influence the adsorption of dissolved and colloidal substances.

During the course of the thesis, this work has been published (Gantenbein et al. 2010; Gantenbein et al. 2011c).

### **6.1 Influence of pH**

#### **6.1.1 Introduction**

In chapter 5, the performance of different phyllosilicates, i.e. talc, chlorite and pyrophyllite, in the adsorption of wood resin constituents, as well as the influence of the available specific surface area of the mineral in the system, was presented. During that work it emerged that the pH can be strongly influenced by the type of mineral added. Significant pH increase was observed after the addition of chlorite or pyrophyllite.

A large number of publications refer to the influence of the three factors, pH, temperature and calcium ion concentration ( $[Ca^{2+}]$ ), on the adsorption efficiency of talc, or on pitch deposition (Allen, Filion 1996; Allen, Douek 1993; Douek, Allen 1991a; Dreisbach, Michalopoulos 1989; Gustafsson et al. 1952; Hamilton, Lloyd 1984; Hassler 1988; Holmbom, Sundberg 2003; Kekkonen, Stenius 2001; Otero et al. 2000; Sihvonen et al. 1998; Trafford 1988). Some authors showed that the affinity of wood resin constituents for talc is progressively weakened as pH increases (Allen, Douek 1993; Douek, Allen 1991a; Hamilton, Lloyd 1984; Hughes 1977; Trafford 1988). These studies, however, were performed using model pitch suspensions, including single compound systems, or contained fibres, on which the pitch was coagulated at low pH.

A recent study investigated the effect of pH on the accumulation of fines and dissolved and colloidal substances in the short circulation water loop in papermaking (Lehmonen et al. 2009). Besides many other findings, it was found that the effect on the pitch particle count is only moderate over the investigated pH range of 4 to 10, and that above pH 6 fatty acids, but especially resin acids, start to dissolve. This might also influence the adsorption behaviour of the wood resin onto a surface.

The pH mainly influences the degree of saponification, the solubility of resin and fatty acids and the electrostatic stability of the colloidal fraction. Less deposition might normally be expected with increasing pH as more free acids would be available (Lehmonen et al. 2009), which could act as emulsifiers, but the opposite is observed in reality. The reason is predominantly the presence of  $Ca^{2+}$  ions which form, in combination with the free acids, insoluble Ca-soaps with a high tendency for deposition (Otero et al. 2000).

Within this overall context, it was the aim of this study to investigate the effect of pH on the adsorption process of dissolved and colloidal substances onto talc.

In order to quantify the effect of pH adsorption isotherms at different pH were measured and interpreted by a operationally defined Langmuir isotherm (see section 2.6.1).

## **6.1.2 Materials and Methods**

### **6.1.2.1 Materials**

14.0 kg of the fresh wet pulp (see section 3.3) (3.6 w/w% solids content) were left for 1 night to cool to room temperature, and then wet pressed through a filter of 2  $\mu\text{m}$  pore size (filter paper, circular 602 EH). A sample taken from the 5.0  $\text{dm}^3$  of filtrate/liquor thus obtained was examined under a light microscope (Olympus AX-70) to check for the absence of fibrils, which might act to distort otherwise purely colloidal adsorption results. The experiments were performed immediately after filtration. The electrophoretic mobility of the suspension at pH 6.6 was measured with a Malvern Zetasizer NS, giving a value of  $-0.81 \times 10^{-8} \text{ m}^2\text{V}^{-1}\text{s}^{-1}$ . The total charge was determined by a streaming current detector (SCD) titration (Mütek PCD-02) and was found to be  $-0.39 \mu\text{Eqg}^{-1}$ , and the polyelectrolyte titration (PET) of the pulp filtrate gave  $-2.0 \mu\text{Eqg}^{-1}$ . Ion chromatography (Dionex DX 120 Ion-Chromatograph) of the TMP sample showed the following ions in solution present in the TMP filtrate:  $\text{SO}_4^{2-} = 0.63 \text{ mM}$ ,  $\text{PO}_4^{3-} = 0.06 \text{ mM}$ ,  $\text{Cl}^- = 0.47 \text{ mM}$ ,  $\text{Na}^+ = 5.30 \text{ mM}$ ,  $\text{K}^+ = 1.18 \text{ mM}$  and  $\text{Ca}^{2+} = 1.03 \text{ mM}$ .

The talc powder in the present study was analysed both by X-ray fluorescence (XRF) and X-ray diffraction (XRD). The talc grade used was shown to contain the minerals talc, chlorite and magnesite. The presence of these constituents was independently confirmed also by FTIR analysis [Perkin Elmer Spectrum One Spectrometer]. XRF [ARL 9400 Sequential XRF] gave a talc content of  $\sim 95 \%$ . The specific surface area was measured on a Micromeritics Tristar based on the BET gas adsorption model (Table 6-1). The weight median equivalent spherical hydrodynamic particle diameter ( $d_{50}$ ) was measured under sedimentation with a Micromeritics Sedigraph 5120.

Additionally, the number median  $d_{N50}$  was determined using the Malvern Zetasizer NS, applying the dynamic light scattering technique. The current talc grade is derived from Finntalc PO5, Mondo Minerals Oy, Finland, with subsequent grinding and delamination to generate fineness, high aspect ratio and enhanced specific surface area. These additional processes maximised the hydrophobically acting planar surface of the talc platelets.

**Table 6-1: Properties of the investigated talc grade. Electrophoretic mobilities were measured in 0.01 M NaCl solution. The  $d_{50}$  measured by Sedigraph is weight based whereas the value from the Malvern Zetasizer NS measurement is number based.**

Description	ssa / m <sup>2</sup> g <sup>-1</sup>	Electrophoretic mobilities / x 10 <sup>-8</sup> m <sup>2</sup> V <sup>-1</sup> s <sup>-1</sup>				$d_{50}$ / $\mu$ m (Sedigraph 5120)	$d_{N50}$ / $\mu$ m (Zetasizer)
		pH 4	pH 5	pH 7.5	pH 10		
High specific surface area talc	45	-2.85	-4.15	-3.92	-4.08	0.8	0.4

### 6.1.2.2 Methods

The filtrate was split into portions of 2 dm<sup>3</sup> and every portion was adjusted to the corresponding pH by the use of hydrochloric acid (0.1 M) or sodium hydroxide (0.1 M) (Table 6-2). The adjustment of the pH to 4 or 9, respectively, requires the presence of 0.10 mM hydronium H<sub>3</sub>O<sup>+</sup> or 0.01 mM hydroxide OH<sup>-</sup> ions. Consequently, the same amount of counter ions are added which correspond to 0.01 mM sodium Na<sup>+</sup> and 0.10 mM chloride Cl<sup>-</sup> ions. As was described above, these ions have the lowest impact on the total ion balance. The use of sulphuric acid was precluded, in order not to increase the sulphate concentration further. 200 g of each pH-adjusted filtrate were placed in a 0.25 dm<sup>3</sup> bottle and the required amount of talc was added in slurry form (solids content of chemical-free talc slurry = 10 wt%). 0, 1, 2, 4, 5, 10 and 20 g talc (dry) were added per 1 dm<sup>3</sup> TMP filtrate. If required, some deionised water was added in order to have the

same dilution. The bottles were air-tight closed and agitated for 2 hours. The suspension was subsequently centrifuged for 15 minutes (Jouan C 312, by IG Instruments) at 2 600 |g|. Two phases were collected; an upper aqueous phase and a lower sedimented mineral-containing phase. Furthermore, mineral alone was centrifuged to confirm that the process removed mineral particles from the upper phase. The upper liquid and the lower solid phase obtained after the centrifugation were separated and analysed according to the following procedures.

**Table 6-2: Trial labelling and corresponding pH adjusted with either hydrochloric acid or sodium hydroxide. For trial point pH 7 no additional acid or base was added. Measured turbidity, COD and gravimetric residue of the pH adjusted TMP filtrates.**

<b>Trial No.</b>	<b>Measured pH after adjustment</b>	<b>Turbidity / NTU</b>	<b>Chemical oxygen demand / mgdm<sup>-3</sup></b>	<b>Gravimetric residue / gdm<sup>-3</sup></b>
pH 4	4.2	496	3 900	1.46
pH 5	5.0	496	4 120	1.41
pH 6	5.8	477	3 940	1.43
pH 7	6.6	451	3 940	1.45
pH 7.5	7.4	438	3 900	1.44
pH 8	8.3	409	3 960	1.45
pH 9	9.1	402	3 910	1.46
Average	-	-	4 100 ± 80	1.44 ± 0.02

A 100 cm<sup>3</sup> sample of the upper aqueous phase, obtained after centrifugation, was placed into a pre-weighed aluminium beaker and dried in an oven (90 °C, 24 hours) to get a total amount of non-volatile residue, by gravimetry, held in the aqueous phase, i.e. that material not adsorbed on talc nor sufficiently agglomerated to be centrifuged into the sediment.

A further 45 cm<sup>3</sup> sample of the upper liquid phase was taken to analyse for turbidity by means of a NOVASINA 155 Model NTM-S (152). Turbidity indicates either that

colloidal material remains in the upper liquid phase or that previously extremely fine material has progressed toward colloidal agglomeration.

A yet further 2 cm<sup>3</sup> sample was taken for chemical oxygen demand (COD) analysis, providing a value for the total organic content, irrespective of its state of dispersion or otherwise. COD was measured using a Lange CSB LCK 014 with a LASA 1/Plus cuvette, range 1 000-10 000 mgdm<sup>-3</sup>.

Particle size was determined on the Malvern Zetasizer NS (photon correlation spectroscopy). The samples were directly measured without any further preparation. The electrophoretic mobility was also measured on the Malvern Zetasizer NS.

### ***6.1.3 Results and Discussion***

Firstly, the turbidity, size and electrophoretic mobility of the TMP filtrate as a function of pH are reported and discussed, and, following that, the adsorption results.

Figure 6-1 shows the turbidity after the addition of acid or base, marked as “pH titration”. The second set of data, “Ref samples”, was recorded 3 hours after the addition of acid or base. The difference between the two lines may indicate the time dependency of the combination of the various processes occurring, namely the saponification reaction of the fatty acid triglycerides, the subsequent dissolving of the saponified fatty acids and the dissolution of the resin acids.

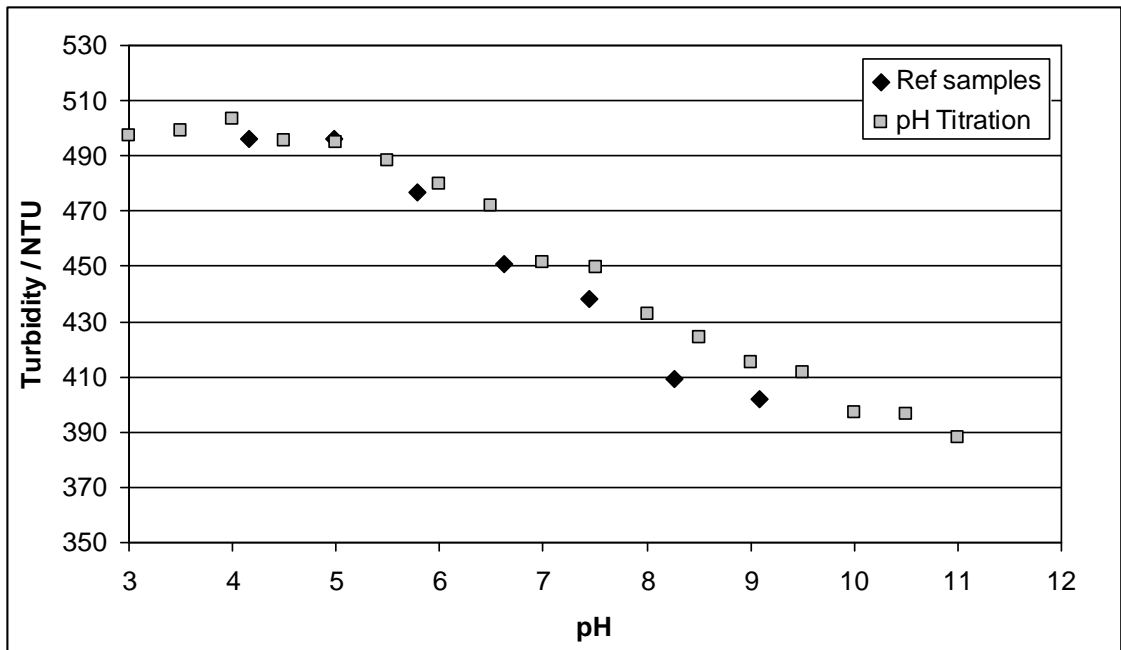


Figure 6-1: Turbidity of the TMP filtrate as a function of pH. The pH was adjusted by either hydrochloric acid or sodium hydroxide (0.1 M). The data set labelled with “Ref samples” was recorded 3 hours after the addition of acid or base.

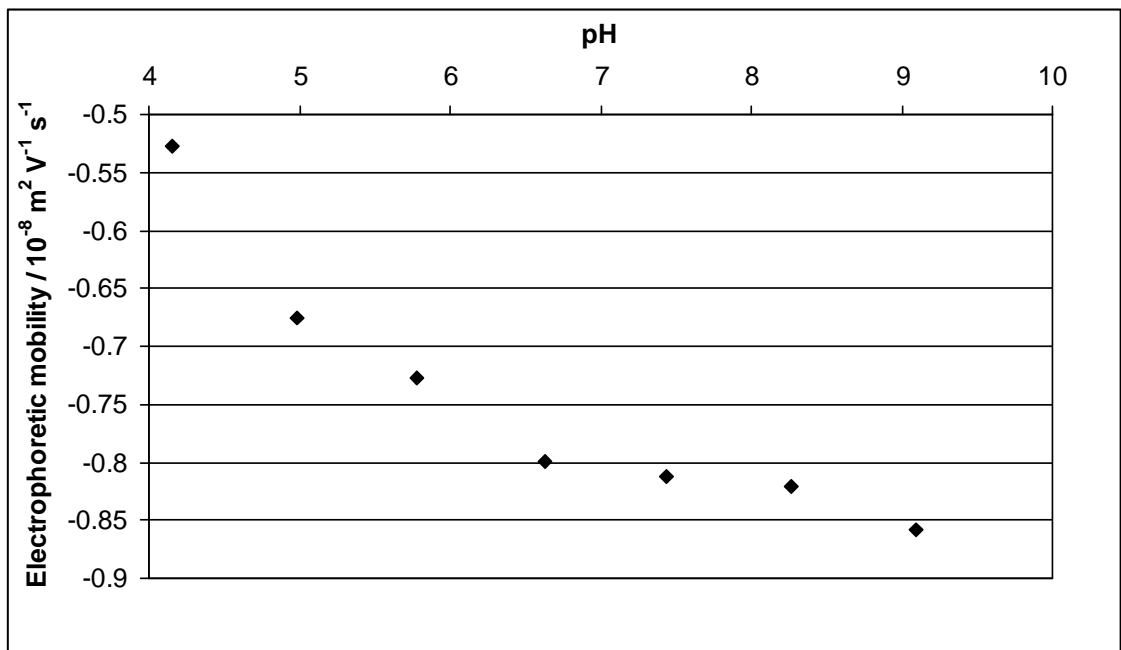


Figure 6-2: Electrophoretic mobility of the pitch particles as a function of pH. Measurements were performed 3 hours after the addition of the acid (hydrochloric) or base (sodium hydroxide), respectively.

Figure 6-2 shows the effect of pH change on the electrophoretic mobility of the pitch particles. As in the turbidity versus pH titration, the electrophoretic mobilities were measured 3 hours after pH adjustment. It can be seen that the lower the pH, the more of the anionic charge carriers (mainly carboxylic groups) on the pitch droplets become

protonated. Increasing pH leads to decreasing electrophoretic mobilities of which the strongest decrease is observed between pH 4 and 7.

The particle size of the pitch colloids remains about the same ( $d_{N50} = 200 - 240 \pm 30$  nm in which the 30 nm are based on the standard deviation of three independent measurements) for all adjusted pH ranges, as shown in Figure 6-3. The pitch droplets have rather comparable particle sizes except for pH 4. This can be expected since at pH 4 the pitch particles will start to coagulate due to their reduced electrostatic stabilisation. The equivalent spherical diameter (*esd*) distribution of the talc is also shown, but it must be remembered that the talc platelet diameters are bigger than those shown in the *esd* distribution (see section 2.4.3 and chapter 4).

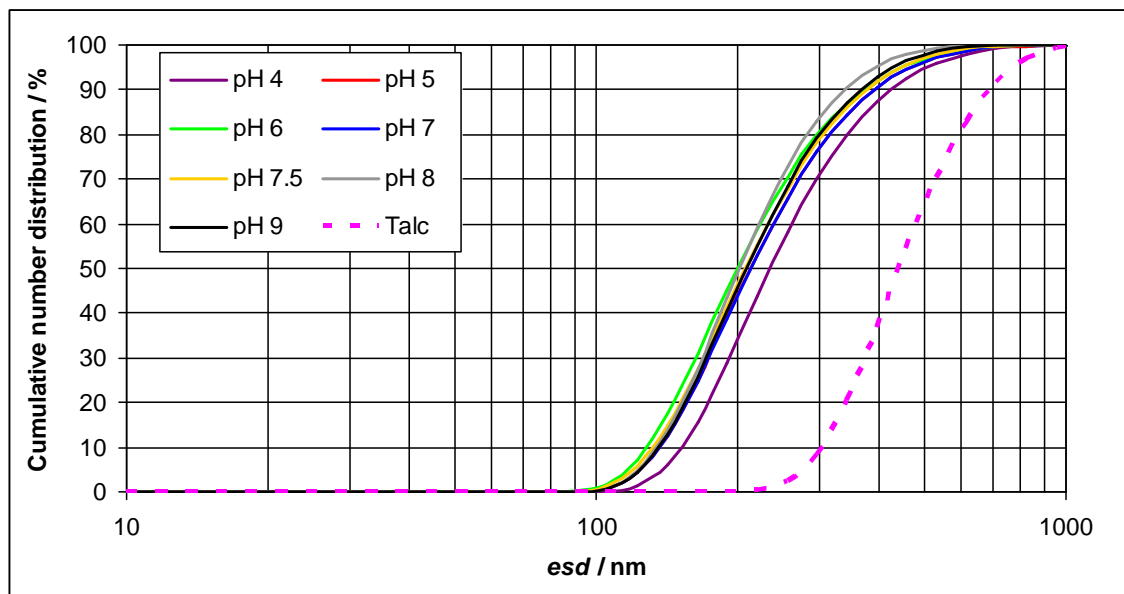


Figure 6-3: Particle size distribution of the pH adjusted TMP filtrates as well as of the talc. The distribution curve is number based.



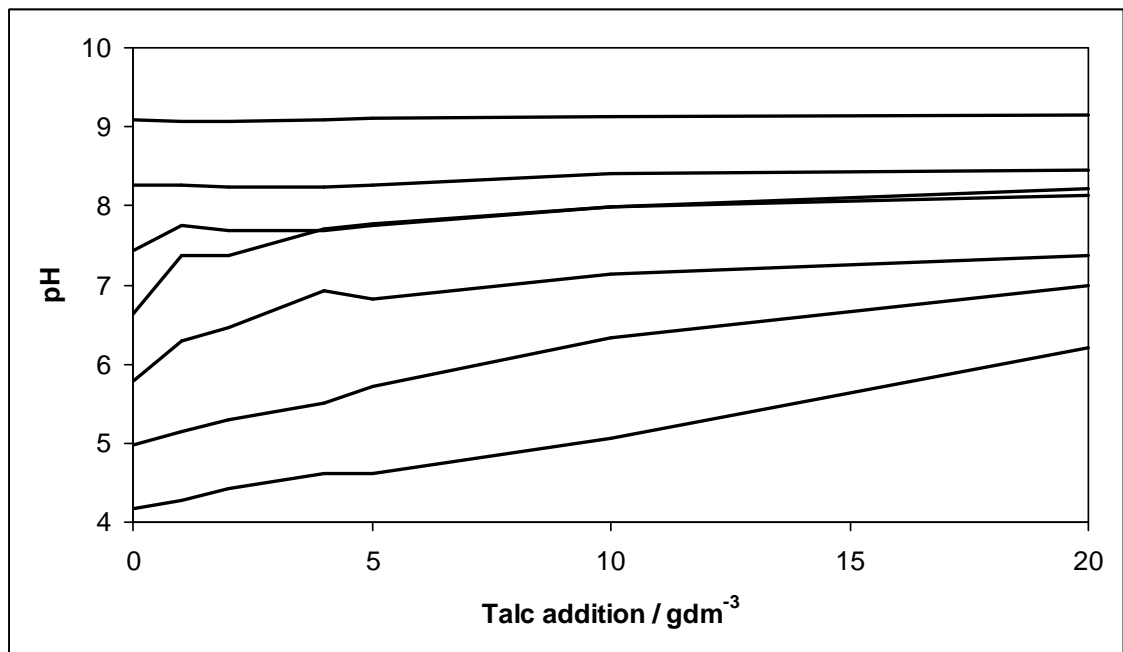


Figure 6-4: pH of the trials, commencing at a range of pH from 4.2 to 9.1, as a function of talc dosage.

The pH was adjusted before talc addition and was not further buffered during the adsorption experiment. As a result of this the added talc basified the system (Figure 6-4) with the strength of this effect proportional to the distance of the initial pH below pH 9. This underlying basification caused the properties of the pitch particles, such as their electrophoretic mobility, to change with increasing talc amount. It also probably changed the surface chemistry of the talc, for example by causing a degree of solubilisation of the  $Mg^{2+}$  from the ancillary dolomite. In the case of the pH 4 experiments the  $Mg^{2+}$  concentration rose from  $< 0.04$  mM to 1.81 mM, whereas at higher pH and lower talc dosage the release of  $Mg^{2+}$  was lower. At pH 4, this increased  $Mg^{2+}$  can have a number of possible effects: raising conductivity, neutralising any carboxyl groups existing on the pitch or surfactant-acting soaps, and depleting the charge balance in the talc structure with the resultant introduction of ionic interactions on the talc surface.

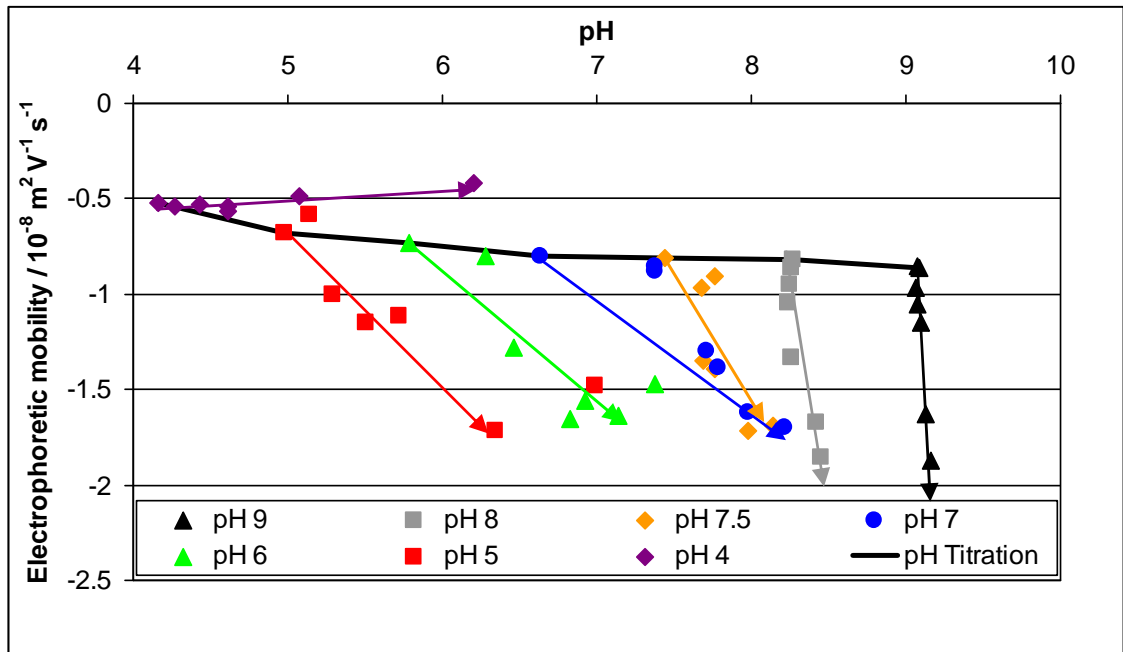


Figure 6-5: Development of the electrophoretic mobility of the particles in the TMP filtrates as a result of increasing talc addition and of pH. The grey shaded line represents the electrophoretic mobility of the original TMP filtrate as already shown in Figure 6-2. Talc dosage increases from there in the direction of the arrows.

Figure 6-5 shows the electrophoretic mobility of the non-adsorbed colloidal particles. Despite the pH development shown in Figure 6-4, the non-adsorbed species follow a different trend. The more talc is added, and the more pitch particles get removed, the more negative the electrophoretic mobility becomes. A possible reason for this could be the presence of very fine talc particles that were not removed by centrifugation. However, IR analyses of the dried supernatants did not show any talc. Therefore, it can be concluded that electrophoretic mobility is that of the remaining colloidal fraction originating from wood resin constituents. It seems either that the material remaining in suspension was even further stabilised, or that the most stable fraction remained in suspension while less stable colloids were adsorbed. The exception is the trial which started at pH 4.

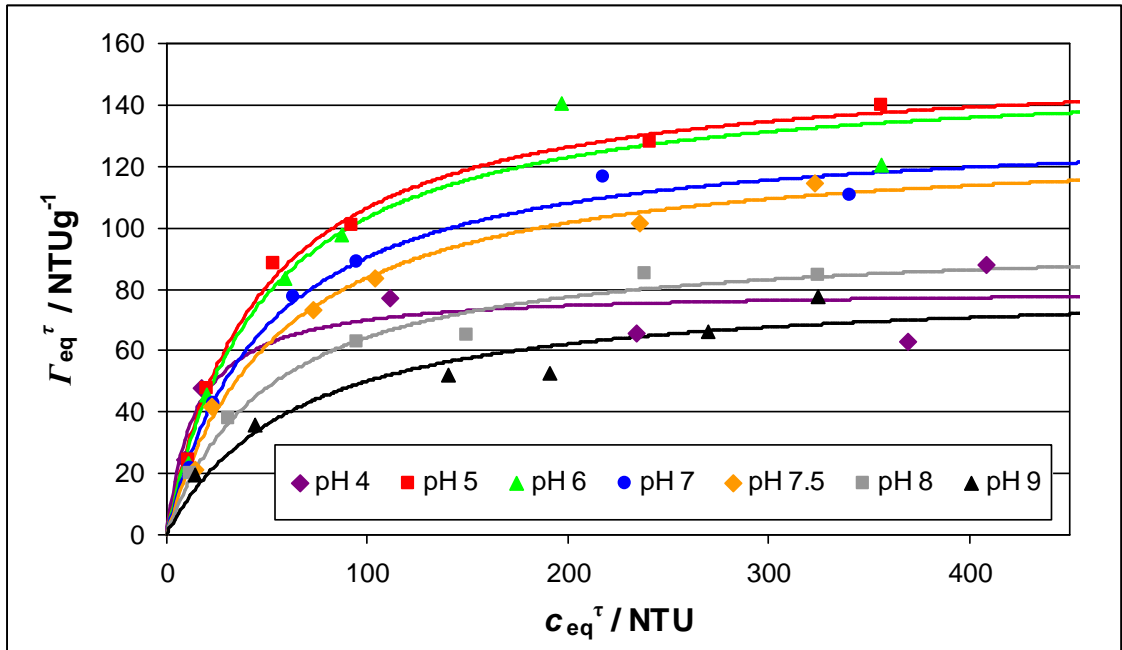


Figure 6-6: Adsorption isotherms of the trials for turbidity analysis.

Figure 6-6 shows the adsorption isotherms for the different pH experiments. The y-axis,  $\Gamma_{eq}^{\tau}$ , is expressed as turbidity removed by 1 g talc added to 1 dm<sup>3</sup> TMP filtrate (Equation 6-1), whereas the x-axis,  $c_{eq}^{\tau}$ , is referring to the equilibrium concentration, following Equation 2-17, or, in this case, the residual turbidity after centrifugation of the talc.

Since

$$\Gamma_{eq}^{\tau} = \frac{c_0^{\tau} - c_{eq}^{\tau}}{m_M}$$

Equation 6-1

where  $c_0^{\tau}$  is the starting concentration (turbidity, COD or gravimetry),  $c_{eq}^{\tau}$  is the equilibrium concentration (turbidity, COD or gravimetry),  $m_M$  is the mineral dosage in gdm<sup>-3</sup> the operationally defined loading  $\Gamma_{eq}^{\tau}$  of sorbate on sorbent, can be derived.

It can be seen that the adsorption capacity of talc is increased at lower pH compared with that at higher pH, what is in agreement with previous work (Hughes 1977). This

adsorption behaviour was characterised in terms of the Langmuir constant ( $K_L^\tau$ ), a measure of the affinity between the adsorbate and the adsorbent, and the maximal loading ( $\Gamma_{\max}^\tau$ ) of the adsorbate onto the adsorbent. These constants (Table 6-3) were found by fitting the data to Equation 2-17 with Tablecurve 2D™ (non linear least squares (NLLS) fit).

**Table 6-3: Summary of the fitting values derived from the turbidity data. The two constants lie all within the confidence interval of 95 %, except for  $K_L^\tau$  at pH 4 and 9 (Given by the t-test with the value of  $P > |t|$ ).**

N°	$K_L^\tau$		$\Gamma_{\max}^\tau$		$R^2$
	Value / NTU <sup>-1</sup>	P >  t	Value / NTUg <sup>-1</sup>	P >  t	
pH 4	0.069±0.092	0.11	80±19	<0.01	0.81
pH 5	0.022±0.006	<0.01	155±13	<0.01	0.99
pH 6	0.021±0.018	0.03	152±40	<0.01	0.95
pH 7	0.021±0.009	<0.01	134±19	<0.01	0.98
pH 7.5	0.018±0.007	<0.01	129±16	<0.01	0.99
pH 8	0.019±0.012	0.01	97±17	<0.01	0.97
pH 9	0.016±0.019	0.09	82±28	<0.01	0.91

It can be seen from Table 6-3 that the behaviour at pH 4 is anomalous with respect to behaviour at higher pH, with a relatively high  $K_L^\tau$  (although not significant) and low  $\Gamma_{\max}^\tau$ . Apart from that  $K_L^\tau$  and  $\Gamma_{\max}^\tau$  decrease monotonically (Figure 6-7). In comparison to the 95 % confidence intervals shown in the graphs, the decrease of  $\Gamma_{\max}^\tau$  with increasing pH is significant. However, although  $K_L^\tau$  also decreases with increasing pH, the decrease is within the 95% confidence intervals, and therefore cannot be attributed any statistical significance.

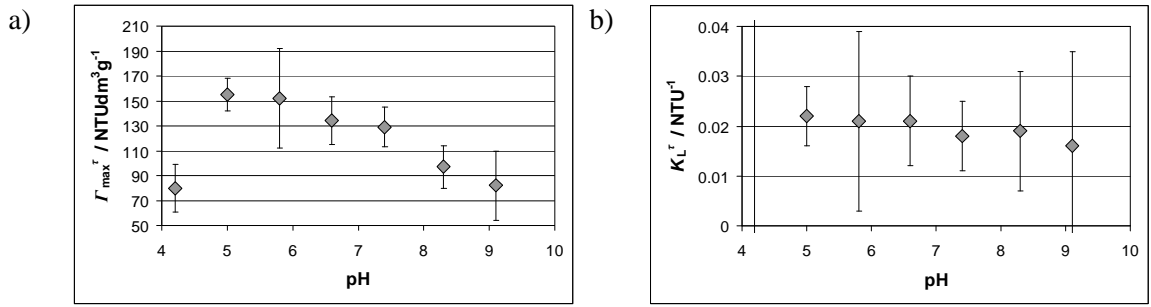


Figure 6-7:  $\Gamma_{\max}^{\tau}$  (a) and  $K_L^{\tau}$  (b) of the isotherm obtained through turbidity analysis against pH. The error bars represent the 95 % confidence intervals.

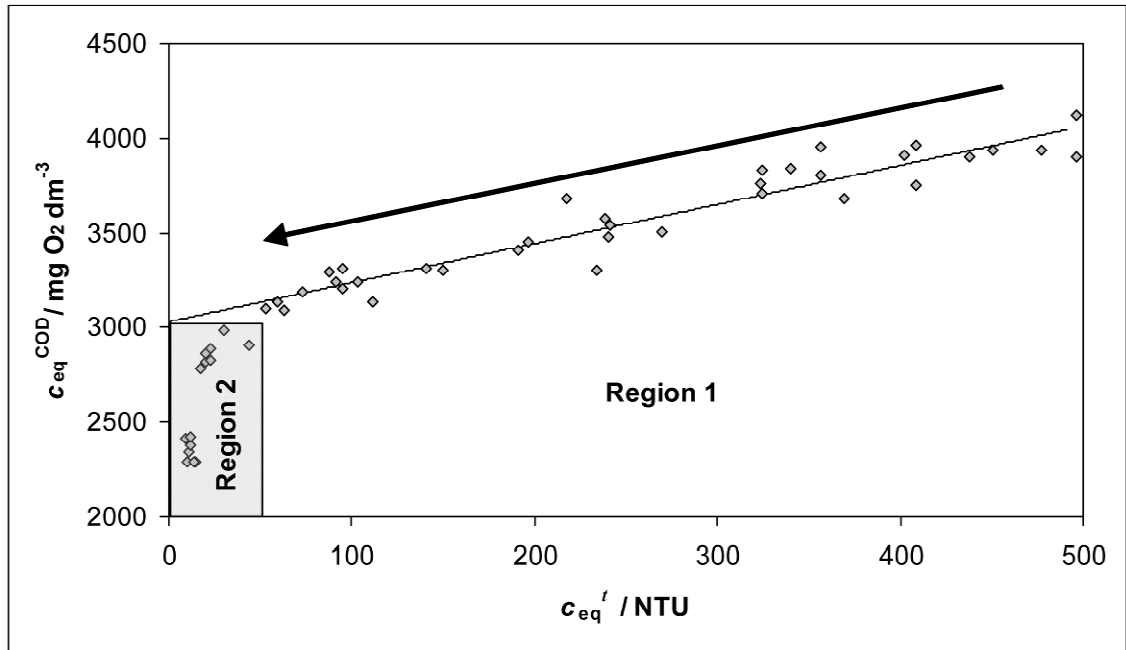


Figure 6-8: Equilibrium COD  $c_{\text{eq}}^{\text{COD}}$  of all trials against equilibrium turbidity  $c_{\text{eq}}^{\tau}$  after adsorption in the supernatant. The arrow shows the direction of increasing talc dosage. The slope of the linear regression line above 50 NTU is  $2.07 \text{ mgdm}^{-3}\text{NTU}^{-1}$ , and its intercept at zero turbidity is  $3\,030 \text{ mgdm}^{-3}$ .  $R^2=0.91$  and  $p$  for both parameters  $< 0.01$ .

Whereas turbidity measures the colloidal fraction, chemical oxygen demand (COD) measures all the material, dissolved and colloidal, which is oxidised under the conditions applied. Therefore plotting equilibrium COD  $c_{\text{eq}}^{\text{COD}}$  against equilibrium turbidity  $c_{\text{eq}}^{\tau}$  (Figure 6-8) allows differentiation between the dissolved and suspended species. As can be seen in Figure 6-8, there is a linear relationship between the two, except at low turbidity at which COD drops markedly. Talc dosage increases from right to left in the figure. So, initially, and as the talc dose increases, the linear relationship moving from right to left in the figure corresponds to the adsorption of colloidal pitch associated with a constant amount of adsorbed dissolved species (region 1). Above a

certain talc dosage, corresponding to the region 2 with lower than 50 NTU on the graph, COD drops markedly because now there is sufficient talc and low enough colloidal material for the adsorption of dissolved material, such as carbohydrates, resin acids or lignin.

The linear relationship above 50 NTU in Figure 6-8 can be extrapolated back to an intercept of  $\sim 3\,030\text{ mg O}_2\text{ dm}^{-3}$  at zero turbidity, as shown on the graph. This intercept corresponds to the hypothetical adsorption of all the colloidal species, without any adsorption of dissolved species.

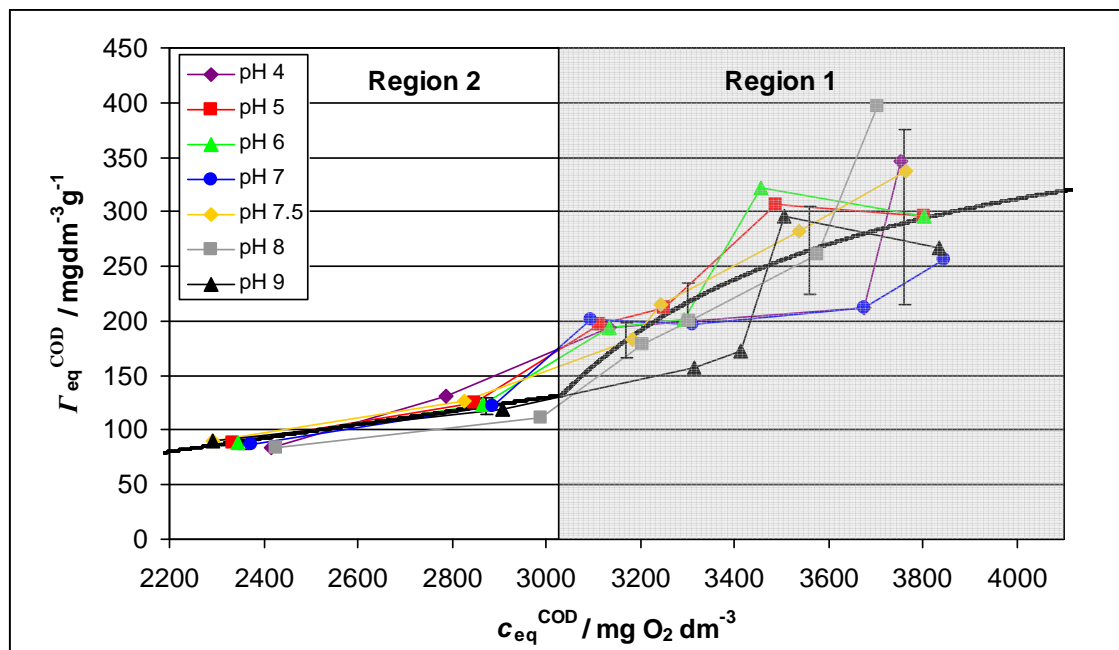


Figure 6-9: Adsorption isotherm of the trials for the COD analysis. The grey area between  $3030\text{ mg dm}^{-3}$  and  $4100\text{ mg dm}^{-3}$  represents the region in which colloids are present in the liquid phase. The scatter of the results in this region is due to the uncertainty of the COD analysis, quantified by the vertical error bars. The error bars were calculated based on the error propagation of Equation 6-1 with the standard deviation of  $c_0$  of  $80\text{ mg dm}^{-3}$  (Table 6-2). The thick line represents a two-stage smoothing curve explained in the text.

The behaviour of the COD isotherm with pH (Figure 6-9) is not clear; it can be seen that the data variation with pH is random and lies within the overall error bars. The intercept of  $3\,030\text{ mg O}_2\text{ dm}^{-3}$  in Figure 6-8 provides a threshold between what we refer to as regions 1 and 2 (Figure 6-9). In region 2 there is only a very minor fraction of the colloidal particles interacting with the talc, and there is very little dependence of

removed COD on pH. In region 1 (shaded), there is significant colloid present. Although in this region there is a general upward trend of removed COD with respect to equilibrium COD, as highlighted by the thick smoothing curve, the effect of pH on this overall trend is apparently fairly random. This scatter is due to the inherent error limits within the COD measurements, the extent of which are shown by the example vertical error bars, and which mask any more subtle trend there is with pH.

The total amount of organics ( $\Gamma_{\text{eq}}^{\text{COD}}$ ) is not clearly affected by pH (Figure 6-9), but that the amount of colloidal material ( $\Gamma_{\text{eq}}^{\text{c}}$ ) is affected. This suggests that the colloidal fraction is in direct competition with dissolved material depending on concentration and pH. In order to make a semi-quantitative characterisation of this effect, the smoothing curves in the two regions are interpreted. In region 2, it is most appropriate to fit a straight line through the 14 data points. This regression line has a steepness of  $0.062 \text{ g}^{-1}$  and an intercept of  $-56 \text{ mgdm}^{-3} \text{ g}^{-1}$  ( $R^2=0.81$ ). In region 1, an operational Langmuir isotherm was fitted (Equation 2-17), with  $K_L = 0.0014 \text{ mgdm}^{-3}$  and  $\Gamma_{\text{max}}^{\text{COD}} = 314 \text{ mgdm}^{-3} \text{ g}^{-1}$  ( $R^2=0.47$ ). The poor  $R^2$  is related to the immense scatter of the data point.

Figure 6-10 shows a linear regression between equilibrium gravimetric analysis (total mass) and equilibrium COD (mass of organic). The intercept of the linear regression line at zero remaining COD, corresponding to the amount of material not involved in the adsorption, is  $1.16 \text{ gdm}^{-3}$ , whereas the maximum value in Figure 6-10 is around  $3.0 \text{ gdm}^{-3}$ . The residual  $1.16 \text{ gdm}^{-3}$  is inorganic material not taking part in adsorption. Around 40 % (i.e.  $1.16 / 3.0$ ) of the mill water filtrate is thus of inorganic nature, whereas the rest (60 %) is organic, of which 25 % ( $1000 / 4100$  as above) is the colloidal fraction.

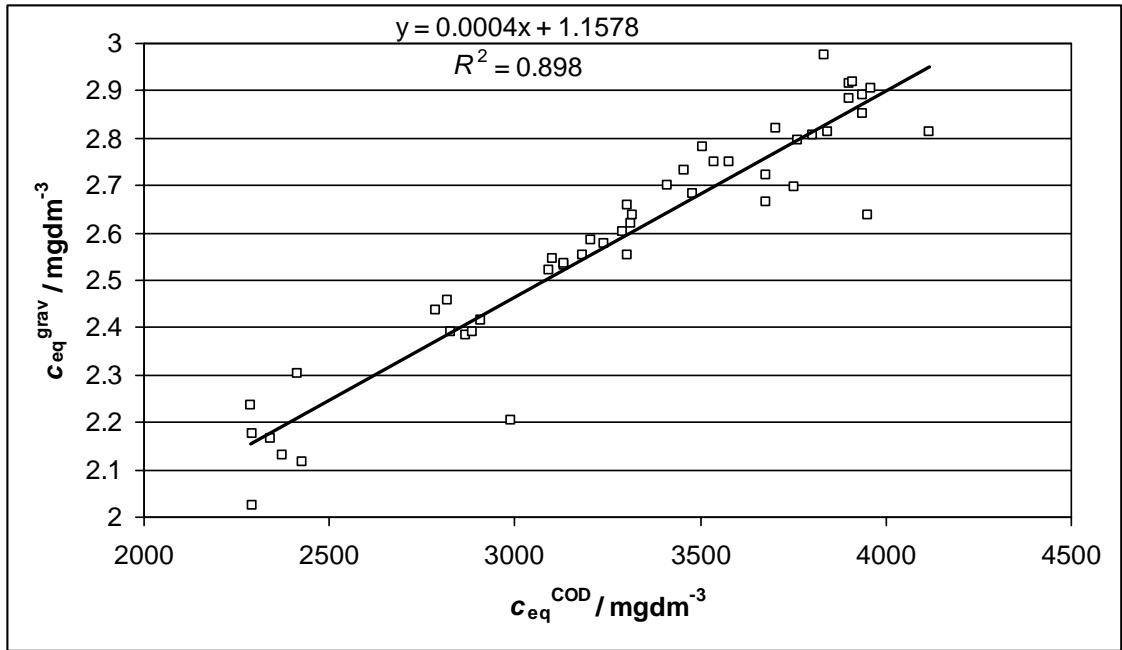


Figure 6-10: Equilibrium gravimetry  $c_{eq}^{grav}$  versus equilibrium COD  $c_{eq}^{COD}$ : enabling the COD to represent mass of organic remaining after adsorption. Both fitted parameters are significant ( $p < 0.01$ ).

Based on the linear regression of COD with turbidity (Figure 6-8) in the region of COD  $> 3\ 030\ \text{mgdm}^{-3}$  and the linear regression of COD with gravimetry (Figure 6-10), it is possible to calibrate turbidity and COD data for absolute mass. The surface covered with dissolved species  $\Gamma_{eq}^{dissolved}$  can be calculated by subtracting the mass of colloidal organic material  $\Gamma_{eq}^{colloidal}$  given by turbidity from the total mass of organic material  $\Gamma_{eq}^{total}$  given by COD as presented in Equation 6-2.

$$\Gamma_{eq}^{dissolved}(c_{eq}) = \Gamma_{eq}^{total}(c_{eq}) - \Gamma_{eq}^{colloidal}(c_{eq})$$

Equation 6-2

The COD isotherm representing the total organic material was transformed to total organic mass by multiplying the equilibrium concentration  $c_{eq}^{COD}$  and the loading  $\Gamma_{eq}^{COD}$  with the steepness found for the linear regression line in Figure 6-10 (0.0004  $\text{mg}^{-1}$ ). For the turbidity isotherm, the Langmuir constant  $K_L^\tau$  and the maximum loading  $\Gamma_{max}^\tau$  expressed earlier were converted in a first step into COD values, using the linear relation in Figure 6-8. In order to do so  $K_L^\tau$  was divided by the steepness of the linear



regression in Figure 6-8 ( $2.07 \text{ mgdm}^{-3}\text{NTU}^{-1}$ ), and  $\Gamma_{\max}^{\tau}$  was multiplied by the same value in order to yield  $K_L^{\text{colloidal}}$  and  $\Gamma_{\max}^{\text{colloidal}}$ , respectively. Also the equilibrium turbidity concentration and loading,  $c_{\text{eq}}^{\tau}$  and  $\Gamma_{\text{eq}}^{\tau}$ , have to be transferred to equilibrium colloidal concentration and loading,  $c_{\text{eq}}^{\text{colloidal}}$  and  $\Gamma_{\text{eq}}^{\text{colloidal}}$ , expressed as in COD. It must be remembered that turbidity recorded a value of zero when COD retained at extrapolated value of  $3\,030 \text{ mgdm}^{-3}$ . This implies that we subtract  $3\,030 \text{ mgdm}^{-3}$  from the equilibrium colloidal fraction concentration leading to Equation 6-3.

$$\Gamma_{\text{eq}}^{\text{colloidal}} = \frac{\Gamma_{\max}^{\text{colloidal}} \cdot K_L^{\text{colloidal}} \cdot (c_{\text{eq}}^{\text{colloidal}} - 3\,030 \text{ mgdm}^{-3})}{1 + K_L^{\text{colloidal}} \cdot (c_{\text{eq}}^{\text{colloidal}} - 3\,030 \text{ mgdm}^{-3})}$$

**Equation 6-3**

The variables ( $\Gamma_{\text{eq}}^{\text{colloidal}}$ ,  $c_{\text{eq}}^{\text{colloidal}}$ ) of Equation 6-3 can then be converted from COD to colloidal mass by multiplication using the steepness of the linear regression, linking mass and COD ( $0.0004 \text{ gm}^{-1}$ ) as already described above for the transformation of COD into mass. The starting point for the colloidal isotherm is at the specific value of  $1.21 \text{ gdm}^{-3}$ . This is due to the intercept in of  $3\,030 \text{ mgdm}^{-3}$  at 0 NTU and transformation with the steepness of  $0.0004 \text{ mgdm}^{-3}\text{g}^{-1}$ . Thus, in summary, the total organic measured by COD is converted into total organic mass, and the organic colloid fraction is converted in 2 steps from turbidity into mass.

The result of this approach is presented in Figure 6-11, Figure 6-12 and Figure 6-13, which refer to pH 5, 7 and 9, respectively. In each figure, the black line is the mass based adsorption isotherm derived from COD, and the blue line is the mass based adsorption isotherm derived from turbidity. The red line, which is the difference between these two isotherms, is the mass based adsorption isotherm for the dissolved organic species. For pH 5 (Figure 6-11), the values for loading of the dissolved material appear to go below zero, whereas the loading of colloidal material goes above the total

loading, but this is an artefact of the errors within the adsorption isotherms, especially observed for the COD analysis.

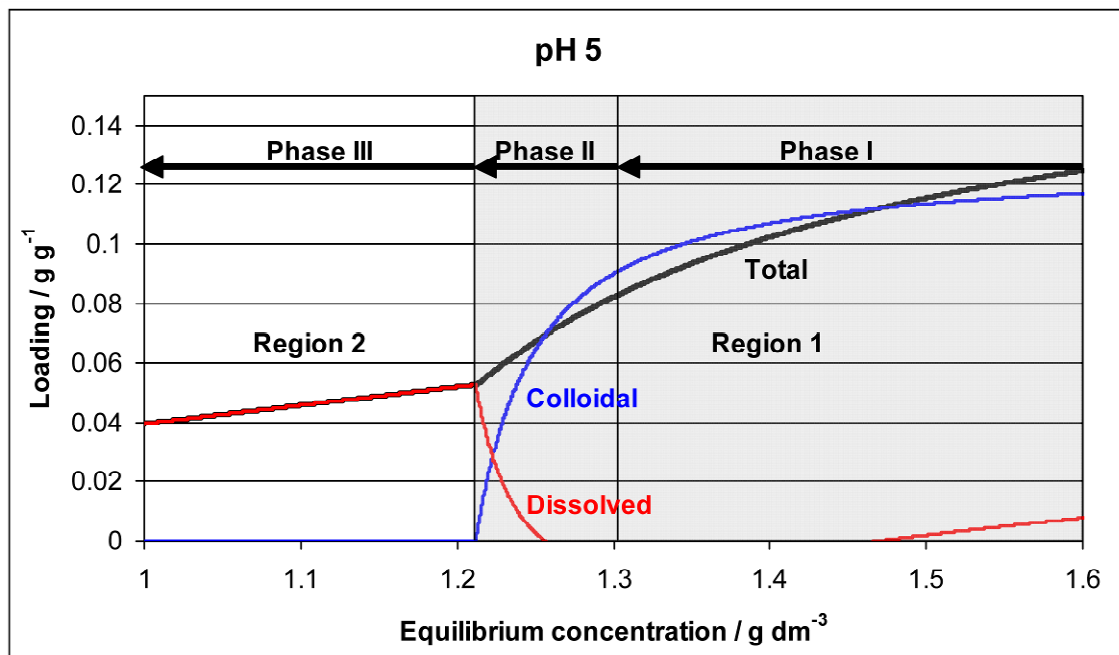


Figure 6-11: Adsorption isotherm at pH 5 for the dissolved and colloidal fractions (black), adsorption isotherm for the colloidal fraction only (blue) and adsorption isotherm for the dissolved fraction only (red). The direction of the arrows indicates the increasing talc dosage, which reduces the equilibrium concentration. The phases are described in the Discussion section.

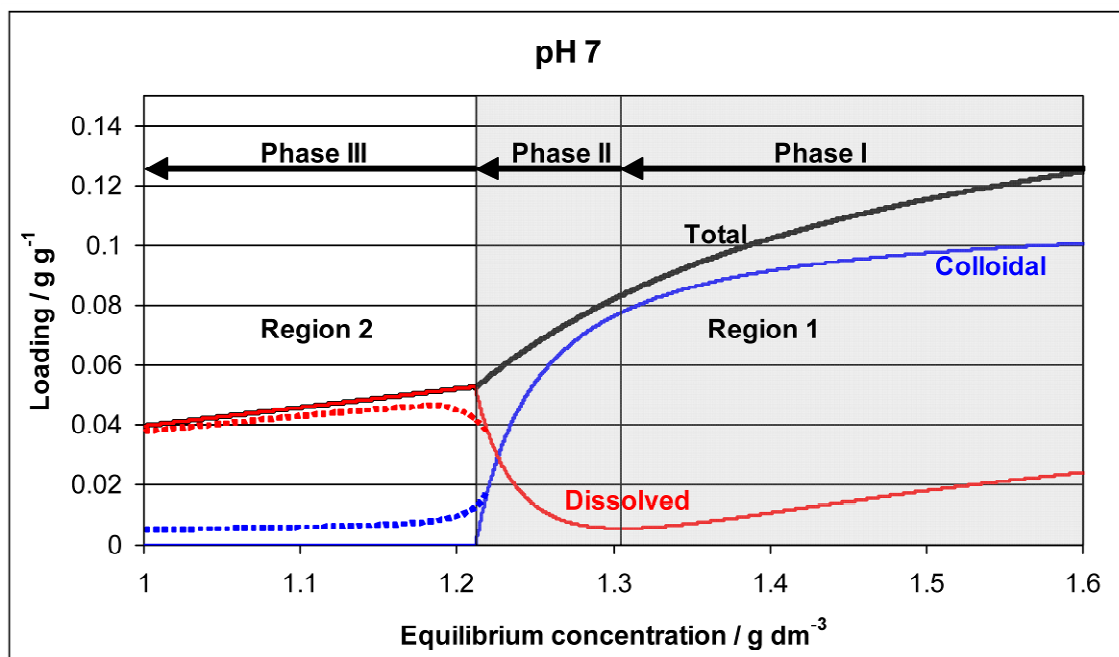


Figure 6-12: Adsorption isotherm at pH 7 for the dissolved and colloidal fractions (black), adsorption isotherm for the colloidal fraction only (blue) and adsorption isotherm for the dissolved fraction only (red). The dotted line indicates the loading of colloidal and dissolved material on talc below the equilibrium concentration of  $1.21 \text{ g dm}^{-3}$ .

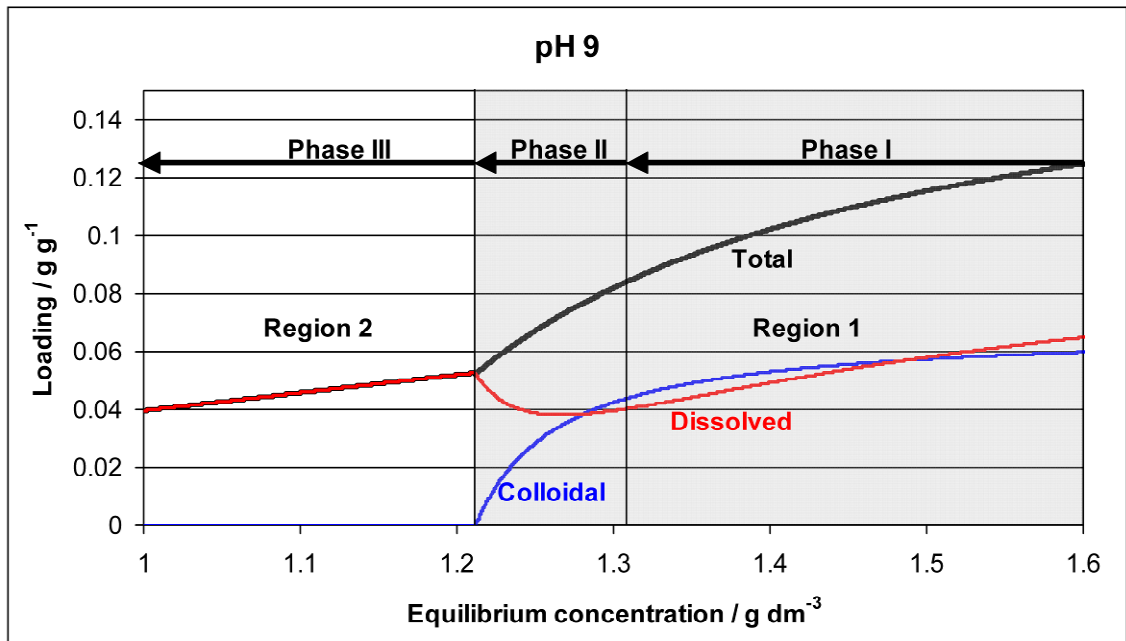


Figure 6-13: Adsorption isotherm at pH 9 for the dissolved and colloidal fractions (black), adsorption isotherm for the colloidal fraction only (blue) and adsorption isotherm for the dissolved fraction only (red).

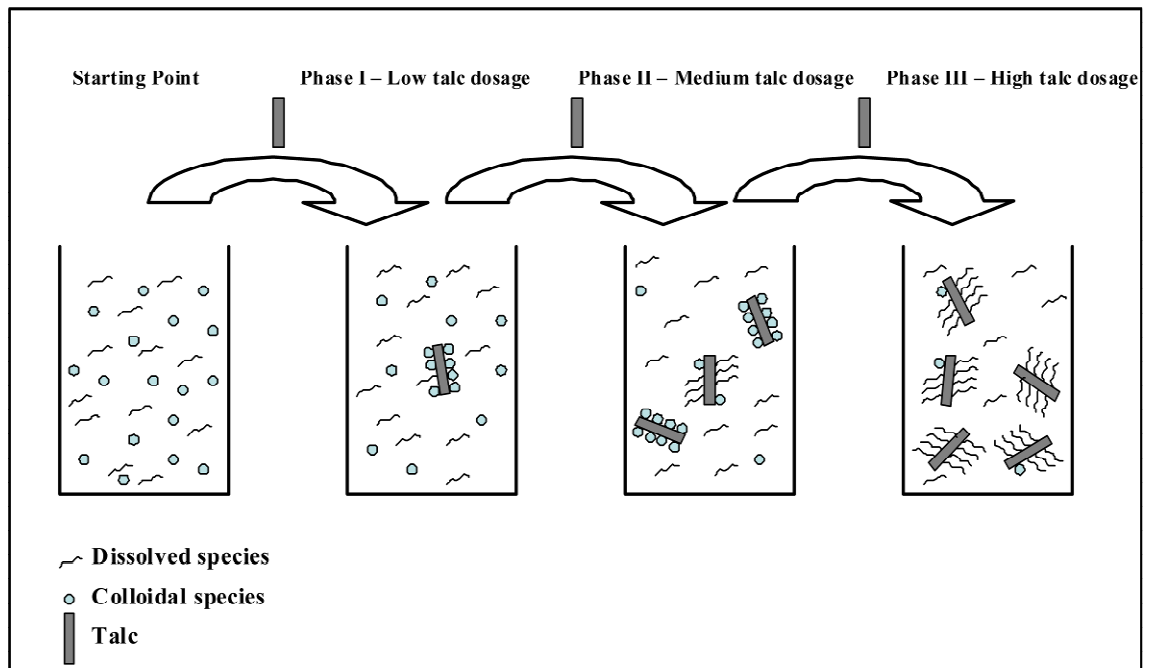


Figure 6-14: Schematic drawing of the adsorption process. Starting point refers to the untreated TMP filtrate. Talc dosage is increased from left to right whereas the equilibrium concentration decreases from left to right.

In order to explain the processes occurring, we split the adsorption process into three phases, as shown in Figure 6-12. Phase I occurs in region 1, and phase III in region 2, with phase II on the borderline of the two regions. The schematic drawing in Figure

6-14 explains the adsorption process in each of these phases, and hence the reason for the trends in Figure 6-11, Figure 6-12 and Figure 6-13. The starting point for each experiment is the TMP filtrate without any talc. Phase I begins on the addition of a low amount of talc. The ratio of colloidal and dissolved species to talc is high, and reduces as more talc is added. In phase I colloidal and dissolved materials compete for the talc surface. By the addition of more talc more and more colloidal and dissolved materials get adsorbed. Due to the limited availability of the colloids, most of them have been adsorbed, the system enters phase II. The ratio of dissolved material to available talc is now increasing and more and more of the talc surface gets covered with dissolved material. At  $c_{eq} = 1.21 \text{ mgdm}^{-3}$ , the border line to phase III, all colloidal particles are removed. At the end of phase II, the entire colloidal fraction has been adsorbed. Therefore, adding more talc has the effect of providing adsorption surfaces for the dissolved fraction only, a state which we refer to as phase III.

In practice, as shown by Equation 6-1, and more precisely by Samiey and Golestan (2010), the adsorption stages cannot be entirely separate and successive. A more realistic plot is therefore shown by the dotted linear line in Figure 6-12, the route described implies that even when the colloid concentration is  $= 0 \text{ mgdm}^{-3}$  the talc loading includes a certain fraction of colloids, which is linearly decreasing the more talc is added. This intercept is presented in Figure 6-12 by the dotted linear line with unknown steepness.

The adsorption of colloidal and dissolved species is controlled by the two equilibria shown in Figure 6-15, where  $K_{\text{Coll-Min}}$  is the colloid adsorption constant and  $K_{\text{Diss-Min}}$  is the constant for the adsorption of the dissolved fraction. While the two equilibria do not directly compete for the same species, they are in competition for the same adsorption sites on the talc. Additionally, a third adsorption equilibrium between dissolved

substances and colloidal substances may also take place, which is also largely influenced by process conditions such as pH and temperature.

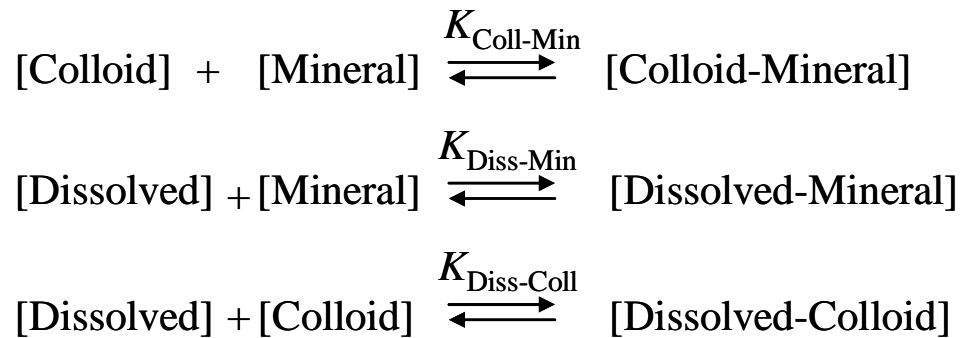


**Figure 6-15: Adsorption equilibriums for the adsorption of colloidal and dissolved species.**

Changing the adsorption constants is directly related to changing affinities that might be caused by a) change of talc surface properties, b) change of colloid surface properties or c) change of properties of the dissolved species. Furthermore, the equilibria shown in Figure 6-15 are also affected by the concentrations of the dissolved species. As discussed previously, a change in talc surface properties (effect a) only occurs at  $\text{pH} < 5$ . Electrophoretic mobilities of talc remain on a comparable level between  $\text{pH} 5$  and  $9$ . It is also known that the properties of talc are not significantly changed by  $\text{pH}$  (Biza 1997; Biza 2001; Parmentier 1979). The change of the colloid surface properties was detected by the electrophoretic mobility measurements presented in Figure 6-2. Since the electrophoretic mobility decreases with increasing  $\text{pH}$  the colloidal stability by electrostatic interaction is increasing as  $\text{pH}$  rises. Willför et al. (2000) proposed a reduced electrostatic stability for wood resin droplets from peroxide-bleached TMP at  $\text{pH} 5$  compared to  $\text{pH} 8$ . However, wood resin droplets of unbleached TMP, as investigated in this study, are known to be electrostatically and sterically stabilised (Sundberg et al. 1996c) and thus the effect b), of changed colloidal stability is expected to be rather minor.

Concerning the concentration of the different species it was shown earlier that turbidity decreases with increasing pH whereas COD remains constant (Figure 6-1, Table 6-2). Additionally to this, the particle size measurements (Figure 6-3) showed no significant change in particle size with different pH values. The decreased concentration of colloidal particles and the increasing solubility of resin and fatty acids with rising pH (Lehmonen et al. 2009; Nyren, Back 1958a; Nyren, Back 1958b) further favour the adsorption of dissolved material in the higher pH ranges due to the changed concentration ratio of the colloidal and dissolved material.

The main effect was seen on the capacity (loading) of the talc but not so much on the affinity of it towards wood resin components. This is another argument suggesting that certain soluble species are covering the surface of talc preferentially at higher pH. It was described earlier that talc has also moderate to strong affinity for components such as carbohydrates, lignin, defoamers, and fatty and resin acids, which might act to suppress the attraction to pitch (Allen et al. 1993; Mosbye et al. 2003; Rogan 1994; Willför et al. 2000). Molecular compounds like fatty and resin acids likely being released at higher pH by saponification and by increased solubility are expected to form molecular mono layers on the talc surface (Rogan 1994). Thus, already very low amounts of these compounds may cover a significant area of the talc surface. Today's continuing trend towards alkaline papermaking is further reinforcing such effects. While the adsorption capacity and surface property of talc are rather stable within the studied range of pH, the chemistry of the papermaking environment changes and with it the capacity of talc to control wood pitch problems is reduced.

In general, a clear effect of pH has been demonstrated [hypothesis **H6(a)**]. Clear trends are apparent, except at pH 4. Such anomalous behaviour has not previously been reported in the literature (Hughes 1977). However, as discussed previously, impurities

present in talc, like dolomite, are strongly affected by pH, and especially at low pH magnesium is observed to be dissolved. Furthermore, Hughes used model pitch which was purely colloidal and did not contain dissolved material. Others (Allen, Douek 1993) observed a reduced amount of pitch particles at  $\text{pH} < 3$ , but this was in the presence of fibrous material on which the pitch heterocoagulated, and so cannot explain what happened during the current trial. Another argument could be that below a certain pH a soluble fraction of the system strongly competes with the colloidal fraction. Douek and Allen (1991b) found that lignin strongly suppresses the adsorption of tall oil especially with decreasing pH. Unfortunately, the investigated pH range reported only covered pH 8 – 12.

## **6.2 Influence of temperature**

### ***6.2.1 Introduction***

During the pulping and subsequent paper production the temperature varies significantly. It is, therefore, important to understand the effect of the temperature on the adsorption of dissolved and colloidal substances onto talc. Despite no data being available in the literature so far directly in respect to adsorption, a lot of work has been performed focusing on the effect of the temperature on pitch deposition (Dreisbach, Michalopoulos 1989; Farley 1977; Gustafsson et al. 1952; Hassler 1988; Qin et al. 2004).

This section aims to investigate the influence of temperature, in a range of 20 – 80°C, representing typical papermaking wet end conditions, on the adsorption of dissolved and colloidal substances originating from an unbleached thermo mechanical pulp (TMP) onto talc, and, after in-depth review of the prior literature, is considered very likely to be the first of such in this field.

In order to study the adsorption behaviour, adsorption isotherms at different temperatures were recorded and interpreted by an operationally defined Langmuir isotherm (section 2.6.1).

The quantification of the adsorption isotherms was made indirectly with analyses such as residual turbidity and chemical oxygen demand (COD) for  $c_{eq}$ , or thermo gravimetric analysis (TGA) for  $\Gamma$ . Therefore, the Langmuir model will not reveal data to identify adsorption energies directly. Nevertheless, the measured trends can indicate the kind of sorption interactions taking place.

## **6.2.2 Materials and Methods**

### **6.2.2.1 Materials**

The fresh wet pulp (see section 3.3) (4.1wt% solids content) was left for one night to cool to room temperature (rt), and further wet pressed through a filter of 2  $\mu\text{m}$  pore size (filter paper, circular 602 EH). The filtrate was checked under a light microscope (Olympus AX-70) for the absence of fibrils. The original TMP filtrate had a turbidity of  $382 \pm 13$  Nephelometric turbidity units (NTU), a chemical oxygen demand of  $3\,440 \pm 65$   $\text{mgdm}^{-3}$  and a gravimetric residue of  $2.85 \pm 0.02$   $\text{gdm}^{-3}$  (the error ranges and the averages refer to the standard deviations of seven measurements). The electrophoretic mobility (EM) at the original pH of 6.6 was  $-0.78 \times 10^{-8}$   $\text{m}^2\text{V}^{-1}\text{s}^{-1}$ . A pH titration of the EM is shown in Figure 6-16. The titration was performed using 0.1 M NaOH and 0.1 M HCl whilst the mobility was measured on a Malvern Zetasizer NS. The electrochemical potential of the TMP filtrate was measured by streaming current detector on a PCD-03 by Müttek, using a solution of 0.0025 M poly-DADMAC [poly-(allyldimethylammonium chloride)] and gave a value of  $-1.1$   $\mu\text{Eqg}^{-1}$ . Polyelectrolyte titration (PET) was performed using 0.01 M PDDPC [poly-(N,N-dimethyl-3,5-dimethylenepiperidiniumchloride)] and 0.01 M KVPS (potassium polyvinyl-



sulphonate). The PET value was  $-2.2 \mu\text{Eqg}^{-1}$ . Ion chromatography was carried out on a Methrom 882 Compact IC plus, and showed:  $\text{Cl}^- = 0.51 \text{ mM}$ ,  $\text{SO}_4^{2-} = 0.35 \text{ mM}$ ,  $\text{Na}^+ = 9.10 \text{ mM}$ ,  $\text{K}^+ = 1.0 \text{ mM}$ ,  $\text{Ca}^{2+} = 0.85 \text{ mM}$  and  $\text{Mg}^{2+} = 0.21 \text{ mM}$ . The resulting conductivity was  $1.89 \text{ mScm}^{-1}$ .

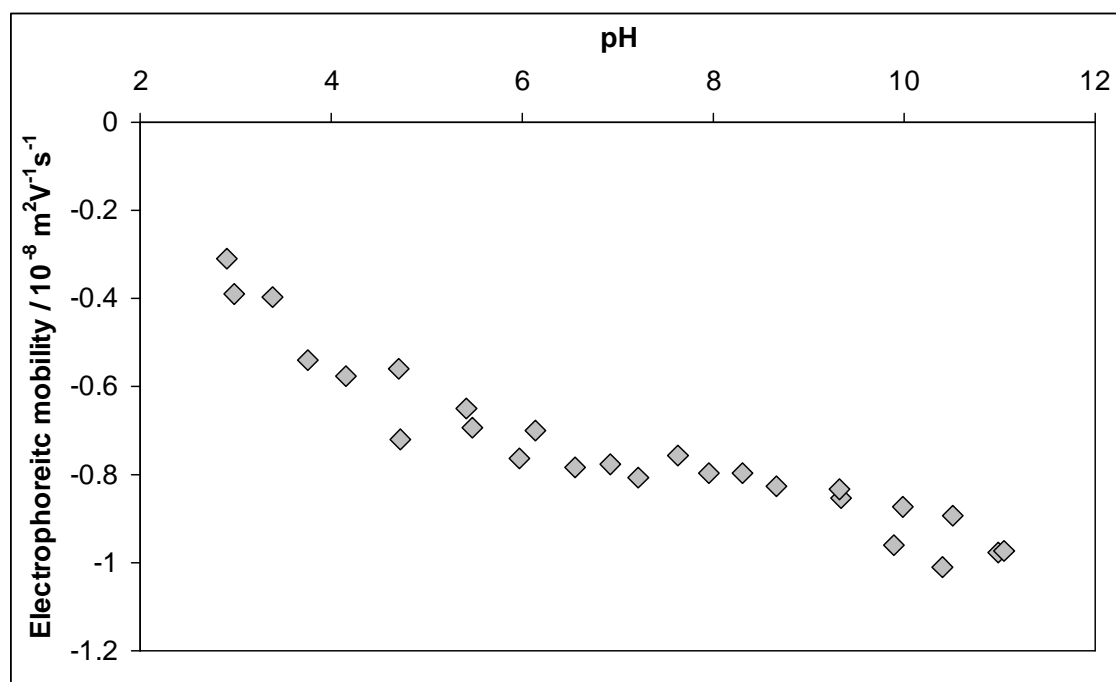


**Figure 6-16: Electrophoretic mobility of the colloidal fraction of the TMP filtrate as a function of pH.**

The talc sample is described in section 6.1.2.1. To check that the initial sample temperature did not affect the thermo-gravimetry of the pure talc, separate samples of talc were stirred into tap water at the various experimental temperatures in the range  $20^\circ\text{C}$  to  $80^\circ\text{C}$ . After a stirring for two hours, the samples were centrifuged and the sediment dried at  $90^\circ\text{C}$ . TGA of the talc samples showed small changes in the weight loss. At  $20^\circ\text{C}$  the weight loss was 6.39 %, at  $40^\circ\text{C}$  6.37 %, at  $50^\circ\text{C}$  6.47 %, at  $60^\circ\text{C}$  6.68 % and at  $80^\circ\text{C}$  7.06 %.

### **6.2.2.2 Methods**

Immediately after filtration the pH of the filtered TMP was adjusted with 0.1 M sodium hydroxide to 7.2, and the sample subsequently split into  $250 \text{ cm}^3$  glass bottles

containing each 200 g of the TMP filtrate. The various samples were then heated to the corresponding temperatures (20, 40, 50, 60 and 80 °C). After having reached the required temperature the talc, also correspondingly pre-heated, was added in slurry form (solids content of the chemical free slurry = 10 wt%). The mineral amounts were chosen to lie between 0 and 50 gdm<sup>-3</sup>. The suspensions were stirred using a magnetic stirrer in temperature controlled water baths for two hours. The temperature of the experiments was measured at the beginning, after one hour and at the end of the experiments. After the two hours of agitation, the experimental mixtures were immediately centrifuged (Jouan C 312 by IG Instruments) for 15 minutes at 2 600 |g|. Two phases were collected; an upper liquid aqueous phase and a lower sediment mineral-containing phase. Centrifugation of the pure mineral did not show any remaining mineral in the supernatant, and centrifugation of the TMP filtrate did not show any sediment coming from the colloidal fraction of the TMP.

Analyses of the two phases were done as described in section 6.1.2.2.

### ***6.2.3 Results and Discussion***

The presentation of the results is split into two sections. In the first section a calibration is presented that allows the transformation of turbidity results, referring only to colloidal material, into mass based results, as well as the transformation of COD results, referring to the total organic material, into total organic mass results. This permits a direct comparison of the two to be made. Within this part a short note is made of the change of pH and electrolyte balance. With this calibration tool in hand the actual sorption results are calculated and reported in the second part.

In the current section a thermodynamic approach was chosen to quantify the sorption behaviour at the different temperatures. Therefore, an equilibrium concentration is obtained after the removal of the mineral. In order to create a mass-based calibration of

the measured parameters, the transformations of turbidity and COD were obtained by plotting them against gravimetry. Figure 6-17 shows the equilibrium turbidity after the removal of the mineral versus the equilibrium gravimetry, also after the removal of the mineral. It can be seen that the two parameters are only linearly dependent within a certain region. This straight line represents the adsorption of colloid species onto mineral. When the mineral, and the colloidal species, are removed from solution at higher concentrations of DCS, what remains are any colloids which have not been adsorbed, and the all of the dissolved fraction. Of these, only the colloidal fraction contributes to the turbidity. However, if the experiment is performed with low concentrations of DCS, then all the available colloid has been preferentially adsorbed, so there are adsorption sites still vacant, which can adsorb some of the dissolved substances. When these adsorption complexes are centrifuged out, what remains in the solution is a negligible quantity of colloids, and a depleted amount of dissolved substances. The steepness of the regression therefore describes the mass equivalent of 1 NTU ( $0.68 \text{ mgNTU}^{-1}$ ), and the intercept of  $2.32 \text{ gdm}^{-3}$  indicates the amount of non-colloidal material. Both fitted parameters are significant ( $p < 0.01$ ).

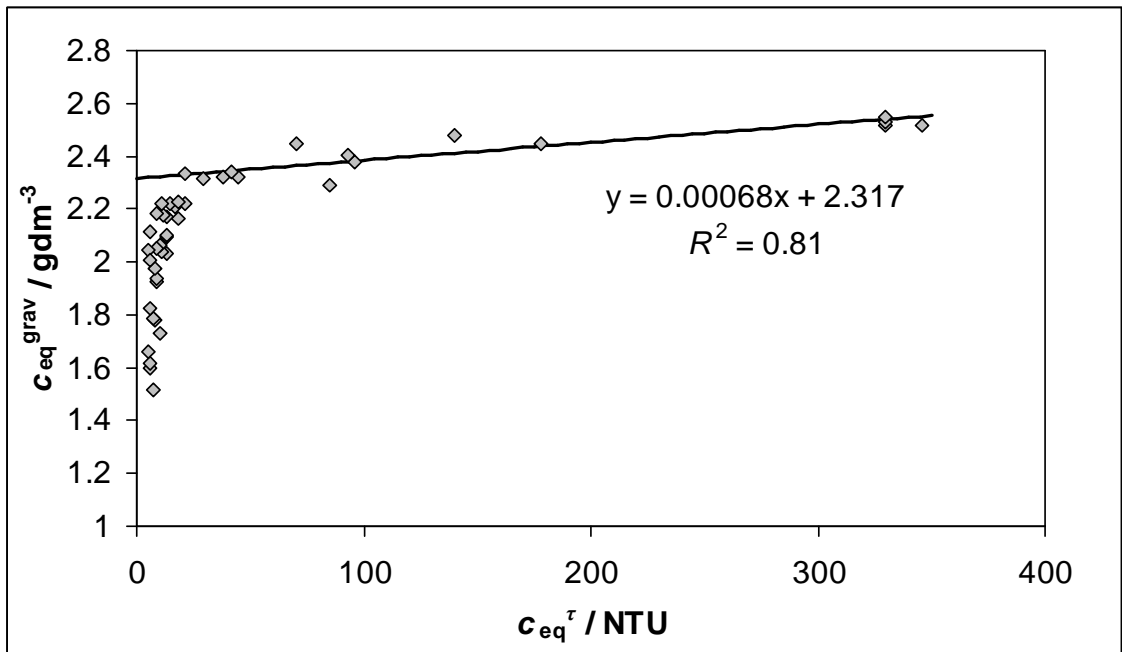


Figure 6-17: Equilibrium turbidity of the TMP filtrate after the removal of the mineral versus equilibrium gravimetry after the removal of the mineral. The presented linear regression is based on all data points with  $x > 45$  NTU. Both fitted parameters are significant ( $p < 0.01$ ).

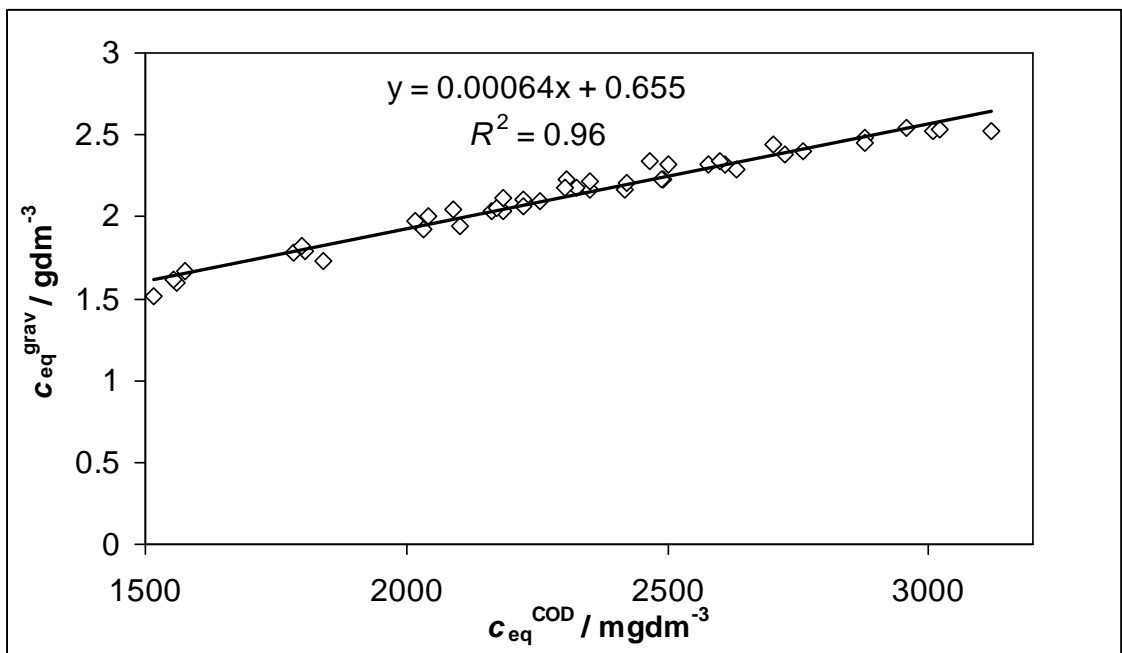


Figure 6-18: Equilibrium COD  $c_{eq}^{COD}$  of the TMP filtrate after the removal of the mineral versus equilibrium gravimetry  $c_{eq}^{grav}$  after the removal of the mineral. Both fitted parameters are significant ( $p < 0.01$ ).

Figure 6-18 shows the equilibrium COD versus the equilibrium gravimetry after the removal of the mineral. In this case (unlike that for Figure 6-17), the properties shown on the two axes are both an indirect measure of the same thing – i.e. the total amount of dissolved and colloidal substances remaining in solution after centrifugation. Therefore,

as expected, the two parameters show a linear dependency, with a regression coefficient  $R^2 = 0.96$ . The steepness suggests that around 0.64 mg of gravimetric residue correspond to 1 mg O<sub>2</sub> required to oxidise the organic material. The intercept of 0.655 gdm<sup>-3</sup> represents the inorganic fraction of the TMP filtrate. Both fitted parameters are significant ( $p < 0.01$ ). Thus, approximately 74% of the total material in the TMP filtrate is organic material. The gravimetric residue may be influenced by the change of inorganic matter with increasing mineral dosage. In respect to this finding, pH and the concentrations of the ions listed in the experimental section were followed. On one hand, the initial pH value of 7.2 before the mineral dosage was seen to increase continuously with increasing mineral dosage, up to pH 8.2 with the highest mineral dosage of 50 gdm<sup>-3</sup>. On the other hand, no change in respect to the analysed ions was observed, except for the magnesium concentration, which increased from 0.21 mM to a maximum of 0.46 mM for the highest mineral dosage. In the case of the lowest gravimetry value (1.52 gdm<sup>-3</sup>) this error contributes less than 1%, and thus it was decided not to correct the data further.

With the above-described calibration, the turbidity and COD data were thus converted into gravimetric mass-based concentrations. In order to obtain the mass-based value for the colloidal organic material  $c_{\text{eq}}^{\text{grav}}(\tau)$  the measured turbidity at equilibrium  $c_{\text{eq}}^{\tau}$  is inserted into Equation 6-4. The reason for the difference in the intercept between Equation 6-4 and the linear regression intercept in Figure 6-17 is the fact that the inorganic material represented by the intercept of the linear regression in Figure 6-18 (0.655 gdm<sup>-3</sup>) has to be subtracted. If only the sorption process of the colloidal material is investigated, the intercept can be completely left out.

$$c_{\text{eq}}^{\text{grav}}(\tau) = 0.00068 \cdot c_{\text{eq}}^{\tau} + 1.662$$

Equation 6-4

$$c_{\text{eq}}^{\text{grav}}(\text{COD}) = 0.00064 \cdot c_{\text{eq}}^{\text{COD}}$$

Equation 6-5

$$\Gamma_{\text{eq}}^{\text{colloidal}} = \frac{c_0^{\text{grav}}(\tau) - c_{\text{eq}}^{\text{grav}}(\tau)}{m_{\text{M}}}$$

Equation 6-6

where the units of concentration are given in  $\text{gdm}^{-3}$ .

The equilibrium COD concentration  $c_{\text{eq}}^{\text{COD}}$  is then converted by Equation 6-5 into total organic equilibrium concentration  $c_{\text{eq}}^{\text{grav}}(\text{COD})$ . Equation 6-5 does not need an intercept like the linear regression previously seen in Figure 6-18, since the excess gravimetry value at zero COD is not organic by definition, i.e. corresponds to zero COD.

With Equation 6-4 it was possible to calculate the mass-based equilibrium concentration of the colloidal material, and thus apply it to the adsorption isotherm for the colloidal fraction. For this isotherm, the loading of colloids on the mineral surface  $\Gamma_{\text{eq}}^{\text{colloidal}}$ , was calculated using the initial colloidal organic material  $c_0^{\text{grav}}(\tau)$ , the equilibrium colloidal organic material  $c_{\text{eq}}^{\text{grav}}(\tau)$ , and the mineral dosage  $m_{\text{M}}$  in Equation 6-6.

**Table 6-4: Summary of the fitting parameters for the colloidal fraction of the TMP filtrate described by a Langmuir isotherm (Equation 2-17). The shown range represents the 95 % confidence interval of the constants and  $P > |t|$  is the probability that the value lies within the confidence interval.**

Temperature	$K_L^{\tau} / \text{dm}^3 \text{g}^{-1}$		$\Gamma_{\text{max}}^{\tau} / \text{mgg}^{-1}$		$R^2$
	Value	$P >  t $	Value	$P >  t $	
20 °C	0.032±0.020	0.01	71±20	<0.01	0.94
40 °C	0.023±0.012	<0.01	108±27	<0.01	0.97
50 °C	0.021±0.014	0.01	125±54	<0.01	0.96
60 °C	0.023±0.009	<0.01	141±25	<0.01	0.98
80 °C	0.031±0.020	0.01	156±59	<0.01	0.95

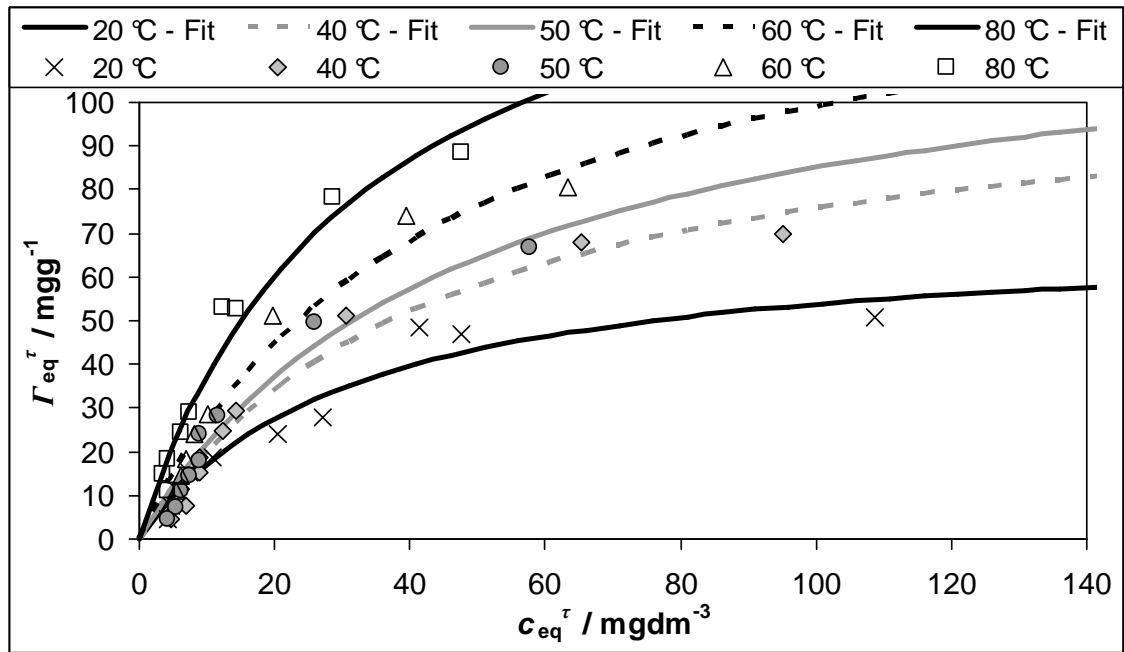


Figure 6-19: Mass-based adsorption isotherm for the colloidal fraction of the TMP filtrate based on turbidity data.

A Langmuir isotherm (Equation 2-17) was fitted at each temperature with Tablecurve 2D<sup>TM</sup> (non linear least squares NLLS fit). Figure 6-19 shows the different isotherms. The fitted parameters  $K_L^\tau$  and  $\Gamma_{\max}^\tau$  are also presented in Table 6-4, together with the regression coefficient  $R^2$ .

The Langmuir constants  $K_L^\tau$  for the adsorption of the colloidal fraction lay between  $0.021 \text{ dm}^3 \text{ g}^{-1}$  and  $0.032 \text{ dm}^3 \text{ g}^{-1}$ . The maximum loading ranges from  $71 \text{ mgg}^{-1}$  at  $20 \text{ }^\circ\text{C}$  to  $156 \text{ mgg}^{-1}$  at  $80 \text{ }^\circ\text{C}$ . The goodness of fit indicated by the regression coefficient  $R^2$  is in all cases  $>0.94$ . A linear regression of the maximum loading  $\Gamma_{\max}^\tau$  versus the temperature gave a steepness of 1.4 ( $R^2=0.96, p<0.01$ ).

In order to quantify the adsorption behaviour of the total organic material  $c_{\text{eq}}$  is obtained via the COD measurement and the loading via the thermo gravimetric analysis (TGA). It was decided to avoid the calculation of the loading according to Equation 6-6 and use the independent parameter of TGA instead. COD measurements can have large errors

( $\pm 65 \text{ mgdm}^{-3}$ ) and, especially in the high equilibrium concentration region, the impact of this error on the calculated loading can be unacceptably high.

Figure 6-20 shows the sorption data for the total organic material in the TMP filtrate onto the mineral at the various temperatures. Following the sorption of the total organic material is more complex than the sorption process of the colloidal fraction. Not only does competition of the colloidal and the dissolved fraction arise, but also competition of the various dissolved species. This makes it very difficult to apply any sorption isotherm throughout the range of the data. Nevertheless, the data were fitted in order to be able to follow the sorption better. In the range between 900 and 1 662  $\text{mgdm}^{-3}$  a linear regression was made (Region II). The point of change to linearity, i.e. at 1 662  $\text{mgdm}^{-3}$ , was chosen based on the intercept in the turbidity versus gravimetry plot in Figure 6-17 minus the intercept in the COD versus gravimetry plot. Above this value, a Langmuir isotherm was fitted (Region I). The parameters thus obtained cannot be regarded as quantitative because for some fits only 3 - 4 data points were available (including the origin) but it was nonetheless decided to use a Langmuir as being qualitatively relevant due to the observation made for the colloidal part. Table 6-5 summarises the fitting parameters derived from the constructed lines in Figure 6-20.

**Table 6-5: Summary of the fitting parameter of the total organic sorption data. The fit is characterised by a linear region in the form of  $y = mx + b$  and the Langmuir region in the form of Equation 2-17. The standard error of the steepness,  $m$ , is in all cases  $\sim 0.01$ . The fitted parameters for the linear regression are significant ( $p < 0.05$ ) except  $m$  and  $b$  at 20 °C which are not significant ( $p > 0.05$ ).**

Temperature	Region II (linear)			Region I (Langmuir)	
	$m$	$b$	$R^2$	$K_L^{\text{COD}}$	$\Gamma_{\text{max}}^{\text{COD}}$
20 °C	0.02	+9	0.44	0.02	12
40 °C	0.07	-66	0.90	0.04	25
50 °C	0.05	-33	0.95	0.05	40
60 °C	0.09	-82	0.87	0.006	100
80 °C	0.05	-38	0.84	0.1	80



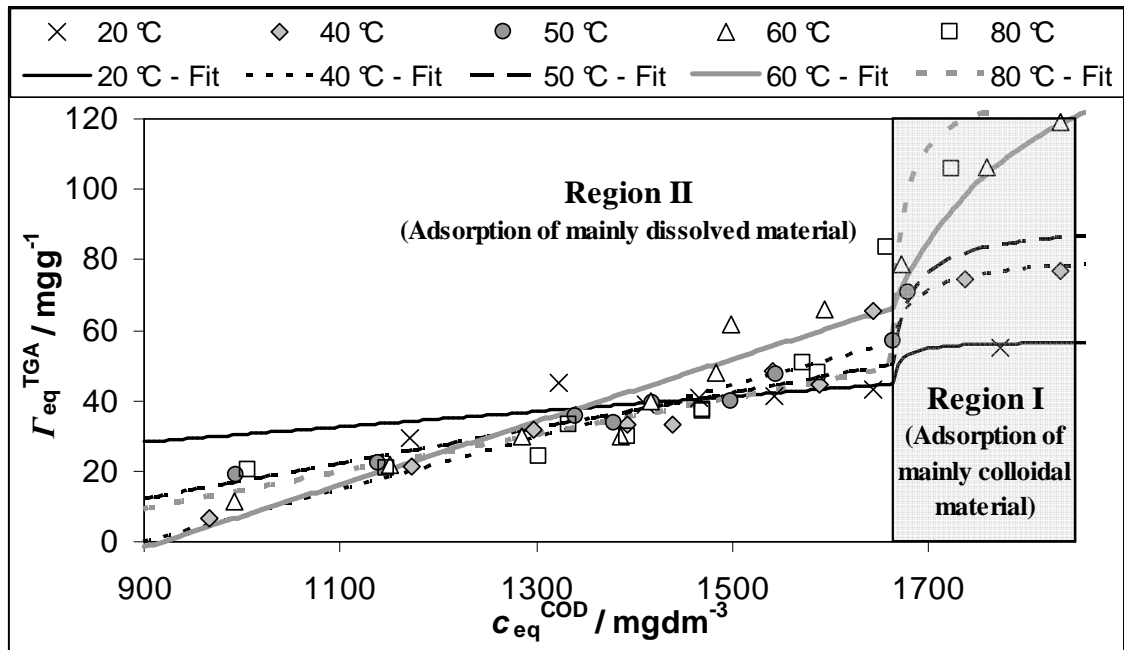


Figure 6-20: Sorption data for the total organic material in the TMP filtrate at various temperatures. The equilibrium concentration in the aqueous phase was determined by COD and transferred into equivalent mass by Equation 6-5. The loading was obtained by TGA  $\Gamma_{eq}^{TGA}$  and refers to mg volatile (200 °C – 1 000°C) material per gram mineral. The fit is based on a linear regression between 900 and 1 662  $\text{mgdm}^{-3}$  and a Langmuir for concentrations  $> 1\,662\ \text{mgdm}^{-3}$ .

The calibration of the turbidity to a mass base in Figure 6-17 showed that the mineral talc adsorbed both colloidal and dissolved species. This can be concluded from the non-linear behaviour of the calibration. However, as soon as colloidal material is available, the adsorption of colloids is preferred, at least on a mass-based consideration. The calibration of COD to a mass base showed that the COD, and thus the total organic material, is linearly related to the removed mass. Extrapolation showed that 26 % of the TMP filtrate is of inorganic nature whereas the other 74 % is of organic nature.

Investigating the adsorption process of the organic colloidal fraction via turbidity showed a significant preferred adsorption of the colloidal material at increased temperatures. No significant change was observed for  $K_L^\tau$  but  $\Gamma_{max}^\tau$  showed a significant increase of adsorbed colloids with increasing temperature (Table 6-4). Hypothesis **H6(b)** is thus proven.

In order to understand this observation better, a few hypothetical mechanisms are discussed in order to elucidate by a process of elimination. With increasing temperature the cohesive force of the individual pitch droplets decreases. Thus, it is more likely that the pitch droplets tend to spread more on the mineral surface, and so covering a larger surface area on the mineral. This would lead to a lower  $\Gamma_{\max}^{\tau}$  but an increased  $K_L^{\tau}$  because of the increased contact area. This was obviously not observed. The temperature also affects the solubility of the dissolved and also colloidal substances in the TMP filtrate. A better solubility of the dissolved substances, which compete with the colloidal fraction for the mineral surface, would lead to an increased adsorption of the colloidal fraction but of course also to a decreased level of dissolved substances on the mineral surface.

In section 6.1.3 we have shown that the pH changes the ratio of dissolved and colloidal substances on the mineral surface, and that with increased pH more and more dissolved substances get adsorbed. This was shown by subtracting the sorption isotherm of the colloidal material from the sorption isotherm of the total organic material. In the current study the pH is around 7.5 – 8.0. Also, according to section 6.1.3, a certain amount of dissolved substances can be found on the mineral surface. As an example, Figure 6-21 at 60°C shows the sorption isotherms of the total organic material, the sorption isotherm of the colloidal material and the difference of the two as the sorption isotherm of the dissolved organic material. The loading of colloids on the mineral appears to be 0 mgg<sup>-1</sup> at an equilibrium concentration of 1 662 mgdm<sup>-3</sup>. It is, however, important to note that also below this critical equilibrium concentration a certain amount of colloids may, nonetheless, be on the mineral surface. In order to account for this, the dotted lines in Region II in Figure 6-21 have been manually inserted. Such plots were also made for the other temperature experiments, but the absolute amount of adsorbed dissolved

substances remained the same. Therefore, an impact coming from the increased solubility of certain compounds is not likely.

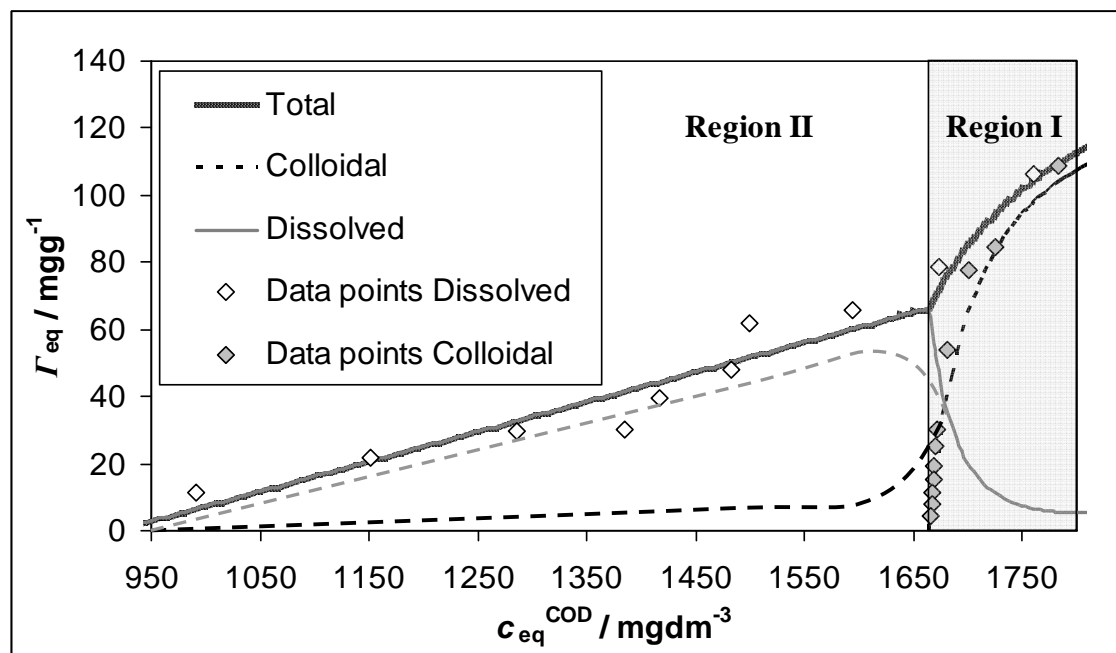


Figure 6-21: Overlay of the total organic adsorption isotherm and the colloidal isotherm with the calculated isotherm for the dissolved fraction at 60 °C. In addition, the measured data points are also shown as  $\Gamma_{eq}^{TGA}$  and  $c_{eq}^{COD}$ .

Another possibility is that the dehydration of both the lyophobic pitch colloids and the hydrophobic mineral surface are the driving forces which control transport, and subsequent adsorption of the colloidal material from the bulk suspension to the hydrophobic surface, as was also described for the sorption process of guar onto talc (Jenkins, Ralston 1998). The dissolved fraction contains also soluble polysaccharides with a hydrophobic backbone, as well as soluble fatty- and resin acids with a hydrophobic carbon chain that would also undergo the same effect. This effect would be manifest as an additional step in region II (Figure 6-20 and Figure 6-21). Although such an effect can be possibly observed in the figures, there are not enough experimental points to make a statistically significant additional fit, whereas the effect for the colloidal fraction is much stronger. In addition, this finding further confirms that

the hydrophobicity of talc and pitch form the relevant pair-wise driving force for the adsorption, as already observed elsewhere (Wallqvist et al. 2007).

The adsorption measurements were interpreted using an operationally defined Langmuir isotherm. An important and fundamental assumption for such an isotherm is that the sorption process is reversible. If this assumption is valid for the adsorption of DCS onto talc, then it is crucial to dose the talc at the right position in the production sequence of the paper mill because desorption may occur if the temperature becomes lower.

### **6.3 Conclusions**

The effect of pH was studied on the adsorption onto talc of dissolved and colloidal substances originating from TMP. It is the first study that deals with the complex system of real pulp mill water without the presence of fibres in the pH range of 4 – 9, and is of particular relevance as papermaking pH continues to trend upwards to neutral and higher.

For the colloidal fraction measured by turbidity, it was possible to apply an operational Langmuir adsorption isotherm. It was seen that with increasing pH, the maximum loading and affinity of colloidal material for talc decreased. Analysis of the total organic material by COD did not show a particular change in the affinity. The impact of increasing soluble species on the adsorption of colloidal material with increasing pH was shown by calculating the total mass of dissolved organics as the difference between the total organic mass and the mass of colloidal organics alone. Thus, it is postulated that the release of dissolved molecular compounds at higher pH, such as fatty or resin acids with a high affinity towards the talc surface, causes a competition with the colloidal fraction and hence reduces the adsorbed amount of colloids on talc.

In today's trend towards neutral or alkaline paper production, there needs to be careful consideration of such effects and the adjustment of the pitch control strategy.

The second section investigated the effect of the temperature on the adsorption of dissolved and colloidal substances from a TMP filtrate onto talc over a temperature range between 20 °C and 80 °C. It was found that talc adsorbs both dissolved and colloidal substances. However, the adsorption of colloids is preferred.

On the one hand, studying the sorption process over the temperature range of the colloidal material only, showed a clear dependency of the process on the temperature. The higher the temperature, the more colloidal material was found to adsorb [Hypothesis **H6(b)**]. The maximum loading of colloids nearly doubled for an increase in temperature of 60 °C. A linear regression of the maximum loading of colloids versus the temperature gave a steepness of 1.4 with a regression coefficient  $R^2$  of 0.96. It was proposed that the main mechanism for this behaviour is the dehydration of the lyophobic colloids, their amphiphilic carbohydrate layers and the hydrophobic talc surface. On the other hand, no significant effect of the temperature was observed on the adsorption of the dissolved fraction of the TMP filtrate onto the mineral, therefore it could only be shown that hypothesis **H6(b)** applies to the colloidal fraction.

The observations reported here also have practical implications. If the assumption of a reversible adsorption is valid then the mineral dosage point has to be chosen carefully in order to minimise desorption.

## **7 The development of hydrophobised ground calcium carbonate and the use of porous high surface area calcium carbonate for the adsorption of dissolved and colloidal substances from thermo mechanical pulp filtrates**

During the course of this thesis it has been shown that process parameters like pH and temperature have a direct impact on the adsorption efficiency of talc. Neutral to alkaline pH especially led to a substantial reduction in the adsorption capacity of talc. Since modern paper production is carried out under these latter conditions, new alternatives to talc are required without losing the beneficial surface properties of talc. To verify this hypothesis, calcium carbonate based particles are developed that have a high affinity for colloidal wood resin. Building on the verification and investigation of hypothesis **H4** and **H5**, we now suggest a further hypothesis:

**H7** On the basis of **H4** and **H5**, tailored mineral particulates can be developed which optimise pitch adsorption while coping with modern trends in paper making.

This work has been published (Gantenbein et al. 2012a; Gantenbein et al. 2012b).

## **7.1 Development of hydrophobised Calcium carbonate particles**

### ***7.1.1 Introduction***

This section aims to develop gcc particles which were treated with stearic acid to hydrophobise for the effective adsorption of mainly colloidal substances from thermo mechanical pulp. The gcc types chosen varied in fineness and the respective amounts of stearic acid used for the surface treatment. The development process was split into four steps. In a first step, hydrophobised gcc products with varying surface area and varying degree of hydrophobicity were screened and compared versus relatively low specific surface area talc. In a second step, the degree of hydrophobicity was optimised. In a third step, adsorption isotherms were recorded for an untreated and optimally hydrophobised gcc and compared with a high surface area talc. Finally, it was investigated if untreated and treated gcc adsorb different components from the TMP filtrate.

The surface properties of gcc have been discussed in section 2.4.2, as well as the treatment with stearic acid. The surface coverage of the calcite was estimated via Equation 2-2.

### ***7.1.2 Materials and Methods***

#### ***7.1.2.1 Materials***

Two Finnish talc grades were used as references. One is commercially available talc, Finntalc P05 from Mondo Minerals and the other talc grade was derived from Finntalc P05 with subsequent comminution and delamination to generate fineness, high aspect ratio and enhanced specific surface area. The Finntalc P05 will be labelled as LSA (low

surface area) talc and the delaminated quality will be labelled as high surface area (HSA-talc) talc. The surface area and particle size are reported in Table 7-1.

Various ground calcium carbonate grades were tested. One is commercially available as Omyacarb 10 (OMC-10), another as Omyacarb 1 (OMC-1) and a third grade was produced from OMC-1 by chemical free grinding to obtain a high surface area gcc (HSA gcc). The ground calcium carbonate samples were supplied by Omya and originating from Avenza, Italy.

**Table 7-1: Specific surface area, particle size ( $d_{50}$ ) and electrophoretic mobility in a 0.01 M NaCl solution of the investigated minerals.<sup>a)</sup> not analysed due to settling problems. <sup>b)</sup> not analysed.**

Name	Abbrev.	Type	Specific surface area / $\text{m}^2\text{g}^{-1}$	$d_{50}$ / $\mu\text{m}$ (Sedigraph 5120)	Electrophoretic mobility / $\times 10^{-8} \text{m}^2\text{V}^{-1}\text{s}^{-1}$
Finntalc P05	LSA-talc	Talc	8.7	2.4	-3.4
Delaminated Finntalc P05	HSA-talc	Talc	45.0	0.8	-3.9
Omyacarb 10	gcc-10	Calcium carbonate	1.3	n.a. <sup>a</sup>	n.a. <sup>a</sup>
Omyacarb 1	gcc-1	Calcium carbonate	3.9	1.5	0.8
Comminuted Omyacarb 1	HSA-gcc	Calcium carbonate	10.2	0.6	n.a. <sup>b</sup>

#### **7.1.2.1.1 Stearic acid treatment and semi-quantitative wetting test**

The stearic acid was a high purity grade from Sigma Aldrich. The gcc powder was filled into the high speed mixer (Type MTI M3/1.5) which was heated to 80 °C. The powder was stirred for a period of 2.5 min at 3 000  $\text{min}^{-1}$  (rpm). The stearic acid was added to the pre-heated powder. The amount of stearic acid was calculated according to Equation 2-2 to derive a product with a defined coverage factor. The blend was again mixed for 2.5 min at 3 000  $\text{min}^{-1}$ . The mixer was opened, the powder manually mixed to ensure



even distribution in the mixer and closed again for another 2.5 minutes mixing time at  $3000 \text{ min}^{-1}$ . During the whole procedure the temperature of the mixer was kept at  $80 \text{ }^{\circ}\text{C}$ .

Mixtures of water and ethanol were prepared in volume ratios of 100:0, 90:10, 80:20, 70:30, 60:40, 50:50, 40:60, 30:70, 20:80, 10:90 and 0:100.  $50 \text{ cm}^3$  of each of these mixtures were placed in a  $100 \text{ cm}^3$  beaker. About 0.5 – 1.0 g of the powder in question was carefully put on top of the liquid. The wetting behaviour was quantified by the time needed for the powder to be wetted according to the following judgement:

- 0 → immediate wetting of the powder (sinks within 30 seconds)
- 0.25 → within 5 minutes all of the powder is wetted
- 0.5 → after 5 minutes more than 50 % of the powder is wetted
- 0.75 → after 5 minutes less than 25 % of the powder is wetted
- 1 → the powder is not wetted within 5 minute

### **7.1.2.2 Methods**

The TMP was left overnight to cool down to room temperature, then filtered through a filter of  $2 \text{ }\mu\text{m}$  pore size (filter paper, circular 602 EH). The filtrate was checked under a light microscope (Olympus AX-70) for the absence of fibres and fibrils. The adsorption experiments were performed immediately after filtration. The pH of the filtrates was usually between 6.0 and 7.0. It was adjusted with 0.1 M sodium hydroxide to 7.0 – 7.5.

A pH titration of the electrophoretic mobility was made in order to quantify the colloidal stability of the wood resin droplets. This was done on a Malvern Zetasizer NS using 0.1 M hydrochloric acid and 0.1 M sodium hydroxide solutions. In addition the total electrochemical charge was determined by titrating the TMP filtrate with 0.0025 M poly-DADMAC [poly-(allyldimethyl-ammonium chloride)] using a streaming current

detector (SCD) (Mütek PCD-03). The ion content was quantified by ion chromatography on a Dionex DX 120 Ion-chromatograph.

After adjustment of the pH, the TMP filtrate was distributed into glass bottles each containing 200 cm<sup>3</sup> of the TMP filtrate. The desired amount and type of mineral was added either as a powder or dispersed in water. In most cases the mineral dosage was 10 gdm<sup>-3</sup> and in the case of the isotherms the mineral dosage was varied between 2.5 and 50.0 gdm<sup>-3</sup>. For all samples in an adsorption isotherm series the same total amount of water was added (usually 18 cm<sup>3</sup>). The bottles were equipped with a magnetic stirring bar, closed with an air-tight lid and stirred on a magnetic stirrer for 2 hours. After this time the magnetic stirring bar was removed and the experimental mixtures centrifuged (Jouan C 312 by IG Instruments) for 15 minutes at 2 600 |g|. Two phases were collected; an upper liquid phase and a lower sediment mineral-containing phase. Centrifugation of the untreated TMP filtrate did not show any sediment, and centrifugation of the pure mineral suspensions showed no remaining mineral particles in the supernatant. However, some mineral suspensions showed in some cases air bubbles with entrapped mineral particles. Thus, the turbidity results might be partially affected by the remaining air bubbles, but not directly by remaining suspended mineral particles. The upper liquid phase was analysed for turbidity by means of a NOVASINA 155 model NTM-S turbidity probe. The particle size was measured by photon correlation spectroscopy on a Malvern Zetasizer NS without any further treatment or dilution. Chemical oxygen demand (COD) was measured using a Lange CSB LCK 014, covering a range 1 000 – 10 000 mgdm<sup>-3</sup> with a LASA 1 / Plus cuvette. 100 cm<sup>3</sup> of the liquid phase was dried in an aluminium dish at 90 °C for 12 hours and the residue weighed to provide a result for the gravimetric residue.

In one trial, the upper liquid phase was also analysed for the wood extractives content and the carbohydrate content. The wood extractives content was determined by extraction of the TMP filtrate with petroleum ether (Saltsman, Kuiken 1959). The GC-FID analysis for the group determination in the wood extractives was performed according to the method of Örsa and Holmbom (1994). The samples were hydrolysed with sulphuric acid at 121 °C in an autoclave according to SCAN-CM 71:09. The solubilised monosaccharides were quantified using an ion chromatograph coupled to a pulsed amperometric detector (IC-PAD). The acid insoluble residue was determined gravimetrically and the acid soluble residue (lignin) was measured with UV spectrophotometry at 205 nm and quantified using an absorption coefficient of 110  $\text{dm}^3\text{g}^{-1}\text{cm}^{-1}$ .

The lower sedimented mineral-containing phase was analysed by thermo gravimetric analysis (TGA) on the Mettler Toledo TGA/STDA 851e. The samples were heated from 20 to 1 000 °C with a heating rate of  $20^\circ\text{Cmin}^{-1}$ . The weight loss was recorded between 200 and 1 000 °C.

### **7.1.3 Results**

In order to screen and optimise the surface treatment, various TMP samples were collected. Table 7-2 summarises the analysed parameters of the tested TMP filtrates. In addition, Figure 7-1 shows the electrophoretic mobility  $u$  of the four TMP filtrates against pH. Despite the difference in the absolute value of  $u$ , it remained stable in the relevant pH range of 7 to 8. Furthermore, below pH 6  $u$  decreases to approach 0 around pH 2 to 3.

**Table 7-2: Properties of the TMP samples 1 to 4. The presented range is based on the standard deviation of three independent experiments. n.a. → not analysed.**

	TMP filtrate 1	TMP filtrate 2	TMP filtrate 3	TMP filtrate 4
Turbidity / NTU	349 ± 1	358 ± 1	393 ± 8	497
Chemical Oxygen demand / mgdm <sup>-3</sup>	3644 ± 21	3944 ± 27	3140 ± 49	4350 ± 40
Gravimetry / gdm <sup>-3</sup>	3.11 ± 0.0005	3.43 ± 0.005	2.84 ± 0.014	3.57
Electrochemical charge (SCD) / $\mu\text{Eqg}^{-1}$	- 2.3	- 1.3	- 1.1	- 0.3
pH	7.0	7.0	7.0	7.2
Conductivity / $\mu\text{Scm}^{-1}$	926	1500	1140	1200
Na <sup>+</sup> / mM	9.5	12.9	9.1	9.2
K <sup>+</sup> / mM	1.1	1.1	1.0	1.2
Ca <sup>2+</sup> / mM	1.4	0.9	0.8	1.4
Mg <sup>2+</sup> / mM	0.2	0.2	0.2	0.3
Cl <sup>-</sup> / mM	n.a.	0.7	0.5	0.7
SO <sub>4</sub> <sup>2-</sup> / mM	n.a.	0.4	0.4	0.4

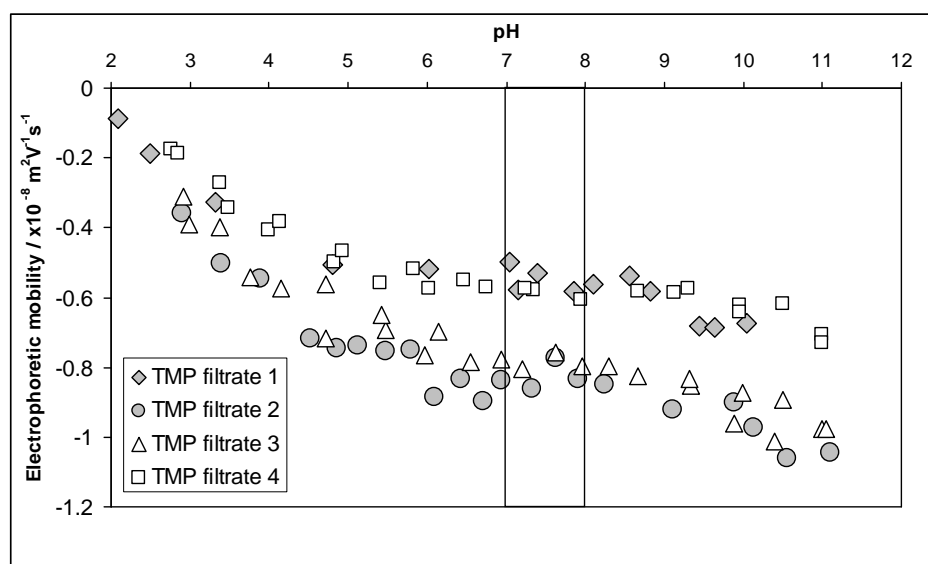


**Figure 7-1: Mean electrophoretic mobility ( $u$ ) of the particles in the TMP filtrates 1-4 against pH. The pH was adjusted with 0.1 M sodium hydroxide and 0.1 M hydrochloric acid.**

### ***7.1.3.1 Screening – 0, 30 and 60 % surface treatment***

The first part of this subsection aims to determine the influence of the degree of stearic acid treatment and the surface area. In order to do so the gcc-10, gcc-1 and the HSA-gcc were treated with 30 % and 60 % stearic acid (based on surface area). For comparison, the untreated gcc and the LSA-talc were also tested.

It was the idea to test also gcc products with 60 % of the surface covered with stearic acid. However, during the experiment it became apparent that these products could not be wetted by the TMP filtrate, leading to foam and undefined phases after centrifugation. Thus, no results were obtained for these products. Even with the 30 % surface treated samples, wetting was a problem. Interestingly, the wetting improved during the experiments, suggesting progressive adsorption of surface active compounds from the TMP filtrate.

The turbidity of the TMP filtrate was clearly reduced as a result of mineral addition (Figure 7-2). An increased specific surface area ( $\epsilon_{\text{BET}}$ ) further improved the removal efficiency for colloidal material. In the case of the 30 % surface covered gcc the turbidity was reduced down to 77 % from the original 349 NTU with the gcc-10, down to 41 % with the gcc-1 and down to 21 % with the HSA-gcc.

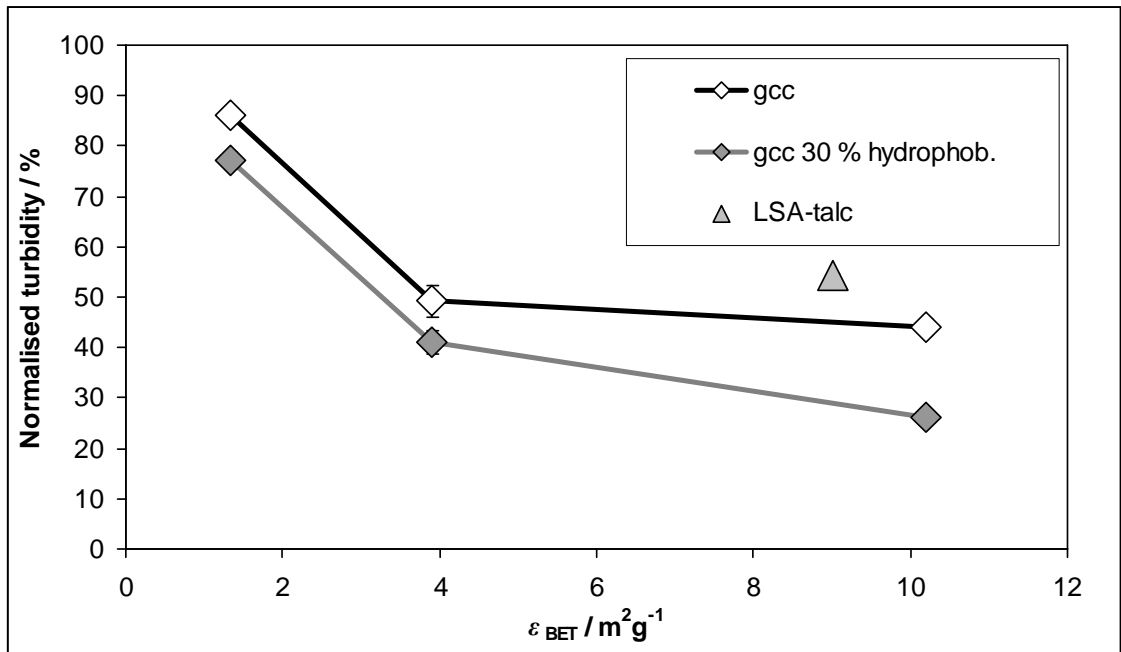


Figure 7-2: Normalised turbidity after the mineral treatment of the TMP filtrate. 100 % corresponds to 349 NTU.

The relation of adsorption efficiency to the surface area was observed earlier for minerals like talc (Chang 1985; Guera et al. 2005), and also shown in the work reported in chapter 5. The treatment with stearic acid increased the efficiency of colloidal pitch adsorption. Both the surface treated and the surface untreated gcc products reduced the turbidity even more efficiently than the LSA-talc, which gave only a reduction of 50 %. The observed efficiency could, however, have also been caused by an agglomeration process of wood resin droplets. The particle size prior and post adsorption in the liquid phase slightly decreased (Table 7-3), which permits one to ascertain on the one hand that the mineral treatment did not induce wood resin self-agglomeration by any mechanism and on the other hand suggests that a preferred adsorption of a larger fraction of the resinous colloids occurred.

**Table 7-3: Number based particle size (photon correlation spectroscopy) of the colloidal fraction in the TMP filtrate prior to and post treatment with the minerals.**

TMP treated with	Particle size / nm	
	$d_{N50}$	$d_{N98}$
-	157	436
gcc-10	160	399
gcc-1	130	382
HSA-gcc	148	365
gcc-10 treated 30%	167	409
gcc-1 treated 30%	144	387
HSA-gcc treated 30%	118	339
LSA-talc	167	449

The size analysis in the liquid phase did not include agglomerates that settled during centrifugation, so it was also important to consider other analyses. The COD analysis (Figure 7-3) showed a slightly different trend. On one hand the values for the gcc-10 and the treated and untreated HSA-gcc did not show significantly different values. The only difference was observed for the gcc-1 for which, oppositely to turbidity, the untreated gcc was seen to be more efficient.

The analysis of the mineral phase after the adsorption experiment (Figure 7-4) confirmed the results of the turbidity analysis. The adsorbed amount on the mineral surface increased with the specific surface area. Partially hydrophobised gcc adsorbed slightly more material than native gcc. Both hydrophobised and native gcc adsorbed more material than talc.

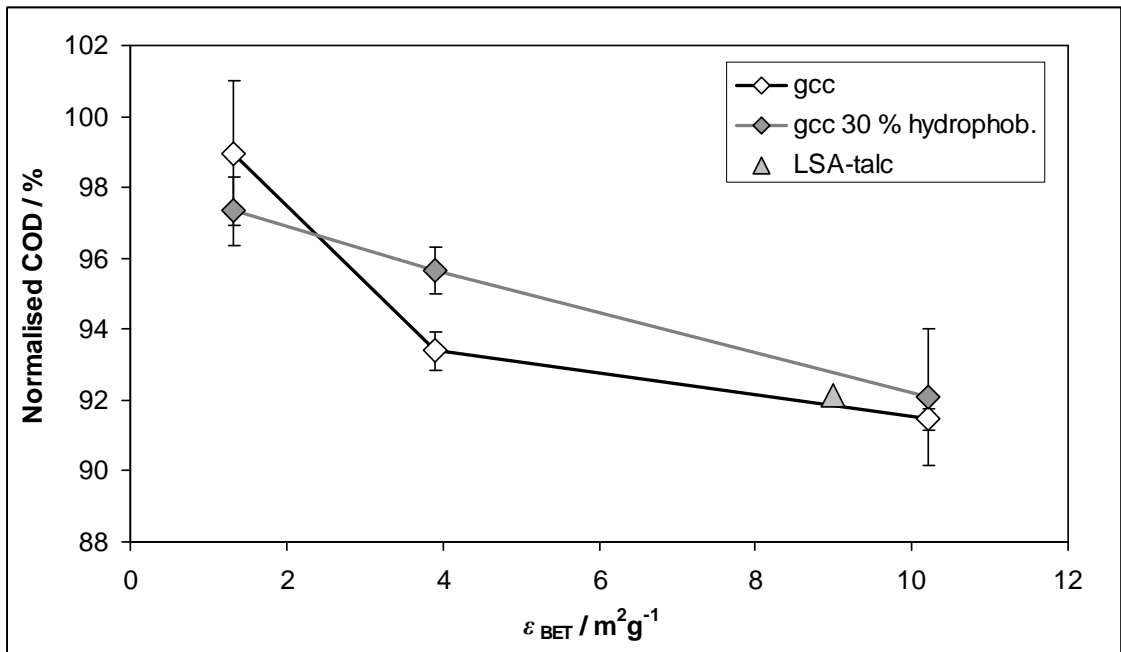


Figure 7-3: Normalised COD after the mineral treatment of the TMP filtrate. 100 % corresponds to 3 644 mg  $\text{O}_2 \text{dm}^{-3}$ .

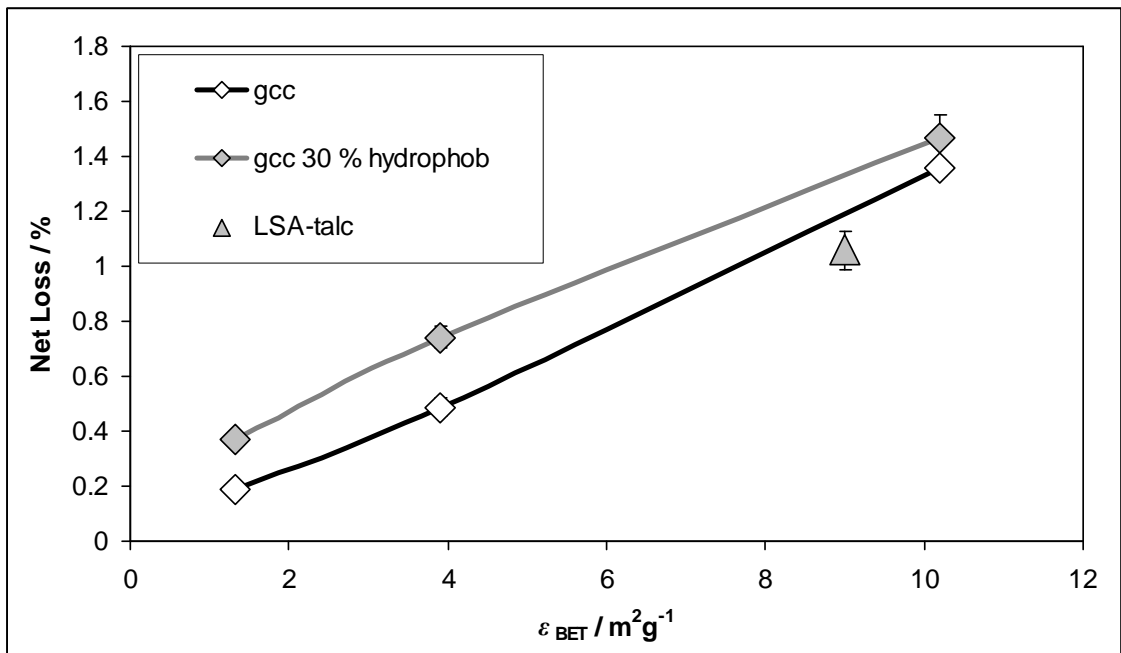


Figure 7-4: Thermo gravimetric analysis of the mineral after the adsorption. The weight fraction lost was recorded between 200 and 1 000 °C and is corrected with the weight loss of the corresponding mineral powder).

The concentration of calcium ions in the supernatant is crucial in paper mill circuits, since they are one of the main contributors to pitch agglomeration. The treatment with gcc increased the pH from 7.0 to 7.8, the conductivity from 926  $\mu\text{Scm}^{-1}$  to 980  $\mu\text{Scm}^{-1}$ ,



and the calcium ion concentration from 1.45 mM to 1.90 mM. The addition of talc had no effect on the calcium ion concentration.

### ***7.1.3.2 Optimisation – defining the degree of surface coverage with stearic acid***

In the previous section it was shown that moderate treatment of up to 30 % of the gcc surface with stearic acid is beneficial for pitch adsorption, but that treating 60 % of the surface caused foaming and phase separation. Therefore, an attempt was made to optimise the amount of stearic acid treatment between 0 and 30 % surface coverage  $X_{SA}$ . The gcc-1 treated and untreated was used for this optimisation, together with TMP filtrate 2. The mean EM of the particles in the original TMP filtrate was  $-0.8 \times 10^{-8} \text{ m}^2 \text{ V}^{-1} \text{ s}^{-1}$  and no significant change was observed within the relevant pH range (7-8). As shown in Figure 7-5, COD and gravimetry showed little difference with surface coverage. Turbidity, however, showed that there was an optimum with respect to turbidity at 15% surface coverage. The rise in turbidity above this level of surface coverage can be attributed to the development of a foamy undefined phase, most clearly seen in the extreme case of 60 % surface coverage described above. Thermo gravimetry (Figure 7-6) showed the optimum surface coverage to be in the range 15 to 25 %. Finally, the semi-quantitative hydrophobicity test (Figure 7-7) showed that the sample with 15 % surface coverage had a comparable hydrophobicity to talc. Therefore, it was decided to use the gcc-1 product with 15 % surface coverage for the investigations.

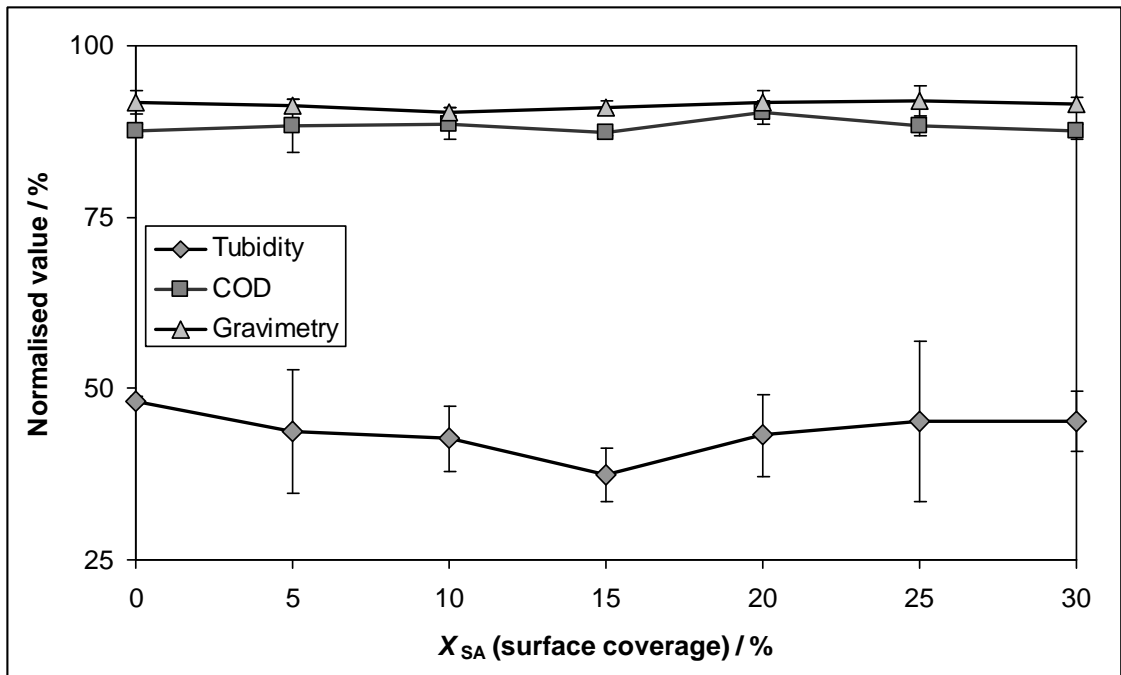


Figure 7-5: Normalised COD, gravimetry and turbidity of the TMP filtrate after the adsorption experiment with the mineral powders against the surface coverage of the mineral powders with stearic acid. The results are normalised with the values obtained for the untreated TMP filtrate.

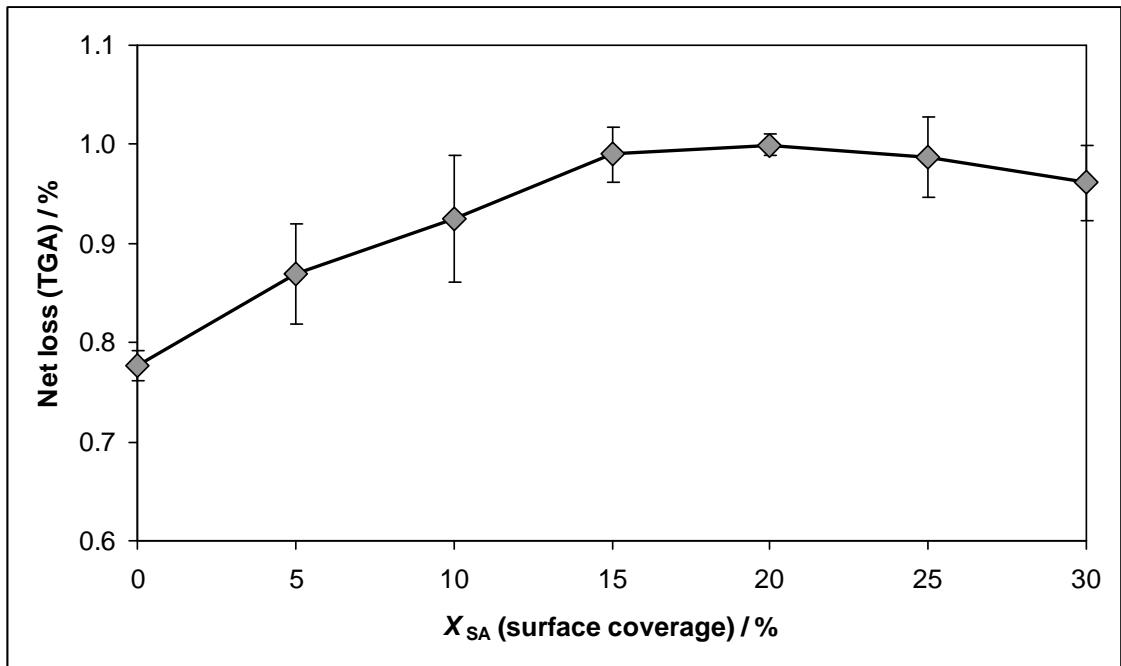


Figure 7-6: Thermo gravimetric analysis of the mineral phase after the adsorption experiments against the surface coverage of the mineral powders with stearic acid. The weight loss of the starting mineral powders (prior the addition to the TMP filtrate) is subtracted (net loss).

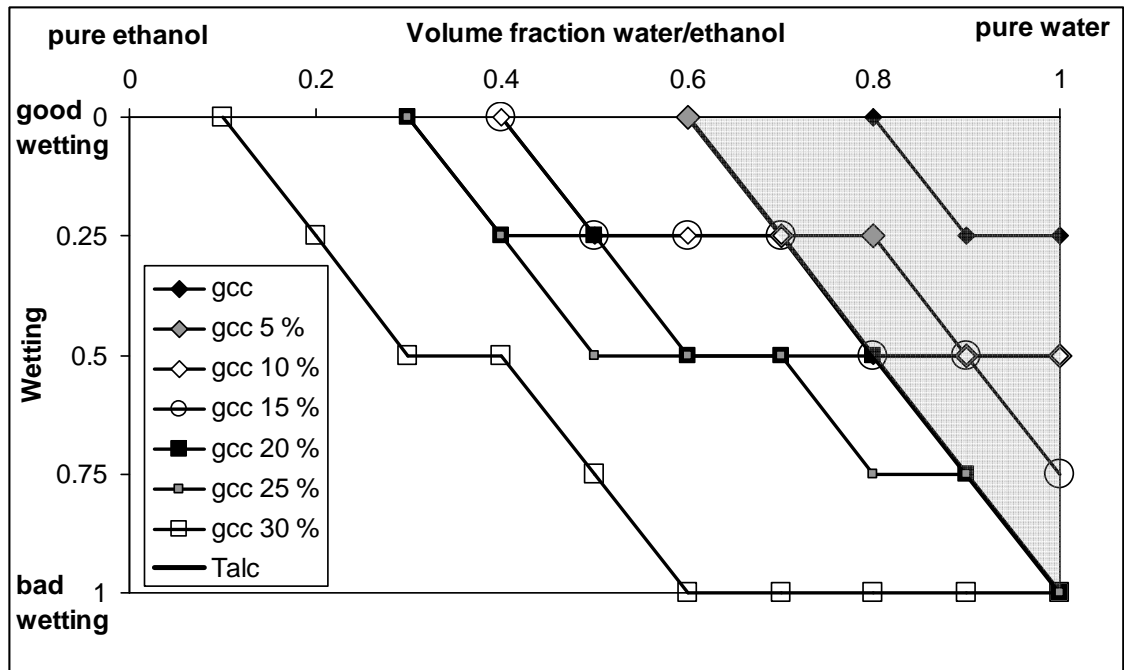


Figure 7-7: Apparent hydrophobicity of the tested mineral powders with their range of stearic acid coverage  $X_{SA}$  including also the HSA-talc sample. The larger the area on the right side of each line the greater the hydrophobicity. The grey area reflects the situation for talc.

### 7.1.3.3 Application – quantify the benefit of surface treatment and chemical analysis

In order to quantify the effect of the stearic acid treatment adsorption isotherms were recorded for an untreated gcc-1 and a gcc-1 with 15 % surface coverage by stearic acid. As a comparison the high surface area talc (HSA-talc) was also included. The isotherm was recorded at 24 °C. TMP filtrate sample 3 was used for this experiment. The mean EM of these filtrate particles was  $-0.8 \times 10^{-8} \text{ m}^2\text{V}^{-1}\text{s}^{-1}$ , and was insensitive to pH in the range 7-8.

The adsorption isotherm is present as the equilibrium concentration defined by turbidity  $c_{eq}^{\tau}$  and the calculated loading  $\Gamma_{eq}^{\tau}$ , which was calculated by Equation 6-1. The isotherm was interpreted by a Langmuir isotherm (Equation 2-17).

**Table 7-4: Adsorption isotherm parameters based on a non-linear least squares (NLLS) fit to the Langmuir equation (Equation 2-17) performed by TableCurve® 2D.**

Mineral	Parameter		95 % Confidence limits		P> t	R <sup>2</sup>
Untreated	$K_L^\tau / \text{NTU}^{-1}$	0.025	0.019	0.032	<0.01	0.98
	$\Gamma_{\max}^\tau / \text{NTUg}^{-1}$	24.9	23.0	26.0	<0.01	
Treated	$K_L^\tau / \text{NTU}^{-1}$	0.013	0.009	0.018	<0.01	0.98
	$\Gamma_{\max}^\tau / \text{NTUg}^{-1}$	37.1	32.9	41.4	<0.01	
HSA-talc	$K_L^\tau / \text{NTU}^{-1}$	0.007	0.003	0.011	<0.01	0.98
	$\Gamma_{\max}^\tau / \text{NTUg}^{-1}$	212.4	127.0	252.2	<0.01	

The Langmuir constant  $K_L^\tau$  (Table 7-4) indicated that the untreated gcc powder has a higher affinity ( $0.025 \text{ NTU}^{-1}$ ) for the colloidal material than the partially hydrophobised ( $0.013 \text{ NTU}^{-1}$ ). The HSA-talc grade had the lowest affinity ( $0.007 \text{ NTU}^{-1}$ ) with the lowest  $K_L^\tau$ . The maximum loading  $\Gamma_{\max}^\tau$  increases from the untreated gcc-1 ( $25 \text{ NTUg}^{-1}$ ) to the treated gcc-1 ( $37 \text{ NTUg}^{-1}$ ) (Figure 7-8 and Table 7-4). As a result of the high  $\epsilon_{\text{BET}}$  of the HSA-talc ( $45 \text{ m}^2\text{g}^{-1}$ ) the maximum loading of colloidal particles on the talc ( $212 \text{ NTUg}^{-1}$ ) was higher, in relation to the  $\epsilon_{\text{BET}}$  of the gcc-1 of only  $4 \text{ m}^2\text{g}^{-1}$ . The parameters are all significant.

Figure 7-8 shows the adsorption isotherms with the loading calculated for the added mass of mineral, whereas Figure 7-9 shows the adsorption isotherm based on the added specific surface area added for each mineral, which shows the higher efficiency of the gcc products in comparison to talc.

Another TMP sample was collected in which the particles had a mean electrophoretic mobility at the original pH of 7.2 of  $-0.6 \times 10^{-8} \text{ m}^2\text{V}^{-1}\text{s}^{-1}$ . The EM was stable in the relevant pH range of 7 – 8.

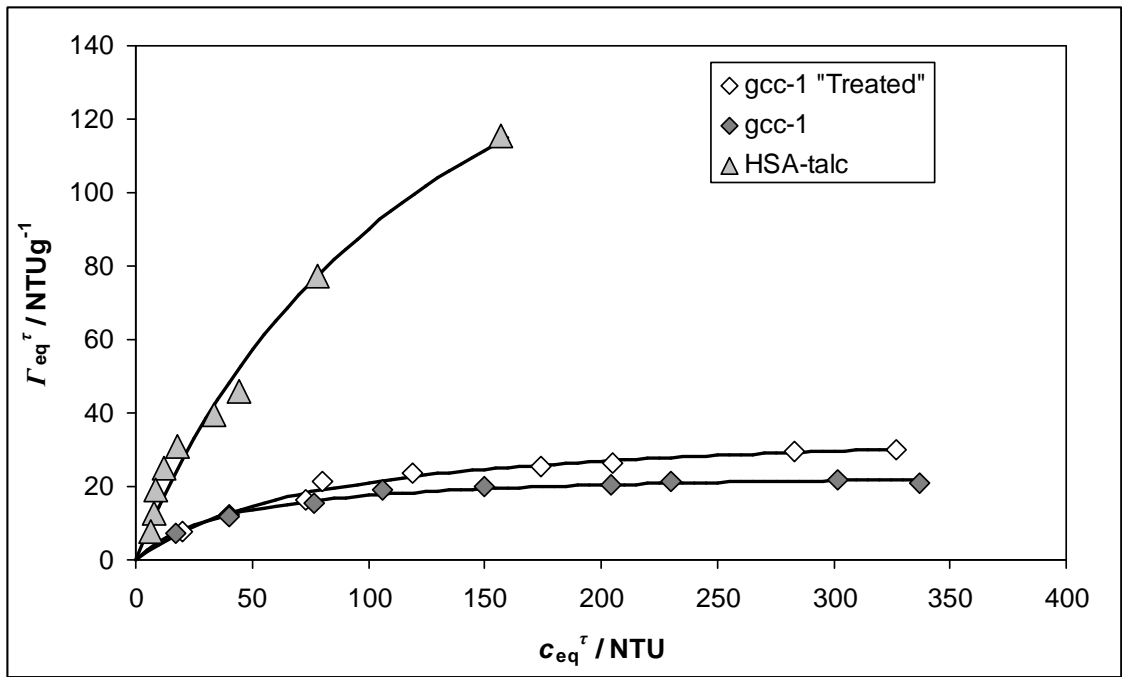


Figure 7-8: Adsorption isotherm based on turbidity data for the untreated gcc-1, the treated (15 % surface coverage) gcc and the HSA-talc.

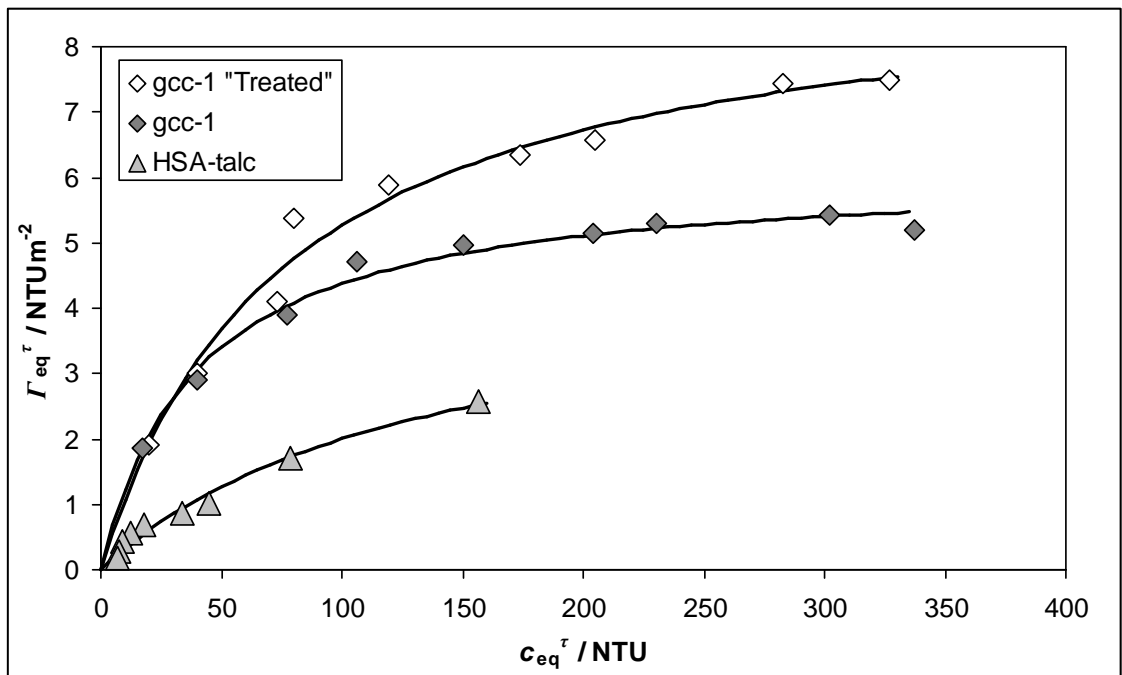


Figure 7-9: Adsorption isotherm based on turbidity data for the untreated gcc-1, the treated (15 % surface coverage) gcc and the HSA-talc. The loading  $\Gamma_{eq}^{\tau}$  is normalised with the specific surface area of the minerals.

In order to cover the relevant regions of the adsorption isotherms different amounts of mineral were added to the TMP filtrate. In the case of the HSA-talc a talc dosage of  $0.4 \text{ gdm}^{-3}$  was used to represent the region where the dissolved and colloidal substances are in excess and a talc dosage of  $4 \text{ gdm}^{-3}$  to represent the region where the talc surface is

available in excess. Because the specific surface area of the gcc powders is much lower than talc, the carbonate addition was increased to 8 and 40 gdm<sup>-3</sup>, respectively.

The petroleum ether extractives content of the TMP filtrate was 142 mgdm<sup>-3</sup> (Table 7-5). This is around 4 % of the total material in the TMP filtrate. The main constituents of the extractives were triglycerides (44 %, triacylglycerides) followed by resin acids (23 %) and sterylesters (18 %). Free fatty acids (6 %), lignans (2 %) and sterols (2 %) formed a minor fraction. The remaining 5 % is of unknown origin.

**Table 7-5: Extractives (petroleum ether) group content, carbohydrate content, acid soluble (lignin) content and acid insoluble content of the TMP filtrate.**

<b>Type</b>	<b>Amount / mgdm<sup>-3</sup></b>
<u>Extractives</u>	
Fatty Acids	9
Resin Acids	32
Lignans	4
Sterols	3
Sterylesters	26
Triglycerides	63
Unknown	<u>5</u>
<b>Total:</b>	<b><u>142</u></b>
Carbohydrates	1052
Acid soluble (Lignin)	527
Acid insoluble	<u>403</u>
<b>Total:</b>	<b><u>1982</u></b>

The addition of 0.4 gdm<sup>-3</sup> HSA-talc reduced the extractives content to 120 mg dm<sup>-3</sup> and the addition of 4 gdm<sup>-3</sup> resulted in a final extractives content of 32 mgdm<sup>-3</sup>. The ratio of the extractives groups was in both cases was not affected (Figure 7-11). The dosage of 8

gdm<sup>-3</sup> gcc-1 reduced the extractives content to 107 mgdm<sup>-3</sup>, and 40 gdm<sup>-3</sup> of gcc-1 to 28 mgdm<sup>-3</sup>, respectively. The ratio of the extractives groups was not affected for the low mineral dosage but was strongly affected for the high mineral dosage. Resin acids were found with an increased ratio and triglycerides were found with a decreased ratio. A similar picture was observed for the hydrophobised gcc-1 (gcc-1 “Treated”). The lower mineral dosage led to a residual amount of extractives of 73 mgdm<sup>-3</sup> and the higher mineral dosage to 23 mgdm<sup>-3</sup>, respectively.

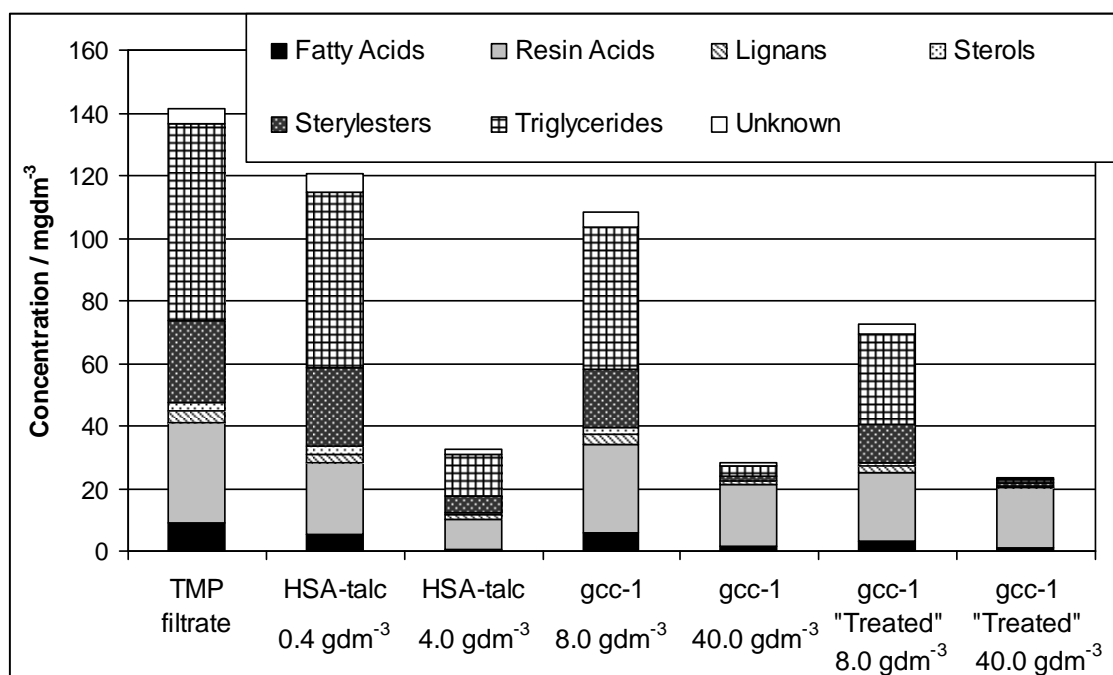


Figure 7-10: Petroleum ether extractives content of the TMP filtrate 4 prior and post adsorption. The extractives are split into the groups; fatty acids, resin acids, lignans, sterols, sterylesters, triglycerides and an unknown fraction.

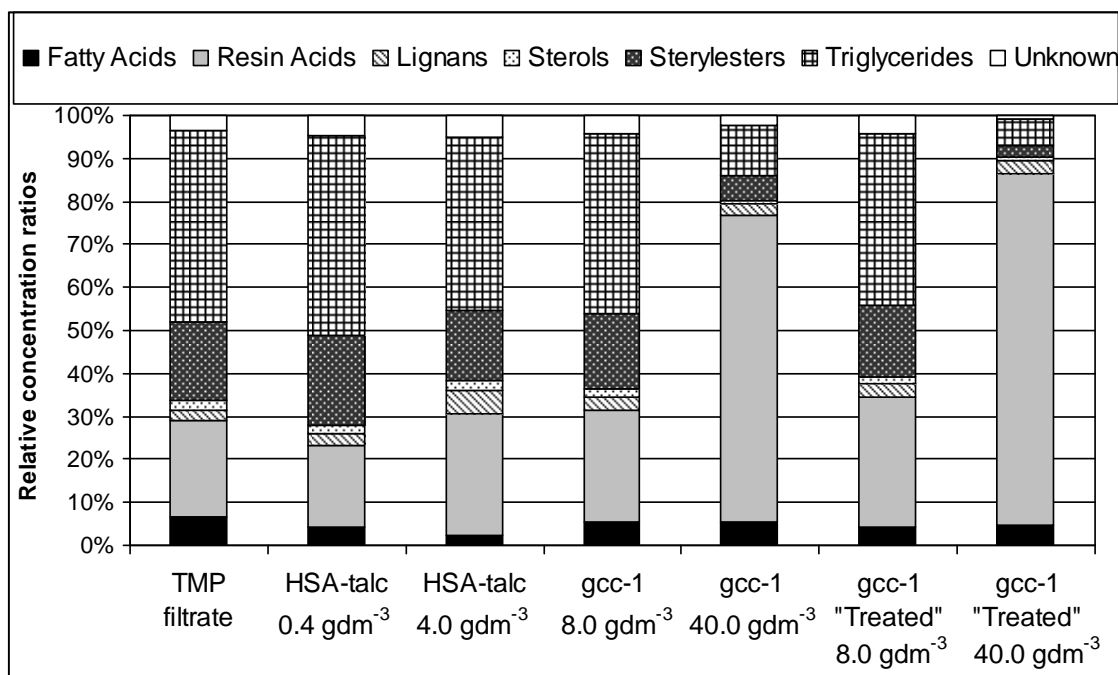


Figure 7-11: Relative composition of the extractives groups in the TMP filtrate prior and post adsorption.

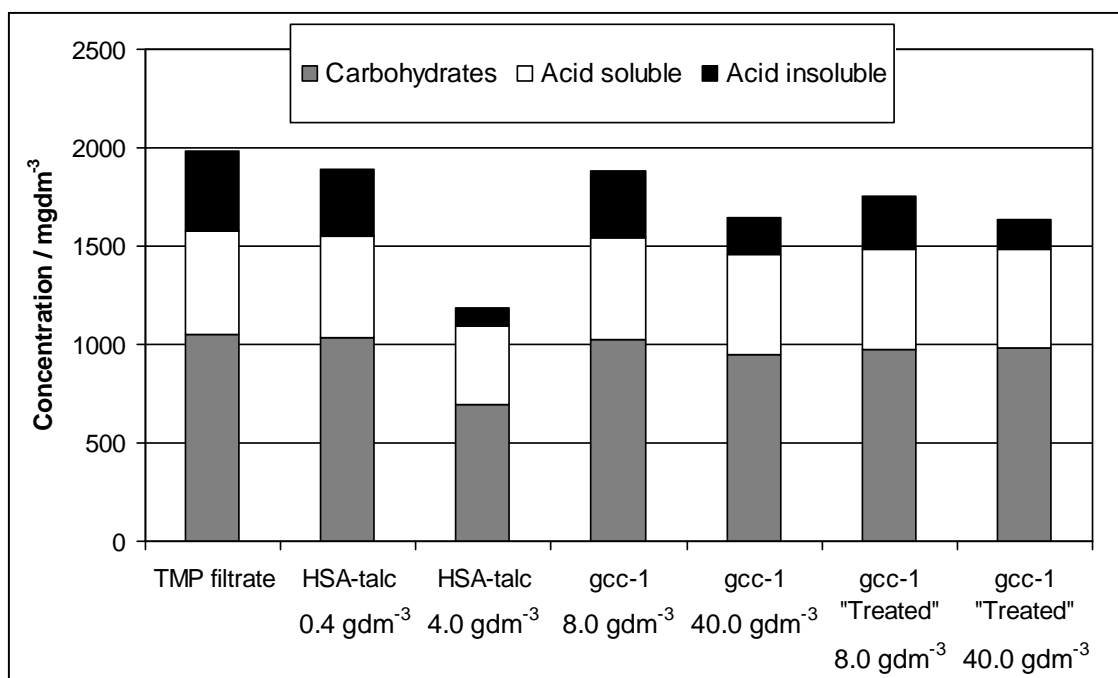


Figure 7-12: Carbohydrate, acid soluble and acid insoluble content in the TMP filtrates prior and post adsorption.

In addition also the water-soluble part of the TMP filtrate was analysed. This analysis is split into three fractions; i) carbohydrates, ii) acid soluble (lignins) and iii) acid insoluble (wood resin, etc.). The original TMP filtrate 4 contains 1 052 mgdm<sup>-3</sup> carbohydrates, 527 mgdm<sup>-3</sup> acid soluble (lignin) and 403 mgdm<sup>-3</sup> acid insoluble



materials (Table 7-5 and Figure 7-12). The carbohydrates content after the talc treatment was reduced only slightly ( $1\ 034\ \text{mgdm}^{-3}$ ) for the low talc dosage but a large reduction in the carbohydrates content was observed for the high talc dosage ( $696\ \text{mgdm}^{-3}$ ). Analysis of the carbohydrate monomers showed the main reduction for glucose and mannose monomers. The untreated gcc-1 adsorbed only a very minor fraction of the carbohydrates (not shown).  $1\ 024\ \text{mgdm}^{-3}$  for the low dosage and  $952\ \text{mgdm}^{-3}$  for the high gcc-1 dosage, respectively. Also the hydrophobised gcc-1 adsorbed a very minor amount. For both mineral dosages the carbohydrate content was approximately  $980\ \text{mgdm}^{-3}$ . In the case of the acid soluble (lignin) fraction the reduction after the mineral treatment was  $< 3\ \%$ , except for the HSA-talc with  $4\ \text{gdm}^{-3}$ . In this case the remaining lignin content was  $396\ \text{mgdm}^{-3}$ . The acid insoluble fraction, finally, varied proportionally to the extractives reduction. The pH of the samples increased as a result of the alkaline nature of the mineral powders. The pH for the lower mineral dosages was between 7.3 and 7.6 and for the higher dosages between 7.7 and 7.8.

#### **7.1.4 Discussion**

In chapter 6 the turbidity data were transformed into mass based data for comparison in the adsorption isotherms. Differentiating the curves then gives the preferred adsorption of either dissolved or colloidal substances from the TMP. For the calibration a plot of either COD or gravimetry versus turbidity was made (Figure 6-8, Figure 6-17 and Figure 7-13). For the HSA-talc we can observe the previously seen trend, namely that below a certain concentration of colloids (e.g.  $< 50\ \text{NTU}$ ) the talc further reduced the content of total COD. Depending on the pH and temperature, this preference can be stronger or weaker. However, in the case of the tested gcc powders this was not observed, but rather a linear dependency was manifest throughout the recorded turbidity range. This implies that only colloidal substances were adsorbed or if also soluble substances were adsorbed then only in a proportional amount to the colloidal

substances. This difference in preferred adsorption should also be manifest in the composition after the adsorption experiment.

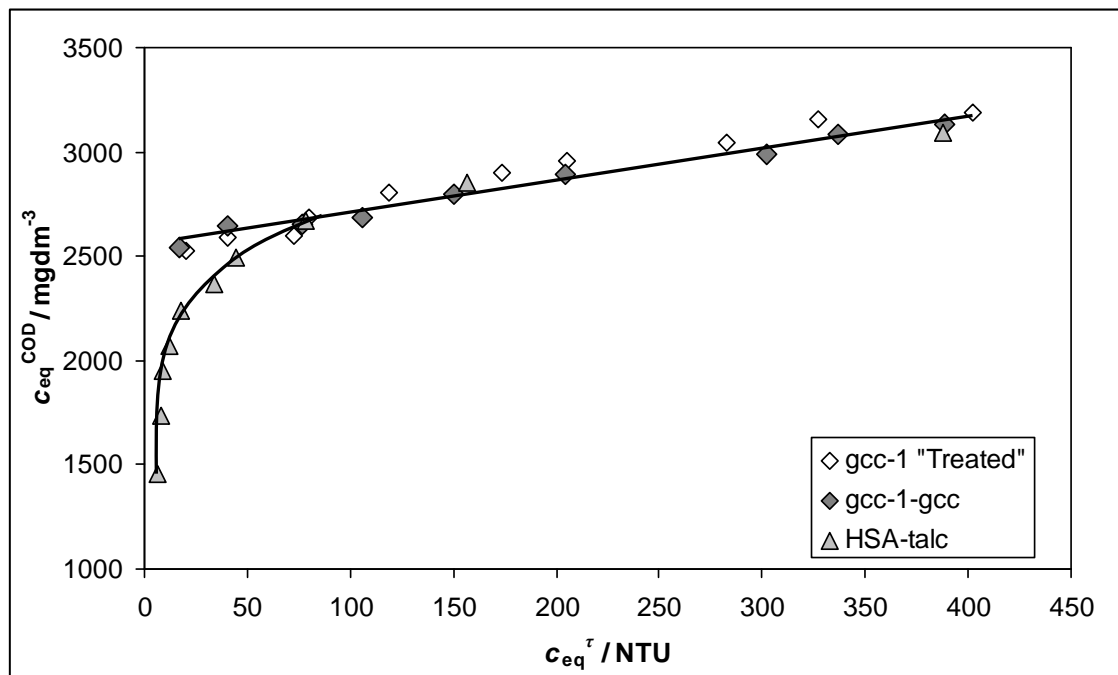


Figure 7-13: Equilibrium COD against equilibrium turbidity.

The carry-through of the difference in preferred adsorption in the data after the experiment is exactly what can be observed (Figure 7-10 and Figure 7-12). On the one hand, in the upper region of high turbidity the adsorption of dissolved materials like carbohydrates and lignins is minor, whereas a substantial amount of carbohydrates and lignins adsorb onto talc in the lower turbidity region. This supports the proposed mechanisms of preferred adsorption at different pH proposed in section 6.1.3. On the other hand only a minor amount of dissolved matter adsorbs onto the gcc powders, independent of the concentration of the colloidal fraction. The ratios of the amount of extractives and the amount of carbohydrates plus acid soluble lignin were calculated (Table 7-6) similarly as in Equation 6-1.

It can be seen in Table 7-6 that the ratio of dissolved to colloidal substances adsorbed onto the mineral remains stable at around 1 to 1.4. However, in the case of high talc dosage (excess of talc surface) the ratio (4.4) is clearly shifted towards the dissolved

fraction which is adsorbed onto the talc surface. A possible explanation could be that the pitch droplets adsorb together with their stabilising carbohydrate layer (low mineral dosage), thus, resulting in a constant ratio (Table 7-6).

**Table 7-6: Ratio between dissolved and colloidal material adsorbed from the TMP filtrate.**

	<b>Dissolved / Colloidal ratio</b>
HSA-talc 0.4 gdm <sup>-3</sup>	1.3
HSA-talc 4.0 gdm <sup>-3</sup>	4.4
gcc-1 8.0 gdm <sup>-3</sup>	1.0
gcc-1 40.0 gdm <sup>-3</sup>	1.1
gcc-1 "Treated" 8.0 gdm <sup>-3</sup>	1.4
gcc-1 "Treated" 40.0 gdm <sup>-3</sup>	0.8

After removal of most of the colloidal fraction at high mineral dosage, the talc also adsorbs dissolved materials such as carbohydrates, lignins and dissolved wood resin constituents (resin acids etc), whereas the gcc does not adsorb material from the dissolved fraction (Figure 7-14). The high affinity of talc for soluble polysaccharides is not surprising and was investigated earlier with guar (Jenkins, Ralston 1998). The major controlling force for the adsorption was attributed to the hydrophobic interactions of the backbone methylene groups of the mannose units with the hydrophobic siloxane surface of the magnesium silicate. The analysis in the current study of the saccharide monomer content after the talc treatment has shown the removal of mainly glucose and mannose monomers. Also the adsorption isotherms for the colloidal substances in the form of the Langmuir constant  $K_L^\tau$  showed these different adsorption preferences (Table 7-4). Talc showed the lowest affinity for the colloidal fraction and the untreated gcc the highest affinity. Interestingly the hydrophobised gcc was in between the two. The trends in the affinity might be explained by the type of interaction. While talc is understood to act

through hydrophobic interactions, charge interactions between the anionic pitch droplets and the gcc particles can be expected. The surface treated gcc, however, is an intermediate of the two and shows therefore both interactions with pitch particles. The difference in the maximum loading ( $\Gamma_{\max}^{\tau}$ ) between the two gcc products could be due to the lower affinity found for the treated gcc, given by  $K_L^{\tau}$ , and may result in a higher mobility of the pitch particles on the mineral surface, and, thus, in a denser packing of the pitch particles on the gcc surface. Including talc in the discussion of surface area based loading can be misleading, because the  $\varepsilon_{\text{BET}}$  can differ from the surface area actually involved in the pitch adsorption.

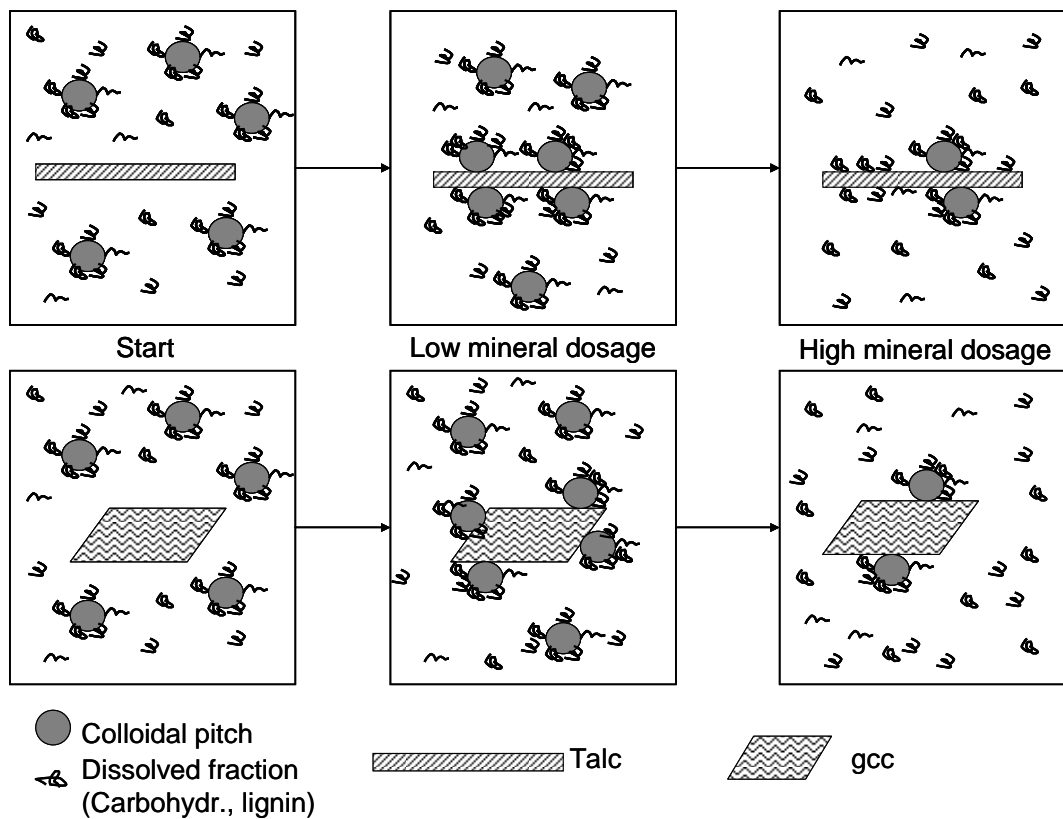


Figure 7-14: Proposed mechanism for the adsorption of dissolved and colloidal substances onto cross-section views of talc platelet (upper route) and gcc rhomboid (lower route).

Willför et al. (2000) have suggested similar mechanisms and made comparable observations. They suggested that the initial interactions occur between the dissolved, hydrophilic polysaccharides and the suspended filler particles.

Another interesting observation is that at high gcc dosages a substantial amount of resin acids were found in the aqueous phase. A possible explanation could be that the resin acids were dissolved during the adsorption experiment. Lehmonen et al. (2009) showed that 20 – 30 mgdm<sup>-3</sup> of resin acids are dissolved in the pH range of 7 to 8. The pH after the adsorption experiments was reported to be 7.8 for the high mineral dosages. Since the system is acidified before the extraction procedure, the resin acids will become insoluble again and will be measured as a part of the extractives. A plot of the extractives content against the turbidity showed a good linear regression coefficient ( $R^2=0.99$ ) (Figure 7-15). Both fitted parameters are significant with  $p$  for the steepness of  $<0.01$  and for the intercept of 0.03. However, the data points for the high gcc dosages with 50 NTU for the untreated gcc-1, and 32 NTU for the treated gcc-1, respectively, do slightly deviate from this linear dependency. Exclusion of these two points, results in an  $R^2>0.99$  and an intercept of only 1.3 mgdm<sup>-3</sup> ( $p = 0.8$ ). This observation indicates that either the amount of extractives is too high or the measured turbidity too low. Both indications can be explained by dissolution of the resin acids during the adsorption experiment (lower turbidity) and the extraction with petroleum ether after acidification (higher extractives content). This can be seen as another indication that treated and untreated gcc particles preferably adsorb colloidal substances rather than dissolved.

An additional benefit in using the analysis shown in Figure 7-15 is that in idealised, colloidal stable systems the turbidity contains all the information that the more complex extractives content analysis also provides. Further, the linear proportionality confirms that the mineral was sufficiently separated from the supernatant during the centrifugation.

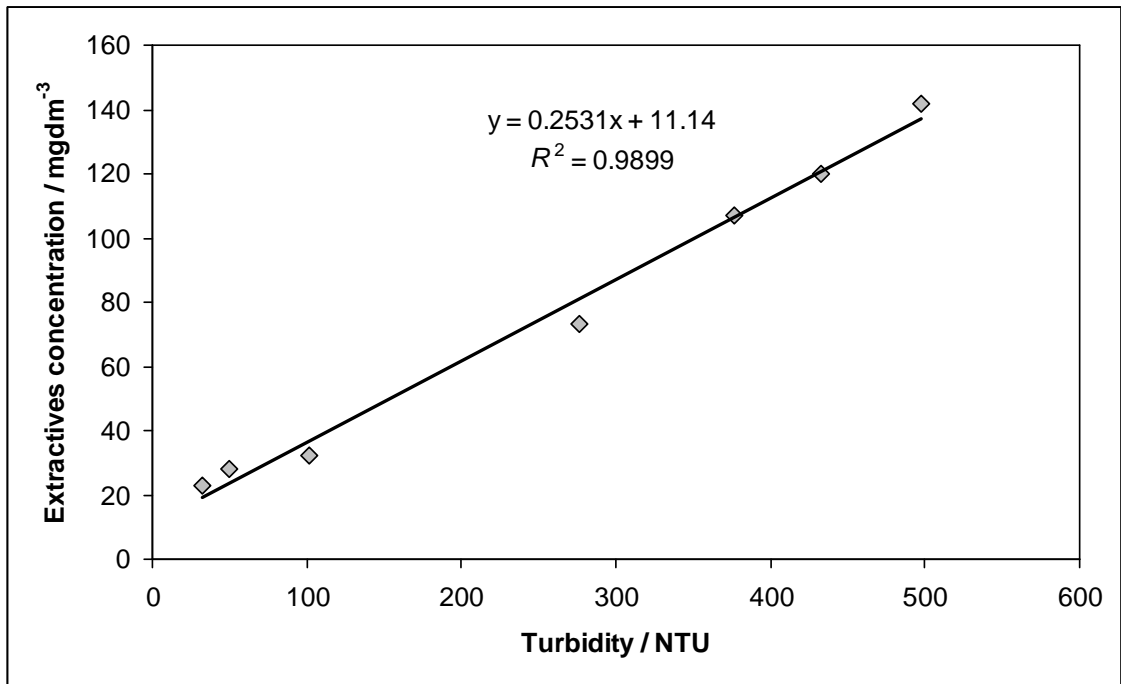


Figure 7-15: Extractives content against turbidity.

A final observation from Figure 7-10 and Figure 7-11 is the strongly reduced triglyceride content after the gcc treatment of the TMP filtrate. Although this can be mainly attributed to saponification a reduction of the triglyceride content is clearly desired since they can be the main contributor to pitch deposition problems (Hubbe et al. 2006; McLean et al. 2005).

## 7.2 The use of porous high surface area calcium carbonate

### 7.2.1 Introduction

In section 7.1 it was shown that by treating natural ground calcium carbonate (gcc) with stearic acid the adsorption capacity for pitch can be increased, engendering a performance approaching that of talc. The use of gcc and precipitated calcium carbonates (pcc) in pitch control has been investigated elsewhere (Rogan 1994; Whiting 1997; Willför et al. 2000). In other studies a surface modified calcium carbonate (mcc) was shown to adsorb efficiently detrimental components (stickies) from recycled fibre processing (Gribble et al. 2010; Gribble et al. 2011; Gribble 2011).

The aim of this work is to investigate the performance of a porous, high surface area mcc in the adsorption of dissolved and colloidal substances from an unbleached thermo mechanical pulp filtrate. The performance of the mcc was compared with that of talc and natural ground calcium carbonate. The comparison is made by measuring operationally-defined adsorption isotherms, with special focus on the colloidal fraction, and a detailed analysis of the constituents to determine the extent of preferential adsorption of some species.

### ***7.2.1.1 Surface properties***

The surface properties of talc and gcc have been described in sections 2.4.1.3 and 2.4.2, respectively. Modified calcium carbonate, as used in this study, is formed from calcium carbonate and phosphate via an in-situ surface re-precipitation (Ridgway et al. 2004). mcs have hydrophilic surfaces and exhibit both calcium phosphate and carbonate crystalline structure. The mcc tested is a porous material with a discretely bimodal pore size distribution when formed into a packed bed, with peaks of the first derivative of mercury intrusion characteristic at 1.31  $\mu\text{m}$  and at 0.18  $\mu\text{m}$ . It is further an amphoteric material showing electrochemical charge values of +71.0 and -35.7  $\mu\text{Eq}^{-1}$  in a polyelectrolyte titration versus KPVS and PDDPC (see section 3.2.7).

## ***7.2.2 Materials and Methods***

### ***7.2.2.1 Materials***

Two Finnish talc grades were used as references. One is commercially available talc, Finntalc P05 from Mondo Minerals and the other talc grade was derived from Finntalc P05 with subsequent comminution and delamination to generate fineness, high aspect ratio and enhanced specific surface area. The Finntalc P05 will be labelled as LSA (low surface area) talc and the delaminated quality will be labelled as high surface area

(HSA-talc) talc. The surface area, particle size and electrophoretic mobility are reported in Table 7-7.

Omyacarb 1 was used as the ground calcium carbonate sample. It consists of a marble originating from Avenza, Italy, and was supplied by Omya. It is labelled as gcc (see also section 7.1.2.1).

**Table 7-7: Specific surface area, particle size ( $d_{50}$ ) and electrophoretic mobility  $u$  in a 0.01 M NaCl solution of the investigated minerals.**

Name	Abbrev.	Type	$\epsilon_{\text{BET}} / \text{m}^2\text{g}^{-1}$	$d_{50} / \mu\text{m}$ (Sedigraph 5120)	$u /$ $\times 10^{-8} \text{m}^2\text{V}^{-1}\text{s}^{-1}$
Finntalc P05	LSA-talc	Talc	9.6	2.4	-3.4
Delaminated Finntalc P05	HSA-talc	Talc	51.0	0.8	-3.9
Omyacarb 1	gcc	Ground calcium carbonate	4.0	1.5	0.8
Modified calcium carbonate	mcc	Modified calcium carbonate	42.7	2.6	-0.8

The surface modified calcium carbonate was produced via a proprietary process which allows a solid-solid crystal transformation using a crystal habit modifier which also acts as a doping agent within the calcite crystal structure to form a metastable inorganic complex which transforms with time under heating and agitation to form a platelet structure as boundaries to internal pores. The final crystal structure and chemical content mimics that of bone. The particle size  $d_{50}$ , specific surface area  $\epsilon_{\text{BET}}$  and electrophoretic mobility  $u$  are reported in Table 7-7.

### **7.2.2.2 Methods**

A detailed description of the method is described in section 7.1.2.2.



### 7.2.3 Results

In this study two different TMP samples, TMP filtrate 1 and TMP filtrate 2, were used. The properties of each filtrate are summarised in Table 7-8. The mean electrophoretic mobility  $u$  (Figure 7-16) of the suspended matter in the TMP filtrates was recorded versus changing pH. Both filtrates have a stable  $u$  in the relevant pH region of 7-8. Nevertheless, the absolute values of the two filtrates slightly differ.

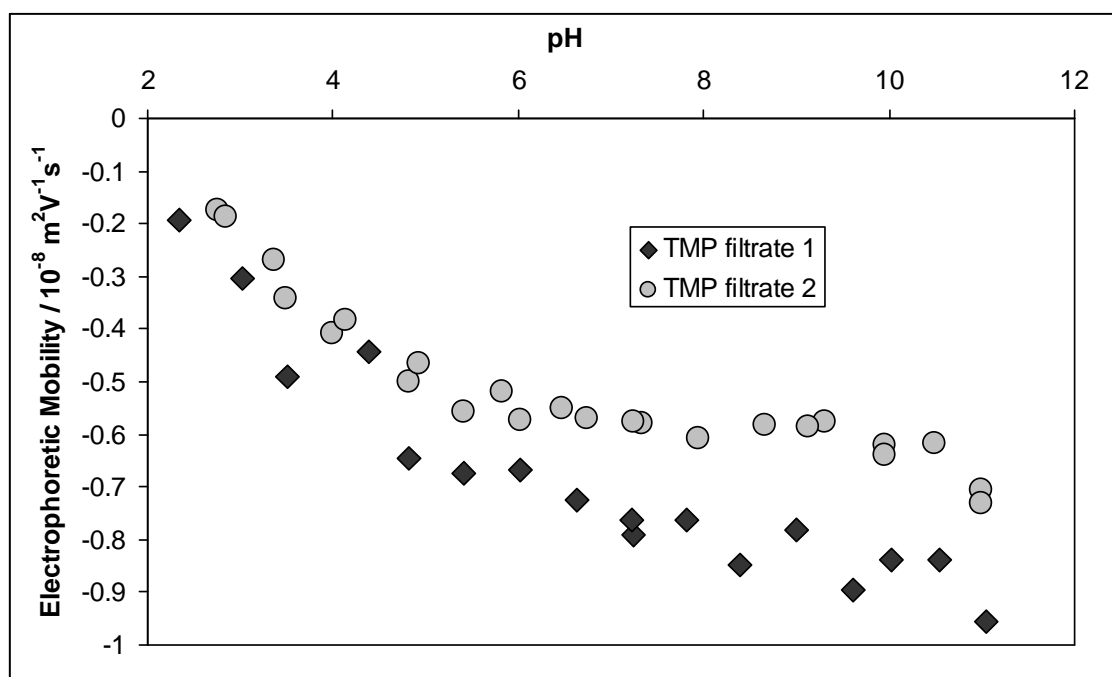


Figure 7-16: Mean electrophoretic mobility of the particles in the TMP filtrates 1 and 2 against pH. The pH was adjusted with 0.1 M sodium hydroxide and 0.1 M hydrochloric acid.

With TMP filtrate 1 the adsorption isotherm was recorded. A special focus was also laid on the electrochemical charge. TMP filtrate 2 was used for a detailed analysis of the components in the TMP filtrate prior and post adsorption.

**Table 7-8: Properties of the TMP samples 1 and 2. The presented range for TMP filtrate 1 is based on the standard deviation of six independent experiments. For TMP filtrate 2 only the COD was measured six times. <sup>1)</sup> Titrated with N-methylglycol-chitosan.**

	TMP filtrate 1	TMP filtrate 2
Turbidity / NTU	307 ± 5	497
Chemical Oxygen demand / mgdm <sup>-3</sup>	3 789 ± 69	4 350 ± 40
Gravimetry / gdm <sup>-3</sup>	3.29 ± 0.11	3.57
Electrochemical charge (SCD) / $\mu\text{Eqg}^{-1}$	- 1.34 ± 0.12	- 0.31 <sup>1</sup>
pH	7.1	7.2
Conductivity / $\mu\text{Scm}^{-1}$	870	1 200
Na <sup>+</sup> / mM	11.2 ± 0.09	9.2
K <sup>+</sup> / mM	1.20 ± 0.03	1.2
Ca <sup>2+</sup> / mM	0.92 ± 0.03	1.4
Mg <sup>2+</sup> / mM	0.22 ± 0.02	0.3
Cl <sup>-</sup> / mM	0.64 ± 0.06	0.7
SO <sub>4</sub> <sup>2-</sup> / mM	0.35 ± 0.01	0.4

### ***7.2.3.1 Effective adsorption isotherm***

The effective adsorption isotherm reported only considers the colloidal fraction of the TMP filtrate. The colloidal fraction was quantified by turbidity measurements, which linearly fit the amount of petroleum ether extractives (Figure 7-15 and Figure 7-17). The amount of adsorbed colloidal substances (loading) from the TMP filtrate in equilibrium  $\Gamma_{\text{eq}}^{\tau}$  was calculated by Equation 6-1.

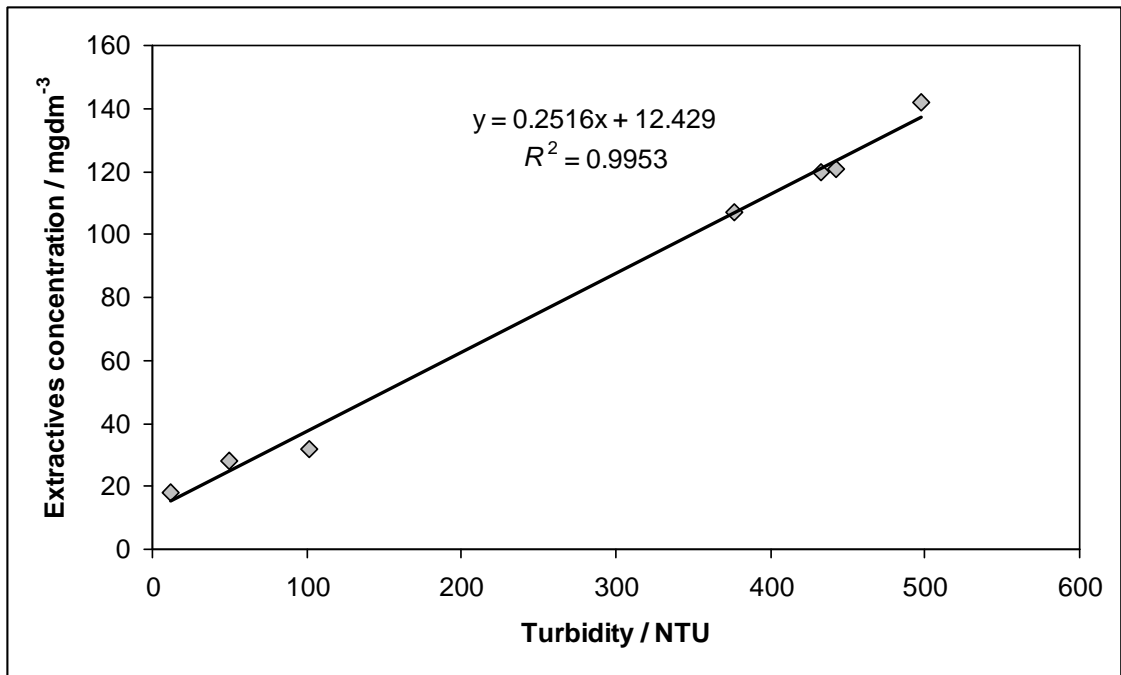


**Figure 7-17: Extractives content against turbidity.**

The mineral with the highest adsorption capacity was the high surface area talc (HSA-talc) (Figure 7-18) with 94 NTUg<sup>-1</sup>. The corresponding low surface area talc (LSA-talc) had a proportional lower capacity of 21 NTUg<sup>-1</sup>. If the capacities are compared based on surface area the two talc grades perform equally (Table 7-9). Both talc grades showed a similar Langmuir constant  $K_L^\tau$  of 0.03 NTU<sup>-1</sup>. It is, however, difficult to compare the  $K_L^\tau$  values because in the case of the low surface area minerals (LSA-talc and gcc) most of the data points occurred in the saturation regime and therefore the fit is biased stronger towards this region. The gcc had a similar adsorption capacity than the LSA-talc with 22 NTUg<sup>-1</sup>. However, the adsorption capacity of the gcc based on surface area was much higher than the capacities of the other tested minerals (Table 7-9). The mcc had a medium adsorption capacity of 34 NTUg<sup>-1</sup> and the highest affinity  $K_L^\tau$  with 0.29 NTU<sup>-1</sup>.

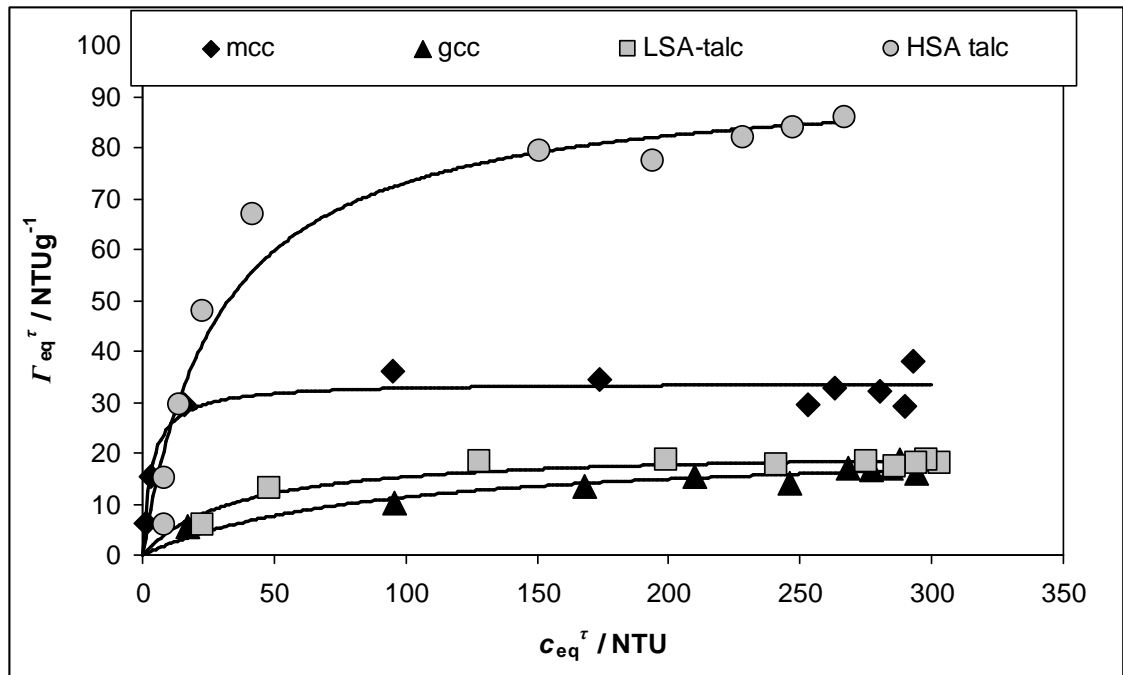


Figure 7-18: Adsorption isotherms for the colloidal fraction of the TMP filtrate measured by turbidity.

Table 7-9: Detailed overview of the fitted Langmuir parameters. The fit was done with TableCurve® 2D using a non-linear least squares (NLLS) fit.

Mineral	Parameter	95 % Confidence limits	P> t	R <sup>2</sup>	
gcc	$K_L^\tau / \text{NTU}^{-1}$	0.01	>0.00	0.02	0.88
	$\Gamma_{\max}^\tau / \text{NTUg}^{-1}$	21.7	16.0	27.4	
	$\Gamma_{\max}^\tau / \text{NTUm}^{-2}$	5.4			
mcc	$K_L^\tau / \text{NTU}^{-1}$	0.29	0.10	0.48	0.92
	$\Gamma_{\max}^\tau / \text{NTUg}^{-1}$	33.9	28.1	31.1	
	$\Gamma_{\max}^\tau / \text{NTUm}^{-2}$	0.8			
LSA-talc	$K_L^\tau / \text{NTU}^{-1}$	0.03	0.01	0.04	0.96
	$\Gamma_{\max}^\tau / \text{NTUg}^{-1}$	20.9	18.8	23.0	
	$\Gamma_{\max}^\tau / \text{NTUm}^{-2}$	2.2			
HSA-talc	$K_L^\tau / \text{NTU}^{-1}$	0.03	0.02	0.05	0.95
	$\Gamma_{\max}^\tau / \text{NTUg}^{-1}$	94.2	82.3	106.1	
	$\Gamma_{\max}^\tau / \text{NTUm}^{-2}$	1.8			

Another parameter that was also analysed was the electrochemical charge of the samples as adsorption progressed (Figure 7-19). The mcc was highly efficient in reducing the anionic charge of the TMP filtrate. The original  $-1.34 \mu\text{Eqg}^{-1}$  was reduced down to  $-0.12 \mu\text{Eqg}^{-1}$ . The pH increased for all minerals from 7.1 for the original TMP filtrate to 7.6 for the highest mineral dosage. Bivalent cations, such as calcium and magnesium increased slightly from 0.92 mM to 1.12 mM for the highest mcc dosage and to 1.20 mM for the highest gcc dosage. The magnesium concentration increased for both talc grades from 0.22 mM to 0.80 mM. The increase in calcium and magnesium concentration is a result of ion release by the minerals.

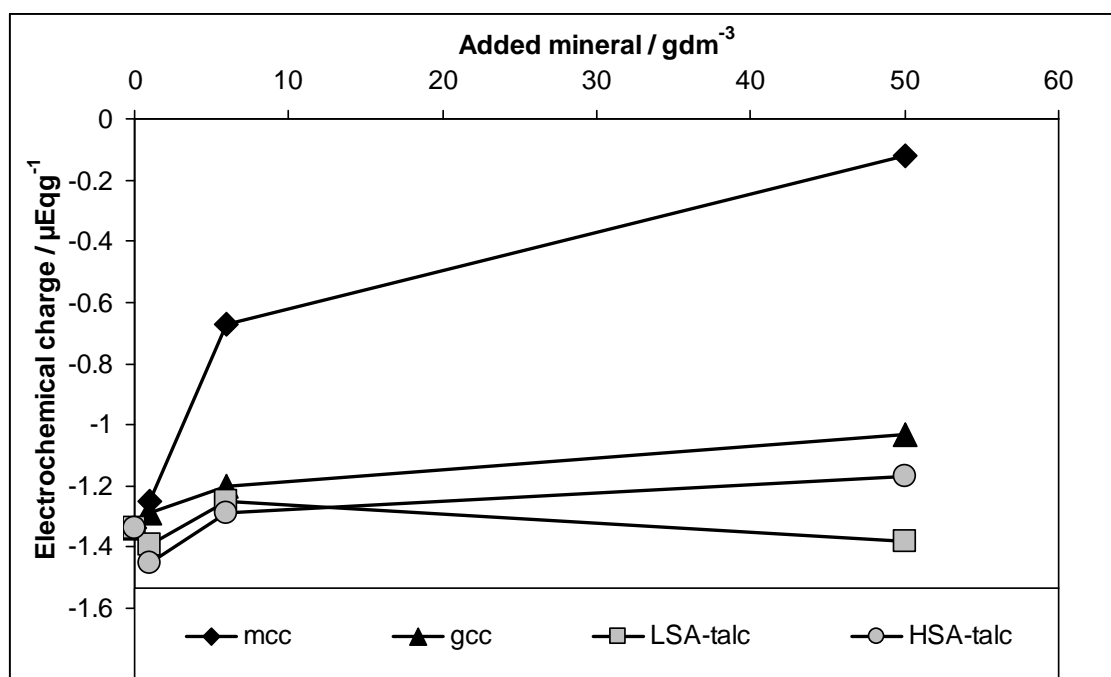


Figure 7-19: Electrochemical charge of the TMP filtrate after mineral separation as a function of added mineral.

### 7.2.3.2 Chemical analysis – selective adsorption properties

The results for the HSA-talc and the gcc have already been shown in section 7.1.3.3. The chemical analysis contained the petroleum ether extractives which represent the lipophilic fraction of the DCS. The carbohydrate content was also analysed and split up into the different saccharide monomers. The analysis includes only the neutral

monosaccharides because the applied acid hydrolysis leads to a decomposition of charge-carrying uronic acids. The lignin was determined by UV photometry as the acid soluble fraction. Additionally, the acid insoluble fraction refers to the rest which includes also the extractives.

The TMP filtrate 2 comprised of 142 mgdm<sup>-3</sup> extractives, of which the main components were triglycerides, followed by the resin acids, sterylesters and fatty acids (Table 7-10). Lignans and sterols were minor components of the system. The TMP filtrate further contained 1 052 mgdm<sup>-3</sup> carbohydrates and 527 mgdm<sup>-3</sup> lignin.

**Table 7-10: Extractives (petroleum ether) group content, carbohydrate content, acid soluble (lignin) content and acid insoluble content of the TMP filtrate 2.**

<b>Type</b>	<b>Amount / mgdm<sup>-3</sup></b>
<u>Extractives</u>	
Triglycerides	63
Resin Acids	32
Sterylesters	26
Fatty Acids	9
Lignans	4
Sterols	3
Unknown	<u>5</u>
Total:	<u>142</u>
Carbohydrates	1052
Acid soluble (Lignin)	527
Acid insoluble	<u>403</u>
Total:	<u>1982</u>

In the case of the HSA-talc treatment, the extractives content was reduced to 120 mgdm<sup>-3</sup> for the lower amount and to 32 mgdm<sup>-3</sup> for the higher mineral dosage, respectively. The composition of the extractives was not changed (Figure 7-20). The treatment of the TMP filtrate with gcc reduced the extractives content to 107 mgdm<sup>-3</sup> for the lower mineral dosage and for the higher mineral dosage to 28 mgdm<sup>-3</sup>, respectively. The composition of the extractives changed for the high mineral dosage sample. The main constituents were resin acids (20 mgdm<sup>-3</sup>) and just minor quantities of the other components. The addition of mcc in low amount reduced the extractives content to 121 mgdm<sup>-3</sup> and did not affect the composition. Adding a high mcc amount reduced the extractives down to 18 mgdm<sup>-3</sup> in turn containing 16 mgdm<sup>-3</sup> resin acids.

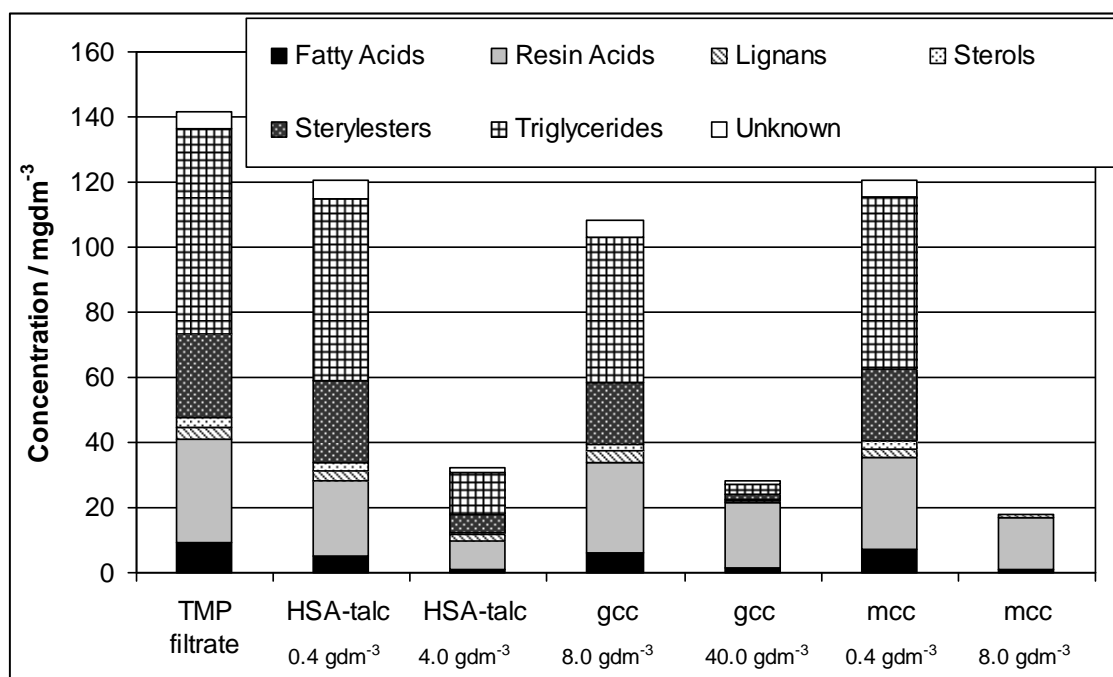
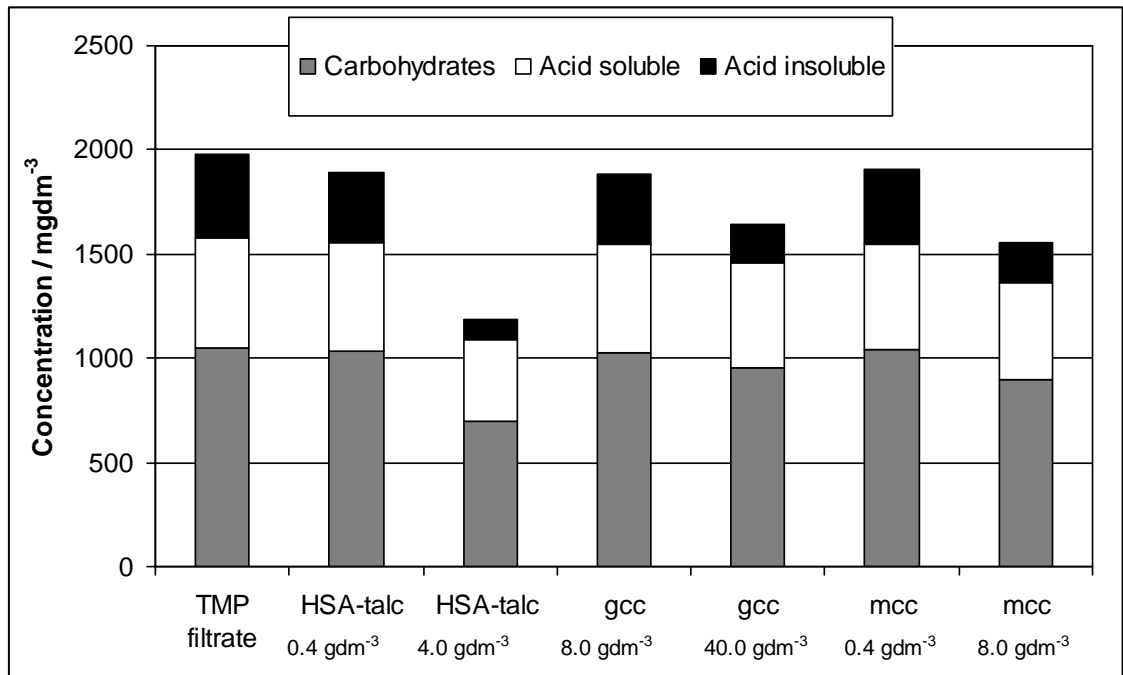


Figure 7-20: Extractives concentration of the original TMP filtrate 2 and after the treatment with HSA-talc at 0.4 and 4 gdm<sup>-3</sup>, gcc at 8 and 40 gdm<sup>-3</sup>, and mcc at 0.4 and 8 gdm<sup>-3</sup>.

With focus on the dissolved substances (carbohydrates and lignin) in the TMP filtrate (Figure 7-21) preferences were observed. With low mineral dosages the removed amount of carbohydrates and lignin was rather minor. The situation changed when the mineral dosage was increased.



**Figure 7-21: Concentration of the carbohydrates, acid soluble (lignin) and acid insoluble content of the TMP filtrate 2 before and after the various mineral treatments.**

Especially in the case of talc but also in the case of mcc substantial amounts of carbohydrates and also lignin were adsorbed. Table 7-11 quantifies the preferential adsorption. The removed amounts of each component (carbohydrates, lignin and extractives) per gram were calculated similarly to Equation 6-1. With high talc addition levels, talc adsorbed not only the colloidal wood resin but also substantial amounts of carbohydrates and lignin. In contrast, the regular ground calcium carbonate did not show a specific preference for dissolved substances even with high dosed amounts. Finally, the mcc showed a very interesting behaviour. If mcc was dosed in low amount, lignin was preferably adsorbed versus the carbohydrates. With a high mcc dosage the ratio changed and preferably carbohydrates were absorbed preferably over lignin.



**Table 7-11: Ratios of removed carbohydrates plus lignin relative to the removed extractives.**

	<b>(Carbohydrates + Lignin) : Extractives</b>	<b>Carbohydrates : Extractives</b>	<b>Lignin : Extractives</b>
HSA-talc 0.4 gdm <sup>-3</sup>	1.3	0.8	0.5
HSA-talc 4.0 gdm <sup>-3</sup>	4.4	3.2	1.2
gcc 8.0 gdm <sup>-3</sup>	1.0	0.8	0.2
gcc 40.0 gdm <sup>-3</sup>	1.1	0.9	0.2
mcc 0.4 gdm <sup>-3</sup>	1.7	0.5	1.2
mcc 8.0 gdm <sup>-3</sup>	1.8	1.3	0.5

Besides the overall carbohydrate content, the mono saccharide composition in the supernatant of the samples was also analysed (Figure 7-22). For the low mineral dosages only a reduction in galactose (Gal), glucose (Glc) and mannose (Man) was observed. The ratio in these samples and in the original TMP filtrate between galactose, glucose and mannose in these cases was always 1:3:4. For the higher talc dosage mannose was especially removed and some arabinose (Ara) and xylose (Xyl). For the high gcc dosage the ratio of galactose, glucose and mannose remained nearly constant but already a substantial amount of arabinose was removed. Most interestingly with the high mcc dosage large amounts of galactose and also more than 50 % of the arabinose were removed. Additionally, this sample showed the strongest decrease of xylose from 20 to 16 mg dm<sup>-3</sup>.

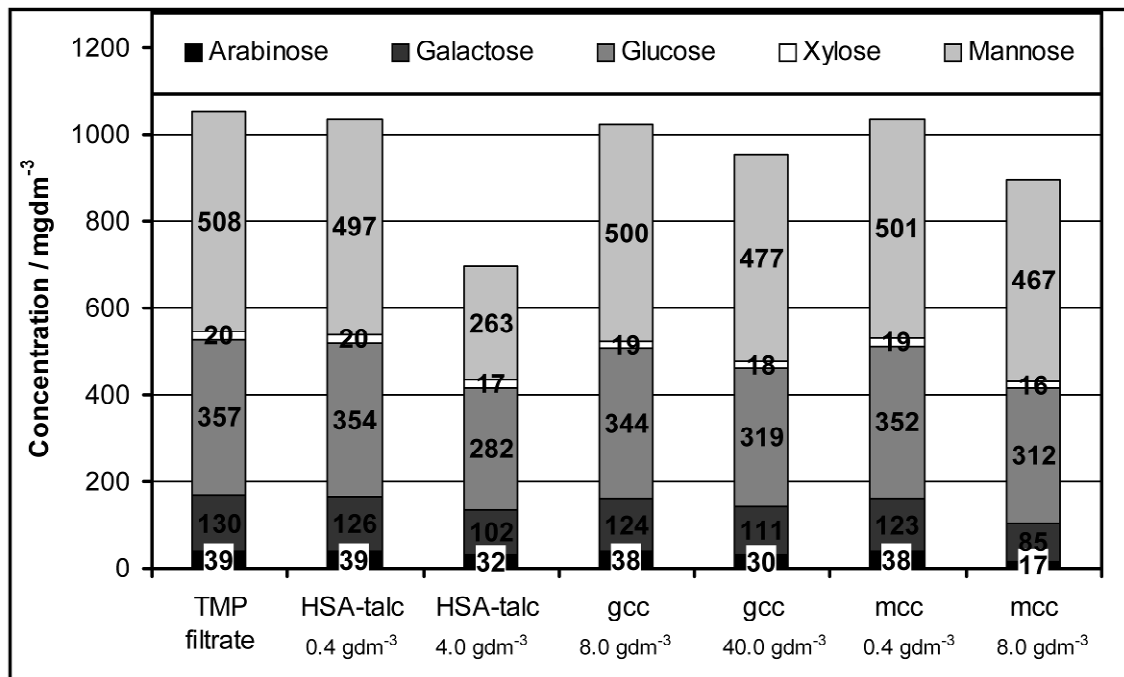
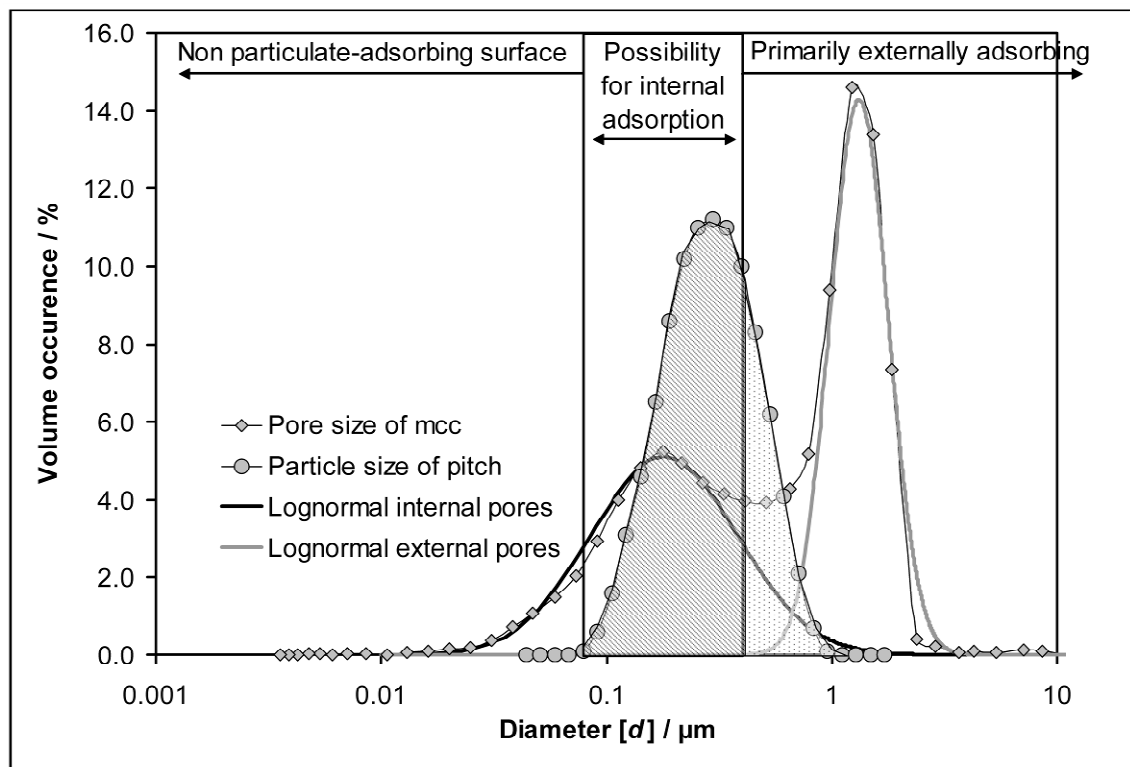


Figure 7-22: Carbohydrate monomer composition of the original TMP filtrate 2 and after the various mineral treatments.

### 7.2.4 Discussion

The adsorption capacity of the HSA-talc was 4.5 times higher than that of the LSA-talc and the surface area was 5.1 times higher, showing a straightforward proportionality between adsorption and surface area. However, this proportionality was not observed for either the gcc or the mcc, implying that in these cases not all the surface area as determined by nitrogen adsorption is involved in the adsorption of colloidal material. Figure 7-23 presents a more detailed analysis of this phenomenon for mcc. The distribution of pore sizes in mcc (grey shaded diamonds) is bimodal, and so in the diagram is split into two log-Gaussian distributions (log-normal) for the smaller (assumed internal) pores and the larger (assumed external) pores. The internal pores have a modal diameter of 0.18  $\mu\text{m}$ . Superimposed on these void distributions is shown the volume-based particle-size distribution of the pitch (grey shaded circles), centred around a modal diameter of 0.29  $\mu\text{m}$ . Therefore part of the mcc pore size distribution,

marked in Figure 7-23 as “Non particulate-adsorbing surface”, is not accessible to the pitch droplets. An additional effect is likely to be that the coarse fraction of the pitch particles primarily adsorb on the external surface, in the region labelled “Primarily externally adsorbing”, and could also prevent smaller pitch droplets reaching the smaller mcc pores by blocking their entrances. To avoid such effects, one could design the pore structure of the mcc to be larger, but in practice it is difficult to predict the size of pitch particles within a particular paper production process.



**Figure 7-23: Overlay of the particle size distribution for the colloidal fraction of the TMP filtrate and the pore size structure of the mcc.**

As described previously in sections 6.1.3, 6.2.3 and 7.1.4 a plot of turbidity to represent the colloidal fraction, versus COD, the total organic fraction, including colloidal and dissolved substances is used to illustrate the preferential adsorption (Figure 7-24). This can serve on the one hand as a means of calibration to convert turbidity results into corresponding organic mass and on the other hand to show that below a certain

concentration of colloidal substances some mineral types start to adsorb more and more dissolved substances.

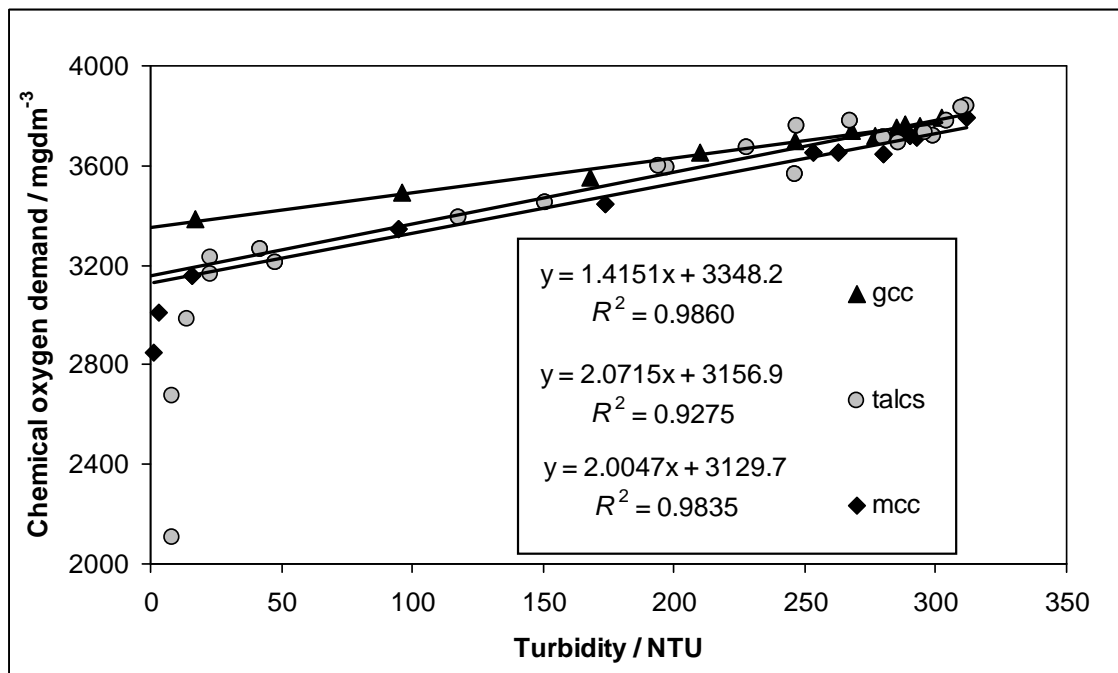


Figure 7-24: Turbidity against chemical oxygen demand (COD) of the recorded isotherm. The linear regression was performed using all data points > 50 NTU. All fitted parameters are significant with  $p < 0.01$ .

Both talc grades showed such preferential adsorption for dissolved substances below a certain turbidity level. The ground calcium carbonate did not have this preference. The affinity of talc for dissolved substances such as carbohydrates and lignin was described previously (Allen et al. 1993; Jenkins, Ralston 1998; Willför et al. 2000) as well as the preferred adsorption of colloidal wood resin onto gcc (Willför et al. 2000). An interesting observation in this study is the preference of the modified calcium carbonate for dissolved substances. A part of the soluble substances already adsorbs in the regions with excess of colloidal pitch droplets with respect to mineral. The carbohydrates, already adsorbed onto the pitch droplets, act as stabilisers for the pitch (Sundberg et al. 1996c) and these composites subsequently adsorb as a unit (Willför et al. 2000). This mechanism is also suggested by the carbohydrate : extractives ratio in the remaining liquid phase (Table 7-11). The ratio remains constant around 0.8 for the low talc dosages and the low and high gcc dosages. These data points are all within the linear

region in the turbidity versus COD plot (Figure 7-24). As listed earlier, the carbohydrate monomer composition in the filtered TMP sample corresponds to a galactoglucomannan (GGM) with a monomer ratio of 1:3:4 (galactose:glucose:mannose). GGMs are the main hemicelluloses present in softwoods like spruce (Willför et al. 2008). It is clear that all the monomers can also be present in other polysaccharides but for a simplified discussion it is assumed that they originate mainly from the GGM. For higher talc dosages the ratio changes and more mannose, most probably in the form of mannan, is removed. With low mcc dosages the ratio of carbohydrates to extractives is lower (0.5) than the ratios obtained for talc and gcc. However, the ratio of Gal : Glc : Man in the aqueous phase of the low dosage mcc treated TMP filtrate is also 1:3:4. The ratio changes drastically for higher mcc addition levels. Galactose is removed in much higher quantities. In addition also arabinose was removed (Figure 7-22). This might indicate the preferred adsorption of arabinogalactans onto mcc. Furthermore, also some xylose was removed. Similarly, also for the high gcc dosage a small quantity of arabinogalactan was removed. Arabinogalactans contain uronic acids that are one of the main charge carriers in the dissolved fraction of TMP (Sundberg et al. 2000). However, the used analysis procedure only captures the neutral saccharide units. Nevertheless, only a part of the arabinose and galactose units in arabinogalactans are charge carriers in the form of uronic acids and, thus, the current findings indicate a possible source of removed charged species which was also observed in the SCD titration (Figure 7-19). The mcc has already shown its affinity for the adsorption of anionic polymers, like KPVS through Coulombic interactions in the polyelectrolyte titration. Neutralisation with bivalent metal ions, like calcium, can be excluded as potential mechanism because the gcc treated samples contain the similar amounts of calcium and also the presence of resin and fatty acids is not substantially different than in the gcc treated TMP filtrates.

Also GGMs can contain anionic charges introduced by uronic acids but are in unbleached TMP mostly methylesterified (Sundberg et al. 2000).

The chosen acid hydrolysis of the polysaccharides results in a degradation of uronic acids and other labile sugar units (Willför et al. 2008). Therefore, the reported values do not represent the complete saccharide content. Nevertheless, the values obtained for the carbohydrate, lignin and extractives content, for example, compare well with earlier work (Wagberg, Odberg 1991).

A plot of turbidity against extractives (Figure 7-17) supports the assumption of Figure 7-24 in which we relate the turbidity to the colloidal fraction and thus to the extractives of the TMP filtrate. Besides the good regression coefficient in Figure 7-17 ( $R^2 > 0.99$ ) it can be recognised that the data points with the lowest turbidity are slightly too high, preventing the line to run through the origin, and thus suggests the presence of an additional species recorded as soluble though found later in the extractives. Considering the extractives composition in Figure 7-20 for these two points, it shows that both points ( $\text{gcc } 40 \text{ gdm}^{-3}$  and  $\text{mcc } 8 \text{ gdm}^{-3}$ ) report mainly the presence of resin acids and some minor parts of the other extractives groups. In section 7.1.4 it is suggested that this is caused by the dissolution of the resin acids during the adsorption experiments due to higher pH levels. Before extraction of the samples for the extractives analysis the samples gets acidified and the resin acids become water insoluble again, thus, appearing in the extractives content and consequently imitating a higher extractives content than suggested in the turbidity analysis. Vice versa, of course, the turbidity does not measure the dissolved resin acids after the mineral removal, and is, thus, suggesting a lower colloidal concentration than measured with the extraction.

A last observation can be made with focus on the extractives composition after the treatment with gcc and mcc (Figure 7-20). By the addition of high amounts of these

minerals the remains mainly consists of resin acids. The original main constituent found in the TMP filtrate, triglyceride, was efficiently removed. Triglycerides are known to be a major cause of deposition problems (Hubbe et al. 2006; McLean et al. 2005) and it is, thus, highly desirable to remove them efficiently.

## **7.3 Influence of electrolytes on pitch stability**

### ***7.3.1 Introduction***

In the previous sections the use of various calcium carbonate types has been presented. The use of these products also bears the risk of Ca-ion release, mainly due to decreased pH. Ca-ions have been found to be a potential cause for pitch agglomeration and deposition problems in paper mills (Allen, Douek 1993; Allen, Filion 1996; Douek, Allen 1991a; Dreisbach, Michalopoulos 1989; Gustafsson et al. 1952; Hamilton, Lloyd 1984; Hassler 1988; Holmbom, Sundberg 2003; Kekkonen, Stenius 2001; Otero et al. 2000; Sihvonen et al. 1998; Trafford 1988). It is, therefore, important to understand if the released  $\text{Ca}^{2+}$  concentrations are sufficient to i) destabilise the system, and ii) eliminate the possibility of failure in the adsorption experiment caused by deposited and agglomerated material.

Clearly, it should be recognised that both the anion and cation can influence the stability depending on three main factors, (i) influence of the sign of charge in respect to opposite charge interaction with the stabilised species surface, depending on its charge, (ii) the impact of electrolyte concentration and (iii) the ratio between mono and divalent cations in respect to cation exchange of stabilising polymers, affecting likely desorption, dissolution and coagulation of same. It is not always possible to identify which of these effects dominates or whether there are cooperative interactions at play.

It is the aim of this section to investigate the stability of TMP filtrates against electrolytes such as calcium ions. The process is followed by turbidity, size and electrophoretic mobility measurements. This is in accordance with other similar studies (Sihvonen et al. 1998; Sundberg et al. 1996c; Sundberg et al. 1996b; Sundberg et al. 1994a; Sundberg et al. 1994b).

### **7.3.2 Materials and Methods**

#### **7.3.2.1 Materials**

The TMP filtrate was already described in section 7.2, and refers here to the TMP filtrate 1 in Table 7-8.

CaCl<sub>2</sub> and NaCl were used to represent mono and divalent cation behaviour. Both were analytical grades and dissolved in deionised water to 0.2 M and 4 M, respectively. HCl and NaOH were also analytical grades and used as 0.1 M solutions for pH adjustment.

#### **7.3.2.2 Methods**

1 000 cm<sup>3</sup> TMP filtrate was placed in a glass beaker equipped with a magnetic stirring bar. The suspension was stirred and the pH adjusted with HCl (pH 5) or NaOH (pH 8). The suspension was stirred for 10 minutes at room temperature (23 °C) and the electrolyte solutions added stepwise (5 cm<sup>3</sup>). pH and turbidity were recorded on-line. After each addition step the electrophoretic mobility and size were measured on the Malvern Zetasizer NS.

40 cm<sup>3</sup> TMP filtrate was placed in a PE centrifuge tube and a defined amount of electrolyte solution was added (0, 0.2, 0.6, 2.0, 6.0, 8.0 cm<sup>3</sup>). The required amount of deionised water was added in order to have a constant volume throughout the trial series. After the addition the lid was closed, the samples shaken for 1 minute and turbidity measured. The sample was left over night (16 hours) at room temperature. The



samples were subsequently centrifuged for 15 minutes at 2 600 |g], followed by turbidity measurement of the supernatant.

The reference sample for turbidity which corresponds to 100 % in the figures is represented by the corresponding sample after electrolyte addition.

### 7.3.3 Results and Discussion

The electrophoretic mobility as a function of pH for this TMP filtrate has been shown in Figure 7-16. It was found to increase below pH 6. The electrophoretic mobility of the particles in the TMP filtrate increased with increasing electrolyte dosage (Figure 7-25). The electrolyte concentration was quantified in terms of ionic strength  $I$  by Equation 7-1, with  $z_i$  being the valency of the ion  $i$  and  $c_i$  the molar concentration of the ion  $i$  in  $\text{mol dm}^{-3}$  (M).

$$I = \frac{1}{2} \sum_i z_i^2 c_i$$

Equation 7-1

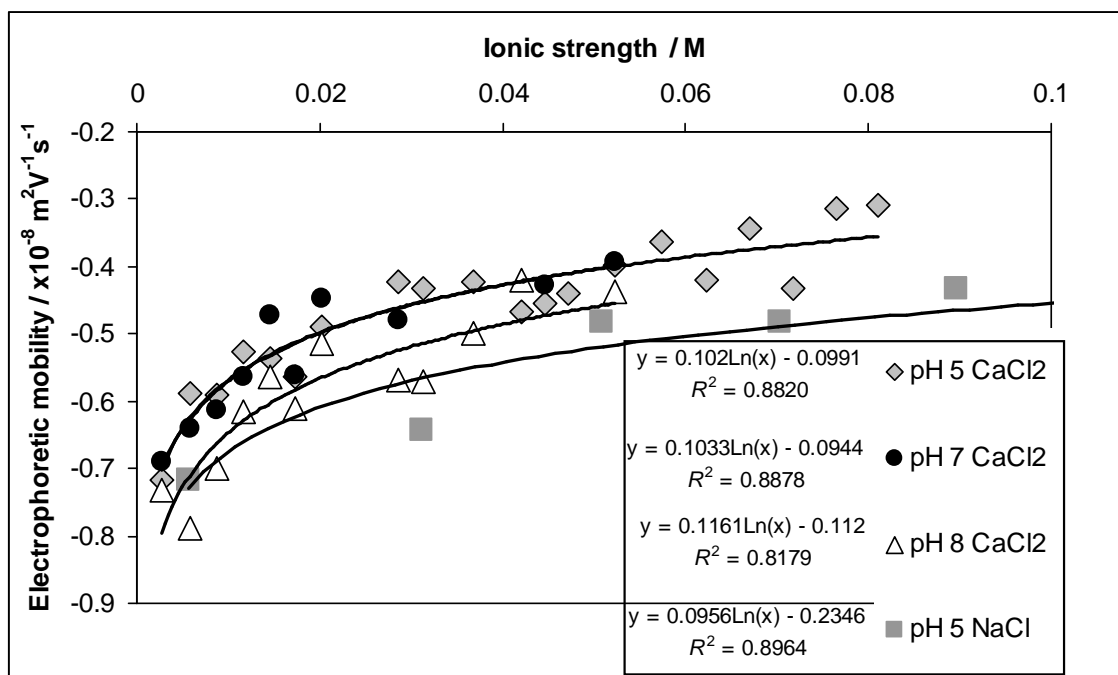


Figure 7-25: Electrophoretic mobility of the particles in the TMP filtrate as a function of  $\text{Ca}^{2+}$  and  $\text{Na}^+$  addition. An ionic strength  $I$  of 0.01 M corresponds to Calcium ion concentration of ~ 3.3 mM.

The electrophoretic mobility  $u$  is proportional to the zeta potential  $\zeta$  (Equation 3-8). The Debye-length  $\kappa^{-1}$  is proportional to the root of the ionic strength (Equation 3-7). Finally,  $\zeta$  can be expressed as a function of the particle charge  $q$ , the Debye-length  $\kappa^{-1}$  and the particle radius  $R_p$  together with  $\epsilon_0$  as the permittivity of free space ( $8.85 \cdot 10^{-12} \text{ C}^2\text{J}^{-1}\text{m}^{-1}$ ), and  $\epsilon_r$  as the dielectric constant of the medium (water at 298 K; 78.64) yielding Equation 7-2 (Hiemenz, Rajagopalan 1997). This might explain the logarithmic dependency between the electrophoretic mobility in Figure 7-25 and the ionic strength  $I$ .

$$u \approx \zeta = \frac{q}{4 \cdot \pi \cdot \epsilon_0 \cdot \epsilon_r \cdot R_p} \cdot e^{-\kappa \cdot R_p}$$

**Equation 7-2**

The turbidity was in some cases immediately affected during the addition of the electrolyte solution (Figure 7-26). If only sodium chloride is added either at pH 5 or at pH 8, no immediate change in turbidity was observed (the data continue up to 250 mM NaCl without any change). Also for the trial at pH 5 with  $\text{Ca}^{2+}$  addition no direct effect on the turbidity was observed. The higher the pH the stronger the turbidity was affected with increasing  $\text{Ca}^{2+}$  concentration. This observation can be explained by the precipitation of calcium fatty and resin acid soaps. The higher the pH, the higher the concentration of dissolved fatty and resin acids is, and hence, the higher the amount of Ca-soap precipitates. In the trials in sections 7.1 and 7.2 the calcium ion concentration slightly increased from 0.92 mM to 1.2 mM, and also pH increased from 7 to 8. These values do not suggest a substantial amount of resin acid is forced to precipitate. In addition, chemical analysis (Figure 7-10 and Figure 7-20) showed a substantial part of the resin acids in solution, and thus, not precipitated. It is clear that also screening of the double layer will influence the stability of the pitch droplets.

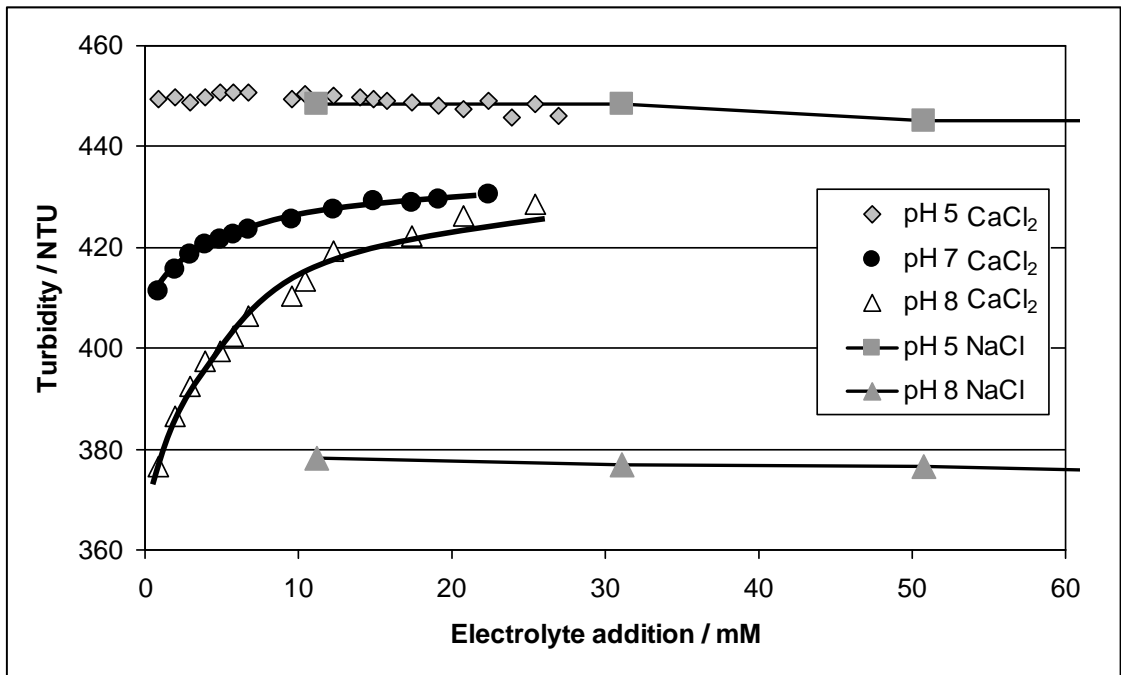


Figure 7-26: Immediate turbidity change during electrolyte addition. Turbidity is dilution corrected.

The particle size, represented by the  $d_{N50}$ , was not observed to change and remained  $280 \pm 20$  nm throughout all the trial points and samples.

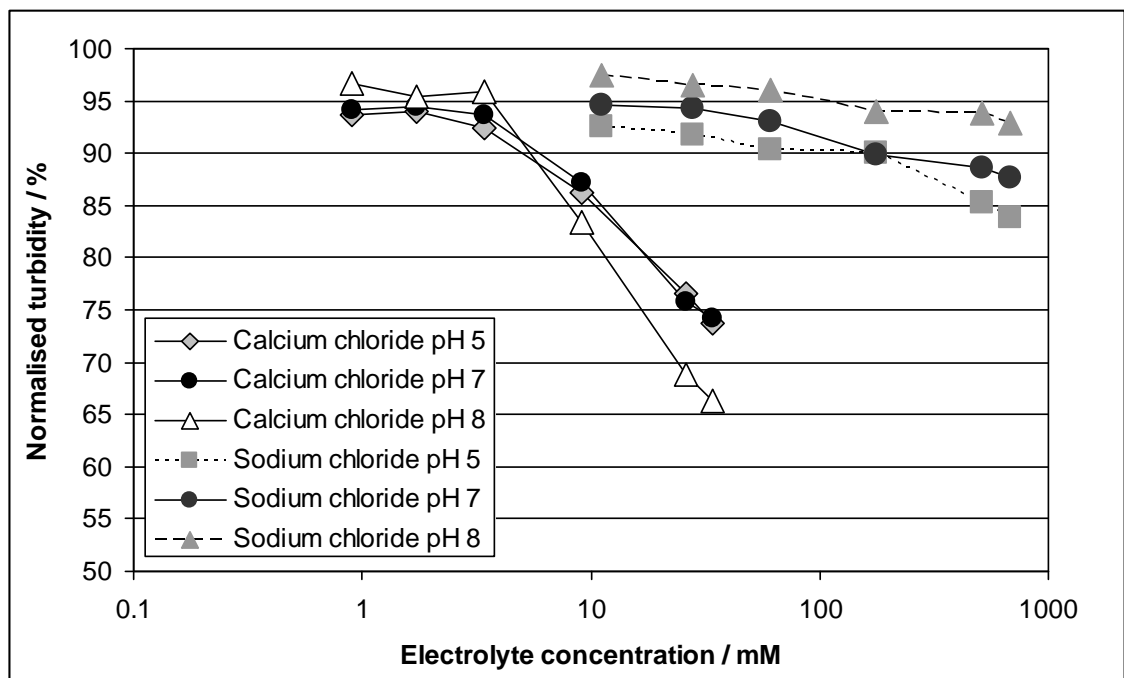


Figure 7-27: Stability of the TMP filtrate with increasing electrolyte concentration quantified by the turbidity prior and after addition of the electrolyte addition.

The stability of the colloidal fraction of the TMP filtrate can be influenced by the addition of electrolytes (Figure 7-27). Adding CaCl<sub>2</sub> resulted in a reduced turbidity after

centrifugation above 5 mM  $\text{Ca}^{2+}$ . Under acidic or neutral conditions the effect of calcium was minor compared to that at alkaline pH 8. The opposite can be observed if sodium is added as the electrolyte. The stability is more affected under acidic or neutral conditions and the highest stability is observed for the alkaline samples. The required sodium concentration in order to observe the destabilisation of the colloidal fraction is around 100 mM. Similar results were obtained previously (Sihvonen et al. 1998; Sundberg et al. 1994a; Sundberg et al. 1994b). The reasons are that calcium ions form soaps with resin and fatty acids which are highly insoluble. The possibility for this calcium-soap formation is higher at increased pH since the acids are present as anions. Furthermore the sodium soaps, especially at increased pH, act as stabilisers, and thus, act to prevent flocculation in a first step. Even more important is the effect of the double layer repulsion screening by the added electrolytes. A calculation of the Debye length  $\kappa^{-1}$  yields a value of 1.8 nm for a 2:1 electrolyte at 0.01 M and 1.4 nm for a 1:1 electrolyte at 0.05 M. In both cases, using sodium or calcium chloride, the amount of ions required to obtain destabilisation is rather high and definitely higher than in the adsorption trials in section 7.1 and 7.2. Additionally, incomplete destabilisation (0 % turbidity) is never realised. This was also observed previously and attributed to the action of acetylated galactoglucomannans (Ac-GGMs) present in unbleached TMP samples (Johnsen et al. 2006; Sundberg et al. 1994b; Tammelin et al. 2007). These hemicellulose types act as sterical stabilisers and are much less sensitive to electrolyte changes and shocks than other dispersing systems based on electrostatic stabilisation.

## 7.4 Conclusions

The development of calcium carbonate particles that can be used in pitch control was described. Optimisation of adsorption capacity and wettability in water led to an estimated surface coverage of gcc-1 of 15 % with stearic acid. Such a product showed

clearly a higher capacity for colloidal pitch materials than an untreated gcc with the same specific surface area.

The ultrafine high surface area talc had a substantially higher capacity for the colloidal wood resin than the rather coarse gcc products. However, calcium carbonate is dosed in much higher quantities than ultrafine talc grades, especially in printing and writing paper qualities. Therefore at typical respective dosing levels, the gcc might compensate or even exceed the adsorption capacities of typically applied talc grades. This observation confirms hypothesis **H7**.

Analysis of the non-adsorbed fractions showed the clear preference of talc for the dissolved carbohydrates fraction especially in the low turbidity region where the concentration of colloids is low. By contrast, both the treated and untreated gcc powders showed a rather weak preference for the dissolved fraction of the TMP.

The use of treated gcc particles for pitch control is likely to be beneficial in alkaline paper making, since there is an advantage over talc which is shifted toward dissolved substances rather than the colloidal substances as pH rises (Hypothesis **H7**). The addition of hydrophobised gcc powders in combination with talc could present a synergistic effect in pitch control due to their different affinities for the dissolved and colloidal fraction.

The study of the adsorption process of dissolved and colloidal substances from unbleached TMP filtrates onto low and high surface area talc, a natural ground calcium carbonate and a surface modified calcium carbonate has shown that for talc the specific surface area is proportional to the adsorption capacity of the mineral (Hypothesis **H4**). Talc adsorbed efficiently the colloidal fraction of the TMP filtrate and showed also the preferences to adsorb dissolved substances like galactoglucomannans, mannans and

lignin as soon as the concentration of colloidal substances also present becomes decreased.

Surface modification of the calcium carbonate provides a porous material with high surface area. Due to size exclusion the BET surface area differed from the effective particulate-adsorbing surface area. In such a case hypothesis **H4** is invalid. Nevertheless, this modified calcium carbonate efficiently adsorbed colloidal wood resin with a very high affinity, a fact that is interesting and important in water circuits. Most importantly, the modified calcium carbonate showed a strong affinity for anionic polyelectrolytes and reduced the anionic charge of the system substantially. The analysis of the remaining saccharide monomers indicated that the observed charge reduction could be related to the adsorption of arabinogalactans and xylans.

Calcium ions were observed to destabilise the colloidal fraction of wood pitch. However, the critical concentration was found to lie above the calcium concentration that is released during the adsorption experiments by the various tested calcium carbonate grades. Nevertheless, it is important to choose the right place in the paper production carefully to add such a product. Clearly, the pH should not become acidic in order to avoid dissolution of calcium.

The destabilisation induced by calcium was most accentuated under slightly alkaline conditions, which is directly linked with the low solubility of calcium-soaps of resin and fatty acids. In contrast to the behaviour of calcium, much higher concentrations of sodium were required to destabilise the colloidal material in the TMP filtrate, and, in addition, the destabilisation was more pronounced under slightly acidic and neutral conditions, where the electrostatic stabilisation induced by fatty and resin soaps is already lower than under alkaline conditions. However, the main contribution to colloidal stabilisation is due to the steric stabilisation through acetylated

galactoglucomannans, being the most common hemicellulose specie in unbleached TMP in softwood.

In summary, it can be concluded that the observed reduction of colloidal material in the TMP filtrates treated with the partially hydrophobised gcc, the regular gcc and the regular mcc was not an agglomeration process of pitch particles but an adsorption process of wood resin colloids onto mineral particles. Several points support this: i) the turbidity-based adsorption isotherms followed an operationally defined Langmuir isotherm, which suggest a formation of a colloidal monolayer, ii) the pitch particle size did not change substantially during the mineral treatment, iii) the apparent calcium ion concentration was below the required concentration to induce strong destabilisation.

## 8 Overview

### 8.1 Findings

**H1** The traditional (Hohenberger) equation relating the aspect ratio of a particle to its diameter and surface area contains false assumptions and can be improved for the case of high aspect ratio particles such as platelets and rods.

- by deriving the Hohenberger model and clearly defining the input parameters hypothesis **H1** was supported.

**H2** Particle size measurements can be made more reliable for high aspect ratio particles by a carefully reviewed choice of method.

- hypothesis **H2** was proven by including various particle sizing methods and comparison amongst each other.

**H3** Equations for aspect ratios based surface area measurements are invalid for particles which (a) agglomerate or (b) are porous.

- hypothesis **H3** was proven by including (a) a water swelling hectorite (Laponite<sup>®</sup> RD) and (b) a porous palygorskite, for which both evaluated aspect ratios differed from the data in the literature or from the one determined by image analysis.

**H4** The adsorption capacity of minerals for dissolved and colloidal substances from wood processing is proportional to the specific surface area of the minerals.

- the proportionality holds, but the constant of proportionality differs across different types of minerals, thus supporting hypothesis **H4**.



- effects of size exclusion limit accessibility of the total surface area for the adsorption of the colloidal fraction.

**H5** The adsorption mechanism of dissolved and colloidal substances from wood processing onto minerals is controlled mainly by hydrophobic interactions, and hence, hydrophobic materials preferably adsorb these substances.

- the comparison of talc and chlorite showed that the hypothesis **H5** is incorrect for the phyllosilicates
- treatment of ground calcium carbonate with stearic acid to increase the hydrophobicity of the particles showed the hypothesis **H5** is correct for cationic charged gcc particles
- preferential adsorption was observed on different types of minerals. More hydrophobic minerals adsorb besides colloidal particles also dissolved substances like hemicelluloses, whereas more hydrophilic / charged minerals seem to have a lower preference for dissolved substances and mainly adsorb colloidal pitch particles together with their hemicellulosic shell.

**H6** Process conditions such as (a) pH and (b) temperature can negatively influence the adsorption of dissolved and colloidal substances.

- increased pH levels reduce the adsorption capacity of talc for colloidal pitch and favour the adsorption of dissolved materials. This observations supports hypothesis **H6(a)**.
- increased temperatures during the adsorption process favours the adsorption capacity of dissolved and colloidal substances on talc. This finding supports **H6(b)**.

**H7** On the basis of **H4** and **H5**, tailored mineral particulates can be developed which optimise pitch adsorption while coping with modern trends in paper making.

- partial treatment of ground calcium carbonate (gcc) with stearic acid led to new particles with improved adsorption properties being as, or even more efficient as talc but offering many other properties talc does not. That all supports hypothesis **H7**.
- modified calcium carbonate (mcc) particles were shown to efficiently adsorb pitch. Size exclusion effects reduced the capacity for colloidal substances from thermo-mechanical pulp (TMP) on these mcc particles. In addition mcc particles have shown a high affinity for the colloidal fraction of TMP and additionally also showed the potential to reduce the anionic charge of TMP filtrates. All these positive observations support hypothesis **H7** further.

## 8.2 Conclusions

In Chapter 4 a model was developed to define the aspect ratios of platy- and rod-like particles by specific surface area and particle size data. The model was derived by combining two already known models and subsequently illustrated with various platy- and rod-like particles, i.e. various talc grades and Laponite<sup>®</sup> to represent platy particles, and aragonite and palygorskite to represent rod-like particles. The relation between the equivalent spherical diameter and the real particle dimensions were discussed and illustrated by measuring the particle size with various techniques (sedimentation, static and dynamic light scattering). The particle size measurement principle has to be chosen carefully to cover the relevant size range and minimise systematic error effects of the anisometric shape of the particles, which prevent the correct determination of the *esd*

under random orientation. Also care has to be taken concerning the specific surface area as input parameter, since it has to describe only the exterior surface of the particles.

Furthermore, in section 4.2 the talc grades used in chapters 6 and 7 LSA-talc and HSA-talc were characterised by the newly developed aspect ratio model.

Chapter 5 showed that the minerals, talc, chlorite and pyrophyllite, act comparably to reduce the colloidal pitch compounds in suspension taken from a TMP-filtrate. A Langmuir adsorption model approach gave reasonable regression. It would be necessary, however, to have a broader statistical range of data to confirm just one single mechanism of adsorption.

Against expectation from a mineralogical point of view, which would suggest that talc exposes approximately twice the hydrophobic surface compared to chlorite, and assuming that the hydrophobic attraction force dominates the adsorption of pitch, talc and chlorite showed similar adsorption behaviour for colloidal pitch. This means that the effectively presented hydrophobic attraction force does not match the crystallographically expected one, and that other factors play a role, including either heterogeneity of the chlorite platelet surface, geometry/association of talc particles and/or the nature of pitch. It was assumed that the colloidal pitch particles exhibit partially also an effective electro-steric/hydrophilic natural stabilisation, which, alongside the more expected lipophilic properties, results in adsorption on a variety of amphiphilic surfaces.

In section 6.1 the effect of pH was studied on the adsorption of dissolved and colloidal substances originating from TMP onto talc. The section dealt with the complex system of real pulp mill water and covered the pH range of 4 to 9, and is thus, of particular relevance in today's paper making environment.

By the application of an operationally defined Langmuir isotherm, it was seen that with increasing pH, the maximum loading and affinity of colloidal material for talc decreased. Analysis of the total organic material by COD did not show a particular change in the affinity. Thus, it was postulated that the release of dissolved molecular compounds at higher pH, such as fatty or resin acids is even more pronounced for dissolved polysaccharides with a high affinity towards the talc surface, causes a competition with the colloidal fraction and hence reduces the adsorbed amount of colloids on talc.

As a result of the current trend towards neutral or alkaline paper production, there needs to be careful consideration given such pH-induced effects, and the adjustment of the pitch control strategy made accordingly.

In section 6.2 the effect of the temperature on the adsorption of dissolved and colloidal substances from a TMP filtrate onto talc over a temperature range between 20°C and 80°C was investigated. On the one hand, studying the sorption process of the colloidal material only over the temperature range, showed a clear dependency of the process on the temperature. The higher the temperature, the more colloidal material was found to adsorb. The maximum loading of colloids nearly doubled for an increase in temperature of 60 °C. It was proposed that the main mechanism for this behaviour is the dehydration of the lyophobic colloids, their amphiphilic carbohydrate layers and the hydrophobic talc surface. On the other hand, no significant effect of the temperature was observed on the adsorption of the dissolved fraction of the TMP filtrate onto the mineral. The observations reported here also have practical implications. If the assumption of a reversible adsorption is valid then the mineral dosage point has to be chosen carefully in order to minimise desorption.

In section 7.1 the development of novel calcium carbonate particles that could be used in pitch control was described. Optimisation of adsorption capacity and wettability in water led to an optimal surface treatment of a gcc with 15 % area coverage using stearic acid. Such a product showed a higher capacity for colloidal materials than an untreated gcc with the same specific surface area. The affinity of the partially treated gcc for the colloidal fraction was slightly reduced, going towards the affinity of talc for the colloidal fraction. The capacity for colloidal substances of both, treated and untreated gcc, when compared on the basis of surface area, was higher than the capacity of talc. Furthermore, in contrast to talc, the gcc particles have a higher affinity for the detrimental colloidal fraction than talc, which can, especially under alkaline conditions, be beneficial.

In section 7.2 it was shown that the adsorption capacity of a non-porous mineral like talc is directly proportional to its surface area. Talc adsorbed the colloidal fraction of the TMP filtrate efficiently, and showed also the preference to adsorb dissolved substances, such as the galactoglucomannans, mannans and lignin, as soon as the colloidal concentration of colloidal substances is first decreased.

The chemical-free ground natural calcium carbonate was based on a material with rather low surface area, but despite this is shown to be very efficient in the adsorption of colloidal wood resin at high dosage. Due to its properties as regularly used paper filler, ground calcium carbonate can be added in much higher quantities than expensive ultrafine talc. The ground calcium carbonate has its main affinity for the colloidal fraction and only adsorbed carbohydrates and other dissolved substances in combination with the colloidal wood resin.

Surface crystal modification of the calcium carbonate was used to provide a porous material with high surface area. Due to size exclusion from the internal pores, affecting

colloidal material, the BET surface area differed from the effective adsorbing surface area. Nevertheless, this modified calcium carbonate efficiently adsorbed colloidal wood resin with a very high affinity, a fact that is interesting and important in water circuits. Most importantly, the modified calcium carbonate showed a strong affinity for anionic polyelectrolytes and reduced the anionic charge of the system substantially.

In section 7.3 calcium ions were observed to destabilise the colloidal fraction of wood pitch. However, the critical calcium ion concentration for destabilisation was found to lie above the calcium concentration that is released by the various tested calcium carbonates, what might eliminate the possibility that agglomeration processes played a deciding role in the previous adsorption experiments when using the various calcium carbonate types. Clearly, the addition point of such calcium carbonates into process has to be chosen carefully to avoid acidic pH, which could release detrimentally high calcium ion concentrations.

Throughout the adsorption studies the impact of dissolved substances, and especially of hemicellulose, was found to be a fundamental factor affecting the adsorption process. The main hemicellulose type in unbleached TMP from softwood is acetylated galactoglucomannan, which, on the one hand acts to stabilise the pitch droplets by steric interactions, and on the other hand plays also a key role in the adsorption of the colloidal part of the wood resinous compounds onto hydrophilic and hydrophobic minerals and may even form the linking unit between pitch and mineral, and so, also render the adsorption process reversible, thus allowing the various adsorption data to be described by an equilibrium process.

### ***8.2.1 Industrial applications and limitations***

The time employed to reach equilibrium in this thesis was typically 120 minutes. According to initial trials this time scale can be considered sufficient to reach

equilibrium conditions. However, contact times in paper making will be much shorter and only in the range of a few minutes. Therefore, even more important it is to have mineral with a high affinity, and, hence, an increased reaction speed.

An efficient pitch control mineral has to fulfil much more than only adsorption properties. The so-called detackification of pitch deposits and agglomerates is a key feature of talc. Therefore, the potential to reduce pitch deposits has to be considered too. A variety of deposition test are available (see section 2.2.6.2) but they all fail to reproduce the situation in a paper mill. The reason for that is the enormous mass and volume flow in a paper mill. Even if only a few ng per m<sup>3</sup> process water tend to form deposits the flow of thousands of m<sup>3</sup> will lead to the formation of deposits on the equipment. As a result only mill trials over weeks and months will reveal the potential of the newly developed mineral particles.

The use of calcium carbonate based minerals is in any case limited to neutral or alkaline conditions. Some paper mills, especially in the US, still run acidic. Also certain pulping technologies are highly acidic (such as the sulfite process). As a consequence the addition point of the pitch control additive has to be chosen carefully. A common rule is to add talc as early as possible in the process in order to guarantee sufficient contact time. This inflexibility of the newly developed calcium carbonate particles is clearly a disadvantage which has to be overcome by increased dosing amounts. An increased dosage of calcium carbonate has positive effects on certain paper properties such as light scattering, brightness or permeability. Also the increased affinity of the mcc and partially hydrophobised gcc may partially compensate for the lost contact time due to the later addition in the process.

### 8.3 Related work

In addition to the presented work in this thesis various other studies were performed. This chapter shall give a short overview of that work, and which is mostly related to the patents listed.

In a first study (Buri et al. 2007) the potential of bentonite in pitch control was evaluated also in combination with talc. Some additive effects of the two minerals were determined and showed the potential of bentonite in pitch control.

Other work (Schoelkopf et al. 2008b; Gane et al. 2008b) described a method for controlling the shape of talc particles as well as the treatment of talc in organic solvents. Both patents are closely linked with the work in Chapter 4.

A series of patents (Gane et al. 2008d; Gantenbein et al. 2008b; Gane et al. 2008c; Gane et al. 2008a) were filed concerning the use of the modified calcium carbonate for water treatment. The surface properties of the mcc can be very beneficial to remove heavy metals, and in processes for removing endocrine disrupting compounds or surfactants from aqueous systems. Also synergistic combinations with more hydrophobic adsorbents like talc and active carbon were presented.

The synergistic use of mcc in combination with talc, or other hydrophobic adsorbents, in pitch control was also studied (Gantenbein et al. 2008a). A serial treatment of TMP filtrates with talc followed by mcc was clearly more beneficial than a single treatment of either individual mineral alone.

Also another process (Buri et al. 2011) to hydrophobise calcium carbonate was tested for its efficacy in adsorbing dissolved and colloidal substances, and other organic material, from aqueous medium, and showed promising results.



During the course of this thesis a Masters study (Benecke 2006) registered at the University of Applied Science in Munich was conducted in the facilities of Omya focussing on the action of talc as sticky control agent. The work (Benecke et al. 2009) showed that talc acts specifically depending on the chemistry of the model sticky polymer. Good adsorbance was seen for polyacrylate, polyvinyl acetate, colophonium (resin) and styrene-butadiene, whereas adsorption was less effective in the cases of fatty acid ester and mineral oil/silicone based defoamers.

## **8.4 Future work**

After this study some open questions remain, as well as the generation of new questions to be asked.

The model presented for the aspect ratio could be expanded to other minerals such as kaolin, smectite or aragonitic pcc qualities with higher aspect ratios.

The difference between talc and chlorite in the adsorption of pitch could be studied in more depth by refining the isotherm. Additionally, a detailed chemical analysis could reveal preferred adsorption tendencies and explain the observed similarity in pitch adsorption for the two mineral types.

A chemical analysis of the adsorption process under different pH and temperature conditions could confirm the proposed mechanisms based on the applied analysis techniques.

The partially hydrophobised calcium carbonate should be applied in a paper mill environment to provide data to investigate its suitability for pitch control in practice.

The size exclusion effect observed for the modified calcium carbonate and colloidal pitch fraction could be investigated in more depth by testing modified calcium carbonate with changing pore sizes. Also defined polymer particles, such as polystyrene

spheres with varying sizes, could be used for a better understanding of the size exclusion effect.

More detailed surface chemistry and surface energy studies made on the microscale could reveal interesting duality in respect to surface adsorption potential, especially when comparing the affinity of chlorite and talc, with their crystallographically differing theoretical surface energies, to complex pitch.

Similarly, microscale studies of the surface charge distribution on modified calcium carbonate could elucidate the simultaneous attraction for anionic and cationic species.

Extraction of the naturally occurring surface active agents could facilitate a better understanding of the impact of cation exchange and cloud point determination. Such findings could establish the role of increasing concentration of divalent ion, likely to be occurring as the closure of the water circuit in industrial installations progresses.

Many interesting experimental trends are presented in this work which could usefully be investigated further. This could be done in conjunction with a more detailed investigation of the fundamental physical processes involved. An example is the variation of electrophoretic mobility with ionic strength (Figure 7-25), and whether the nature of that variation does indeed stem from Equation 7-2.

## 9 Literature

- Ackermann, Ch., Putz, H.-J. and Götttsching, L.** (1996): Herkunft und Gehalt klebender Verunreinigungen im Graphischen Altpapier, Wochenbl. Papierfabr., 11, 508.
- Adamczyk, Z., Nattich, M. and Barbasz, J.** (2009): Deposition of colloid particles at heterogeneous and patterned surfaces, Adv. Colloid Interface Sci., 147-148, 2.
- Adamczyk, Z., Weronki, P. and Musial, E.** (2002): Colloid particle adsorption at random site (Heterogeneous) surfaces, J. Colloid Interface Sci., 248, 67.
- Adamczyk, Z., Zembala, M., Siwek, B. and Warszynski, P.** (1990): Structure and ordering in localized adsorption of particles, J. Colloid Interface Sci., 140, 123.
- Adamson, A. W.** (1990): "Physical chemistry of surfaces", Wiley, New York.
- Aitchison, J. and Brown, J. A.** (1957): "The lognormal distribution", Cambridge University Press, Cambridge, UK.
- Allen, L. H.** (1977): Pitch particle concentration: an important parameter in pitch problems, Trans. CPPA, 3, 32.
- Allen, L. H.** (1980): Mechanism and control of pitch deposition in newsprint mills, Tappi J., 63, 81.
- Allen, L. H., Cavanagh, W. A., Holton, J. E. and Williams, G. R.** (1993): New understanding of talc addition may help improve control of pitch, Pulp Paper, 13, 89.
- Allen, L. H. and Douek, M.** (1993): Effectiveness of talc for pitch control in kraft pulp manufacture, J. Pulp Paper Sci., 19, 131.

- Allen, L. H. and Filion, D.** (1996): A laboratory white pitch deposition test for screening additives, *Tappi J.*, 79, 226.
- Allen, L. H. and Lapointe, C. L.** (2005): Effectiveness of retention aids for pitch control in TMP newsprint manufacture. Part I: low shear, *Pulp Paper*, 106, 102.
- Allen, T. A.** (1990): "PARTICLE SIZE MEASUREMENT", Chapman and Hall, London,
- Aris, R.** (1957): On shape factors for irregular particles - I. The steady-state problem. Diffusion and reaction, *Chem. Eng. Sci.*, 6, 262.
- Asselman, T. and Garnier, G.** (2000): Adsorption of model wood polymers and colloids on bentonites, *Colloids Surf. A*, 168, 175.
- Auhorn, W. and Melzer, J.** (1979): Untersuchung von Störsubstanzen in Geschlossenen Kreislaufsystemen, *Wochenbl. Papierfabr.*, 107, 493.
- Baak, T. and Gill, G. J.** (1971): The adsorptive property of talc and its application to pitch control, *Paperi Puu*, 53, 449.
- Back, E. L. and Allen, L. H.** (2000): "Pitch Control, Wood Resin and Deresination", Tappi Press, Atlanta.
- Bailey, S. W.** (1988): Chlorites: structures and crystal chemistry, *Rev. Min. Geochem.*, 19, 347.
- Baltar, C. A. M., da Luz, A. B. and Baltar, L. M.** (2009): Influence of morphology and surface charge on the suitability of palygorskite as drilling fluid, *Appl. Clay Sci.*, 42, 597.
- Barber, P. W. and Hill, S. S.** (1990): "Light scattering by particles: computational methods", World Scientific, Singapore.

- Barret, E. P., Joyner, L. G. and Halenda, P. P.** (1951): The determination of pore volume and area distributions in porous substances. I. Computations from nitrogen isotherms, *J. Am. Chem. Soc.*, 73, 373.
- Baudet, G., Bizi, M. and Rona, J. P.** (1993): Estimation of the average aspects ratio of lamellae-shaped particles by laser diffractometry, *Part. Sci. Tech.*, 11, 73.
- Benecke, F.** (2006): Wirkungsweise von Talkum als sticky-Bekämpfungsmittel, MSc Thesis, Fachhochschule München.
- Benecke, F., Gantenbein, D., Schoelkopf, J., Gane, P. A. C. and Gliese, T.** (2009): Organic contaminants in recycled paper: a model study of the adsorbent properties of talc for idealised component suspensions, *Nord. Pulp Pap. Res. J.*, 24, 219.
- Bergaya, F., Theng, B. K. G., and Lagaly, G.** (2006): "Handbook of Clay Science", Elsevier, New York.
- Beuleke, E. and Burri, P.** (1999): Coating pigment concepts of the future, *Wochenbl. Papierfabr.*, 127, 1482.
- Biza, P.** (1997): Talc solutions for deposition problems in pulp and paper processes, Use of minerals in papermaking, Manchester, UK, February 26-27, 1997, PIRA, Letherhead, UK, pp. 193-200.
- Biza, P.** (2001): Talc - A modern solution for pitch and stickies control, *Pap. Technol.*, 42, 22.
- Boardman, D.** (1996): The use of organophilic mineral particulates in the control of anionic trash like pitch, Tappi Papermakers Conference, Philadelphia, PA, US, March 24-27, 1996, Tappi Press, Atlanta, US, pp. 533-538.

- Bonn, D., Kellay, H., Tanaka, H., Wegdam, G. and Meunier, J.** (1999): Laponite: what is the difference between a gel and a glass, *Langmuir*, 15, 7534.
- Bos, J. H., Veenstra, P., Verhoeven, H., and de Vos, P. D.** (2006): "Das Papierhandbuch", Wolters-Noordhoff, Houten.
- Brownsey, G. J. and Jennings, B. R.** (1978): Electrically induced variations of rayleigh scattering: simultaneous monitoring of the intensity and spectral width from macromolecular solutions, *J. Chem. Phys.*, 68, 926.
- Brunauer, St., Emmett, P. H. and Teller, E.** (1938): Adsorption of Gases in multimolecular layers, *J. Am. Chem. Soc.*, 60, 309.
- Buri, M., Karth, B., Gantenbein, D., and Gane, P. A. C.**(2007): Method for processing crude bentonite, Patent No. EP2144850,
- Buri, M., Rentsch, S., Gane, P. A. C., Gantenbein, D., and Schoelkopf, J.,**(2011): Process for the preparation of surface-treated calcium carbonate material and use of same in the control of organic material in an aqueous medium, Patent No. WO2012010466,
- Capozzi, A. M. and Rende, D. S.** (1995): Particle management: Innovations in sticky control, Recycling Symposium, New Orleans, LA, US, February 20-23, 1995, Tappi Press, Atlanta, US, pp. 79-89.
- Carre, B., Brun, J. and Galland, G.** (1998): The incidence of the destabilization of the pulp suspension on the deposition of secondary stickies - new test shows propensity for stickies formation, *Pulp Paper*, 99, 75.
- Casal, J., Lucas, A. and Arnaldos, J.** (1985): A new method for the determination of shape factor and particle density, *Chem. Eng. J.*, 30, 155.

- Cathie, K.** (1994): The effect of packaging adhesives on wastepaper recycling - A review, *Int. J. Adhes. Adhes.*, 14, 63.
- Cathie, K., Haydock, R. and Dias, I.** (1992): Understanding the fundamental factors influencing stickies formation and deposition, *Pulp Paper*, 93, 157.
- Champion, J. V., Downer, D., Meeten, G. H. and Gate, L. F.** (1978): Magnetic and optical properties of kaolinite particles in aqueous dispersion, *J. Chem. Soc., Faraday Trans.*, 2, 843.
- Champion, J. V., Meeten, G. H., Moon, B. R. and Gate, L. F.** (1979): Optical Extinction of Randomly Orientated and Shear Flow Orientated Colloidal Kaolinite Particles, *J. Chem. Soc., Faraday Trans.*, 2, 780.
- Chang, Y. C.** (1985): An analytical method for determining pitch adsorptivity, *Tappi J.*, 68, 112.
- Charnay, C., Lagerge, S. and Partyka, S.** (2001): Assessment of the surface heterogeneity of talc materials, *J. Colloid Interf. Sci.*, 233, 250.
- Compton, R. G. and Brown, C. A.** (1995): The inhibition of calcite dissolution / precipitation: 1,2-Dicarboxylic acids, *J. Colloid Interf. Sci.*, 170, 586.
- Conley, R. F.** (1966): Statistical distribution patterns of particle size and shape in the Georgia kaolins, *Clay. Clay Miner.*, 14, 317.
- Derjaguin, B. and Landau, L.** (1941): Theory of the stability of strongly charged lyophobic sols and of the adhesion of strongly charged particles in solutions of electrolytes, *Acta Physicochim. URSS*, 14, 633.

- Dixit, M. K., Maleike, T. A. and Jackowski, C. W.** (1991): Retention strategies for Alkaline fine papermaking with secondary fiber: a case history, *Tappi J.*, 74, 107.
- Doshi, M. R.** (1991): Properties and control of stickies, *Progress in Paper Recycling*, 1, 54.
- Douek, M. and Allen, L. H.** (1983): A laboratory test for measuring calcium soap deposition from solutions of tall oil, *Tappi J.*, 66, 105.
- Douek, M. and Allen, L. H.** (1991): Some aspects of pitch control with talc in unbleached kraft pulps, *J. Pulp Paper Sci.*, 17, 171.
- Douek, M. and Guo, X.-Y.** (1997): An overview of the chemical nature of deposits/stickies in mills using recycled fibre, *TAPPI Recycling Symposium*, April 14-16, 1997, Chicago, IL, US, Tappi Press, Atlanta, US, pp. 313-330.
- Douillard, J. M., Malandrini, H., Zoungrana, T., Clauss, F. and Partyka, S.** (1994): Surface tension of talc and talc-chlorite mixtures, *J. Thermal Anal. Calorim.*, 41, 1205.
- Dreisbach, D. D. and Michalopoulos, D. L.** (1989): Understanding the behavior of pitch in pulp and paper mills, *Tappi J.*, 72, 129.
- Dunlop-Jones, N., Douek, M. and Allen, L. H.** (1987): A new method for measuring retention of talc used for pitch control in bleached Kraft pulp and newsprint mills, *J Pulp Pap. Sci.*, 13, 18.
- Eadie, G. S.** (1942): The inhibition of cholinesterase by physostigmine and prostigmine, *J. Biol. Chem.*, 146, 85.



- Ekman, R. and Holmbom, B.** (1989): Analysis by gas chromatography of the wood extractives in pulp and water samples from mechanical pulping of Spruce, Nord. Pulp Paper Res. J., 4, 16.
- Evans, B. W. and Guggenheim, S.** (1988): Talc, pyrophyllite, and related minerals, Rev. Min. Geochem., 19, 225.
- Farley, E. C.** (1977): Causes of pitch problems and a laboratory method of evaluating control agents, TAPPI Papermakers Conference, Chicago, IL, US, April 8-20, 1977, Tappi Press, Atlanta, US, pp. 23-32.
- Fenter, P. and Sturchio, N. C.** (1999): Structure and growth of stearate monolayers on calcite: first results of an in situ x-ray reflectivity study, Geochim. Cosmochim. Acta, 63, 3145.
- Ferrage E., Martin F., Petit S., Pejo-Soucaille S., Micoud P., Fourty G., Ferret J., Salvi S., De Parseval P. and Fortune J.P.** (2003): Evaluation of talc morphology using FTIR and H/D substitution, Clay Miner., 48, 141.
- Fowkes, F. M.** (1963): Additivity of intermolecular forces at interfaces. I. Determination of the contribution to surface and interfacial tensions of dispersion forces in various liquids, J. Phys. Chem., 67, 2538.
- Freundlich, H.** (1907): Über die Adsorption in Lösungen, Z. Phys. Chem., 57, 385.
- Gane, P. A. C.** (2001): Mineral pigments for paper: structure, function and development potential (Part I), Wochenbl. Papierfabr., 129, 110.
- Gane, P. A. C., Buri, M. and Blum, R.** (1999): Pigment co-structuring: new opportunities for higher brightness coverage and print-surface design,

International Symposium on Paper Coating Coverage, Helsinki, FI, February 16-17, 1999, AEL/METSKO, Helsinki, FI, pp. 2-17.

- Gane, P. A. C. and Coggon, L.** (1987): Coating blade Geometry: its effect on coating color dynamics and coated sheet properties, *Tappi J.*, 70, 87.
- Gane, P. A. C., Gantenbein, D., and Schoelkopf, J.** (2008a): Surface-reacted calcium carbonate in combination with hydrophobic adsorbents for water treatment, Patent No. WO2008151991,
- Gane, P. A. C., Gantenbein, D., and Schoelkopf, J.** (2008b): Treatment of talc in a solvent, Patent No. WO2008148666,
- Gane, P. A. C., Hooper, J. J. and Grunewald, A.** (1997): Coating pigment orientation: a comparative analysis of the application mechanisms and properties of blade and roll coatings, *Tappi J.*, 80, 109.
- Gane, P. A. C., Kettle, J. P., Matthews, G. P. and Ridgway, C. J.** (1996): Void space structure of compressible polymer spheres and consolidated calcium carbonate paper-coating formulations, *Ind. Eng. Chem. Res.*, 35, 1753.
- Gane, P. A. C., Schoelkopf, J., Gantenbein, D., and Gerard, D. E.** (2008c): Process for the removal of endocrine disrupting compounds, Patent No. EP2180943,
- Gane, P. A. C., Schoelkopf, J., Gantenbein, D., and Gerard, D. E.** (2008d): Surface treated calcium carbonate and its use in waste water treatment, Patent No. EP2180944,
- Gane, P. A. C. and Watters, P.** (1989): Pigment particle orientation: an analysis of the opportunities for optimising blade coater runnability and coated sheet properties by controlled flow geometry, *Paperi Puu*, 5, 517.

**Gantenbein, D., Schoelkopf, J., and Gane, P. A. C. (2008a):** Process for the control of pitch, Patent No. WO2008113839,

**Gantenbein, D., Schoelkopf, J., and Gane, P. A. C. (2008b):** Process for the purification of water, Patent No. EP2180945,

**Gantenbein, D., Schoelkopf, J., Gane, P. A. C. and Matthews, G. P. (2010):**  
Influence of pH on the adsorption of dissolved and colloidal substances in a thermo mechanical pulp filtrate onto talc, Nord. Pulp Paper Res. J., 25, 288.

**Gantenbein, D., Schoelkopf, J., Hunziker, P., Matthews, G. P. and Gane, P. A. C. (2009):** Efficiency of colloidal pitch Adsorption onto phyllosilicates: comparing talc, chlorite and pyrophyllite, Nord. Pulp Paper Res. J., 24, 448.

**Gantenbein, D., Schoelkopf, J., Matthews, G. P. and Gane, P. A. C. (2011a):**  
Determining the size distribution-defined aspect ratio of platy particles, Appl. Clay Sci., 53, 544.

**Gantenbein, D., Schoelkopf, J., Matthews, G. P. and Gane, P. A. C. (2011b):**  
Determining the size distribution-defined aspect ratio of rod-like particles, Appl. Clay Sci., 53, 538.

**Gantenbein, D., Schoelkopf, J., Matthews, G. P. and Gane, P. A. C. (2011c):**  
Influence of the temperature on the adsorption of dissolved and colloidal substances from a thermo mechanical pulp filtrate onto talc, Nord. Pulp Pap Res. J., 26, 329.

**Gantenbein, D., Schoelkopf, J., Matthews, G. P. and Gane, P. A. C. (2012a):** The development of hydrophobised ground calcium carbonate particles for the effective adsorption of dissolved and colloidal substances (DCS) from thermo mechanical pulp (TMP) filtrates, Nord. Pulp Paper Res. J., 27, 93.

- Gantenbein, D., Schoelkopf, J., Matthews, G. P. and Gane, P. A. C. (2012b):** The use of porous high surface area calcium carbonate for the adsorption of dissolved and colloidal substances from thermo mechanical pulp filtrates, accepted in Nord. Pulp Paper Res. J.
- Garver, T. M., and Yuan, H. (2002):** Measuring the response of pitch control strategies, Pulp Paper, 103, 24.
- Gavelin, G. (1949):** The effect of mill water on pitch troubles in paper mills, Pulp Paper, 50, 59.
- Giese, R. F., Costanzo, P. M. and van Oss, C. J. (1991):** The surface free energies of talc and pyrophyllite, Phys. Chem. Miner., 17, 611.
- Gill, G. J. (1974):** Controlling pitch deposits in pulp mills with talc, Pulp Paper, 48, 104.
- Glazer, J. A. (1991):** Overview of deposit control, Tappi J., 74, 72.
- Gribble, C. M. (2011),** Surface adsorption and pore-level properties of mineral and related systems of relevance to the recycling of paper, Ph.D. Thesis, University of Plymouth, Plymouth, United Kingdom.
- Gribble, C. M., Matthews, G. P., Gantenbein, D., Turner, A., Schoelkopf, J. and Gane, P. A. C. (2010):** Adsorption of Surfactant-Rich Stickies Onto Mineral Surfaces, J. Colloid Interface Sci., 352 , 483.
- Gribble, C. M., Matthews, G. P., Turner, A., Gantenbein, D., Schoelkopf, J. and Gane, P. A. C. (2011):** Equilibrium coefficients for the adsorption of colloidal stickies onto mineral suspension particulates to improve paper recycling, Nord. Pulp Paper Res. J., 26, 421.

- Groszek, A. J. and Partyka, S.** (1993): Measurements of hydrophobic and hydrophilic surface sites by flow microcalorimetry, *Langmuir*, 9, 2721.
- Gruber, E., Gattermayer, J. and Pätzold, R.** (2001): Zur Bildung von Ablagerungen durch mikrodisperse klebende Verunreinigungen und Füll- und Faserstoffe, *Wochenbl. Papierfabr.*, 20, 1326.
- Guera, N., Schoelkopf, J., Gane, P. A. C. and Rautma, I.** (2005): Comparing colloidal pitch to adsorption on different talcs, *Nord. Pulp Paper Res. J.*, 20, 156.
- Gustafsson, Ch., Tammela, V. and Kahila, S.** (1952): On pitch troubles caused by sulphite pulp, *Paper Trade J.*, 124, 38.
- Hamilton, K. A. and Lloyd, J. A.** (1984): Measuring the effectiveness of talc for pitch control, *Appita*, 37, 733.
- Hassler, T.** (1988): Pitch deposition in papermaking and the function of pitch-control agents, *Tappi J.*, 71, 195.
- Hayes, P. J. and Kauffman, T. F.** (1993): The impact of hot-melt adhesives on the paper recycling process, *Tappi J.*, 76, 162.
- Helmy, A. K., de Buseti, S. G. and Ferreiro, E. A.** (2007): The surface energy of palygorskite, *Powder Technol.*, 171, 126.
- Henry, D. C.** (1931): The cataphoresis of suspended particles, *Proc. Roy. Soc. (London)*, A133, 106.
- Henry, W.** (1803): Experiments on the quantity of gases absorbed by water at different temperatures and under different pressures, *Phil. Trans. Roy. Soc.*, 93, 29.
- Hiemenz, P. C. and Rajagopalan, R.** (1997): "Principles of colloid and surface chemistry", CRC Press, Boca Raton.

- Hinrichsen, E. L., Feder, J. and Jossang, T.** (1986): Geometry of Random Sequential Adsorption, *J. Stat. Phys.*, 44, 793.
- Hofstee, B. H. J.** (1959): Non-inverted plots in enzyme kinetics, *Nature*, 184, 1296.
- Hohenberger, W.** (2001): "Plastics Additives Handbook", Hanser Publishers, Munich.
- Holmbom, B.** (1977): Improved gas chromatographic analysis of fatty and resin acid mixtures with special reference to tall oil, *J. Am. Oil Chem. Soc.*, 54, 289.
- Holmbom, B. and Sundberg, A.** (2003): Dissolved and colloidal substances accumulating in papermaking process water, *Wochenbl. Papierfabr.*, 131, 1305.
- Holton, J. E. and Moebus, C. R.** (1982): Control of pitch, stickies, gunk and tramp organics in pulp and paper mills, *Pulp Paper*, 83, 52.
- Holysz, L. and Chibowski, E.** (1994): Surface free energy components of calcium carbonate and their changes due to radiofrequency electric field treatment, *J. Colloid Interface Sci.*, 164, 245.
- Horn, D.** (1978): Optisches Zweistrahlverfahren zur Bestimmung von Polyelektrolyten in Wasser und zur Messung der Polymeradsorption an Grenzflächen, *Prog. Colloid Polym. Sci.*, 65, 251.
- Horn, D.** (1979): Über die Wirkungsweise organischer Polyelektrolyte bei der Papierherstellung, *Zellstoff und Papier*, 28, 129.
- Horvath, A. E.** (2003), Appropriate conditions for polyelectrolyte titration to determine the charge of cellulosic fibers, Ph.D. Thesis, Royal Institute of Technology, Stockholm, Sweden.
- Hubbe, M. A., Rojas O.J. and Venditti R.A.** (2006): Control of tacky deposits on paper machines - A review, *Nord. Pulp Paper Res. J.*, 21, 154.

- Hückel, E.** (1924): Die Kataphorese der Kugel, *Phys. Z.*, 25, 204.
- Hughes, D. A.** (1977): A method for determining the pitch adsorption characteristics of mineral powders, *Tappi J.*, 60, 144.
- Inoue, S.** (1998): Measurement and analysis of light scattering characteristics of paper by modulation transfer function, Pan-Pacific and International Printing and Graphic Arts Conference, October 6-8, 1998, Québec, Canada, CPPA, Montreal, Canada, pp. 155-163.
- Janczuk, B., Bialopiotrowicz, T. and Chibowski, E.** (1987): Interpretation of the contact angle in marble/organic liquid film-water system, *Mater. Chem. Phys.*, 16, 489.
- Jenkins, P. and Ralston, J.** (1998): The adsorption of a polysaccharide at the talc-aqueous solution interface, *Colloid. Surf. A*, 139, 27.
- Jennings, B. R.** (1993): Size and thickness measurement of polydisperse clay samples, *Clay Miner.*, 28, 485.
- Jennings, B. R. and Parslow, K.** (1988): Particle size measurements: the equivalent spherical diameter, *Proc. Roy. Soc. A*, 419, 139.
- Johnsen, I. A., Stenius, P., Tammelin, T., Osterberg, M., Johansson, L. and Laine, J.** (2006): The Influence of dissolved substances on resin adsorption to TMP fine material, *Nord. Pulp Paper Res. J.*, 21, 629.
- Kallio, T., Kekkonen, J. and Stenius, P.** (2004): The formation of deposits on polymer surfaces in paper machine wet end, *J. Adhesion*, 80, 933.
- Kekkonen, J. and Stenius, P.** (2001): Adsorption of wood materials on silica surface with a wettability Gradient, *Nord. Pulp Paper Res. J.*, 16, 4.

- Keller, D. S. and Luner, P.** (2000): Surface energetics of calcium carbonates using inverse gas chromatography, *Colloids Surf. A*, 161, 401.
- Keller, G. and Trojna, G.** (2001): Laser systems used for sticky measurement, *Assoc. Tech. Ind. Pap.*, 56, 26.
- Kerman, N., Eronen, H., Burke, T. and Vanninen, S.P.** (2006): Neue Ansätze bei der Auswahl und Optimierung von Fixiermitteln zur Pitch- und Sticky-Kontrolle bei unterschiedlichen Faserstoffsystemen, *Wochenbl. Papierfabr.*, 21, 1203.
- Kinniburgh, D. G.** (1986): General purpose adsorption isotherms, *Environ. Sci. Technol.*, 20, 895.
- Kiser, A. R.** (1976): The use of talc to control pitch deposition, TAPPI Conference: Alkaline Pulping and Testing, September 13-15, 1976, Dallas, TX, US, Tappi Press, Atlanta, US, pp. 133-134.
- Koppel, D. E.** (1972): Analysis of macromolecular polydispersity in intensity correlation spectroscopy. The method of cumulants, *J. Chem. Phys.*, 57, 4814.
- Kröhl, T., Lorencak, A., Gierluski, H., Eipe, L. H. and Horn, D. A.** (1994): A new laser-optical method for counting colloidal dispersed pitch, *Nord. Pulp Paper Res. J.*, 9, 26.
- Kroon, M., Vos, W.L. and Wegdam, G.H.** (1998): Structure and formation of a gel of colloidal disks, *Phys. Rev. E*, 57, 1962.
- Kroon, M., Wegdam, G. and Sprik, R.** (1996): Dynamic light scattering studies on the sol-gel transition of a suspension of anisotropic colloidal particles., *Phys. Rev. E*, 54, 6541.



- Langmuir, I.** (1916): The constitution and fundamental properties of solids and liquids, J. Am. Chem. Soc., 38, 2221.
- Lawler, D. M.** (1995): "Encyclopedia of Analytical science", Academic Press, London.
- Lee, H. K. and Sumimoto, M.** (1991): Pitch problems in pulping and bleaching of sarawak hardwoods. Part 4. An efficient method of resin speck removal from dipterocarpaceae pulps, Appita, 44, 201.
- Lehmonen, J., Houni, J., Raiskinmäki, P., Vähäsalo, L. and Grönroos, A.** (2009): The effects of pH on the accumulation of fines, dissolved and colloidal substances in the short circulation of papermaking, J. Pulp Paper Sci., 35, 46.
- Li, L., Collis, A. and Pelton, R.** (2002): A new analysis of filler effects on paper strength, J. Pulp Paper Sci., 28, 267.
- Lide, D. R.** (2002): "CRC Handbook of Chemistry and Physics", CRC Press, London.
- Likitalo, M. and Gantenbein, D.** (2009): "Pigment Coating and Surface Sizing of Paper", Paperi ja Puu Oy, Helsinki, pp. 110-124.
- Lindberg, L.E., Vahasalo, L.J. and Holmbom, B.** (2004): Flow cytometry of bacteria and wood resin particles in paper production, Nord. Pulp Paper Res. J., 19, 412.
- Lindström, M., Ödberg, L. and Stenius, P.** (1988): Resin and fatty acids in kraft pulp washing: physical state, colloid stability and washability, Nord. Pulp Paper Res. J., 3, 100.
- Lineweaver, H. and Burk, D.** (1934): The determination of enzyme dissociation constants, J. Am. Chem. Soc., 56, 658.
- Lloyd, J. A. and Stratton, L. M.** (1986): The determination of extractives and pitch by chromic acid oxidation, Appita, 39, 287.

- Lohmander, S.** (2000): Aspect ratios of pigment particles determined by different methods, *Nord. Pulp Paper Res. J.*, 15, 221.
- Lucas, R.** (1918): Ueber das Zeitgesetz des Kapillaren Aufstiegs von Flüssigkeiten, *Kolloid Z.*, 23, 15.
- Maat, P. and Yordan, J. L.** (1998): Use of the microfoam (doshi) method for assessing the effectiveness of talc in controlling stickies, TAPPI Recycling Symposium, March 8-12, 1998, New Orleans, LA, US, Tappi Press, Atlanta, US, 197-203.
- Mal, D., Sinha, S., Middy, T. R. and Tarafdar, S.** (2008): Desiccation crack patterns in drying laponite gel formed in an electrostatic field, *Appl. Clay Sci.*, 39, 106.
- Malandrini, H., Clauss, F., Partyka, S. and Douillard, J. M.** (1997): Interactions between talc particles and water and organic solvents, *J. Colloid Interface Sci.*, 194, 183.
- McGregor, C. and Philippaerts, J.** (1998): A systematic approach to preventing pitch and stickies deposition in mill furnishes, 51e Congress Annuel ATIP.
- McLean, D. S., Stack, K. R. and Richardson, D. E.** (2005): The effect of wood extractives composition, pH and temperature on pitch deposition, *Appita*, 58, 52.
- Menke, L.** (1998): Mikro-Stickies - Störenfriede im Wasserkreislauf, *Wochenbl. Papierfabr.*, 126, 187.
- Michot, L. J., Villieras, F., Francois, M., Yvon, J., Le Dred, R. and Cases, J. M.** (1994): The structural microscopic hydrophilicity of talc, *Langmuir*, 10, 3765.
- Mie, G.** (1908): Beiträge zur Optik trüber Medien, speziell kolloidaler Metallösungen, *Annalen der Physik, Ann. Phys-Leipzig*, 330, 377.

- Moebius, C. H.** (1978): Ursachen und Bekaempfung von Harzschwierigkeiten, Wochenbl. Papierfabr., 23, 889.
- Morris, H. H., Sennett, P. and Drexel, R. J.** (1965): Delaminated clays - physical properties and paper coating properties, Tappi J., 48, 92.
- Mosbye, J., Foss, H. M., Laine, J. and Moe, S.** (2003): Interaction between model colloidal wood resin, fillers and dissolved substances, Nord. Pulp Paper Res. J., 18, 194.
- Mourchid, A., Delville, A., Lambard, J., Lécolier, E. and Levitz, P.** (1995): Phase diagram of colloidal dispersions of anisotropic charged particles: equilibrium properties, structure, and rheology of laponite suspensions, Langmuir, 11, 1942.
- Mourchid, A. and Levitz, P.** (1998): Long-term gelation of laponite aqueous dispersions, Phys. Rev. E, 57, 4887.
- Murray, H. H. and Kogel, J. E.** (2005): Engineered clay products for the paper industry, Appl. Clay Sci., 29, 199.
- Naito, M., Hayakawa, O., Nakahira, K., Mori, H. and Tsubaki, J.** (1998): Effect of particle shape on the particle size distribution measured with commercial equipment, Powder Technol., 100, 52.
- Napper, D. H.** (1983): "Polymeric stabilization of colloidal dispersions", Academic Press, London.
- Nyren, V. and Back, E. L.** (1958a): The ionization constant, solubility product, and solubility of abietic and dehydroabietic acid, Acta Chem. Scand., 12, 1516.
- Nyren, V. and Back, E. L.** (1958b): The ionization constant, solubility product, and solubility of lauric and myristic acids, Acta Chem. Scand., 12, 1305.

- Opedal, M. T., Stenius, P. and Johansson, L.** (2011): Colloidal stability and removal of extractives from process water in thermomechanical pulping, *Nord. Pulp Paper Res. J.*, 26, 248.
- Orsa, F. and Holmbom, B.** (1994): A convenient method for the determination of wood extractives in papermaking process waters and effluents, *J. Pulp Paper Sci.*, 20, 361.
- Osman, M. A. and Suter, U. W.** (2002): Surface treatment of calcite with fatty acids: structure and properties of the organic monolayer, *Chem. Mater.*, 14, 4408.
- Otero, D., Sundberg, K., Blanco, A., Negro, C., Tijero, J. and Holmbom, B.** (2000): Effects of wood polysaccharides on pitch deposition, *Nord. Pulp Paper Res. J.*, 15, 607.
- Pabst, W. and Berthold, C.** (2007): A simple approximate formula for the aspect ratio of oblate particles, *Part. Part. Syst. Charact.*, 24, 458.
- Pabst, W., Berthold, C. and Gregorova, E.** (2006a): Size and shape characterization of polydisperse short-fiber systems, *J. Eur. Ceram. Soc.*, 26, 1121.
- Pabst, W., Berthold, C. and Gregorova, E.** (2007): Size and shape characterization of oblate and prolate particles, *J. Eur. Ceram. Soc.*, 27, 1759.
- Pabst, W., Gregorova, E. and Berthold, C.** (2006b): Particle shape and suspension rheology of short-fiber systems, *J. Eur. Ceram. Soc.*, 26, 149.
- Pabst, W., Kunes, K., Gregorova, E. and Havrda, J.** (2001): Extraction of shape information from particle size measurements, *Br. Ceram. T.*, 100, 106.
- Pabst, W., Kunes, K., Havrda, J. and Gregorova, E.** (2000): A note on particle size analyses of kaolins and clays, *J. Eur. Ceram. Soc.*, 20, 1429.

- Paltakari, J** (2009): "Pigment coating and surface sizing", Paperi ja Puu Oy, Helsinki, Finland.
- Papirer, E., Balard, H., Jagiello, J., Baeza, R., and Clauss, F.** (1992): "Chemically Modified Surfaces", Elsevier, Amsterdam, pp. 351-368.
- Papirer, E., Schultz, J. and Turchi, C.** (1984): Surface properties of a calcium carbonate filler treated with stearic acid, *Eur. Polym. J.*, 20, 1155.
- Parmentier, C. J.** (1973): Electron microscopic observation of pitch problems associated with closed water systems, *Tappi J.*, 56, 80.
- Parmentier, C. J.** (1979): The adsorptive concept of pitch control with talc, case histories using new methods of analysis, Tappi Papermakers Conference, April 9-11, 1979, Boston, MA, US, Tappi Press, Atlanta, US, pp. 165-176.
- Patel, S. N. and Banerjee, S.** (1999): Deposition of hot melt and wax on surfaces, *Tappi J.*, 82, 99.
- Pelton, R. and Lawrence, D.** (1991): A new laboratory approach for evaluating kraft mill pitch deposit control additives, *J. Pulp Paper Sci.*, 17, 80.
- Pereira, F. W.** (1990): Expanding the talc pitch-control market in Japan, *Industr. Miner.*, 55, 55.
- Podczek, F.** (1997): A shape factor to assess the shape of particles using image analysis, *Powder Technol.*, 93, 47.
- Putz, H.-J., Hamann, A. and Gruber, E.** (2003): Untersuchungen zur Stickybildung und Stickybekämpfung, *Wochenbl. Papierfabr.*, 131, 883.
- Qin, M., Hannuksela, T. and Holmbom, B.** (2004): Deposition tendency of TMP resin and related model mixtures, *J. Pulp Paper Sci.*, 30, 279.

- Randall, M. G.** (1989): "Particle packing characteristics", Metal Powder Industries, New Jersey.
- Ravnjak, D., Zule, J. and Moze, A.** (2003): Removal of detrimental substances from papermaking process water by the use of fixing agents, *Acta Chim. Sloven.*, 50, 149.
- Redlich, O. and Peterson, D. L.** (1959): A useful adsorption isotherm, *J. Phys. Chem.*, 63, 1024.
- Reynolds, J. and Yordan, J.** (2002): Laboratory and mill experiences with a novel talc for deposit control of pulps rich in anionic trash, 88th PAPTAC Annual meeting, January 29-31, 2002, Montréal, Canada, pp. 53-57.
- Ridgway, C. J., Gane, P. A. C. and Schoelkopf, J.** (2004): Modified calcium carbonate coatings with rapid absorption and extensive liquid uptake capacity, *Colloid. Surf. A*, 236, 91.
- Rogan, K. R.** (1994): Adsorption of oleic acid and triolein onto various minerals and surface treated minerals, *J. Colloids Interface Sci.*, 272, 82.
- Saarimaa, V., Vahasalo, L., Sundberg, A., Pranovich, A., Holmbom, B., Svedman, M. and Orsa, F.** (2006): The influence of pectic acids on aggregation and deposition of colloidal pitch, *Nord. Pulp Paper Res. J.*, 21, 613.
- Saltsman, W. and Kuiken, K. A.** (1959): Estimation of tall oil in sulphate black liquor, *Tappi J.*, 42, 873.
- Salvador, A. R., Soria, F. G. O. and Sierra, A. C.** (1992): Modelling resin extraction from wood different solvents, *Tappi J.*, 75, 141.

- Samiey, B. and Golestan, S.** (2010): Adsorption of triton X-100 on silica gel: effects of temperature and alcohols, *Cent. Eur. J. Chem.*, 8, 361.
- Scatchard, G.** (1949): The attractions of proteins for small molecules and ions, *Annals New York Acad. Sci.*, 51, 660.
- Schaaf, P. and Talbot, J.** (1989): Surface exclusion effects in adsorption processes, *J. Chem. Phys.*, 91, 4401.
- Scherrer, P.** (1918): Bestimmung der Grösse und der inneren Struktur von Kolloidteilchen mittels Röntgenstrahlen, *Nachr. Ges. Wiss. Göttingen*, 26, 98.
- Schmidt, W.** (2000): "Optische Spektroskopie - Eine Einführung", Wiley-VCH, New York.
- Schoelkopf, J.** (2002), Observation and modelling of fluid transport into porous paper coating structures, Ph.D. Thesis, University of Plymouth, Plymouth, United Kingdom.
- Schoelkopf, J., Gantenbein, D., Dukhin, A. S., Goetz, J. P. and Gane, P. A. C.** (2008a): Novel particle size characterization of coating pigments: comparing acoustic spectroscopy with laser light scattering and sedimentation techniques, Tappi Advanced Coating Fundamentals Symposium, June 8-11, 2008, Montreal, Canada, Tappi Press, Atlanta, US.
- Schoelkopf, J., Gantenbein, D., and Gane, P. A. C.**,(2008b): Method for controlling the shape of talc particles, Patent No. EP2146793,
- Schrader, M. E. and Yariv, S.** (1990): Wettability of clay minerals, *J. Colloid Interface Sci.*, 136, 85.

- Schwarzenbach, R. P., Gschwend, P. M., and Imboden, D. M.** (2003): "Environmental Organic Chemistry", Wiley, Hoboken.
- Semmler, M., Mann, E. K., Ricka, J. and Borkovec, M.** (1998): Diffusional deposition of charged latex particles on water-solid interfaces at low ionic strength, *Langmuir*, 14, 5127.
- Semmler, M., Ricka, J. and Borkovec, M.** (2000): Diffusional deposition of colloidal particles: electrostatic interaction and size polydispersity effects, *Colloid. Surf. A*, 165, 79.
- Senger, B., Voegel, J. C. and Schaaf, P.** (2000): Irreversible adsorption of colloidal particles on solid substrates, *Colloid. Surf. A*, 165, 255.
- Sihvonen, A.-L., Sundberg, K., Sundberg, A. and Holmbom, B.** (1998): Stability and deposition tendency of colloidal wood resin, *Nord. Pulp Paper Res. J.*, 13, 64.
- Slepetys, R. A. and Cleland, A. J.** (1993): Determination of shape of kaolin pigment particles, *Clay Miner.*, 28, 495.
- Smoluchowski, M. v.** (1903): Contribution a la theorie de l'endosmose electrique et de quelques phenomenes correlatjjs, *Bull. Int. Acad. Sci. Cracovie*, 8, 184.
- Stockwell, J.** (1997): Bentonite in the paper industry, *Pira*, 177.
- Stoylov, S. P. and Petkanch, I.** (1972): Transient electric light-scattering. 3. Investigation of stability of palygorskite colloid solutions, *J. Colloid Interface Sci.*, 40, 159.
- Sundberg, A., Pranovich, A. and Holmbom, B.** (2000): Distribution of aionic groups in TMP suspensions, *J. Wood Chem. Technol.*, 20, 71.



- Sundberg, A., Sundberg, K., Lillandt, C. and Holmbom, B.** (1996a): Determination of hemicelluloses and pectins in wood and pulp fibers by acid methanolysis and gas chromatography, *Nord. Pulp Paper Res. J.*, 4, 216.
- Sundberg, K., Ekman, R. and Holmbom, B.** (1994a): Interactions between simple electrolytes and dissolved and colloidal substances in mechanical pulp, *Nord. Pulp Paper Res. J.*, 9, 125.
- Sundberg, K., Pettersson, C. and Eckerman, C.** (1996b): Preparation and properties of a model dispersion of colloidal wood resin from Norway spruce, *J. Pulp Paper Sci.*, 22, 248.
- Sundberg, K., Thornton, J., Holmbom, B. and Ekman, R.** (1996d): Effects of wood polysaccharides on the stability of colloidal wood resin, *J. Pulp Paper Sci.*, 22, 226.
- Sundberg, K., Thornton, J., Pettersson, C., Holmbom, B. and Ekman, R.** (1994b): Calcium-induced aggregation of dissolved and colloidal substances in mechanical pulp suspensions, *J. Pulp Paper Sci.*, 20, 317.
- Swanson, J. W.** (2003): "Colloid chemistry of papermaking materials", Tappi Press, Atlanta, US.
- Swerin, A., Ödberg, L. and Wagberg, L.** (1993): Preparation and some properties of the colloidal pitch fraction from a thermomechanical pulp, *Nord. Pulp Paper Res. J.*, 8, 298.
- Tammelin, T., Johnsen, I. A., Osterberg, M., Stenius, P. and Laine, J.** (2007): Adsorption of colloidal extractives and dissolved hemicelluloses on thermomechanical pulp fiber components studied by QCM-D, *Nord. Pulp Paper Res. J.*, 22, 93.

- Terayama, H.** (1952): Method of colloid titration (a new titration between polymer ions), *J. Polym. Sci.*, 8, 243.
- Thompson, D. W. and Butterworth, J. T.** (1992): The nature of laponite and its aqueous dispersions, *J. Colloid Interface Sci.*, 151 (1), 236.
- Thornton, J., Ekman, R., Holmbom, B. and Örsa, F.** (1994): Polysaccharides dissolved from norway spruce in thermomechanical pulping and peroxide bleaching, *J. Wood Chem. Technol.*, 14, 159.
- Tijero, A., Monte, M. C., Blanco, A., Negro, C. and Tijero, J.** (2009): Pitch adsorption on natural and modified talcs, *J. Pulp Paper Sci.*, 35, 130.
- Toth, J.** (1971): State equations of the solid-gas interface layers, *Acta Chim. Acad. Sci. Hung.*, 69, 311.
- Trafford, J.** (1988): Pitch investigations with pinus radiata bisulphite and thermomechanical pulps, *Appita*, 41, 207.
- Vahasalo, L., Degerth, R. and Holmbom, B.** (2005): The use of flow cytometry in wet end research, *Paper Technol.*, 44, 45.
- van Oss, C. J., Chaudhury, M. K. and Good, R. J.** (1988): Interfacial Lifshitz - van der Waals and polar interaction in macroscopic systems, *Chem. Rev.*, 88, 927.
- Verwey, E. J. W. and Overbeek, J. T. G.** (1948): "Theory of the stability of lyophobic colloids", Elsevier, New York.
- Wagberg, L.** (2000): Polyelectrolyte adsorption onto cellulose fibres - A review, *Nord. Pulp Paper Res. J.*, 15, 586.

- Wagberg, L. and Odberg, L.** (1991): The action of cationic polyelectrolytes used for the fixation of dissolved and colloidal substances, *Nord. Pulp Paper Res. J.*, 3, 127.
- Wallqvist, V., Claesson, P. M., Swerin, A., Schoelkopf, J. and Gane, P. A. C.** (2006): Interaction forces between talc and hydrophobic particles probed by AFM, *Colloid. Surf. A*, 227, 183.
- Wallqvist, V., Claesson, P. M., Swerin, A., Schoelkopf, J. and Gane, P. A. C.** (2007): Interaction forces between talc and pitch probed by atomic force microscopy, *Langmuir*, 23, 4248.
- Washburn, E. W.** (1921): The dynamics of capillary flow, *Phys. Rev.*, 17, 273.
- Whiting, P.** (1997): Contaminant control on a high speed paper machine, Tappi Engineering and papermakers conference, October 6-9, 1997, Nashville, TN, US, Tappi Press, Atlanta, US, pp. 661-668.
- Willför, S., Sundberg, A., Sihvonen, A.-L. and Holmbom, B.** (2000): Interactions between fillers and dissolved and colloidal substances from TMP, *Paperi Puu*, 82, 398.
- Willför, S., Sundberg, K., Tenkanen, M. and Holmbom, B.** (2008): Spruce-derived mannans - A potential raw material for hydrocolloids and novel advanced natural materials, *Carbohydr. Polym.*, 72, 197.
- Williams, G. R.** (1987): Physical Chemistry of the absorption of talc, clay and other additives on the surface of sticky contaminants, Tappi Pulping Conference, South Yosemite, CA, US, Tappi Press, Atlanta, US, pp. 563-571.

- Yang, H., Tang, A., Ouyang, J., Li, M. and Mann, S.** (2010): From natural attapulgite to mesoporous materials: methodology, characterisation and structural evolution, *J. Phys. Chem.*, 114, 2390.
- Yekeler, M., Ulusoy, U. and Hicyilmaz, C.** (2004): Effect of particle shape and roughness of talc mineral Ground by different mills on the wettability and floatability, *Powder Technol.*, 140, 68.
- Yildirim, I.** (2001), Surface free energy characterization of powders, Ph.D. Thesis, Virginia Polytechnic Institute and State University, Blacksburg, United States.
- Yin, H., Mo, D. and Chen, D.** (2009): Orientation behaviour of attapulgite nanoparticles in poly(acrylonitrile)/attapulgite solutions by rheological analysis, *J. Polym. Sci.*, 47, 945.
- Yordan, J. L. and Maat, P.** (1997): Application of new analytical tools to determine efficiency of talc as a pitch/stickies control agent, *Recycling Symposium*, April 14-16, 1997, Chicago, IL, US, Tappi Press, Atlanta, US, pp. 361- 366.
- Yu, L., Allen, L. H. and Esser, A.** (2003): Evaluation of a laser-optical resin particle counter, *Tappi J.*, 2, 13.